Role of the SAA and SMB neurons in locomotion in the nematode *Caenorhabditis elegans*, with a focus on steering

Elpiniki Kalogeropoulou

Submitted in accordance with the requirements for the degree of
Doctor of Philosophy

The University of Leeds
School of Computing

March, 2018

The candidate confirms that the work submitted is her own and that appropriate credit has been given where reference has been made to the work of others.

All experiments were planned, designed and conducted by the author.

All data collection and analysis was conducted by the author, expect for the video analysis on neural calcium imaging of freely moving worms (Chapter 4), which was conducted by Christopher Brittin.

Acknowledgements

To my loving husband, Andrew.

Abstract

The nematode *C. elegans* can orient itself towards sensory cues. Two mechanisms of orientation have been observed in the worm; pirouettes and steering. Past studies have identified a number of neurons that contribute to either orientation strategy.

Here I investigate the role of the motor neuron SMB and the interneuron SAA in locomotion, with a focus on steering. SMB motor neurons have been postulated to be part of the steering circuit. SAA interneurons, which are close to and highly synaptically connected with the SMB motor neurons, have not been previously explored. Here, for the first time, the function of SAA in locomotion is investigated.

I report the generation of integrated transgenic lines where the SMB neuron and/or the SAA neuron are genetically ablated. A two-component ablation system was used to genetically ablate the neurons by targeted expression of a reconstituted caspase specifically in these neurons. Imaging confirmed targeted ablation.

The SMB- and SAA- ablated strains demonstrate similar phenotypes different to those of the wild type in both probabilistic and deterministic locomotion. The phenotypes suggest that SMB and SAA suppress pirouettes, while also facilitating steering, and regulate the amplitude of sinusoidal movement and omega turns. Double ablation mutants revealed that these two neurons are integral to steering, but are not the sole head neurons regulating the amplitude of undulatory movement. Dorsal asymmetric ablation strains revealed differing contributions of SMB and SAA to each orientation strategy. The expression of the *trp-1*, *trp-2* and *trp-4* genes encoding known stretch receptors suggests that these neurons might also have a proprioceptive function. Calcium imaging on the SMB neurons revealed increased activity of these neurons after the onset of omega turns.

Using these results I proposed a new neural network model that integrates both orientation strategies, and a testable model for head movement.

Table of Contents

List of Tables

List of Figures

Chapter 1
General Introduction

'Now we see that the living creature is moved by intellect, imagination, purpose, wish, and appetite. And all these are reducible to mind and desire. For what is painful we avoid, what is pleasing we pursue.'

Aristotle, 4th century BC

'On animal movement'

1.1 Introduction

1.1.1 On animal movement

Humans, have always been fascinated by observing, describing, comparing and sometimes even collecting all creatures, great and small, surrounding us. As early as 4th century BC, when Aristotle wrote his book 'On animal movement', we have strived to understand how and why animals move and adapt their behaviour to different contexts and environments. Our ultimate aim being, consciously or not, to use this knowledge to understanding and know ourselves.

After Aristotle's and prior to Darwin's time, little was done within the field of animal behaviour, let alone locomotion. When Darwin's book 'Origin of Species' was published in 1859, all fields of biology, including animal behaviour, advanced faster than ever before (Darwin, 1859). Early works on movement at this time consisted of research done mostly on plants and motile unicellular organisms' directed movement. It is at this time that directed movement was divided between tropism (directional turning of organisms like plants or fungi) and taxis (directional movement of motile animals) (Sachs, 1887). Moreover, it was also the time that terms like phototaxis and chemotaxis were coined, to infer the reasons behind directed movement, from studies conducted on spores and flagellates' attraction to light, and fern sperms movement towards chemicals (Strasburger, 1878; Pfeffer, 1888). Research conducted on multicellular animals was mostly compared with human behaviour and, as such, interpreted in a very anthropomorphic way. The zoologists at that time seemed to have found the work conducted in plants and unicellular organisms irrelevant to their research (Fraenkel, G.S. and Gunn, 1961).

A big breakthrough in the study of animal movement came with Fraenkel and Gunn's book 'The orientation of animals', where the classification of directed movements was established

(Fraenkel, G. and Gunn, 1940). A classification system we still use today. Fraenkel and Gunn's book, alongside with the research on animal behaviour by Karl von Frish (honey bees), Konrad Lorenz (geese and crows) and Nikolaas Tinbergen (geese and honey bees), established the grounds of modern animal behaviour and movement (Tinbergen, 1951; Frisch, 1954; Lorenz, 1970). The three authors mentioned above, envisioned behaviour in a more mechanistic way than any of their peers before, won the Nobel Prize on 1973 for their work, and are now regarded as the founding fathers of animal behaviour.

Behaviour is the final output of the integration of all sensory stimuli, both internal and external, of an animal's environment. Most behaviours observed across the animal kingdom are carried out with movement. This sensory-motor integration can be quite complex and is of high importance as it results in a variety of behaviours that allow animals to find food, avoid predators and other noxious stimuli, find mates and reproduce, interact with other animals, navigate and migrate. But how does this integration occur and how do neural circuits result in the variety of behaviours we observe? This remains the most fundamental question in behavioural neuroscience. The soil nematode *Caenorhabditis elegans*, with its simple nervous system but wide range of behaviours, is an attractive and ideal model organism to investigate neural function, the link from gene expression to behaviour and sensory-motor integration. In this thesis, I use this animal model to investigate the role of two neurons, a motor neuron and an interneuron, in the orientation strategies this animal employs to navigate. Through this focused research I will try to improve our understanding of the neural circuits controlling the orientation strategies behind navigation.

1.1.2 *Caenorhabditis elegans* as an animal model for behavioural neuroscience

Caenorhabditis elegans is a nematode found in nature in soil and rotten fruit, approximately 1mm in length (Figure 1.1, Image A). Although it is a hermaphrodite nematode, males of the species do exist, but in very low numbers (approximately 0.1-0.2%) (Ward, S. and Carrel, 1979). Since its identification and introduction as an animal model in the lab it has been regarded as a powerful and well established model for neurosciences (Brenner, 1974). Although it has been considered a simple and hard wired animal due to its neural circuitry, *C. elegans* has been shown to have a wide range of behaviours and exhibits neuronal plasticity (de Bono and Maricq, 2005). These behaviours include foraging, feeding, avoidance of and taxis towards various soluble chemicals, odours, heat, oxygen, light (i.e. chemotaxis, thermotaxis, aerotaxis and phototaxis) (Ward, S., 1973; Bargmann, C. I. and Horvitz, 1991; Bargmann, C. I. *et al.,* 1993; Hedgecock, E. M. and Russell, 1975; Ward, A. *et al.,* 2008). However, more complicated behaviours have also been observed, such as mating, imprinting, aggregation (social feeding), sleep and drug dependence, learning and memory (White, J.Q.

et al., 2007; Gray, J.M. *et al.,* 2004; de Bono *et al.,* 2002; Rankin *et al.,* 1990; de Bono and Maricq, 2005).
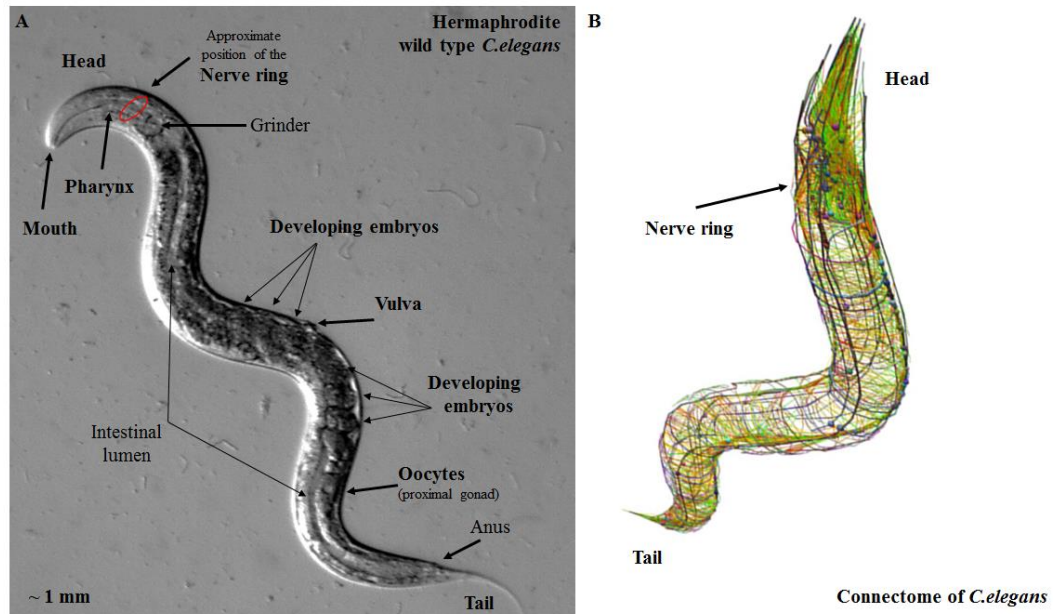
Figure 1.1 *Caenorhabditis elegans* annotated images. A) An image of a hermaphrodite worm using DIC microscopy, taken and annotated by the author. B) A 3D reconstruction of the worm's connectome using the OpenWorm project's visualisation browser (www.openworm.org).

All the behaviours mentioned above are remarkably regulated by a neural circuit of only 302 known neurons. *C. elegans* is the only animal whose entire nervous system has been completely reconstructed by electron microscopy and this is the major reason why it has become such a valuable model for understanding neural control of behaviour (Ward, S. *et al.,* 1975; White, J.G. *et al.,* 1986; Hall and Russell, 1991). Due to the amount of effort put into its circuit being reconstructed by White and colleagues, it was also one of the first animal models to have its connectome (neural wiring) created and it's connectome is still by far the most complete (Chen *et al.,* 2006) (Figure 1.1, Image B). The cell lineages of its neurons, and their neural development, have also been described to a full extent (Sulston *et al.,* 1983; Sulston and White, 1980; Sulston and Horvitz, 1977; Hedgecock, E.M. *et al.,* 1987). In addition, the mapped and sequenced compact genome of *C. elegans*, the available forward and reverse genetics and RNAi techniques, all together make it an excellent animal model for genetic manipulations (Hodgkin *et al.,* 1998). Amongst other advantages are its short lifecycle; the worm reaches adulthood within approximately three days at a temperature of 20°C. Finally, its transparent body has proved to be a major advantage when imaging, identifying and laser-ablating neurons.

Recent technical advances in the *C.elegans* field, such as patch clamp recording (Goodman *et al.,* 1998), calcium imaging (Tian *et al.,* 2009), optogenetics (Nagel *et al.,* 2005), microfluidics (Lockery, S. R. *et al.,* 2008) and most importantly the combination of them, have contributed to a fast pace progress of behavioural neuroscience and have made the worm an even more attractive animal model (Leifer *et al.,* 2011; Wen *et al.,* 2012; Akerboom *et al.,* 2013; Li, Z. *et al.,* 2014).

.

1.1.3 An introduction to *Caenorhabditis elegans'* nervous system

An adult hermaphrodite *C. elegans* has 302 neural cells regulating two neural systems: the somatic and the pharyngeal. The pharyngeal nervous system is responsible for the transfer of the food that the nematode feeds on (bacteria) through the worm. The somatic nervous system is responsible for all the rest of the nematode's behavioural processes, such as locomotion, sensing the environment, avoidance, attraction etc. Most neurons are clustered in ganglia in the head or tail, and more than half project their processes into the nerve ring (Ware *et al.,* 1975). According to their known function and synaptic connectivity, the somatic neurons fall into three functional groups: the sensory neurons, which sense information from the worm's environment (i.e. detect attractant or repellant chemicals, temperature, touch, osmotic levels, carbon dioxide etc.), the motor neurons, which are connected to muscle cells via neuromuscular junctions and the interneurons where the information of the worm's environment is being processed (White, J.G. *et al.,* 1986; Chalfie and White, 1988). The absence of voltage gated channels in the worm has resulted in the view that *C. elegans* does not fire classic sodium-dependent action potentials (Bargmann, C. I., 1998; Lockery, S. R. and Goodman, 2009). Ever since, the *C.elegans* research community has postulated that synaptic transmission between the neurons of the worm is most likely graded. Few studies have demonstrated evidence supporting this idea (Liu *et al.,* 2009; Lindsay *et al.,* 2011). However, this begs the question of how can the worm exhibit both dynamic (in a sense graded) and digital-like (on/off) behaviours with only graded synaptic transmission? Li *et al.* (2014) demonstrated in their recent multifaceted study that this can be achieved by bifurcation of the information flow (recruitment of two different postsynaptic neurons) and differential biophysical properties of the postsynaptic receptors. This achieves the regulation of two behaviours with different mechanistic qualities (speed vs. forward/backward movement switch) from one first layer interneuron (AIY), using remarkably one neurotransmitter (Ach), and graded transmission (Li, Z. *et al.,* 2014)

1.1.3.1 Sensory neurons

The sensory neurons are the amphid and inner labial neurons localized in the head, and the phasmid neurons found in the tail (Ware *et al.,* 1975; Ward, S. *et al.,* 1975). Most sensory

neurons are located in the head, possess axons in the nerve ring and consist of two cells, one right and one left. These cells are ciliated and sense the environment through sensory pores in the head of the animal. Phasmid neurons are not necessary for chemotaxis (Ward, S., 1973). Through years of research we have quite a clear picture of which stimuli each neuron responds to (especially for the amphid neurons that mediate chemotaxis) and have observed that they often can be polymodal (each sensing more than one stimuli and sometimes opposing ones) (Bargmann, C. I. and Horvitz, 1991; Bargmann, C. I. *et al.*, 1993). Recent studies however, have shown that sensory neurons are multifunctional and more complex than initially thought (Bargmann, Cornelia I., 2012). Some exhibit a functional left and right asymmetry (i.e. ASEL and ASER sensing Na^+ and Cl^-, and activity increase in up-steps and down-steps of concentration respectively) (Suzuki *et al.*, 2008; Thiele *et al.*, 2009). Some sensory neurons have been shown to asymmetrically express odorant receptors (i.e. AWCL and AWCR) (Troemel *et al.*, 1999). In addition, some can adapt their response and interneuron 'recruitment', not only to previous experiences, but also to changes in the concentration of the stimuli (i.e. the opposing responses of AWCL and AWCR to different concentrations of isoamyl alcohol) (Yoshida *et al.*, 2012) (Satoh *et al.*, 2014).

In this thesis I explore part of the chemotaxis circuit of the worm, with an emphasis on the output (lower layer of interneurons and head motor neurons) and not the sensory layer as much. To this end, I have included a table in the Appendix Section G with the amphid sensory neurons and their known role in chemotaxis, as it will aid the unaccustomed reader (Table G1). Briefly, ASE, ASI, ADF, ASJ and ASG neurons primarily sense water soluble chemicals (Bargmann, C. I. and Horvitz, 1991). AWA and AWC neurons mediate response to odor attractants, whereas AWB, ASH, and ADL neurons respond to odor repellants (Bargmann, C. I. *et al.*, 1993; de Bono *et al.*, 2002). ASK seems to be a redundant neuron regarding chemotaxis, with minor contributions to the avoidance response and lysine attraction (Bargmann, C. I. and Horvitz, 1991). The AFD neuron responds to changes in temperature (Mori and Ohshima, 1995). The attractant used in the behavioural assays in this thesis is a soluble salt (NH_4Cl), and the sensory neurons responding to it are ASE, and to a lesser degree ASI, ASG, ADF (Ward, S., 1973; Bargmann, C. I. and Horvitz, 1991).

1.1.3.2 Motor neurons

Motor neurons are located all over the worm's body and control all locomotory behaviours, as well as egg laying and defecation. There are 113 motor neurons and they regulate the characteristic undulatory movement of the animal, but also control the movement of the head. The head motor system is separate from the body motor system, which is controlled by the ventral nerve cord (VNC). VNC motor neurons are thought to excite or inhibit the muscles that they are coupled with via neuromuscular junctions (NMJs), resulting to the contraction

or relaxation of the muscles respectively. There are 5 classes of VNC motor neurons, each with a different number of cells [A (21), B (18), D (19), VC (6), and AS (11)]. The A, B, and D classes are further distinguished by whether they innervate the dorsal or ventral muscles [DA (9), VA (12), DB (7), VB (11), DD (6), and VD (13)](Von Stetina *et al.,* 2005). On the other hand, the head motor neurons are arranged in a four or six part symmetry (reflecting the number of cells in the same neural class) [(i.e. SMB(4), RMD(6)]. Further distinction of a head motor neuron is, using as an example the SMB neuron, as follows: SMBVL, SMBDL, SMBVR, SMBDR. Letters D and V indicate dorsal and ventral side, whereas L and R the left and right side of the animal.

The evidence so far suggests that motor neurons that utilize the neurotransmitter acetylcholine (ACh) are likely to be excitatory, whereas the ones that utilize GABA as their transmitter are inhibitory to the muscles (McIntire *et al.,* 1993). However, a recent study has shown the acetylcholine neurotransmitter to also be used for inhibitory connections (Li, Z. *et al.,* 2014). In this thesis I focus on the head of the worm, and therefore the motor neuron investigated (SMB) innervates the head and neck muscles (White, J.G. *et al.,* 1986). See section 1.2.5 for more detail on the SMB neurons. Amongst the other head motor neurons relevant to the project, due to their function in the navigational system of the worm, are SMD, RME, RMD, RIM and RIV (Gray, J.M. *et al.,* 2005). Amongst them the motor neuron highly relevant to the project, due to its position in the head, NMJs to the head and neck muscles (White, J.G. *et al.,* 1986) and function is the SMD motor neuron and will be taken into consideration in the discussion sections (Gray, J.M. *et al.,* 2005; Shen *et al.,* 2016).

1.1.3.3 Interneurons

Perhaps the least defined cells in *C. elegans* research are the interneurons. Most interneurons have a cell body in the nerve ring and make contacts with sensory neurons and other interneurons. Most interneurons are bilaterally symmetric comprising of two cells (i.e. AIYL, AIYR; L for left and R for right). However, some classes consist of four cells (i.e. SAAVL, SAADL, SAAVR, SAADR). Although, their anatomy and localization is known, their functionality is far from defined. More often than not, a set of interneurons and not a single interneuron are responsible for a behavioural output or for multiple outputs. This makes it difficult for researchers to draw out functional profiles of these cells with simple laser ablations. Recently, a combination of techniques, such as calcium imaging and optogenetics, have helped identify interneuron function, such as the AIY interneuron's role in turning bias and the RIA interneuron's differential activity (Kocabas *et al.,* 2012; Hendricks *et al.,* 2012). The AIY interneuron has also been shown to be part of two directionally opposing behaviours (Satoh *et al.,* 2014). Also, a single interneuron can encode a digital-like (on/off) and analog-like (graded) output (i.e speed and direction switch, AIZ-AIY-RIB circuit)(Li, Z. *et al.,* 2014).

The interneurons mostly researched to date are the ones directly regulating backward and forward movement and the switch between the two, via regulation of the VNC motor neurons. These interneurons are called 'command interneurons' (more on them in the next section that covers the worm's sinusoidal movement). In this thesis the interneuron investigated is the SAA, localized in the nerve ring, adjacent to the SMB and SMD motor neurons, and highly synaptically connected to them (see 1.25 for more details on the SAA neurons).

1.1.4 The sinusoidal locomotion of *C.elegans*

Behaviour in *C. elegans,* more often than not, involves locomotion. The worm moves on an agar plate on its side, either left or right, by generating sinusoidal dorsoventral waves that are propagating along the length of its body via alternate muscle contractions (Croll, 1975). As with most nematodes' locomotion the body follows the trajectory of the head (Gray, J. and Lissmann, 1964). Locomotion consists of forward crawling (where waves propagate from head to tail), backward crawling (where waves propagating from tail to head) and turns (shallow or deep). Its undulatory movement is accompanied by rapid exploratory head movements at the tip of the head (often called nose) that are similar to those when the worm is foraging on food. These foraging head movements are suppressed in backward locomotion and during turns (Chalfie *et al.,* 1985; Alkema *et al.,* 2005). A specific form of deep turn has been dubbed "Omega turn" because of the characteristic shape of the body that resembles the Greek letter 'Ω' (Gray, J.M. *et al.,* 2005). In this turn, the head over flexes so much that it touches the rest of the body before resuming its forward movement in a direction at least 90° degrees different than before the turn. The omega turns that have a dorsoventral reorientation and where the head crosses over the mid body rather than sliding off of it, were recently coined 'delta' turns (Broekmans *et al.,* 2016).

During forward or backward crawling the body wall muscles positioned along the worms body alternatively contract. When the ventral muscle of a body bend is contracted then its corresponding dorsal muscle is relaxed, and vice versa. Since the focus of this project is on steering, I will focus more on the work that has been done on forward, rather than backward, movement. I consider turns, shallow or deep, to be part of the forward movement during this thesis, albeit distinct as well.

1.1.4.1 Body movement

The body wall muscles are coupled with and thus controlled by the 4 classes of VNC motor neurons that drive forward movement [VD (13), VB (11), DD (6), DB (7)](Chalfie *et al.,* 1985). It is important to mention again that VNC motor neurons are arranged in repeating groups along the body, 'virtually' segmenting an otherwise anatomically non-segmented

animal (Von Stetina *et al.,* 2005). The cholinergic B-type neurons are excitatory to the muscle cells, whereas the D-type GABAergic neurons are inhibitory to muscle cells (Richmond and Jorgensen, 1999; McIntire *et al.,* 1993). VB and VD innervate ventral muscles, whereas DB and DD innervate dorsal muscles (White, J.G. *et al.,* 1976). The D-type inhibitory neurons are postsynaptic to the excitatory B-type motor neurons that innervate muscles on the opposite side of the body. This neuronal architecture allows for a pattern of contralateral inhibition such that DB motor neurons can excite a dorsal muscle cell as well as VD motor neurons, and in turn VD motor neurons inhibit the opposing ventral muscle cell, and vice-versa. Asymmetric inhibition of VD to VB resets the whole pattern, and so on so forth. Figure 1.2 gives a good simplified example of how the worm's body wall muscles achieve the sinusoidal posture.
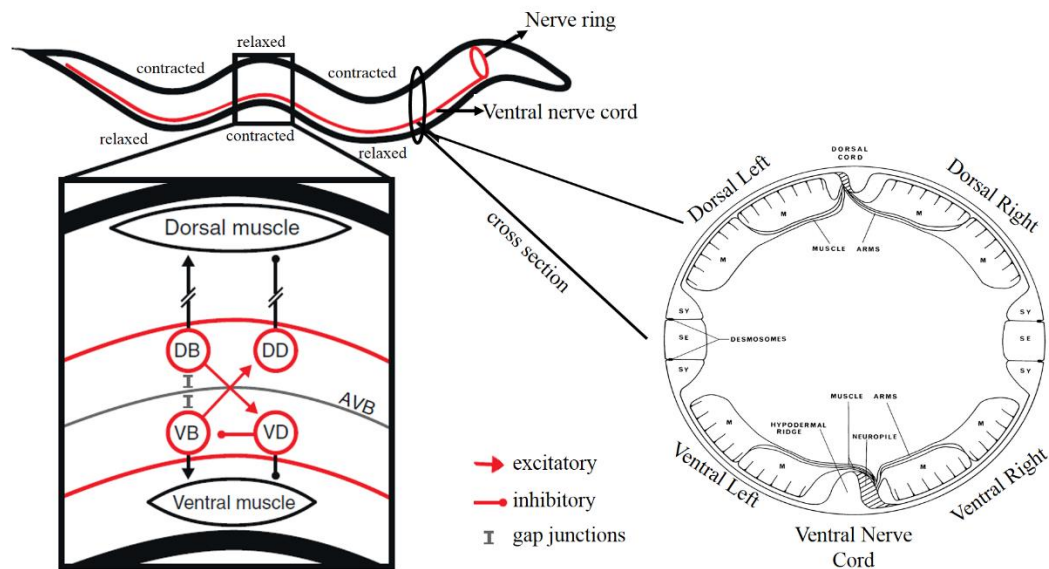
Figure 1.2 (Left) A simplified schematic of one part of the repeated groups of VNC motor neurons and their connection to the muscle quadrants. Body wall muscles contracting and relaxing along the body. Image edited from Cohen and Sanders (Cohen and Sanders, 2014). (Right) A cross section schematic of the worm's body with an emphasis in the anatomy of the body wall muscle quadrants and the position of the VNC. Image edited from White *et al.,* (1986) (White, J.G. *et al.,* 1986).

VNC motor neurons are deeply synaptically connected with a set of interneurons called command interneurons. These are AVA, AVB, AVD, PVC and AVE. The circuit including command interneuron AVB (and to a lesser extend the PVC ventral cord interneuron) and the B-type and AS VNC motor neurons directs forward locomotion, whereas the circuit including AVA, AVD, AVE interneurons and the A-type VNC motor neurons directs backward locomotion (Chalfie *et al.,* 1985).

However, although AVA/AVD/AVE are important for initiating reversals, they have been shown to not be essential. A study by Piggot *et al.* (2011) showed that worms lacking these command interneurons could still initiate reversal, thus providing evidence of two parallel reversal circuits The first layer interneuron AIB, and the motor neuron RIM, are the alternative circuit for backward locomotion (Piggott *et al.,* 2011). At this point, and having in mind this example, it is good to emphasize to the reader the presence of a lot of redundancy in the neural circuits of the worm. Having parallel circuits for important behaviours, such as in this case the reversals, makes the worm able to find food or escape threatening or noxious stimuli even when part of its neural system is damaged or not functioning due to overriding conditions in the environment. It also enables the worm to regulate the time of its response, and act faster when it is essential for survival. Recently, another case of parallel circuits for the same type of behaviour has started to be explored and is relevant to this study. Forward locomotion driving the worm away from a stimuli (ipsilateral steering) has been shown to include AIY first layer interneurons, however, curving towards the stimuli (contralateral steering) is not driven by AIY, but most likely by one of the other first layer interneurons (AIA, AIB, AIZ) (Satoh *et al.,* 2014).

Finally, and because it is also relevant to this project, command interneurons have been shown not to generate the sinusoidal forward movement (Zheng *et al.,* 1999). Which brings us to one of the most intriguing question in the field of *C.elegans* locomotion.

How does the worm generate and maintain its undulatory movement? Is there any rhythm pattern generator or is proprioception at work, or both? Neuroanatomical insights from biological data and theoretical studies have suggested that the worm's sinusoidal locomotion is generated by motor neuron sensory feedback via stretch receptors (a.k.a. proprioception) (Boyle *et al.,* 2012; Fang-Yen *et al.,* 2010; de Bono and Maricq, 2005; Von Stetina *et al.,* 2005; White, J.G. *et al.,* 1986). Computational models integrated with biophysics, such as the one proposed by Boyle and colleagues, assume that proprioception forms the rhythm the worm requires to form and maintain the sinusoidal locomotion (Boyle *et al.,* 2012). In each repeated unit of VNC motor neurons, DB and VB excitatory neurons are represented as binary and bistable. Input from command interneurons switches the circuit on and induces the oscillatory response. Stretch input on the ventral side activates VB, which by activating the ventral muscles will gradually increase stretch on the opposite side thus activating DB, which will reset VB via inhibition from VD. When the stretch input now on the dorsal side falls below a threshold it will release VB from inhibition (Figure 1.2 can aid in envisaging the model). This motif can maintain a repeated rhythm that can propagate up and down adjacent units via proprioception. In fact, Boyle *et al.*'s model suggests that proprioception would be sufficient, without the requirement of a central pattern generator (CPG). Recently, an exciting new study has shown that the previously unresearched AS VNC motor neurons, facilitate, but

don't play an instructive role in generating, the forward undulatory wave (Tolstenkov *et al.,* 2018). Soon new computation models will surely be developed, giving us even more insight on the worm's undulatory movement.

One of the first studies using optogenetic activation on freely moving worms shed some light on the proprioceptive function of the VNC (Leifer *et al.,* 2011). Leifer *et al.* (2011) were able to suppress undulatory wave propagation by optogenetically inhibiting parts of the repeated units of VB and DB motor neurons. The region posterior to the illuminated segment was suppressed whereas the region anteriorly still exhibited wave propagation. Experimental work by Wen *et al.* (2012), where they artificially bend the worm at different parts of the body in a microfluidic device, provided even more evidence that proprioception is indeed present in the worm, and is integral for the propagation of body bends from head to tail via anterior facing stretch receptors (Wen *et al.,* 2012). In addition, mutant worms lacking a TRP homologue stretch receptor (*trp-4*) in DVA neuron bend their body abnormally, suggesting that stretch-receptor-mediated proprioception is at work in *C.elegans* (Li, W. *et al.,* 2006). It is unclear whether the worm lacks a CPG, or one exists (most likely in the area of the head according to most models entertaining the idea of a central oscillator), and that it might be modulated by proprioceptive information from stretch receptors along the body.

1.1.4.2 Head movement

In this section I want to explore a little further the head motor neurons that have been experimentally shown to regulate head movement (Figure 1.3 shows the head motor neurons and which muscle quadrants they innervate). Gray *et al.*'s extensive study of the head motor neurons was the first to shed some light on head movement (Gray, J.M. *et al.,* 2005). Laser ablation of the SMB head motor neurons exhibited a 'loopy' phenotype in the locomotion of the worm, hinting at the inhibitory regulation of head movement and it was one of the incentives for me to focus on them in this study. The RIV motor neuron was found to facilitate the ventral bias of omega/delta turns (Gray, J.M. *et al.,* 2005). The laser ablation of SMD head motor neurons resulted in shallow turns, and from personal communication with Manuel Zimmer's lab, locomotion is also affected; SMD- ablated worms exhibit shallow undulatory movement. Recently, Hendricks *et al.,* showed with calcium imaging some evidence of SMD's effect on head bending mediated by RIA motor neurons (Hendricks *et al.,* 2012). Gray *et al.,* discuss in their study, without though showing the data, that by laser killing the ventral cells of SMD, RMD and SMB a gentle curvature of forward movement was observed. RME seems to regulate foraging, which is the oscillation of the nose of the head (Gray, J.M. *et al.,* 2005). This result has been supported by Shen and colleague's study using calcium imaging and microfluidics (Shen *et al.,* 2016). Their videos of ablated RMEs show clearly the nose movement being affected, however, not all the head and neck is. Once again, I want to mention

that the head bending regulation has been shown to be transmitted to the remainder of the body, mainly by proprioceptive feedback (Wen *et al.,* 2012).
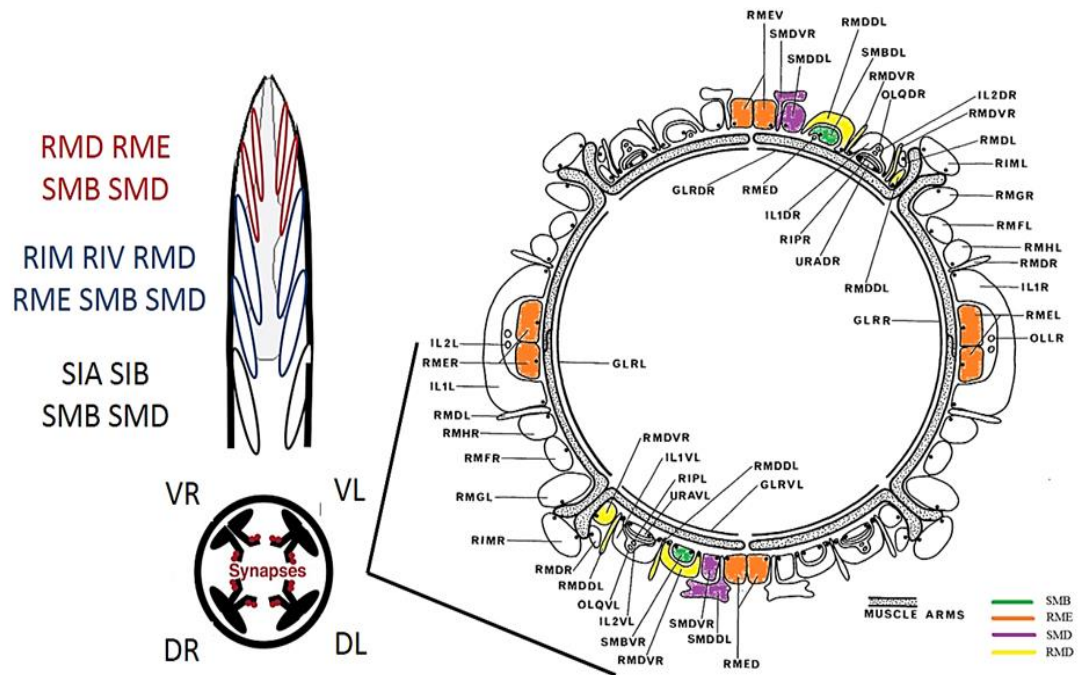
Figure 1.3 A schematic of the worm's head and the main head motor neurons innervating muscles at the head or neck or both (left). A cross section of the head showing in a simplified way the synaptic connectivity between head motor neurons and the body wall muscle quadrants (right). Image edited from (Gray, J.M. *et al.,* 2005) and (White, J.G. *et al.,* 1986).

Since I am a molecular biologist and this is in fact a biological study of two neurons, it is not necessary to go through all computational models for head movement. However, I came across two that are based on a good amount of biological data, can give us good insight into what to research next and are re-enforcing my own project's hypothesis (Sakata and Shingai, 2004; Karbowski *et al.,* 2008). I will explore them further in section 1.2.5.

1.1.4.3 Extrasynaptic neuromodulators affect locomotion

To add to the complexity of the worm's sensory-motor integration, there is evidence of extrasynaptic regulation of behaviours. This added complexity makes it harder for us to fully understand the circuit, and reflects increased circuit flexibility that enables the worm to portray a big number of behaviours with a small number of neurons/subcircuits (i.e. low developmental cost). Neuromodulators, monoamines, and peptides have been shown to affect many aspects of *C. elegans* behaviour (Bargmann, Cornelia I., 2012; de Bono and Maricq, 2005; Horvitz *et al.,* 1982).

Alkema *et al.* showed in 2005 that tyramine has a role in the inhibition of egg laying and in the regulation of the escape response (Alkema *et al.,* 2005). He later went on to show with Donnely, Pirri and other colleagues, that tyramine can inhibit head movements and forward locomotion through the activation of a tyramine-gated chloride channel expressed in neuronal and muscle cells (Pirri, J. K. *et al.,* 2009). In addition, they showed that tyramine acts as an inhibitory neurotransmitter in the GABAergic motor neurons that synapse onto the ventral body wall muscles that can contribute to the sharp ventral turns observed during the escape response (Donnelly *et al.,* 2013).

Harris *et al.* (2011) showed that serotonin release from NSM neurons (stimulating response) and ADF neurons (inhibiting response) acts differentially on ASH-mediated aversive responses (Harris *et al.,* 2011). In the same research paper another neuropeptide was found to inhibit serotonin release altogether. A study published in the same year showed serotonin to promote swimming while dopamine promotes crawling in the worm (Vidal-Gadea *et al.,* 2011). Another example of two neuromodulators affecting two linked but different motor outputs in the worm, is seen with serotonin and PDF neuropeptide. When serotonin is released by two motor neurons it promotes dwelling (staying in the area of food while performing tumbles), whereas when the PDF neuropeptide is released by an interneuron it promotes roaming (exiting the area of food while performing runs) in the worm (Flavell *et al.,* 2013).

1.1.4.4 An overview of the information flow within the neural system that drives locomotion.

To sum up everything so far, from the structure of the nervous system of the worm, to the connections between the neurons and the studies I referred to, and to help the reader grasp the complex information flow within the neural system of the worm that drives locomotion, I have drawn Figure 1.4 and Figure 1.5. Figure 1.4 shows a putative simplified schematic of the main information flow in the worm and how the community has categorised the layers of neurons. Figure 1.5 shows a broadened network of postsynaptic and presynaptic partners on the neurons relevant to this project, from the amphid neurons to the muscles. The reader should bear in mind that each layer sends information to almost every other layer, and possibly each layer has its own feedback loop well.
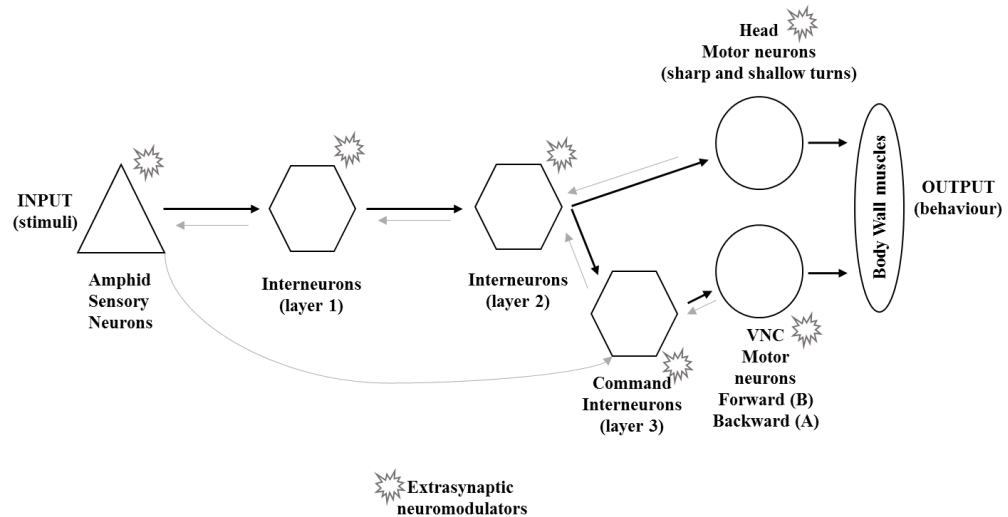
Figure 1.4 An oversimplified schematic of the main flow of information from the input (amphid sensory neurons) to the output (muscles). Updated and adapted from Gray *et al.,* (2005)(Gray, J.M. *et al.,* 2005). Studies have shown that all layers can be affected by extrasynaptic neuromodulators, and some sensory neurons directly synapse and affect motor neurons when the worm has to respond fast (i.e. ASH to the command interneurons regulating the escape response).
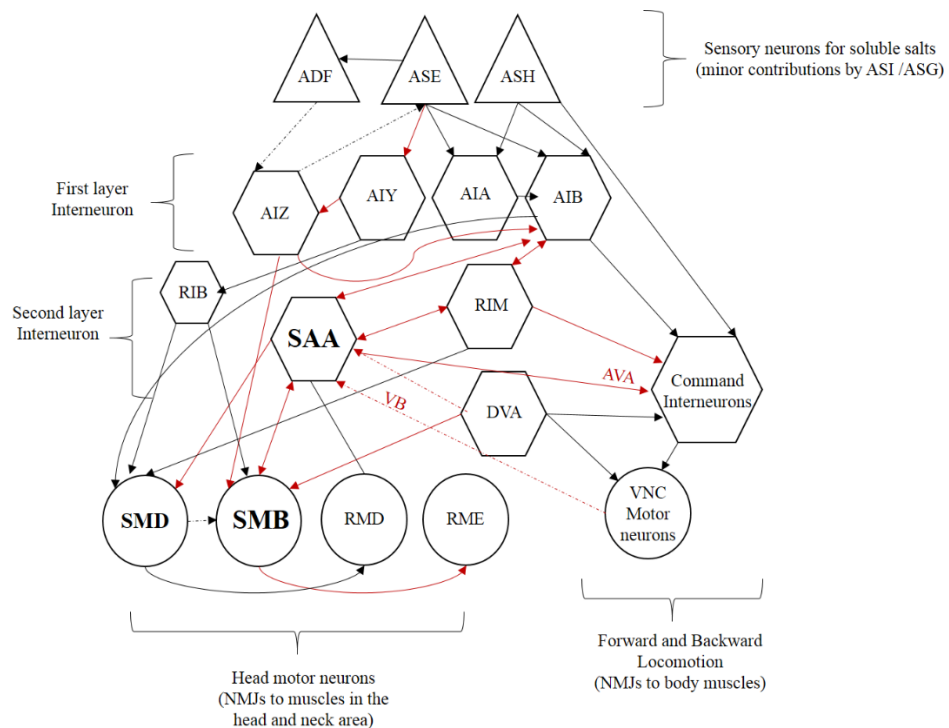
Figure 1.5 A broadened network of postsynaptic and presynaptic partners on the neurons relevant to this project. Starting from the input layer (amphid sensory neurons responding to soluble salts) to the output (muscles). In bold the neurons of high relevance to the project. Dashed lines are weak connections, solid lines are strong. In red colour are the connections of high relevance to the project.

1.2 The focus of this thesis: Navigation and spatial orientation strategies in *C.elegans*

It has already been emphasized in this chapter that *C.elegans*, in order to explore and navigate its environment, senses and computes a variety of stimuli, which in turn result in various behaviours and adaptations of them. Faumont *et al.* (2012) created an umbrella term for all the behaviours described below, which are necessary for survival: 'habitat and resource localization' (Faumont *et al.,* 2012).

While feeding on bacteria the worm will stay in the area via a barrage of pauses, turns and reversals exhibiting a behaviour described as 'dwelling', interrupted every so often by a switch to the behaviour described as 'roaming' (Croll, 1975; Gray, J.M. *et al.,* 2005; Fujiwara *et al.,* 2002; Flavell *et al.,* 2013). When the worm roams away from food, it exhibits long runs until the time comes to return back to the area of the food. If the worm finds itself away from any kind of stimuli it will apply a 'local-search'. While in this mode the worm exhibits an approximately equal number of short and long reversals, turns and short runs. With this behaviour the worm samples its environment for cues to follow while staying relatively close to its starting position. As time goes by without positive or negative cues to follow or averse from respectively, the frequency of turns and reversals decreases while it exhibits long runs (Gray, J.M. *et al.,* 2005). In this way, the worm covers more area and increasingly gets further away from its starting point. These 'runs' are interrupted by short instances of local searches but these diminish in time too ('long-range dispersal').

When the worm senses an attractive cue it will re-orient itself to follow it, whereas it will try to re-orient itself away from a repellent cue (taxis). As previously mentioned in this chapter, according to the nature of the cue, the orientation behaviour overall can be a chemotaxis, thermotaxis, phototaxis etc. For the soluble salts used in this project the worm has been shown to chemotaxis towards them as early as the 70s (Ward, S., 1973).

In simple words, the worm uses reversals, sharp turns (deep turns, omega or delta turns) and shallow turns (that results in gradual turning) to change direction (Kim, D. *et al.,* 2011). In fact, it is not much different to what researchers in navigation call 'runs and tumbles'. Observed motifs, computational elements and repeated combinations of these behaviours have separated them in two strategies of spatial orientation observed in the worm in the context of various sensory inputs (Lockery, Shawn R., 2011). These strategies are the 'pirouette' strategy (which is regarded as a klinokinesis response; directional movement governed by a biased random walk) and 'weathervane' strategy (or steering, which is regarded as a klinotaxis response; directional movement with continuous adjustment) (Pierce-Shimomura *et al.,* 1999; Iino and Yoshida, 2009; Lockery, Shawn R., 2011; Faumont *et al.,* 2012; Dusenbery, 1980; Ward, S., 1973). These strategies, and the sensory stimuli that can

evoke them, are easily observed and are comparable in simple chemotaxis assays. Being a biologist interested in researching sensorimotor integration it made sense for these strategies to be the primary focus of my investigation.

1.2.1 The 'pirouette' strategy (klinokinesis response)

During the pirouette strategy the worm exhibits short runs interrupted by sharp re-orientations via events the *C.elegans* research community have come to call 'pirouettes'. A pirouette is the event where the worm stops its forward movement, reverses, performs a deep or sharp turn and resumes forward locomotion in a trajectory at least ~90° different than the original (pirouettes are circled in red in Figure 1.6). Overall, pirouettes are performed at a rate of 2 per minute, unless the worm is moving down an attractant gradient and their rate increases until the worm re-adjusts up the gradient again (Pierce-Shimomura *et al.,* 1999). Indeed, pirouette frequency is strongly regulated by the rate of change in the concentration of the attractant, and is employed by the worm for rapid course correction, in both chemotaxis assays, but also *in silico* computational models (Pierce-Shimomura *et al.,* 1999; Lockery, Shawn R., 2011). The change in attractant concentration has been shown to be computed within on/off type of cells of sensory neurons. Specifically, for the soluble attractants that my investigation uses, the on-cells are ASEL and ADF that sense up-steps in concentration, whereas the off-cells are ASER and ASH that sense down-steps in concentration(Suzuki *et al.,* 2008; Thiele *et al.,* 2009). When a down-step in concentration is sensed, the off-cells recruit the command interneuron network to initiate backward movement and then perform a pirouette, as seen in the simplified model in Figure 1.7 (Lockery, Shawn R., 2011). Iino and Yoshida demonstrated with a large study of neural ablations and chemotaxis assays that AIZ mediates the pirouette frequency, probably via the command interneurons AVA and AVE (Iino and Yoshida, 2009). Their more recent study with chemotaxis assays of isoamyl alcohol confirmed previous findings and added AVD command interneuron and AIB first layer interneuron to their neural circuit model (Yoshida *et al.,* 2012). Looking back to their original study there was indeed a hint of AIB mediating pirouettes, but as they commented their transgenic animals were unreliable.

For a time this strategy was considered to be sufficient for all chemotactic behaviours exhibited by the worm (Pierce-Shimomura *et al.,* 2005). And if it is considered on its own it is indeed a klinokinesis response (Fraenkel, G. and Gunn, 1940), although most metazoans exhibit more complicated behaviours than eukaryote cells, like *E.coli* that exhibits only klinokinesis (L. Gunn, 1975). Differences between the *in silico* models and experimental data hinted on another strategy existing as well, which was described (it had already been

observed) and named 'weathervane' by the *C.elegans* research community (steering) (Iino and Yoshida, 2009).
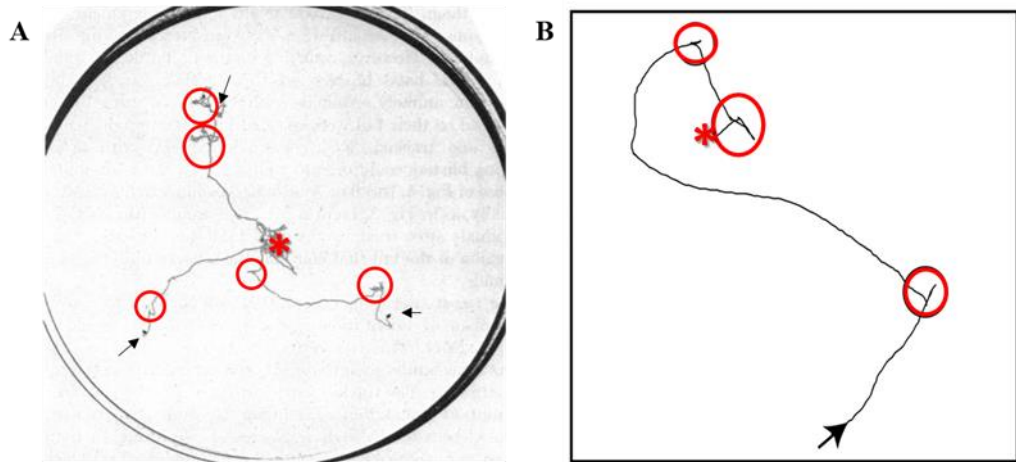
Figure 1.6 Real and *in silico* worms orienting up a chemical gradient. A) Actual trajectories made by worms orienting towards a NH_4Cl radial gradient (Ward, S., 1973). B) *In silico* simulation of a worm going up a gradient (Iino and Yoshida, 2009). The red circles indicate pirouettes. The black arrows indicate starting points of the worms. The red stars indicate the peak of the gradient.
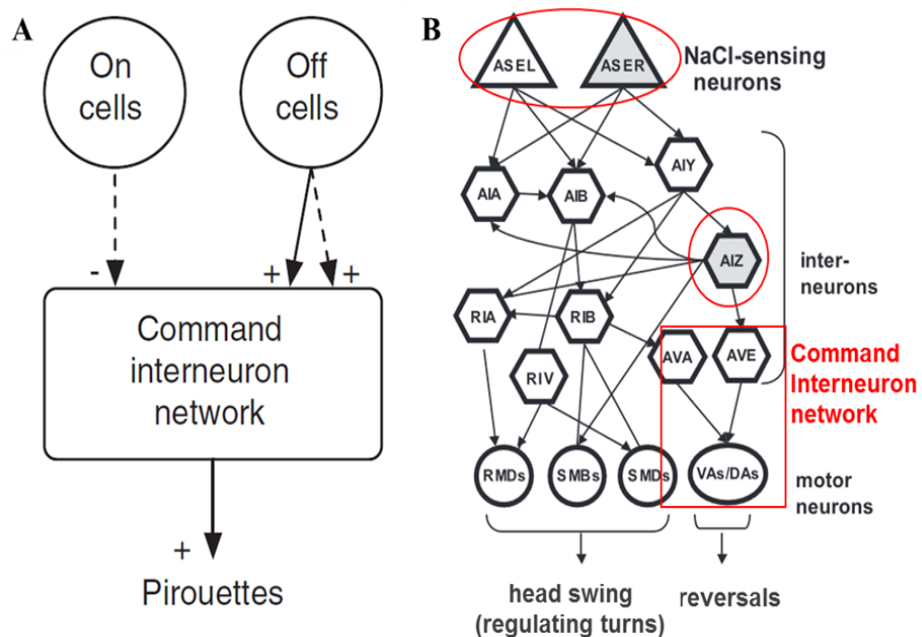
Figure 1.7 Examples of pirouette models. A) A simplified pirouette strategy network model. Plus and minus symbols are excitatory and inhibitory connections respectively. Solid lines represent monosynaptic pathways. Dashed lines represent polysynaptic pathways (Lockery, Shawn R., 2011). B) A candidate neural circuit schematic for the pirouette strategy (in red the circuit mediating pirouettes). Edited from Iino and Yoshida (2009) (Iino and Yoshida, 2009).

1.2.2 The 'weathervane' strategy (steering or klinotaxis response)

Steering in general is the term applied to the collection of components (external or internal), and the continuous adjustments of those components, required for an organism, or any kind of vehicle, to follow a specific course. The motor system (output) is constantly modified by the sensory system (input) via a precise integration and fine-tuning. Stimuli received from the environment establish the animal's position, and proprioceptive feedback establishes the internal state of the animal. Steering relies on this continuous feedback, and the animal's course is continuously corrected because of it during its ascent toward the stimuli it follows.

In the context of *C. elegans* one could define steering as the continuous adjustment of the body of the worm, through a modulation of neurons and muscles, in order to move towards the direction of the source of the cue it is sensing. The worm is steering its body, like we steer the wheel of a car in an open long turn on the road, in order to make a long gradual turn up a gradient. The weathervane strategy, or steering, is therefore a more deterministic course correction strategy than the pirouettes. It has been demonstrated that the worm steers by gradually adjusting the turning angle of its head and the body follows it (Iino and Yoshida, 2009; Kim, D. *et al.,* 2011). This turning bias has been shown to be due to the changes in concentration sensed during head swings, and not the concentration *per se* (Iino and Yoshida, 2009). This was hinted at since Ward's study decades ago, when he used mutants with blisters at different parts of the body, and observed that only the ones with blisters on the head could not steer up a radial NH_4Cl gradient (Ward, S., 1973). He also observed and compared the tracks of mutants following a gradient with deficiencies in the sensory neurons or the head muscles. His experiments indicated for the first time that the response is indeed a klinotaxis (Fraenkel, G.S. and Gunn, 1961); that orientation is mediated by sensory neurons via dorso/ventral displacement of receptors, and therefore is facilitated by the side to side movement of the head. Course correction via steering therefore occurs faster than the pirouettes, as it takes place between head swings. In the tracts of a worm, steering is observed as very long biased runs, gradually turning towards the peak of the gradient (Figure 1.6).

Iino and Yoshida demonstrated that, as with pirouettes, in this strategy ASE sensory neurons provide most of the input, with ASER (off-cell in Lockery's network model in Figure 1.8, Image A) playing a more important role than ASEL (Iino and Yoshida, 2009). ASER ablation, but less so ASEL ablation, exhibited a strong defect in the turning bias towards the peak of the gradient, indicating the worms could not steer properly. Full ablation of the ASE neurons hinted at a redundancy in the steering circuit, with other sensory neurons, most likely the ones required for chemotaxis of soluble attractants mentioned earlier, playing some role as well. Several ablations of first and second layer interneurons have highlighted candidate interneurons mediating steering, such as AIZ and AIY (Iino and Yoshida, 2009). It is through

these interneurons in Lockery's network model and Izquierdo and Beer's model that inhibition and excitation of the head motor neurons is mediated (Figure 1.8) (Lockery, Shawn R., 2011; Izquierdo and Beer, 2016). In both models a putative unknown oscillator gives feedback information to these head motor neurons for undulatory movement.

The head motor neurons have been postulated to be the SMB neurons by most studies, both experimental and computational (Iino and Yoshida, 2009; Izquierdo and Lockery, 2010; Lockery, Shawn R., 2011), including all of the Izquierdo and Beer's model revisions (Izquierdo and Beer, 2013; Izquierdo *et al.,* 2015; Izquierdo and Beer, 2016) (Figure 1.8, Image B). Experimental data from only one study, using a combination of odor stimulation and optogenetic activation of the SMB neurons, has supported this hypothesis (Kocabas *et al.,* 2012). These studies, Gray's finding that SMB ablation result in a 'loopy' worm posture and anatomical data for the SMB neurons make them an excellent candidate for my research (White, J.G. *et al.,* 1986; Gray, J.M. *et al.,* 2005).

Again though, as with the pirouette strategy, this strategy has been shown to be only partially efficient for chemotaxis (Iino and Yoshida, 2009).
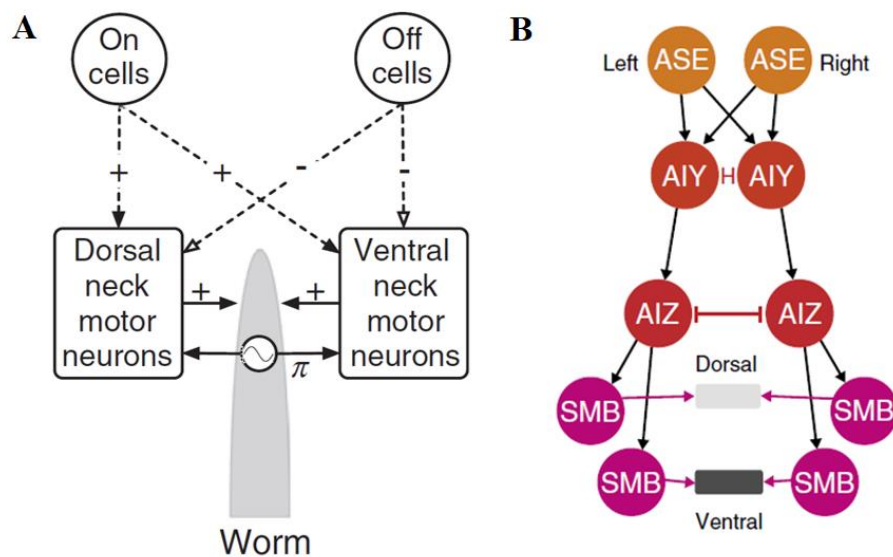
Figure 1.8 Examples of klinotaxis models. A) A simplified klinotaxis (steering) network model. (Lockery, Shawn R., 2011). Sensory on and off cells, excite and inhibit the neck muscle motor neurons via polysynaptic pathways. The sine wave symbol represents a putative pattern generator. B) A proposed neural circuit schematic for klinotaxis (steering). (Izquierdo *et al.,* 2015; Izquierdo and Beer, 2016). ASE left and right are the on and off cells from the klinotaxis model in Image (A). AIY and AIZ are the interneurons integrating sensory information from the on/off cells to the motor neurons SMB. SMB excite dorsal and ventral muscles.

1.2.3 Is there a circuit distinction between the two strategies of orientation?

The two strategies share neurons in their regulation and have been observed in the same sensory modalities [i.e in chemotaxis (mediated by ASE sensory neurons)(Iino and Yoshida, 2009), odor taxis (mediated by AWC sensory neurons)(Yoshida *et al.,* 2012) and thermotaxis (mediated by AFD sensory neurons)(Hedgecock, E. M. and Russell, 1975; Ryu and Samuel, 2002; Luo *et al.,* 2006)]. In addition, graphical analysis of them showed that they are driven by the same function of concentration change over time (Pierce-Shimomura *et al.,* 1999; Iino and Yoshida, 2009; Izquierdo and Lockery, 2010; Lockery, Shawn R., 2011). As Lockery stated in his review in 2011 discussing computational models of these two strategies, both strategies seem to be working 'in concert in the real worms' (Lockery, Shawn R., 2011).

Some studies have exclusively focused on one of the two strategies and consider them as distinctive behaviours, most probably governed by distinct neural circuits (Pierce-Shimomura *et al.,* 1999; Pierce-Shimomura *et al.,* 2005). Some studies, such as Iino and Yoshida's, have considered them parallel behaviours mediated by a parallel circuit, overlapping at least in the first interneuron layer (Figure 1.8 B)(Iino and Yoshida, 2009; Yoshida *et al.,* 2012). For the sake of quantifying and comparing these strategies amongst my transgenic and wild type worms, I will consider them distinct to begin with. However, I am in agreement with the argument that they are part of a parallel circuit, with some differences at the sensory input layer, but overall with a great overlap, especially at the layer of the head neurons my investigation focuses on (2nd interneuron layer and head motor neurons). This will be discussed further in the General Discussion (Chapter 8), when I propose a candidate neural circuit for orientation.

1.2.4 How does the worm steer? Izquierdo and Beer model: Integrating forward locomotion with steering

The steering mechanism must involve the ability of the worm to rhythmically modulate the side-to-side head swings, and the turning of these head swings should be biased towards the source of the cue the worm is sensing. For example, if the worm is following an attractant to its left side then the head swings will be gradually biased to the left, thus resulting in the worm orienting itself towards the attractant. It means that, on average, the head swings to the left must be deeper than the ones to the right side, and on average the head muscles to the left will be more contracted and the muscles to the right side of the head more relaxed. Steering therefore requires a means whereby the dorso/ventral symmetry of the undulations are 'broken' within fast timescales, continuously and gradually. How this is achieved is still not

fully understood. Computational models have been increasingly helpful in giving insights into how a system might work, and giving the experimental biologists potential targets to investigate. For this reason, I would like to give a special mention to the integrated biomechanical model that partly aided my hypothesis(Izquierdo and Beer, 2013).

A model of symmetry breaking was first proposed by Izquierdo and Lockery (2010) and was revised and upgraded with the neuronal circuitry from Beer and Izquierdo in 2013, with their latest model integrating body movement from Boyle's model as well (Izquierdo and Lockery, 2010; Boyle *et al.,* 2012; Izquierdo and Beer, 2016; Izquierdo and Beer, 2013)(Figure 1.9). In their model they used the shortest and strongest connections between neurons, and through stochastic optimisation they inserted the variables of parameters they had no experimental data on. The model, in addition to assuming an oscillator working with the SMB head motor neurons, predicted that the worm's direction changes as a function of the phase the undulation is in when the stimuli is/are being sensed. This was supported by experimental work using optogenetic phasic activation on ASER neurons and observing the changes in head curving that resulted (Satoh *et al.,* 2014). For example, when light was shone on the ASER and the worm was bending ventrally it resulted on significantly different curving than when the worm was bending dorsally.

As the experimental data on the neurons increase, the predictions of the computational models will become be more accurate, and the representation of the worm's movement more life-like. This is where experimental biologists, like myself, can aid with the biological and behavioural data computational neuroscientists can use to improve their models.
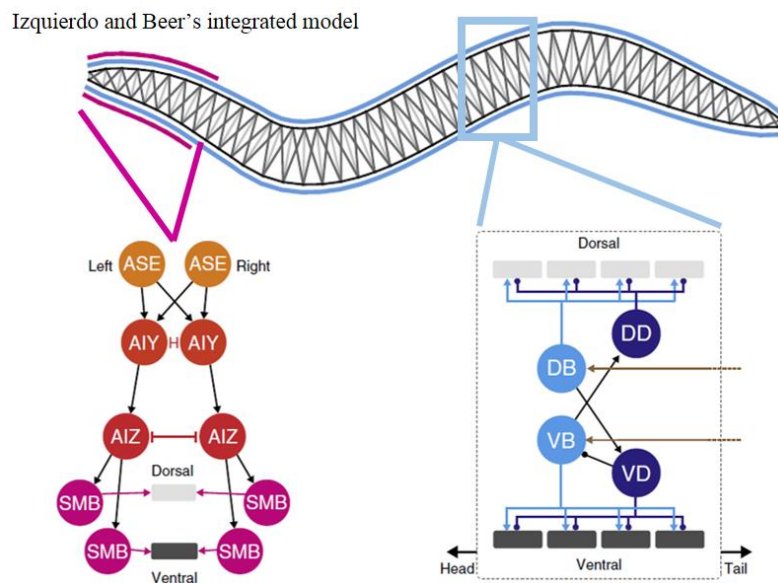
Figure 1.9 A proposed integrated model for steering. Model includes a head movement circuit integrated with a body movement model updated from Boyle's model (Boyle *et al.,* 2012). Edited from (Izquierdo and Beer, 2016).

1.2.5 Neural focus of the project: SAA and SMB neurons

1.2.5.1 Inspiration

At the same time as the first Izquierdo and Beer (2013) model was published, my colleague Tom Sanders was exploring neuro-computational motifs capable of steering for his PhD (Sanders, 2016). His computational model of steering showed that reciprocal inhibitory connectivity could function as a bistable component and facilitate gradual turning in the worm (steering). In this model, hidden interneurons drove a motor neuron in antiphase via the motor neuron's self-reciprocal inhibition (Figure 1.10). This connectivity resulted in an oscillator generating undulations and smooth steering in response to sensory input. The sensory neurons in the model were set to excite both interneurons equally, similar to the Lockery model (2010). However, because the small oscillations ensured that one of the two interneurons was hyperpolarized in half of their duty cycle, during these times any sensory input produces a stronger excitation in the hyperpolarized than in the depolarized interneuron. This difference is further amplified by the mutual inhibition. The interneuron cells each excite one of the two motor neuron cells downstream, producing a bias in the undulations and thus steering the worm. However, in contrast to the Beer and Izquierdo model, the worm is represented as a dot, head movement or body is not incorporated and the pair of neurons work as one component.
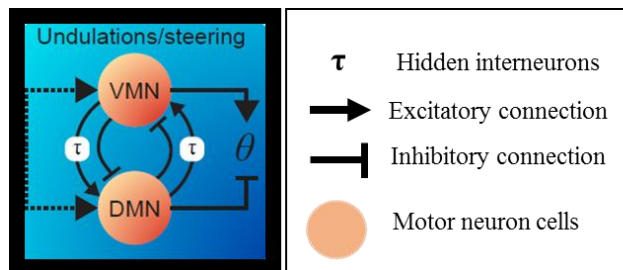
Figure 1.10 Tom Sander's model component suggesting that a reciprocal inhibition motif could facilitate generating undulation and steering. Image edited from Sanders (2016) (Sanders, 2016).

The synaptic connectivities between RME, SMB and SAA seemed to him to be of potential interest for a motif of reciprocal inhibition, albeit their actual connections were not reflected by the model's component. I chose to focus entirely on the SAA and SMB neurons as with my lab experience I knew generating the transgenic strains would take time, the SMB neurons function was then largely unknown but many models included them as the head motor neuron implicated in steering, and the SAA interneurons had not been investigated at all.

Similar computational models, but that incorporate head movement, have implicated SAA and SMB in the head turning circuit, either due to the fact that their synaptic connectivity to each other allows for a potential reciprocal motif or because they are hypothesized to have a stretch receptor neuron function (Sakata and Shingai, 2004; Karbowski *et al.,* 2008). A few models have incorporated SMB only, without mentioning SAA (Iino and Yoshida, 2009; Yoshida *et al.,* 2012; Izquierdo and Beer, 2013; Izquierdo and Beer, 2016). However, none of these models have used experimental data for the neurons of interest to inform their construction.

1.2.5.2 SMB head motor neuron

Considering the sum of all experimental studies and computational models mentioned previously, it is strongly suggested that the regulation of head movements are the important component in orientation of the worm. It makes sense then to focus on the head neurons, when exploring the orientation strategies of the worm. SMB is a very good candidate for the motor neuron of the circuit. SMB is a set of four motor neuron cells, they innervate muscles in the head via neuromuscular junctions and send processes posteriorly down the sub-lateral cords (White, J.G. *et al.,* 1986). In addition, it is one of the two head motor neurons that innervate all anterior muscle rows in the head, the other being the SMDs, and therefore may potentially control head movement from the height of the 'neck' to the 'nose' of the head (White, J.G. *et al.,* 1986; Gray, J.M. *et al.,* 2005) (Figure 1.3). This view is supported by the fact that killing the SMB head motor neurons with laser ablations resulted in high-amplitude sinusoidal movement (Gray, J.M. *et al.,* 2005). This behavior, termed 'loopy' by the authors, hints that SMB is capable of modulating the amplitude of the undulations. However, Gray *et al.* proceeded no further in examining the phenotype. The most recent experimental data for SMB comes from Kocabas et al's study: By asymmetrical optogenetic activation of the SMB neurons they observed head bending of the worm on the direction of the side of the neurons that were activated (Kocabas *et al.,* 2012).

Modulating the amplitude of the head swing during forward locomotion suggests a potential role for the neural circuits underlying the formation of undulations in the control of gradual turning. Lebois et al study, where they observed adaptation of locomotion by applying mechanosensory pressure to the worm, revealed that the control of maximum curvature is a key ingredient of the locomotion regulation (Lebois *et al.,* 2012). SMB motor neuron cells have unusual connections with each other. The ventral SMB cells, which have neuromuscular junctions with the ventral head muscle cells, are completely separate with the dorsal SMB cells, which in turn are connected with the dorsal head muscle cells (Figure 1.11). Hence, SMB motor neurons could potentially require a 'coordinator' for dorso/ventral regulation. The coordinator is not absolutely required, but it would make the circuit more robust as it

would prevent all SMB cells from being activated simultaneously. Simultaneous activation of both ventral and dorsal sides would only result in the worm's head shrinking. This putative coordinator has a prerequisite; connections that would allow a breaking in the symmetry of the undulatory movement, and dense synaptic connectivity towards SMB since better connected cells are more likely to have stronger and faster interactions. SAA is a likely candidate (Figure 1.12).
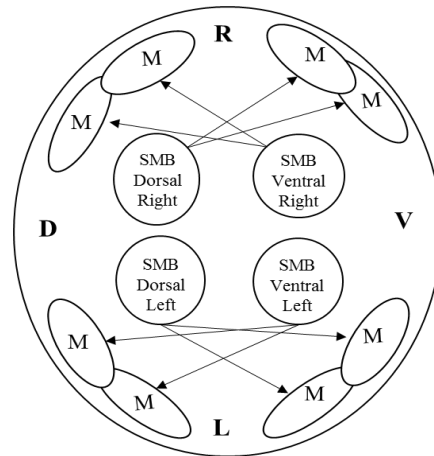
Figure 1.11 A simplified cross section drawing indicating the connections of the SMB motor neurons to the body wall muscles. The nature of the connections, inhibitory or excitatory, are unknown.
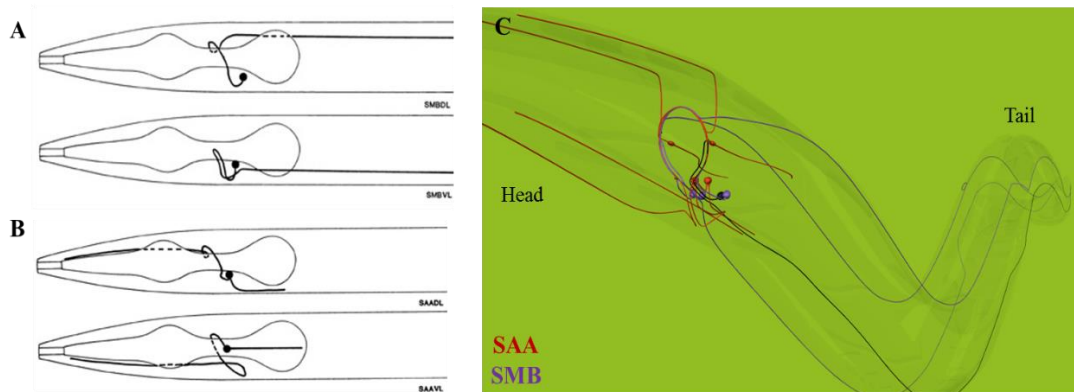
Figure 1.12 Localisation of the SAA and SMB neurons. A) SMBDL (top) and SMBVL (bottom) drawings indicating localisation of the somas and the processes (only the left side cells are shown) (White, J.G. *et al.,* 1986). B) SAADL (top) and SAAVL (bottom) drawings indicating localisation of the somas and the processes (only the left side cells are shown) (White, J.G. *et al.,* 1986). C) A 3D reconstruction of all the cells of SAA and SMB class of neurons using the OpenWorm project's visualisation browser (www.openworm.org).

1.2.5.3 SAA interneuron

There is no experimental evidence so far implicating SAA in steering or the control of undulations. Due to its gene expression pattern (no unique genes being expressed in the SAA neurons) and its extremely close proximity to adjacent neural cells (i.e. SMD), it has been difficult to either laser ablate the cell or manipulate it genetically. This fact makes this class of interneurons all the more interesting and worthwhile to focus on. The SAA class of neurons includes a set of four interneuron cells that send processes anteriorly up the sub-lateral cords in the head (White, J.G. *et al.,* 1986). There are numerous gap junctions between SAA and SMB, which makes it a good candidate for a co-ordinator, as it can facilitate fast responses via these electrical synapses (Table 1.1 and Figure 1.13). The synaptic connections in Table 1.1 are updated with data from recent worm wiring computational work done on the connectome (Jarrell *et al.,* 2012; Xu *et al.,* 2013). Other than the wiring circuit, which gives us the chemical synapses and gap junctions between the cells, plus knowledge of their anatomy and localization, there are no other experimental data for the SAA neurons. Interestingly, anatomy alone can give insights into function, and White and colleagues hypothesised the presence of stretch receptors in SAA decades ago due to their long undifferentiated processes (White, J.G. *et al.,* 1986; O'Hagan and Chalfie, 2005). The existence of them in SAA is still unknown. Although the SAA neurons have been included in two computational networks modelling the movement of the head, they have not been specifically modelled themselves (Sakata and Shingai, 2004; Karbowski *et al.,* 2008).

Table 1.1 Table showing the synaptic connectivity of SAA and SMB neurons. In grey colour the weak synapses that were not included in the schematic connectivity in Figure 1.13. These synapses were weak even when the left and right cells' connections were merged to show only dorsoventral symmetry between the neurons.

source	target	weight	type	source	target	weight	type
SAADR	SMBDR	2	chemical	SAADL	SMBDL	3	electrical
SAADR	SMBVR	1	chemical	SAAVL	SMBDR	2	electrical
SAAVL	SAADR	5	chemical	SAAVL	SMBVR	17	electrical
SAAVL	SMBDR	2	chemical	SAAVR	SMBDL	1	electrical
SAAVR	SAAVR	1	chemical	SAAVR	SMBVL	16	electrical
SAAVR	SMBDL	1	chemical	SAAVL	SAAVR	1	electrical
SMBDL	SAAVR	9	chemical	SMBDR	SMBVR	2	electrical
SMBDL	SMBVL	2	chemical				
SMBDR	SAAVL	8	chemical				
SMBDR	SMBDL	3	chemical				
SMBVL	SAADL	16	chemical				
SMBVL	SMBDL	2	chemical				
SMBVR	SAADR	12	chemical				
SMBVR	SMBDR	2	chemical				

1.2.6 The SAA and SMB oscillator hypothesis

Neural patterns showing reciprocal connectivity are of interest because they can function as oscillators (Marder and Bucher, 2001), and under the right conditions they can facilitate the break in the symmetry required for the worm to steer as previously discussed. The synaptic connectivity pattern of the SMB and SAA neurons that I generated, after filtering out weak synapses to keep just the ones with a weight of 3 and above, shows a lot of potential to fit this hypothesis (Figure 1.12). Connection information in Left and Right neurons was merged and the schematic shown in Figure 1.13 has a dorso-ventral perspective, reflecting the worms movement on the agar plates they are kept in and assayed in the lab. It is unknown whether the chemical synapses from SMB to SAA are inhibitory or not, but in order for the putative oscillator to work, I predict they are. Moreover, there are numerous gap junctions from SAA to SMB that can facilitate fast responses and render the SAAD SMBD cells as one component and SAAV and SMBV as another, having them work in unison but with a delay.
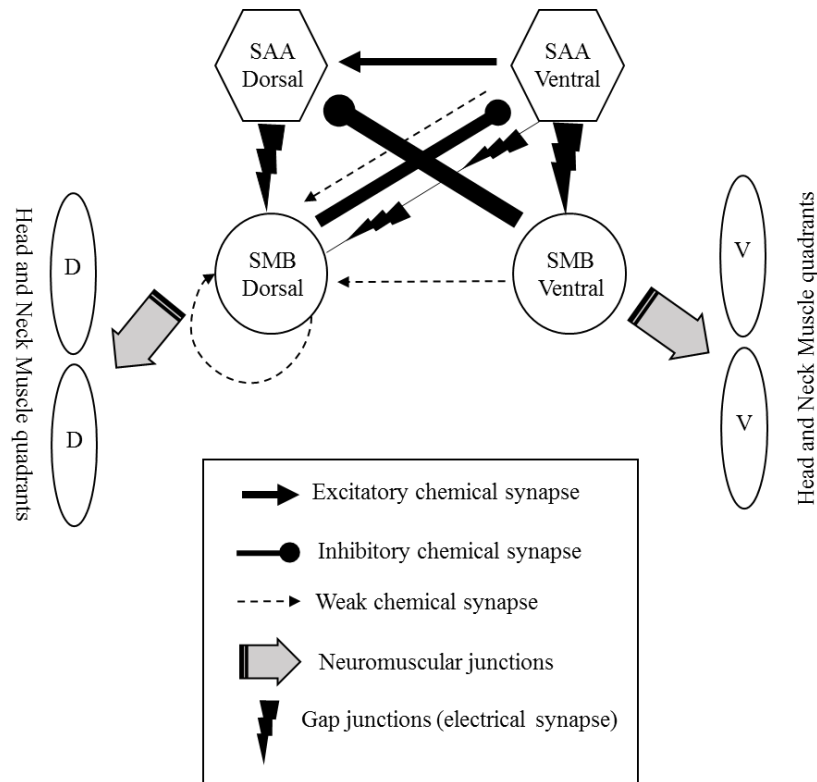
Figure 1.13 SAA and SMB connectivity diagram drawn to illustrate the potential for an oscillator mediating a rhythmic pattern. The schematic is drawn with a dorso-ventral perspective. Each body wall muscle bundle represents two bundles. Solid lines represent strong synapses, while dotted lines represent weaker synapses. The thickness of the solid lines are proportional to the strength of the synapses. For example the synaptic weight of SMBV to SAAD is 28, whereas the synapse from SMBV to SAAV is 17. Connections assembled by computational work (Jarrell *et al.,* 2012; Xu *et al.,* 2013) done on the EMs generated by White and colleagues (White, J.G. *et al.,* 1986).

Thus, if one of two neurons is 'on' (depolarized) the other is 'on' as well. Because of the inhibitory connection to the other side, the other two are then 'off' (hyperpolarized). If the 'on' original pair starts to fall to an 'off' hyperpolarised state, the other two become less inhibited and depolarize. In the end we have a pair going on, off, on, off, and the other pair going off, on, off, on etc. But how it would generate the rhythm in the first place? There are some possibilities. There could be an intrinsic oscillator in either of the cells. Recent research has showed that to be a possibility, especially in motor neurons, since within that study the excitatory A-class motor neurons exhibited intrinsic and oscillatory activity sufficient enough to drive backward locomotion (Gao *et al.,* 2018). The other possibility would be to have a proprioceptive signal kick-start the oscillator and keep it at check. The asymmetry in synaptic connectivity of the Ventral side of the oscillator to the Dorsal side might hint towards that way of resetting the pair. With a biased over-flex on the one side stretch receptors would activate the motor neuron on the other side. If the pair cannot maintain an intrinsic oscillator/rhythmic pattern, or do not have a proprioceptive function then perhaps they are kick-started by an unknown external oscillator. This oscillator would preferably show a pattern of self-sustainable rhythm and would be highly synaptically connected to them. The SMD motor neuron, with its dorsoventral intrinsic dense connections, and its dense connections with SAA, seem a probable target (Figure 1.14). Therefore, its known function will be closely discussed along with the results of experiments on my neurons of interest in most result chapters.

On a side note, it's important to briefly mention the connectivity of SAA with RIM and SAA with AIB [two interneurons controlling backward locomotion; Piggott *et al.,* 2011 (Piggott *et al.,* 2011)], and also the dense connections of the interneurons AIZ and RME to SMB. AIZ has also been implicated in steering (Iino and Yoshida, 2009; Kocabas *et al.,* 2012) and the RME head motor neuron has been shown to regulate the foraging movement of the tip of the head (Gray, J.M. *et al.,* 2005; Shen *et al.,* 2016).
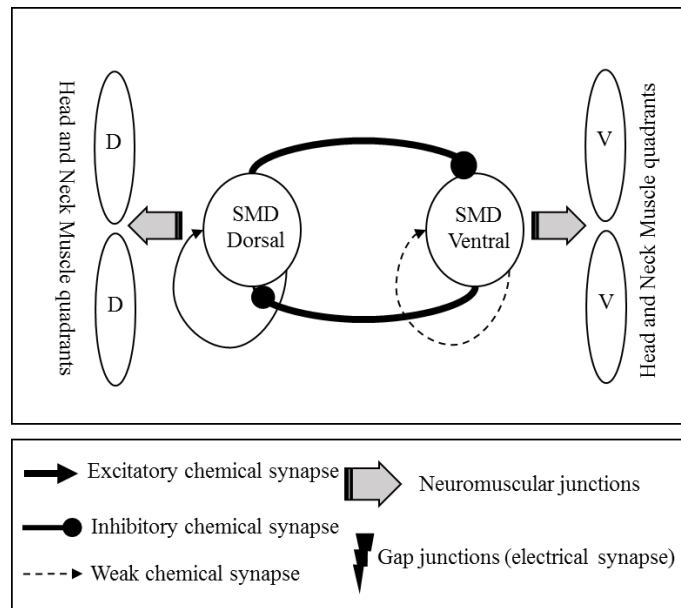
Figure 1.14 SMD self-connectivity diagram drawn to illustrate the potential for an intrinsic oscillator. The schematic is drawn with a dorso-ventral perspective. Each body wall muscle bundle represents two bundles. Solid lines represent strong synapses, while dotted lines represent weaker synapses. The thickness of the solid lines are proportional to the strength of the synapses. Connections assembled by computational work (Jarrell *et al.,* 2012; Xu *et al.,* 2013) done on the EMs generated by White and colleagues (White, J.G. *et al.,* 1986).

1.2.6.1 Predictions and questions I will try to answer

The minimal experimental evidence that exists has implicated SMB in the modulation of the amplitude of head swings and in steering. I hypothesize that SAA neurons are also involved in the mechanism of steering, and are within the same neuronal circuit for steering as the SMB motor neurons. I hypothesize that they indirectly control steering in the area of the head by modulating the amplitude of the head swings via regulating SMB. The modulation is likely mediated via their dense dorsoventral synaptic connectivity with the SMB motor neurons.

In order to test this hypothesis, I will attempt to carry out a series of genetic ablations, specifically SAA ablations, SMB ablations and SAA/SMB double ablations, including dorsal and/or ventrally restricted ablations. I will then test the effect of these ablations on the worms' performance in behavioural steering assays.

If my hypothesis is correct, and SAA is involved in the modulation of undulations alongside SMB, then without the reciprocal indirect inhibition to each of the SAA neuron, and the feedback information from the SAA, the SMB won't be able to coordinate themselves with regards to their alternate relaxation/contraction of the muscles that they innervate in the head

and neck. Therefore, I predict that SAA single ablation will result in a similar phenotype to that observed when the SMB neurons were laser ablated by Gray *et al.,* (2005); in a high-amplitude sinusoidal movement (i.e. the head bending angle will be higher than wild type measurements). As a side note, SAA- ablated worms may also exhibit a defect during backward locomotion due to the synaptic connection SAA has with AIB and RIM, as explained earlier in this section. For this reason, I also expect a defect in the frequency of pirouettes when the SAA neurons are ablated.

SMB single ablation should result in a similar 'loopy' sinusoidal movement to that observed by Gray *et al* following their laser ablations of SMB; the head bending angle will be higher than the wild type measurements.

What effect will the undulatory defects following SAA or SMB ablation have in the radial chemotaxis assays? By eliminating either part of the putative oscillator will the worm's efficiency in steering be decreased? Will the results for each neuron be similar, or hint at different functions within the oscillator motif? Is the asymmetry in connectivity from the Ventral to Dorsal side of the oscillator mirrored in some way in the undulations of SMB abated worms?

The double ablation of SAA and SMB should also produce informative results. What will happen when the putative oscillator is gone entirely? Will the undulatory movement be completely defective, meaning that SAA and SMB generate the undulations? Will the results hint at another external oscillator (i.e. SMD)? Will the worm be able to steer at all? Indeed, if SAA and SMB generate or regulate undulations the double ablated worms shouldn't be able to follow up a gradient.

Finally, Asymmetrical Dorsal and/or Ventral ablation also have the potential to give interesting results. For example, with the SMBD and SAAD gone, the SAAV and SMBV will be either always contracting the ventral muscles (Ventrally biased sinusoidal movement) and/or the dorsal muscles will be permanently relaxed. In this case, I should observe a ventrally biased sinusoidal movement over the course of many undulations, as Gray *et al.,* (2005) observed the opposite by laser ablating the ventral half of various head motor neurons (SMD, RMD and SMB), but did not assay further (Gray, J.M. *et al.,* 2005). Will ventral asymmetrical ablations show different results to the dorsal half ablations? Will the mutants take a longer time to reach the peak of the gradient?

The actual results will not likely be so absolute as the predictions here, because there is likely to be redundancy in the circuitry of the worm, and other head motor neurons might also generate, maintain and/or regulate undulatory movement and mediate steering.

If my hypothesis proves incorrect, the SAA ablation will produce a distinct phenotype that I have not considered, irrelevant to steering. SMB ablation however should still give a similar phenotype to the one observed by Gray *et al.,* 2005.

In addition, I will try to observe the effect the neurons of interest have in the muscles in the area of the head. This will not only show SMB's nature of connection to the muscle but it might also infer some relationship between SAA's overall connections to the SMB. If they are inhibitory in contrast to what I have hypothesized here I should see an opposite effect on the muscle with each individual ablation.

Finally, I will try to assess the overall nature of the connectivity between the cells of interest, and investigate if there is a proprioceptive function in either of the neurons, and what that might mean for the steering efficiency of the worm.

1.3 Thesis outline

In this thesis, I investigate the role of the SAA and SMB neurons in the locomotion of *C.elegans* with the use of a combination of fine-tuned genetic and molecular approaches to experimentally answer functional questions about the neurons. In particular, I focus on the potential role they have in the orientation strategies observed in the worm, by conducting different types of chemotaxis assays. I also try to provide for the first time some evidence of proprioceptive function in the SAA or the SMB, or both.

In Chapter 2, I discuss the method I used to genetically and specifically target the neurons of interest, and highlight its advantages. For the SAA interneurons, it is the first time that they have been individually targeted.

In chapter 3, using single-worm and multi-worm video tracking and manual locomotion/ behavioural analysis, I describe the phenotypes resulting from the successful ablation of the neurons of interest.

In chapter 4, I consider the effect these neurons have on the BWMs and try to infer their activity during locomotion via calcium imaging.

In chapters 5 and 6, I conduct chemotaxis assays of fully ablated and half ablated neurons that highlight SAA and SMB's role in steering, but also inform us on their role in the pirouette strategy and their subtle differences in function. It is also the first time, to my knowledge, that strains were generated with half of their neurons genetically ablated in *C.elegans* (dorsal cells).

In chapter 7, following hints of proprioception within the neurons of interest from chapters 3 and 6, I further investigate this via the observation of the expression of known stretch receptors.

Finally, in chapter 8, I discuss the sum of all the major findings, and try to infer the underlying function of the SAA and SMB neurons in locomotion, in the regulation of the undulatory movement of the worm, in the context of either or both of the orientation strategies. Moreover, I discuss how they might regulate head movement as part of an oscillator, whether they may be stretch receptor neurons and also refer to additional neural targets. Taking into consideration my results and the extensive literature on the worm's navigational circuits, I propose my own neural network integrating both strategies of orientation. This chapter, and the thesis as a whole, ends with a section where I identify important future experiments, and discuss the prospects for our understanding of locomotion and steering.

Chapter 2
Targeted ablation of the SAA and SMB neurons: A genetic approach

2.1 Introduction

2.1.1 Aim of this chapter

The aim of this chapter was to generate transgenic strains with SAA neurons or SMB neurons independently ablated. Once the genetic approach was pinned down, I had to clone the constructs required to specifically target SAA and SMB neurons, and generate the transgenic strains via means of microinjection. Imaging of the transgenic strains' progeny confirmed SAA and SMB's localisation and successful ablation.

2.1.2 The advantages of targeting SAA and SMB using genetic ablation

A common goal of neuroscientists is to understand the function of individual neural cells with respect to the behaviours they help to control in living organisms. One of the most powerful methods to study cell function is targeted cell killing. If my hypothesis for the role of neurons SAA and SMB in the worm's undulations and control of head movement (explained in Chapter 1) is right, then the targeting and killing of one or both of these neurons should result in a behavioural defect while the worm steers towards an attractant, or lead to an abnormal undulatory phenotype, or both. An unexpected locomotion defect might also be observed, since the function of these neurons is largely uncharacterized.

Laser ablation is a classic and commonly used approach to study the role of specific cells in *C. elegans*, as well as many other model organisms (Sulston and White, 1980; Shah and Jay, 1993; Bernhardt *et al.,* 1992; Bargmann, C. I. *et al.,* 1993). However, the laser ablation of cells requires precision. The location of SAA and SMB in the nerve ring makes it difficult to accurately ablate these cells without affecting adjacent neurons, or damaging nearby muscle cells. Moreover, laser ablation of some cells in late larval stages does not always result in complete removal of the neuron's function (Avery and Horvitz, 1987). In addition, I would like to take my functional analysis one step further by conducting asymmetric ablation of these neurons (i.e. ablating either the dorsal or ventral neural cells; see Chapter 1 & 6), and this is even more difficult via the laser ablation technique due to the proximity of the dorsal and ventral cells. Finally, with laser ablations you can create and handle only a small number of worms for use in behavioural assays.

Another way of conducting cell ablation is via cell-specific expression of a toxin gene such as the diphtheria toxin A-chain gene, an approach that has previously been used successfully in mice (Breitman *et al.,* 1987). However, diphtheria brings some obvious health and safety implications, and there is also the risk that it won't work in *C. elegans,* since it has previously been tried only in mammalian cells. Other cytotoxic molecules that have been used in the past in *C. elegans* research are the degenerins. Degenerins kill neural cells via the pathway of neurodegeneration (Hong and Driscoll, 1994). However, cell-specific targeting using this approach requires expression of these toxic molecules under the control of a cell-specific promoter, which are in fact rare; not all cells have unique genes being expressed.

Recently, a photo-inducible cell ablation approach in *C. elegans* was established using the genetically encoded singlet oxygen generating protein miniSOG (Qi *et al.,* 2012). miniSOG is a 106 amino acid protein, obtained from *Arabidopsis thaliana*, that expresses reactive oxygen species upon exposure to blue-light. Targeted cells are killed by over-oxidation. Qi *et al.* expressed it in the mitochondria in neurons of *C. elegans* and observed a rapid and effective cell death within 30 minutes of light exposure. Although this system provides a means of cell killing that is easier, better controlled as it is light inducible and more precise than laser ablation, miniSOG would still need to be expressed under a cell-specific promoter, and cell specific promotors have not yet been identified for the SAA and SMB neurons.

2.1.2.1 Targeted cell killing using a two-component ablation system

Since there is not a single cell-specific promoter for either the SAA or SMB neurons, it became clear to me that I needed to find an alternative genetic approach. Fortunately, I then discovered elegant work conducted by Chelur and Chalfie, back in 2007, in which they overcame the cell-specific promoter 'requirement' by developing a two-component system for selective or conditional ablation of targeted cells (Chelur and Chalfie, 2007). This is a combinatorial method where co-expression, but not individual expression, of two caspase subunits kills the targeted cells. Caspases are a family of enzymes essential for programmed cell death that are found across the animal kingdom. The nematode caspase is encoded by the *ced-3* gene (Ellis and Horvitz, 1986). Chellur and Chalfie generated transgenes containing non-overlapping fragments of the *ced-3* gene that encoded small (p15) and large (p17) subunits of the CED-3 protein. In each transgene the sequence encoding the CED-3 subunit was linked to sequence encoding an N-terminal or C-terminal leucine-zipper domain (Figure 2.1, Image A). The fusion proteins encoded by these two transgenes can interact via their shared leucine-zipper domains such that the p15 and p17 subunits come into close proximity and reconstitute a functional CED-3 protein. This reconstituted caspase is then competent to trigger programmed cell death. However, this will obviously only happen in cells where the expression of both subunits overlaps. Chelur and Chalfie (2007) showed that expression of

the subunits on their own did not cause cell death. Integrated lines, however, containing interacting versions of both subunits showed apoptotic death of nearly 100% of the cells in which they were co-expressed. Moreover, over-expression of the caspase subunits did not lead to non-specific cell killing.

I designed this project using exclusively the genetic cell ablation technique described above. The expression of each caspase subunit will be driven under the control of one of two promoter regions cloned from genes that are expressed in the targeted cells, as well as others cells. However, pairs of promotors will be carefully selected such that they only exhibit co-expression in the SAA or the SMB neurons. Therefore, a function caspase will only be reconstituted in the neurons of interest, resulting in cell-specific ablation.
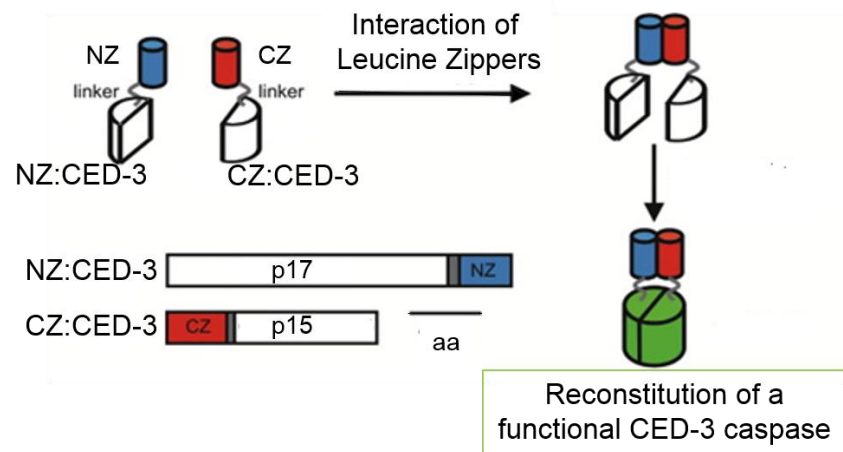
Figure 2.1 A schematic representation of the reconstituted CED-3 caspase components. Same pattern applies for the reconstituted GFP caspase subunits. Leucine-zipper domains (blue and red) are shown connected to the linker domains (grey) which are in turn connected to partial subunits of the CED-3 caspase. Interaction between these two leucine zipper domains will lead to the activation of the caspase subunits (reconstitution). The caspase then becomes functional. Image edited from Zhang *et al.,* (2004) (Zhang *et al.,* 2004), on the description of the technique established by Ghosh *et al.,* (2000) (Ghosh *et al.,* 2000).

2.1.2.2 GFP reporter strains using the same two-component system

It was essential not only to be able to confirm the genetic ablation of the targeted neurons, but also to ensure that the two-component system worked accurately under the promoter regions used in this project; i.e. that there was not unexpected leaky expression from a promoter, or promoters, resulting in off-target cell ablations. Therefore, it was important to confirm that

the selected promoter regions drove expression only in the locations originally described in the literature. Thus, additional strains needed to be generated expressing a reporter protein fused to the promoter regions of the genes selected to genetically ablate the SAA and SMB neurons. The green fluorescent protein, since its introduction as a biological marker years ago, has been an important and reliable reporter protein and was therefore used throughout this project (Chalfie *et al.,* 1994). As an additional control, the selected promoter regions were also cloned into the same two-component system described above, however, this time driving expression of two subunits of the GFP that only fluoresced when reconstituted, following the same principle of reconstituted CED-3 (Zhang *et al.,* 2004; Ghosh *et al.,* 2000) (see Figure 2.1, Image B).

2.2 Material and methods

2.2.1 Nematode maintenance

Animals were kept at 20°C at all times, fed *E.coli* (OP50 strain) and were maintained as previously described (Brenner, 1974). *C. elegans* variety N2 Bristol strain was provided by the Caenorhabditis Genetics Centre (CGC), which is funded by NIH Office of Research Infrastructure Programs (P40 OD010440).

2.2.2 Cloning of the GFP reporter and CED-3 ablation constructs

2.2.2.1 CED-3 caspase, reconstituted GFP and GFP plasmids

CED-3 plasmids carrying the CED-3 large subunit (p17) and the CED-3 small subunit (p15) were a gift from Martin Chalfie (Addgene plasmid # 16081 [TU#807] and Addgene plasmid # 16080 [TU#806], respectively). They originally carried the *mec-18p* promoter region, which had to be excised (see Figure 2.2).

Reconstituted GFP plasmids rec-GFP (707) and rec-GFP (708) were also a gift from Martin Chalfie (Addgene plasmid # 15276 [TU#707] and Addgene plasmid # 15277 [TU#708], respectively). Although the rec-GFP plasmids share a similar structure with the CED-3 plasmids, they did not carry any promoter region to begin with. In addition, in the place of the CED-3 caspase they each carry a part of the GFP.

pPD95_75 GFP plasmid was a gift from Andrew Fire (Addgene plasmid # 1494). All plasmids share the pPD95_75 backbone manufactured by Andrew Fire.
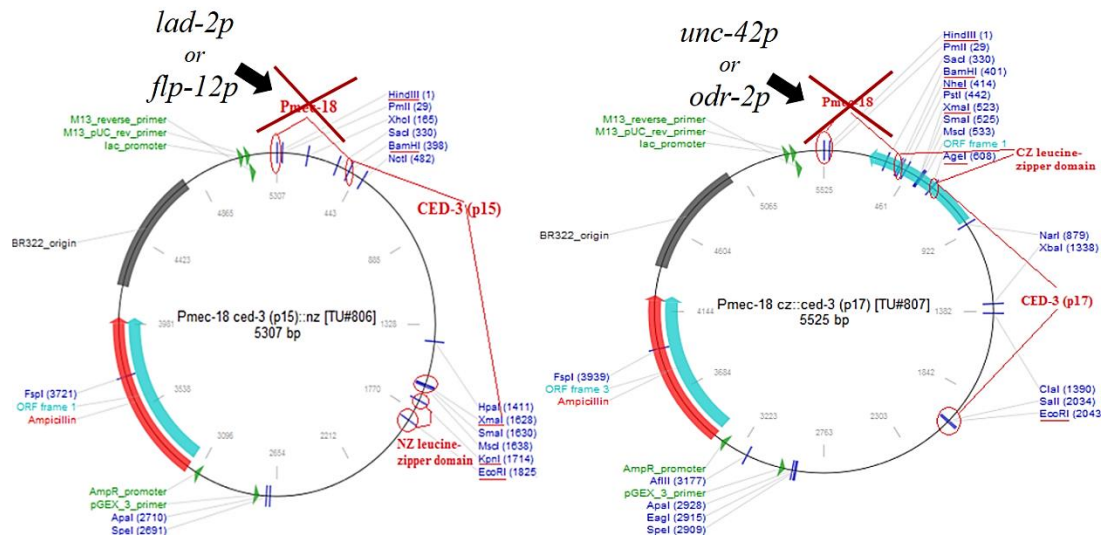
Figure 2.2 Annotated CED-3 caspase plasmid DNA maps. (Left) The CED-3 small subunit (p15) plasmid. Underlined with red colour are the restriction enzymes cutting the touch neurons promoter *mec-18p* (HindIII and BamHI), the CED-3 protein encoding the sequence of the small subunit (p15) (BamHI and XmaI) and the NZ leucine zipper domain (KpnI and EcoRI). (Right) The CED-3 large subunit (p17) plasmid. Underlined with red colour are the restriction enzymes cutting the touch neurons promoter *mec-18p* (HindIII and BamHI), the CED-3 protein encoding the sequence of the large subunit (p17) (AgeI and EcoRI) and the CZ leucine zipper domain (NheI or BamHI and AgeI). *mec-18p* promoter regions were excised (red crosses) and the constructs were re-ligated with the promoter regions targeting the neural cells of interest (SAA and SMB neurons)(thick black arrows). Original plasmid DNA maps provided by Addgene (www.addgene.org).

2.2.2.2 Molecular biology

After thorough research amongst all genes expressed in the SAA and SMB neurons I identified the unique gene pairs whose promotors would only result in co-expression in either SAA or SMB, but not any other *C.elegans* cell (see results of search in Result section 2.3.1). To target the SAA neurons, *unc-42p* (2.8kb) and *lad-2p* (4kb) promoter regions were selected to be amplified by PCR (see appendix Table A.2) from the nematode's genomic fosmid library (Aurelio *et al.,* 2002; Brockie *et al.,* 2001). Those regions were then cloned in the CED-3, reconstituted GFP and GFP plasmids (see CED-3 example in Figure 2.2). For the GFP plasmids the selected promoter regions did not replace any existing sequences. To target the SMB neurons *flp-12sp* (350bp, sp = small promoter region), *flp-12lp* (2.6 kb, lp=large promoter region) and *odr-2p* (2.4kb) promoter regions were selected to be cloned in the

plasmids described above (see also Table 2.1) (Kim, K. and Li, 2004; Chou *et al.,* 2001) (and Kyuhyung Kim, personal communication).

Amplified regions were cloned into the ablation and reporter GFP and reconstituted GFP plasmids using sticky or blunt ends as shown in Table *A.1* of the appendix section. Diagnostic enzymatic digestions with BamHI, XhoI, SalI or HindIII followed each time to confirm the constructs identity.

ApE – A plasmid editor v2.0.47 software was used for the annotation of all genomic regions, predictions of enzymatic digestions and ligation results (Paradis *et al.,* 2004). Primer3 v0.4.0 software was used for primer design (Untergasser *et al.,* 2012; Koressaar and Remm, 2007). Oligocalc v3.27 software was used to check self-complementarity in primers and melting temperature (Tm) (Kibbe, 2007). The Ecl136II restriction enzyme was purchased from Thermoscientific. The rest of the restriction enzymes and ligase that were used were purchased from Promega and Invitrogen respectively. Primers were purchased from Sigma.

2.2.3 Generating and integrating transgenic animals

The parent wild type strain used for generating the transgenic strains was the *C. elegans* variety N2 Bristol strain (Brenner, 1974). Transgenic worms were generated by the means of microinjection (Mello *et al.,* 1991), whereby the constructs described above were microinjected into the distal gonad of a young adult worm alongside with a transformation marker (Hobert, 2002; Evans, 2006). The transformation marker used to select the transgenic GFP reporter lines was the pRF4 plasmid that induces a dominant "roller" phenotype (Kramer *et al.,* 1990), whereas for the ablation lines the *myo-2p*::mCherry plasmid was used that expresses the red fluorophore mCherry in the pharynx. pCFJ90 - *myo-2p*::mCherry::unc-54utr was a gift from Erik Jorgensen (Addgene plasmid # 19327).

The extrachromosomal arrays formed after microinjection and transmitted to the progeny of the injected worms, were integrated into the genome using the rapid protocol for integrating extrachromosomal arrays by Mariol (Mariol *et al.,* 2013).

2.2.4 Microscopy and imaging

To confirm ablation, transgenic worms were imaged for the expression of GFP, or the lack of it, in the neurons of interest, after being anaesthetised by the use of azide (5mM). A ZEISS stereo Lumar V12 was used to screen for transgenics. For imaging, a Leica M165 FC fluorescent stereoscope fitted with a Q-imaging Qi-CLICK COOLLED pE-300 camera and a ZEISS Axioplan fluorescent microscope fitted with a Q-imaging RETIGA 2000R camera,

were used. Images were captured with Q-Imaging's Q-capture Pro 7 software. Images were processed with the use of FIJI software (Schindelin *et al.,* 2012).

2.3 Results

2.3.1 Identification and selection of unique gene pairs expressed in the SAA and SMB neurons

Thus far, there is no evidence of a unique gene been expressed in the SAA neurons. However, there are four unique gene pairs that were found after a thorough search of the SAA's genetic expression pattern (Table C.1). These pairs are: *flp-12* and *pdf-1*, *flp-12* and *rig-6a*, *flp-7* and *syg-1*, *lad-2* and *unc-42*. SAA was targeted in this project using the promoters of the pair *lad-2* and *unc-42,* as these genes are expressed in a relatively small number of cells, making the subsequent confirmation of ablation easier.

The same process was followed for the SMB neurons (Table C.2). Initially, there was no unique gene known to be expressed in the SMB neurons, but my screen of gene expression patterns revealed two unique gene pairs. These pairs are: *flp-12* and *odr-2*, *unc-42* and *odr-2*. However, after personal communication with Kyuhyung Kim, I was informed that a small part of the *flp-12* promoter region of 350bp seems to drive expression solely in the SMB neurons. Although I had already cloned the whole *flp-12* promoter region and the *odr-2* promoter region to target the SMB neurons, only the strains generated with the small *flp12sp* promoter region were used in consequent experiments in this project, as the transmission rate of the injected plasmids in these strains was higher.

For the genetic manipulations to be accurate and successful I decided it was necessary to: (i) choose pairs that were expressed in the same life stage of the worm, (ii) to avoid promoter regions that were the same both for the SAA and SMB neurons as it could introduce unexpected implications in generating strains with both neurons ablated, and (iii) to avoid genes that were expressed in far too many neurons alongside the ones this project targets as it would make confirmation of neural ablation difficult.

2.3.2 Cloned constructs and transgenic strains generated

The promoter regions selected in the previous section were cloned in the ablation, reporter GFP and reconstituted GFP plasmids (see Table *A.1*). Twenty one plasmids were cloned in total. Co-injection of those plasmids with transformation markers in wild type worms generated eleven transgenic worm strains. Resultant plasmids and strains are shown in Table *2.5*. Strain names, expected ablated cells and expression of GFP are also included in the Table.

Table 2.1 Generated transgenic strains for the project.

	Plasmids injected	Marker	Ablated cell	Expected expression/localisation of GFP	Strain name
GFP strains	*unc-42p*::GFP	pRF4	none	SAA, AVA, AVD, AVE, ASH, RMD, SMB, AIN, AVH, AVJ, AVK, RIV, SIB, DD, PVT	UL4183
	lad-2p::GFP	pRF4	none	SAA, SMD, ALN, PLN, SDQ	UL4213
	flp-12lp::GFP	*myo-2p*::mCherry	none	SMB, AVJ, AVH, BAG, PDA, PVR, SAA, SDQ, BDU (?)	UL4237
	odr-2p::GFP	*myo-2p*::mCherry		SMB, RME, ALN, PLN, RIG	UL4238
	flp12sp::GFP	pRF4	none	SMB	UL4187
rec-GFP strains	*lad-2p*::rec-GFP(707), *lad-2p*::rec-GFP(708)	pRF4	none	SAA, SMD, ALN, PLN, SDQ	UL4184
	lad-2p::rec-GFP(707), *unc-42p*::rec-GFP(708)	pRF4	none	SAA	UL4214
	lad-2p::rec-GFP(708), *unc-42p*::rec-GFP(707)	pRF4	none	SAA	UL4216
Ablation Strains	*flp12sp*::CED-3 (p15), *flp12sp*::CED-3 (p17), *flp12sp*::GFP	*myo-2p*::mCherry	SMB	Absence of GFP expression in SMB	UL4230*
	lad-2p::CED-3 (p15), *unc-42p*::CED-3 (p17), *lad-2p*::GFP	*myo-2p*::mCherry	SAA	SMD, ALN, PLN, SDQ	UL4207*
Control strains	*flp12sp*::CED-3 (p15), *flp12sp*::GFP	*myo-2p*::mCherry	none	SMB	UL4224
	unc-42p::CED-3 (p17), *lad-2p*::GFP	*myo-2p*::mCherry	none	SAA, SMD, ALN, PLN, SDQ	UL4219

(?) = unclear

* = integrated

2.3.3 Neural localisation and confirmation of ablation by microscopy

2.3.3.1 GFP reporter strains confirmed the localisation of the SAA and SMB neurons

The GFP strain carrying the *lad-2p* promoter region (UL4213) drove expression of the GFP protein in five neurons (Figure 2.3, Images A, C and D) as expected and previously described (Aurelio *et al.,* 2002; Kim, J. *et al.,* 2015a). In the head and in the area of the nerve ring SAA and SMD neurons were visible (Figure 2.3, Images A and C). By focusing in on the head area all four cells of each of these neurons were identifiable (Figure 2.3 C). The two cells of SDQ were observed in the anterior and posterior body flanking the general area of the vulva (Figure

2.3, Image A). In the area of the tail four cells in close proximity to one another were observed (Figure 2.3, Image D). These were ALN and PLN, consisting of two cells each.
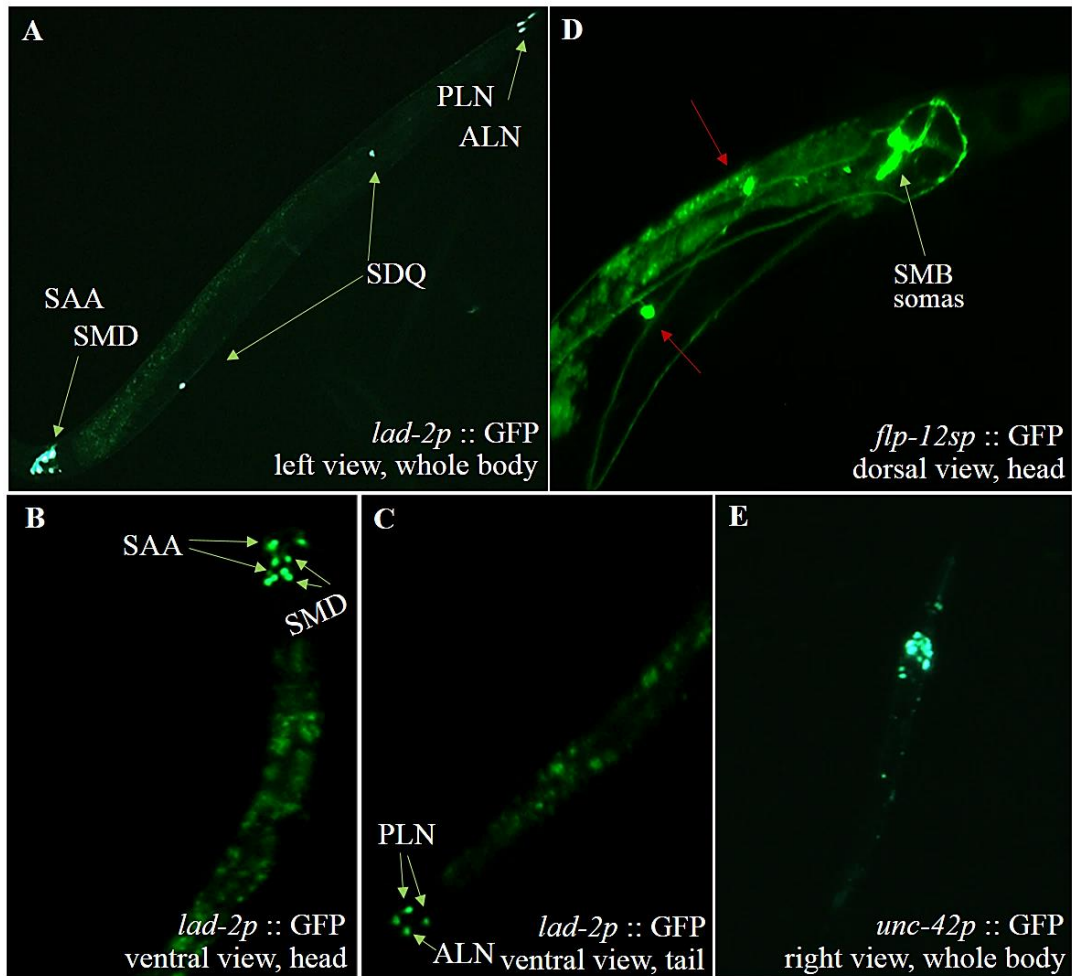
Figure 2.3 GFP reporter strains images. Worms expressing GFP driven by the *lad-2p* (Images A, B and C), *flp-12sp* (D) and *unc-42p* (E) promoter regions. Green arrows indicate neural cells. Red arrows indicate a temporary expression of GFP on the dorsal-right and ventral-left SMB's axons that was gone after some generations of worms passed.

The GFP strain carrying the *flp-12sp* promoter region (UL4187) drove expression of the GFP protein solely in the SMB neurons (Figure 2.3, Image B) as expected (personal communication with Kyuhyung Kim). Within the area of the nerve ring four SMB cells were visible with four axons extending from the nerve ring towards the tail. The ventral axons were always longer than the dorsal ones.

The GFP strain carrying the *unc-42p* promoter region (UL4183) drove expression of the GFP in many cells, rendering them very difficult to identify, and the levels of expression varied (Figure 2.3, Image E).

2.3.3.2 rec-GFP reporter strains showed successful expression of the two-component system

Worms expressing the two subunits of the reconstituted-GFP driven by the same *lad-2p* region (UL4184) showed the same expression pattern as the *lad-2p*::GFP reporter strain (UL4213).

Furthermore, there was no non-specific GFP expression observed by the rec-GFP strains (Figure 2.4, Images A, B and C). When the two subunits of the reconstituted-GFP were driven by the two different promoter regions (*lad-2p* and *unc-42p*), with expression overlapping only in SAA, the whole GFP protein was expressed solely there (strain UL4214) (Figure 2.4, Image D). Same expression result was observed with strain UL4216, were the promoter regions were switched to different rec-GFP subunits. The two-component system thus far worked successfully and as expected (Chalfie *et al.,* 1994).
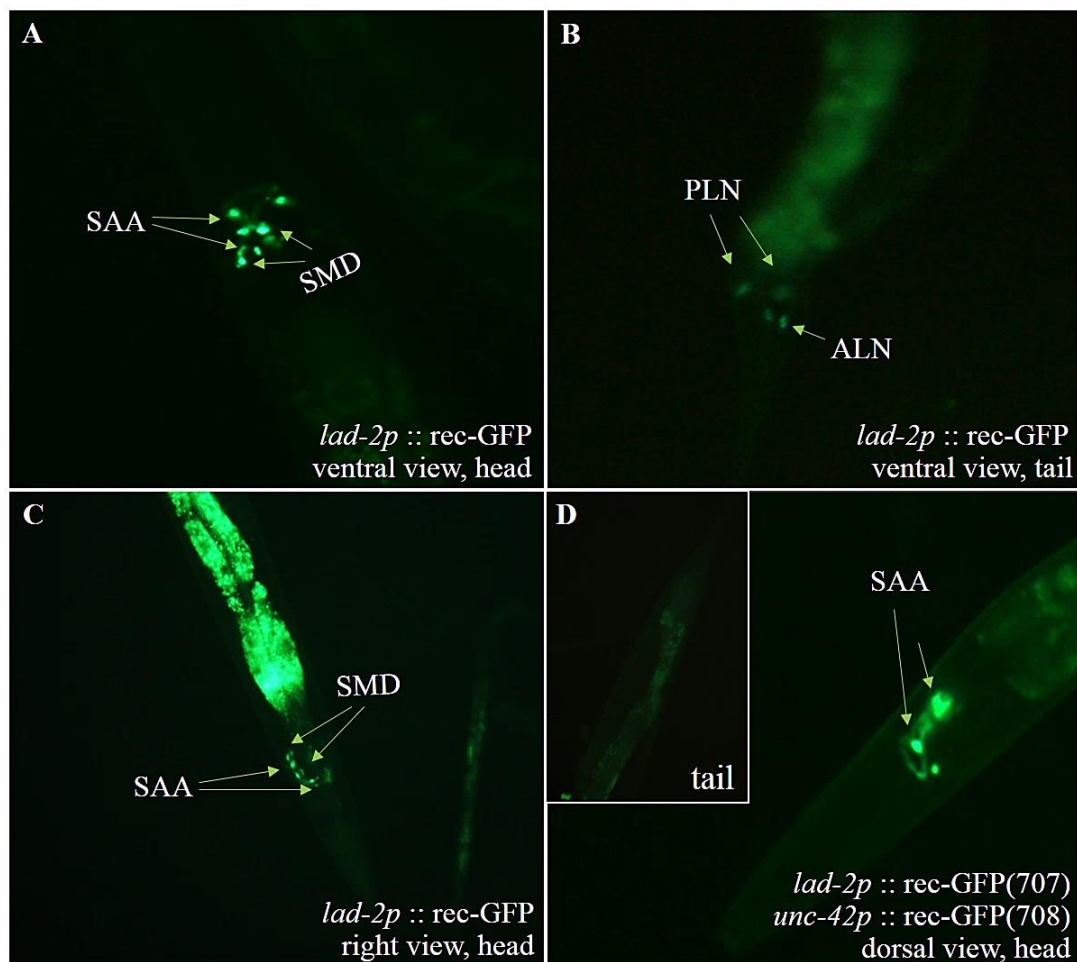
Figure 2.4 rec-GFP reporter strains images. Worms expressing the two subunits of the reconstitute - GFP driven by the *lad-2p* (A, B and C) and by both the *lad-2p* and the *unc-42p* (D) promoter regions.

2.3.3.3 Ablation and control strains confirmed successful genetic ablation of the SAA and SMB neurons

GFP plasmids were co-injected along the caspase ones, so that I would be able to confirm ablation of the targeted neural cells via microscopy. SMB cell ablation occurred in worms expressing the two subunits of the reconstituted CED-3 caspase driven by the *flp12-sp* promoter region [Figure 2.5, Image A, worm in the bottom has the SMB- ablated (strain UL4230), whereas worm in the top has not (strain UL4224)]. When the reconstituted CED-3 caspase was driven by both the *lad-2p* and the *unc-42p* promoter regions, SAA ablation took place (Figure 2.5, Image C; strain UL4207). GFP expression in other cells, and the lack of it in the targeted ablated cells, confirmed the genetic ablation,. In the 'control ablation' strains, where only one of the two ablation constructs were injected, the neural ablation does not take place (Figure 2.5, Image A top worm and 2.5B; strains UL4224, UL4219 respectively). Ablation of the targeted cells with the caspase two-component system therefore occurred successfully, as previously described with other neural cells (Chelur and Chalfie, 2007).
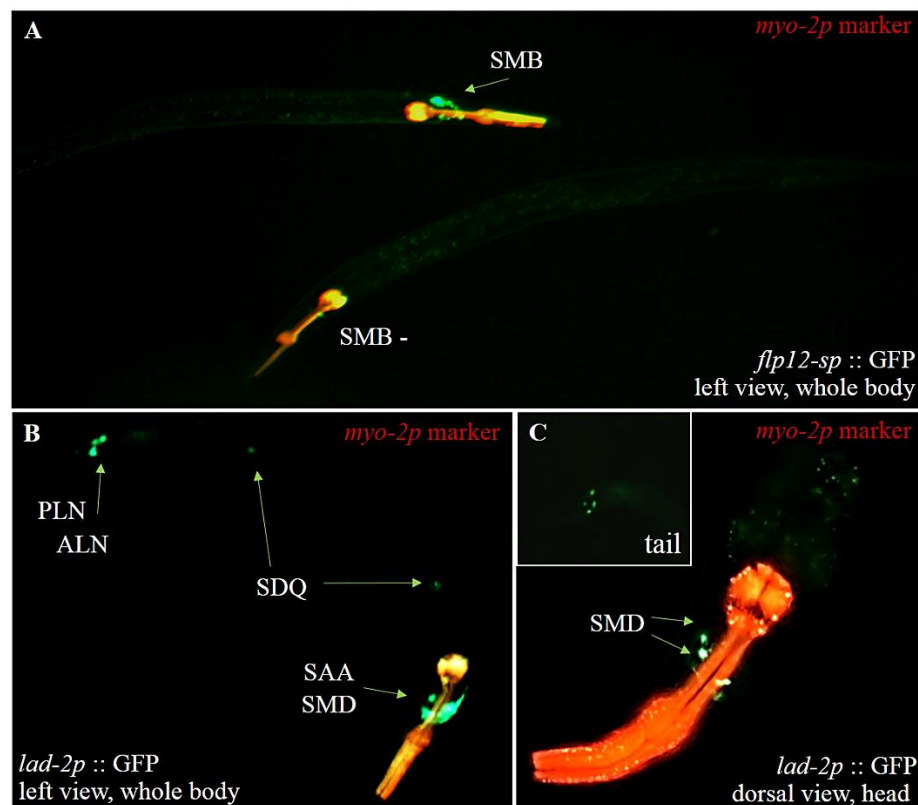
Figure 2.5 Ablation and control strains images. Worms expressing the two subunits of the reconstitute CED-3 caspase driven by the *flp-12sp* (A bottom worm), and by both the *lad-2p* and the *unc-42p* promoter regions (C). GFP expression, and the lack of it, confirms the genetic ablation. Control ablation strain (Image A top worm and Image B) expresses only one of the two ablation constructs, therefore the neural ablation (SMB and SAA respectively) does not take place.

2.4 Discussion

In order to gain a more detailed understanding of individual neural function in the worm, and link that function to the role of complex neural circuits and specific behaviours, the need for more fine-tuned genetic manipulations and techniques arises. In this project, the neurons of interest were difficult or even impossible to target by commonly used laser or genetic techniques. The two-component system created by Chellur and Chalfie (2007) used here, proved to be both specific and consistently successful.

The general anatomy and localisation of the neurons of interest, SAA and SMB, was confirmed as previously described (Aurelio *et al.,* 2002; White, J.G. *et al.,* 1986). The promoter regions selected to target the neurons worked well with the two-component system. Ablation of the targeted cells was confirmed.

Ablated strains showed locomotion phenotypes different to that of the wild-type animals, all described in detail in the next chapter (Chapter 3). The SAA and SMB ablation strains generated in this chapter are the main strains that were used throughout this project.

Although generating these strains took the better part of a year, it enabled the behavioural assays to move forward faster. Having strains transmitting the genetic ablation to their progeny, gave me a continuous supply of mutants, and prevented me from having to keep doing independent laser ablations on individual worms for each and every assay. On that note, it increased the reliability and reproducibility of the all behavioural analysis I conducted in the following chapters.

This reconstitute system was first published in 2007 by Chelur and Chalfie, however, when I started my project only four other studies had used it for neural ablations; to ablate RIA interneuron (Ha *et al.,* 2010), BAG interneuron (Bendesky *et al.,* 2011), AFD sensory neuron (Glauser *et al.,* 2011), AWC sensory neuron (Beverly *et al.,* 2011) and ASI sensory neuron (Gallagher *et al.,* 2013). It's been gaining more attention the last three years. It is my hope that by showing how reproducible and successful it is, more *C.elegans* researchers will use it in the future to target cells that were otherwise difficult to target. Using this genetic approach, we will also expand our mutant strain library in the CGC with strains that will be easily accessible to all labs and directly comparable.

Chapter 3
Locomotion analysis of the SAA- and SMB- ablated strains

3.1 Introduction

The aim of this chapter was to observe and describe any phenotypes that resulted from the transgenic strains generated in the previous chapter, and to assess the role of SAA and SMB in locomotion by means of behavioural analysis.

3.1.2 Behavioural phenotype of the SAA and SMB ablation strains

In order to infer neural cell function, neuroscientists often kill a neuron of interest and examine the resulting behaviours of the ablated animals. Neural ablation studies and behavioural characterisation of genetic mutants have shed much light on the neural circuits regulating the different behaviours *C.elegans* demonstrates (Bargmann, C. I., 1993; Bargmann, C. I. *et al.,* 1993; Gray, J.M. *et al.,* 2005; Pierce-Shimomura *et al.,* 1999; Zhao *et al.,* 2003; Iino and Yoshida, 2009). Such studies can also suggest functional overlap or circuit proximity between neurons. Regarding the neurons of interest of this project, SMB has been partially characterised whereas SAA has been largely overlooked. As previously discussed in Chapter 1: General Introduction, SMB and SAA's relationship has not been explored any further than their known synaptic connectivity, and SAA has not yet been linked to any behavioural circuit.

Therefore, in this chapter I focused on an extensive behavioural analysis of the SAA and SMB genetically ablated strains. Well-defined behaviours were studied, such as local search behaviour, dispersal (Croll, 1975; Gray, J.M. *et al.,* 2005), escape response to harsh touch (Chalfie *et al.,* 1985; Pirri, Jennifer K and Alkema, 2012) and swimming (used to be called thrashing) in liquid M9 (Vidal-Gadea *et al.,* 2011). The performance and frequencies of reversals, turns and the amplitude of undulations during those behaviours were measured. Wild type and control ablation animals, where only one of the two CED-3 subunits were expressed, were used as controls. Albeit a laborious work as everything was measured manually, observation and description of the various behavioural phenotypes created a 'behavioural envelop' or 'ethogram' for each strain, highlighting the mutant strains' locomotion defects in comparison to the wild type animals.

3.2 Material and methods

3.2.1 Nematode maintenance and strains

Animals were kept at 20°C at all times, fed *E.coli* (OP50 strain) and were maintained as previously described (Brenner, 1974). *C. elegans* variety N2 Bristol wild-type strain was provided by the Caenorhabditis Genetics Centre (CGC), which is funded by NIH Office of Research Infrastructure Programs (P40 OD010440). Ablated strains SAA- (UL4207), SMB- (UL4230) and control ablation strain (UL4223) used throughout this chapter were generated for this project (see previous chapter for details). Animals were assayed in the first 2 days of adulthood.

3.2.2 Amplitude of undulations

The body bends of the worm's sinusoidal movement leave behind tracks consisting of undulations. Each half undulation is either a hyperbolic or parabolic-like curve (Figure 3.1, Image A). In order to quantify and compare the undulatory phenotype of the ablated strains to the wild type worms and control worms, the degree of curve was measured (Figure 3.1, Image B). Most commonly used by civil engineers to define and compare curves and arcs (Schofield, 2001), the degree of curve defines the sharpness or flatness of a curve. The degree of curve is directly proportional to curvature and inversely proportional to the radius of the circle fitting in the curve measured.

Nematode growth medium 9cm plates were plated with OP50 bacteria in order to produce thin lawns, and were left overnight at room temperature. Well-fed adults were transferred with the use of an eyelash to the 9cm plate and were left 1 minute to recover. Tracks left on the thin bacterial lawn were captured by StreamPix 7 (version 7.2.1) video capturing software, built by NorPix. Images were processed with FIJI software (Schindelin *et al.,* 2012) and GeoGebra 4.4 software (Hohenwarter, 2002) in order for the angle of the curve to be measured. 50 random tracks were measured from 10 worms for each strain.
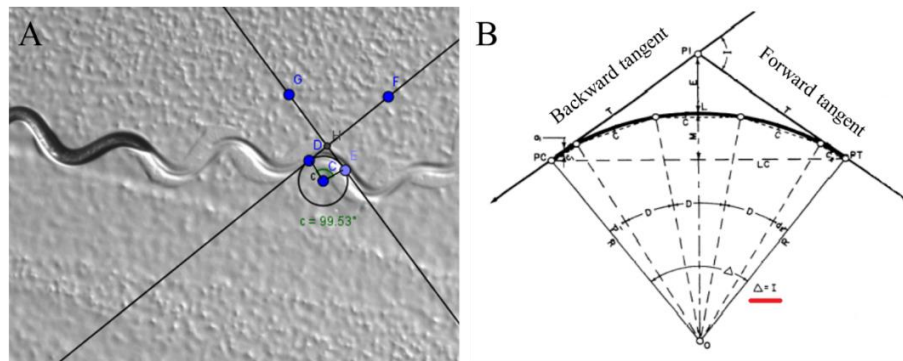
Figure 3.1 Angle curve measurement method. A) Example of an angle curve measured on an image of a worm track. Lines G and F are the backward and forward tangents to the circle fitted on a random undulation. Spot D is the point of intersection of the two tangents. C is the angle referring to the degree of curve. B) Elements of a simple curve. Δ is the angle depicting the degree of curve. Image obtained and adapted from http://www.tpub.com/inteng/11a.htm (Integrated Publishing, 2013).

3.2.3 Behavioural assays

3.2.3.1 Locomotion analysis of local search via single-worm video-tracking

Well-fed adults were transferred with the use of an eyelash to a fresh, foodless nematode growth medium plate (9cm diameter). They were left 1 minute to recover because the transfer suppresses turning for about a minute (Zhao *et al.,* 2003). Video-tracking was initiated immediately and lasted for approximately 11 minutes as reversals, stops and turns decrease to a minimum after 11 minutes in the absence of food (Gray, J.M. *et al.,* 2005). Videos were captured at our group's custom built single-worm tracker consisting of a Nikon dissecting microscope, a XIMEA xiQ super-speed camera and a Prior Optiscan II (x, y) stage installed, so that the animal could be observed as it moved across the plate (Figure 3.2, Image A). Six animals were tracked for each strain (control ablation n=4), resulting in approximate 4 hours of video tracking.

Any backward movement was scored as a reversal event. How reversal lengths were scored is shown by the schematic in Figure 3.2, Image C. Reversals of three or more head swings or body bends (1.5 undulation and above) were scored as long reversals. Less than three head swings or body bends (up to 1.25 undulation) were scored as short reversals (Zhao *et al.,* 2003; Gray, J.M. *et al.,* 2005). A body bend or head swing was scored whenever a bend reached a maximum just posterior to the pharynx (Koelle and Horvitz, 1996). Backward movement that was interrupted by a brief period of forward movement was scored as two distinct reversals. Stops longer than 1 second were scored as 'pauses'. Forward movement

included also all kinds of turns; omega and delta. Omega turns were visually identified by the head touching the mid-body and sliding off the tail, the resulting posture forming the Greek letter Ω (Gray, J.M. *et al.,* 2005). Delta turns were distinguished by the head passing underneath or above the tail the posture forming the Greek letter δ (Gray, J.M. *et al.,* 2005; Broekmans *et al.,* 2016). All behaviours were scored as events (counts) and the length of time it took for them to be performed by the worms noted down (seconds). Videos were captured at 25fps with StreamPix 7 (version 7.2.1) software built by NorPix. Experiments were conducted at 20°C. The order in which plates and strains were used was randomised with the use of a dice. For representative ethograms for each strain see Appendix section D (Figure D1).
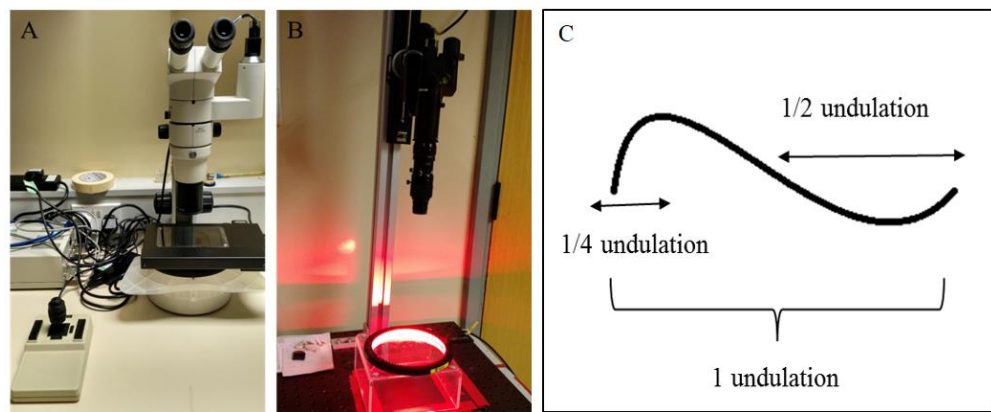
Figure 3.2 Images of our group's worm trackers and undulations measurements. A) Shows the single-worm tracker in our group.   B) Shows the multi-worm tracker set up by my postdoc colleague Robert Holbrook. C) Schematic representation of undulation measurements during reversal scoring (long ≥ 1.5 undulations, short ≤ 1.25 undulations).

3.2.3.2 Dispersal (Long-range search) behavioural assay

After the first approximate 10-15 minutes without access to food the worm enters an exploratory behaviour of long runs and fewer tumbles to cover more area. This behaviour is called dispersal. Well-fed adults were transferred with the use of an eyelash to a drop of M9 buffer and immediately afterwards to the centre of a fresh, food-free nematode growth medium plate (9cm diameter). The base of the plate was divided into squares by an 86 square-grid petri-sticker (Figure 3.3). Video-tracking was initiated immediately and lasted for an hour. Squares covered by the worms' tracks were scored and percentage of area covered compared between the strains (Flavell *et al.,* 2013).

For these experiments a custom built multi-worm tracker was used, set up by my postdoc colleague Robert Holbrook, consisting of a Navitar telemetric lense and a XIMEA xiQ super-

speed camera mounted on a Fotomate macro slider / Manfrotto 410 geared head, and a Polytech LED red light circular system (Figure 3.2, Image B). Videos were captured at 4fps with the use of StreamPix 7 (version 7.2.1) software built by NorPix. Trajectories were visualised with FIJI software (Schindelin *et al.,* 2012). Experiments were conducted at 20°C. The order in which plates and strains were used was randomised with the use of a dice. Four animals per strain were tracked.
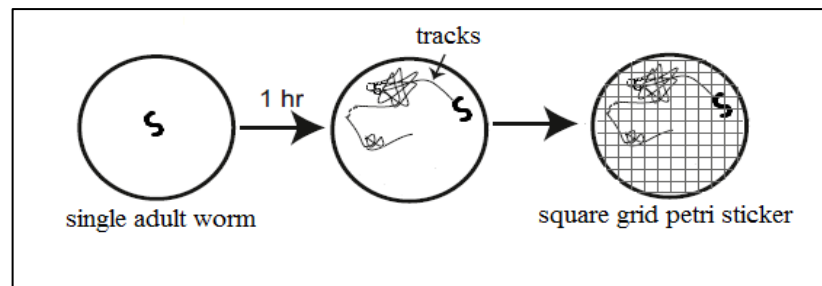
Figure 3.3 Simplified schematic showing the dispersal assay for measuring search behaviour based on worm tracks formed for an hour, on a plate without a cue. Number of squares entered by the worm demonstrates an approximation of the area of the plate covered during exploration. Image adapted from (Flavell *et al.,* 2013).

3.2.3.3 Escape response via harsh touch

Well-fed adults were transferred with the use of an eyelash to a fresh, food-free nematode growth medium plate (5cm diameter) and were left 5 minutes to make sure they recovered and none of the responses observed were due to the transfer. They were then poked with an eyelash on the tip of the head. Percentage of response to the harsh touch was scored. From those adults that responded, undulations of the reversals were scored as described in the previous section (Figure 3.2, Image C). Whether the reversals were followed by omega or delta turns was also scored and the turn's performance posture was observed. Turns were visually identified as described in section 3.2.3.1. Experiments were conducted at 20°C. The order in which plates and strains were used was randomised with the use of a dice, and their genotypes blinded to me. Sham experiments were conducted alongside as an additional control, whereby the worms were not poked and their spontaneous response observed. 50 worms were poked from each strain and 30 were observed for the sham experiments.
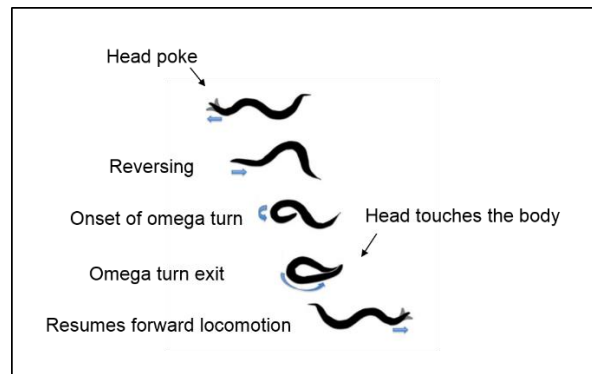
Figure 3.4 Escape response, coupled with an omega turn, of a wild type worm after a harsh touch on the tip of the head with an eyelash. Original image edited from (Pirri, Jennifer K and Alkema, 2012).

3.2.3.4 Swimming in liquid M9

Assessing motility in liquid has proved useful in identifying mutants affecting locomotion behaviours (Brenner, 1974). Well-fed adults were transferred with the use of an eyelash to a 24 well microtiter plate filled with M9 buffer (22mM KH_2PO_4, 34mM K_2HPO_4, 86mM NaCl, 1mM $MgSO_4$ in H_2O) and were left 1 minute to recover. Body bends, turns and reversals were scored for a whole minute in 50 animals per strain. Experiments were conducted at 20°C. The order in which plates and strains were used was randomised with the use of a dice, and their genotypes blinded to me.

3.2.4 Lifespan assay

Adult worms were left to lay eggs on OP50 seeded nematode growth medium plates (5cm diameter) and after 2 hours were removed. The resulting synchronised eggs were left to develop at 20°C and were observed twice daily until they reached adulthood. The adults were then transferred to newly seeded plates and their survival rate was scored daily until all worms were dead. A Kaplan-Meier plot was drawn to depict the survival rates (Rich *et al.,* 2010). Initial population for all strains was 80 animals (4 plates of 20 animals). Those few that were lost crawling to the lid of the plates, resulting in them drying out, were removed from the analysis.

3.2.5 Statistical analysis

Comparisons between tested animals and matched controls were conducted by using one-way or two-way analysis of variance (ANOVA) followed by Tukey's multiple comparisons test.

For the lifespan assay the Log-rank (Mantel - Cox) test and Gehan-Breslow-Wilcoxon test were used as recommended by the statistical package. Analysis was performed using GraphPad Prism (version 6.01), GraphPad Software, La Jolla California USA, www.graphpad.com.

3.3 Results

3.3.1 SAA- and SMB- ablated animals exhibit exaggerated undulation amplitudes

The first and most apparent difference between the wild type and the ablated animals was the amplitudes of their undulations. The curves of the undulations left on the thin bacterial lawn by the ablated animals were deeper than the wild type and the controls (Figure 3.5, Images A-D). The measurements of the angle of the curves revealed that the SMB- ablated strain has the highest curvature of the strains, with the SAA ablation strain curving less, but still significantly higher than the controls (Figure 3.5, Image E).
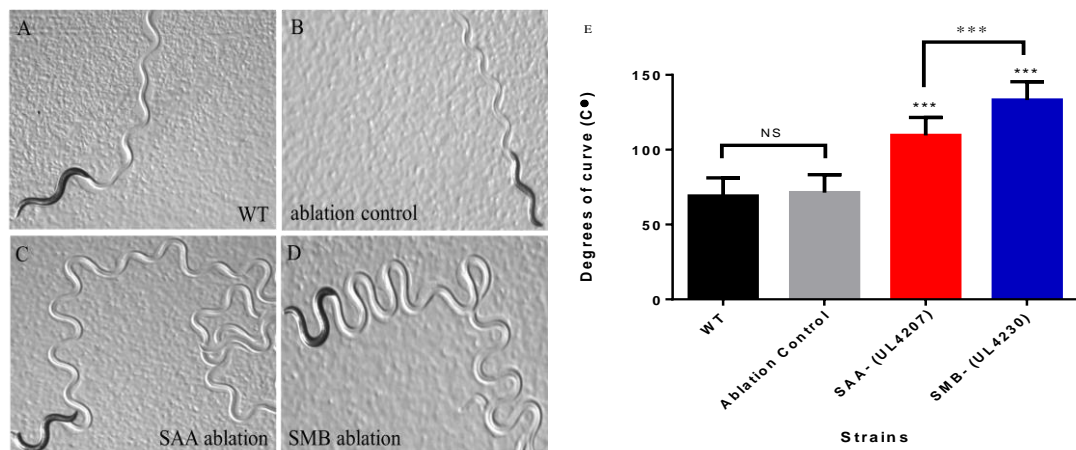
Figure 3.5 Images of tracks and curve angle measurements. Images A,B,C and D depict tracks of the ablated and wild type animals on thin bacterial lawns. Graph E shows the mean degree of curves from tracks left by the body bends of each strain examined (n=10, average of 5 bends measured from 10 animals per strain, 50 bends in total per strain). Statistical significance, and error bars as STDEV, are indicated. (One-way analysis of variance (ANOVA) and Tukey's multiple comparison; ***$p < 0.001$).

3.3.2 SAA- and SMB- ablated animals perform a coiled phenotype version of an omega turn
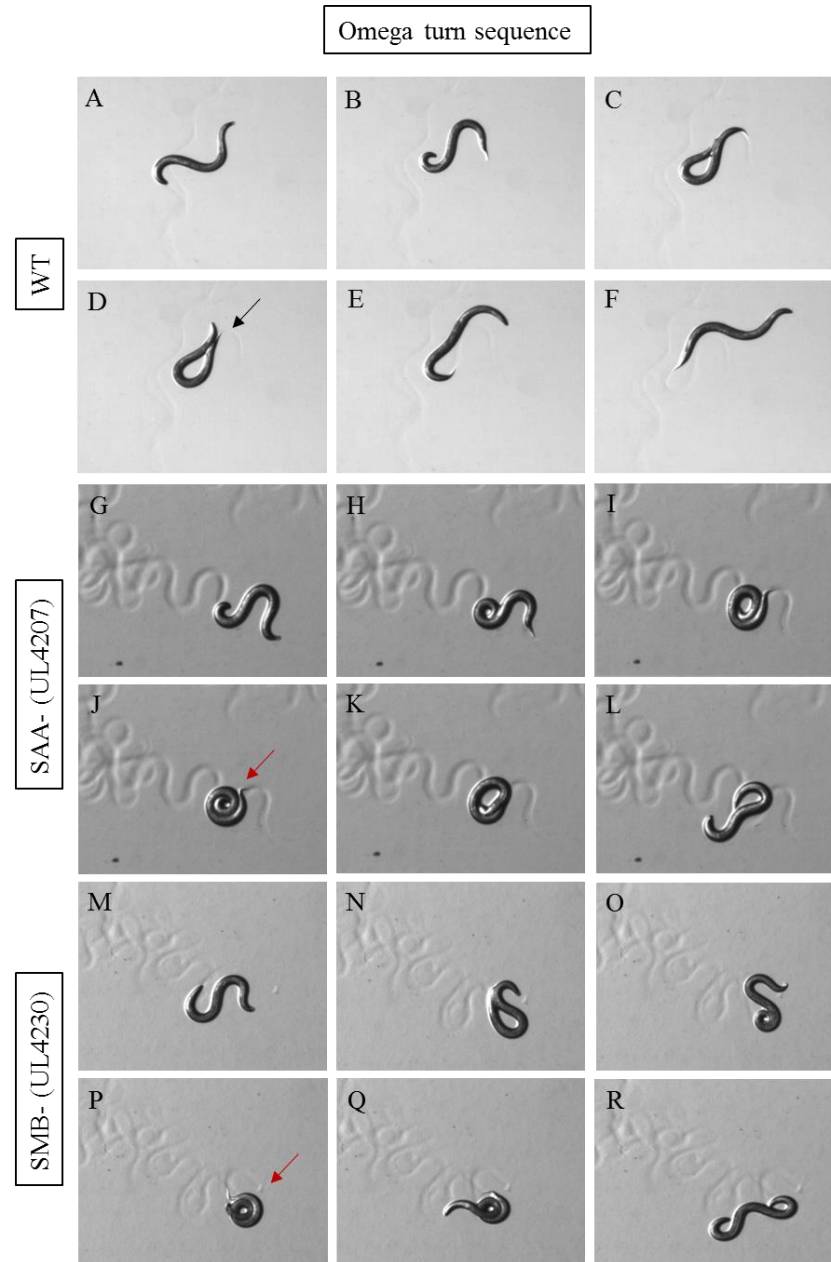
Figure 3.6 Omega turn sequence images. Images A to F depict snapshots of an omega turn of a wild type animal. Black arrow indicates the posture resembling the Greek letter Ω that gave this behaviour its name. Control ablation animals exhibited the same postures as the wild types. Images G to L depict snapshots of an omega turn from a SAA- ablated animal and snapshots M to R from a SMB- ablated animal. Red arrows depict the coiled posture observed during the omega turns of the ablated strains.

Initial direct observation of the ablated strains also revealed a phenotype during omega turns. This was examined more carefully by video-tracking on food-free plates.

When an SAA- or SMB- ablated worm bent its head to initiate the omega turn, it did so with an overstretch that made the most of the body coil to the side it was bending (Figure 3.6, Images O and I). The head could not then slide off the body and bent to the other side as happens during the recovery of a wild-type omega turn. In order for the worm to exit the posture, the head had to either lift upwards and cross over the body (Figure 3.6, Image Q), or the animal had to roll its whole body until it uncoiled enough for the head to slide free (Figure 3.6, Image K). I have dubbed this very specific abnormal version of an omega turn a 'coiled' omega turn (Figure 3.6, Images J and P). The ablated animals also exhibited normal omega turn behaviours as well, but at a lower observed frequency relative to coiled turns.

3.3.3 SAA- and SMB- ablated animals exhibit a different local search pattern than the wild type

The locomotion analysis via continuous single worm video-tracking highlighted not only the obvious differences between the strains, but also the more subtle ones. The SAA- ablated animals exhibit 3D movement in the form of a head lift, especially before performing a turn (Figure 3.7, Images A-D). Although, the time spent in forward, backward movement and pauses was no different than the control strains (Figure 3.7, Image E), the behaviours within those timeframes were in some cases significantly different (Figure 3.7, Images F and G). The SMB- strain exhibited a high frequency of all types of turns (omega, delta and coiled) leaving its remaining forward movement as the lowest percentage across all strains. The SAA- strain exhibited a similar phenotype, however not as strong, and its delta turns were at control levels. Backward movement for SMB was similar to the wild-type animals, whereas, the SAA- ablated animals exhibited a higher frequency of sort reversals and a higher length of longer reversals (Figure 3.7, Images H, I and J). Both ablated strains required more time to perform long reversals and turns than the control strains, but this was not true for short reversals (Figure 3.7, Image K).
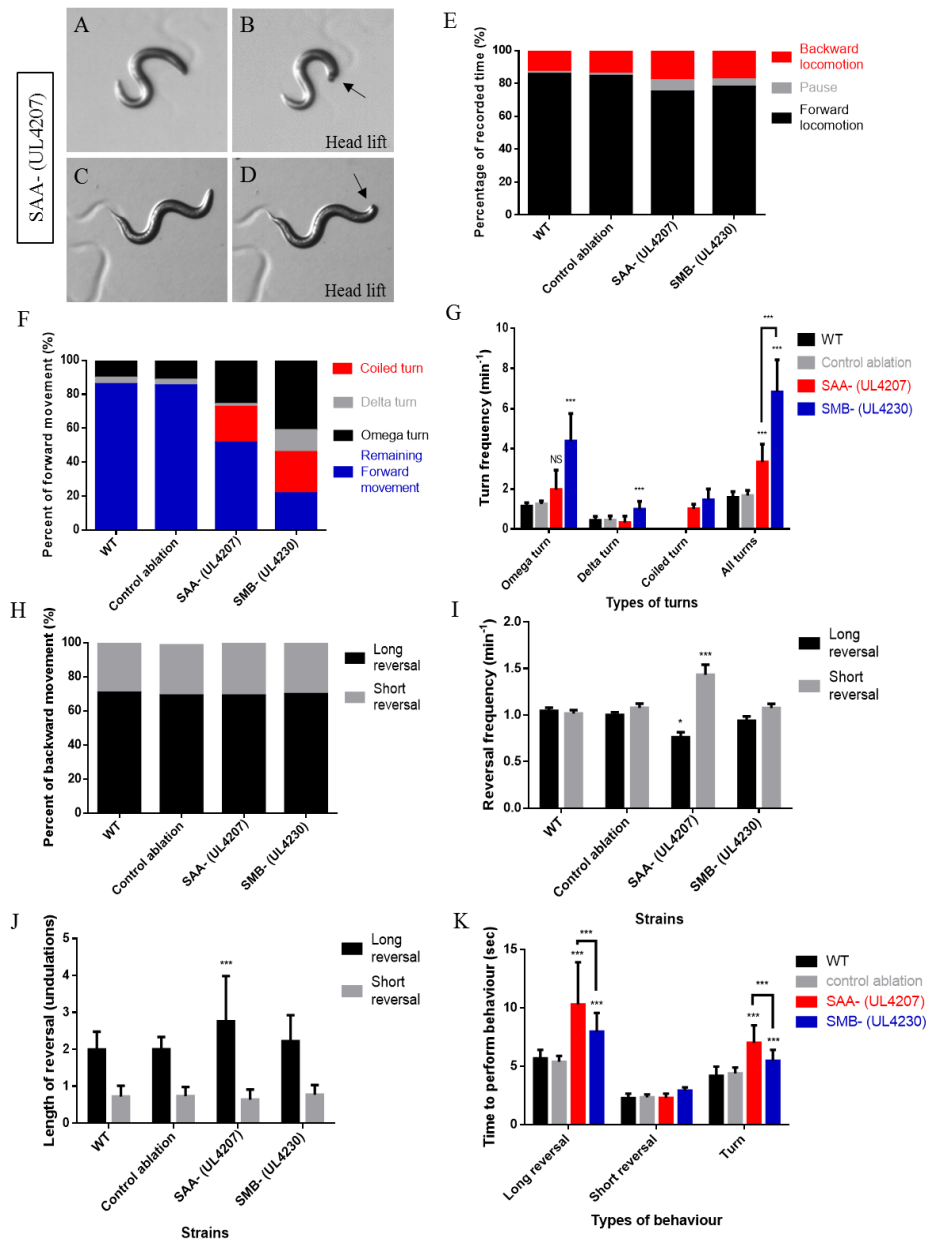
Figure 3.7 Spontaneous locomotion analysis. Images A to D depict a head lifting behaviour observed in the SAA- ablated animals. Graph E shows the percentage of time spent in forward, backward locomotion or pause during the recording by the animals of the tested strains. Graphs F and H show the specific behaviours performed during forward and backward movement respectively. Graph G shows the frequency and type of turns during forward movement, and graph I the frequency and type of reversals during backward movement. Graph J shows the mean length of the reversals (measured as undulations) performed during long and short reversals. Graph K shows a comparison of the time it took each strain to perform the different behaviours. Statistical significance, and error bars as STDEV, are indicated. [A two-way analysis of variance (ANOVA) and Tukey's multiple comparison were used; ***$p<0.001$; *$p<0.05$; 6 animals were tracked for 11 minutes for each strain (control ablation n=4)].

3.3.4 SAA- and SMB- ablated animals exhibit a decrease in exploratory behaviour
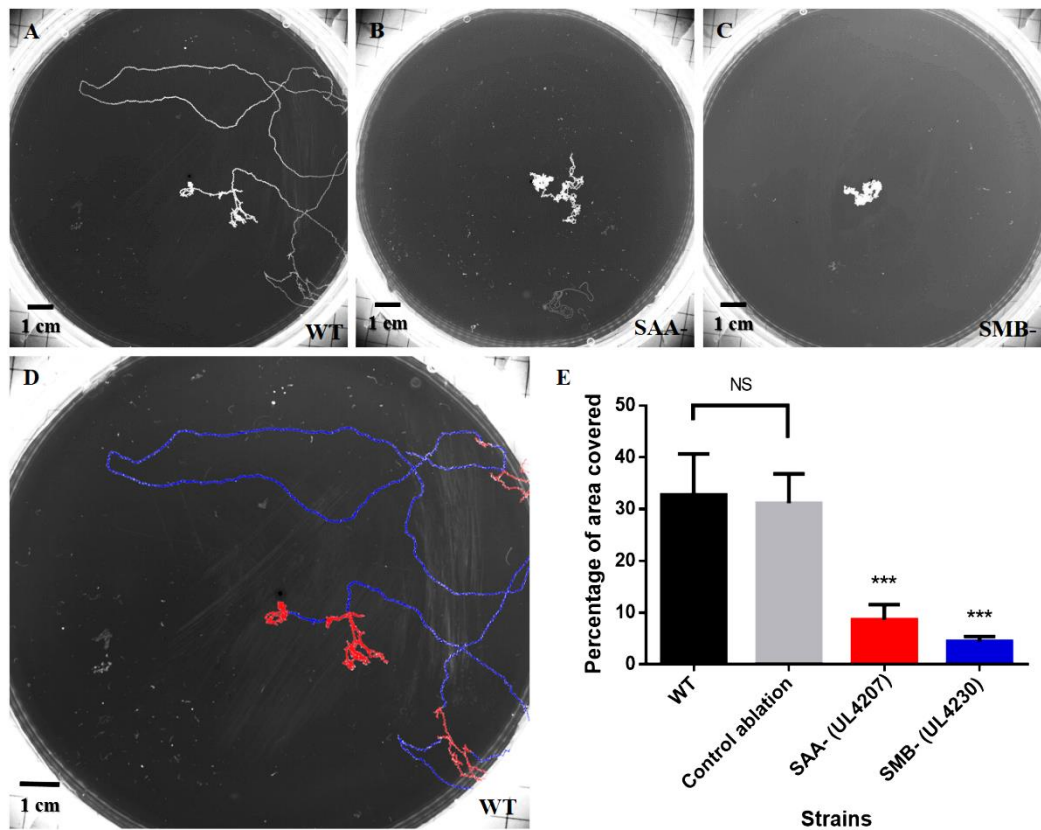
Figure 3.8 Long-range dispersal behaviour of assayed strains. Image A shows a representative example of the tracks formed by a wild-type animal for an hour, B a representative example of the tracks formed by a SAA- ablated animal and C a representative example of the tracks formed by a SMB- ablated animal. Ablation control animals showed similar tracks to the wild-type (data not shown). Image D depicts the dispersal behaviour of a wildtype animal with the tumbles and turns indicated with red and blue coloured tracks, respectively. Graph E shows the approximate area covered by the animals tracked for 1 hour. Statistical significance, and error bars as STDEV, are indicated. [One-way analysis of variance (ANOVA) and Tukey's multiple comparison were used; ***p<0.001; n=6 for each strain].

Once their local search behaviour was analysed, I moved on to observe their long-range dispersal behaviour (Figure 3.8, Images A-C). As has been previously observed in Gray *et al.,* (2005), the worm, after spending the first minutes exhibiting a high frequency of reversals and turns (local search), switches to a behaviour where 'runs' last longer and 'tumbles' decrease exponentially (long-range dispersal) (see red and blue tracks in Figure 3.8, Image

D). There was a statistically significant change in the area explored between the ablated strains and the controls. The SAA- ablated animals showed a 3-times decrease and the SMB animals a 6-times decrease of the area explored (Figure 3.8, Image E). From direct observation of the movies, this was due to the fact that SAA- and SMB- ablated animals performed more tumbles and less runs during the one hour of video-tracking.

3.3.5 The escape responses of SAA- and SMB- ablated animals differed to those of wildtype and ablation control animals.

Once spontaneous behaviour was largely covered, I next examined whether similar phenotypes would be observed during an evoked response, a deterministic behaviour of the worm. Moreover, I was interested in checking whether the ablated animals do respond to touch, and whether the reversals are coupled to omega turns, just as happens in wildtype animals (Croll, 1975; Gray, J.M. *et al.,* 2005). The escape response the worm exhibits on the application of a harsh head poke, is a well-defined response (Figure 3.9, Images A - I). The experiments revealed that the ablated worms do respond to harsh touch, the majority of the reversals that follow the touch are long and coupled with turns, just like the wild-type worms (Figure 3.9, Images J, K and M). However, the majority of the turns were coiled for the ablated animals (Figure 3.9, Image N). Moreover, the SMB- ablated animals exhibited more long reversals and significantly longer in length (Figure 3.9, Images K and L, respectively).
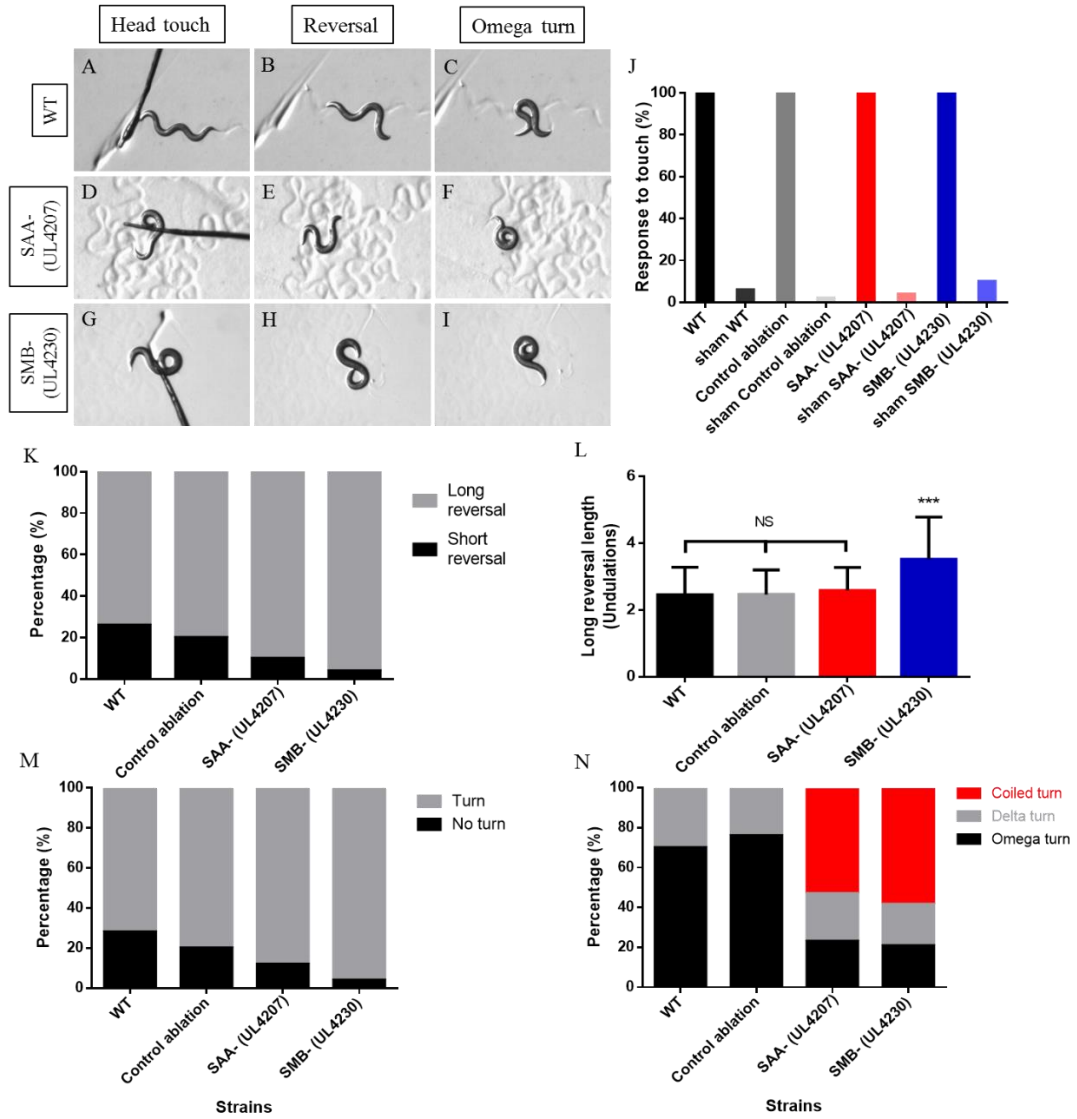
Figure 3.9 The escape response of ablation, control and wildtype strains following the application of a harsh touch on the tip of the head. Images A to I show some snapshots taken during the response from the wild-type and ablated animals. Ablation control animals showed similar postures to the wild-type (data not shown). Graph J shows the percentage of animals responding to the harsh touch, compared to mock experiments. Graph K depicts the percentage of long and short reversals as a response to the touch, while graph L shows the length of the long reversals measured as the number of undulations. Graph M depicts the percentage of the reversals that were coupled with a turn as a response to the touch, while graph N shows the relative frequencies of different types of turn; omega, delta or coiled. Statistical significance, and error bars as STDEV, are indicated. (For graph L a One-way analysis of variance (ANOVA) and Tukey's multiple comparison were used; ***$p < 0.001$; n=50 for each strain).

3.3.6 SAA- and SMB- ablated animals exhibit a decrease in motility in liquid compared to wildtype and ablation control animals.

In order to check the motility of ablated, control and wildtype strains in liquid, and to observe their swimming behaviour, they were transferred into M9 medium. The body bends per minute of SAA- and SMB- ablated animals were considerably lower than for wild-type animals (Figure 3.10 J) and the SMB- ablated worms' turn frequency was higher than the other strains (Figure 3.10 K). The SAA- and SMB- ablated animals also exhibited a coiled turn behaviour as previously observed on agar (Figure 3.10 F and I). The difficulty they exhibited in exiting that coiled shape, in combination with the exaggerated body bends, contributed to the decreased motility observed. Some of the liquid experiments were video-tracked and their images revealed a difference between the ablated strains. The body bends of the ablated strains, as expected after the results in the previous section, were deeper but the over stretch was at different parts of the body. The SAA- ablated worms over-bend at the tip of the head (arrow in D and E), whereas the SMB worms over-bend at the neck (arrow in G and H) (Figure 3.10 D, E, G, H). Last but not least, the SMB- ablated worms demonstrate a rod-like stiffness towards the tail, not following the curvature of the rest of the body.
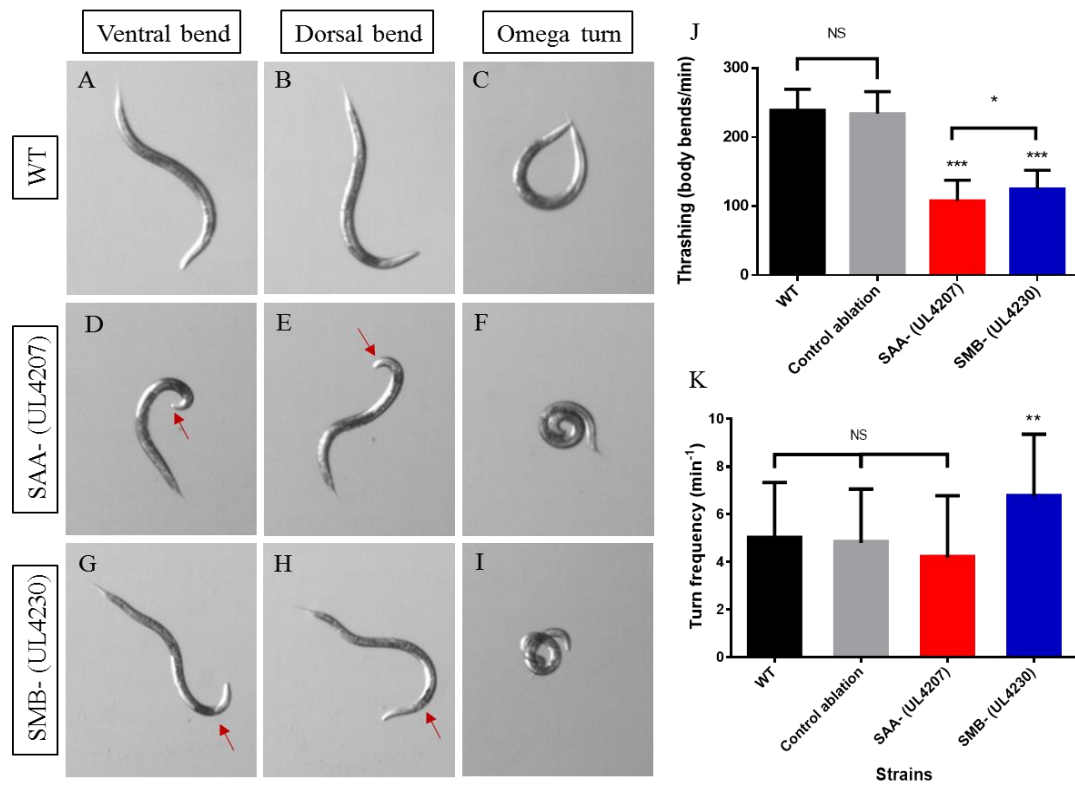
Figure 3.10 Swimming behaviour of assayed strains. Images A-I show examples of ventral or dorsal bends, and omega turns, of the ablation, control and wildtype strains in liquid M9 medium. The ablation control strain showed similar bends and turns when compared with the wild-type animals (data not shown). Graph J shows the motility of the tested strains depicted as body bends per minute. There was a statistically significant decrease in the body bend rate between the ablated and the wild-type animals. (One-way analysis of variance (ANOVA) and Tukey's multiple comparison were used; ***p <0.001;*p <0.05; n=50 for each strain). Graph K shows the omega turn frequency of the tested strains depicted as turns per minute. There was a statistically significant difference in the turn rate between the SMB- ablated strains and the wild-type. Statistical significance, and error bars as STDEV, are indicated. (One-way analysis of variance (ANOVA) and Tukey's multiple comparison were used; **p <0.01; n=50 for each strain). Experiments comparing reversal frequency across the strains revealed no statistically significant difference amongst all animals tested (graph not shown). Red arrows highlight head bend.

3.3.7 SAA- and SMB- ablated animals show no obvious developmental or survival defects

There was no statistically significant change in the trend of survival between the strains (Figure 3.11). Moreover, with the exception of a minor delay in development of the SMB-ablated strain during day 3, no obvious developmental defects were detected via direct observation until animals reached adulthood (Table 3.1).
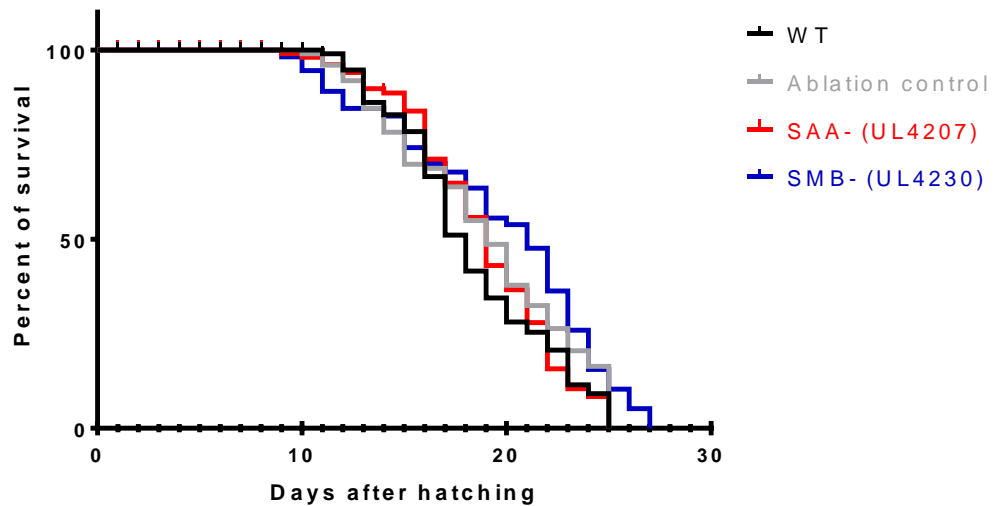
Figure 3.11 Graph showing a Kaplan-Meier survival plot for the main strains used throughout the project. Initial population for all strains was 80 animals (4 plates with 20 animals each). There was no statistically significant change in the trend of survival between the strains. Log-rank (Mantel - Cox) and Gehan-Breslow-Wilcoxon tests were used; $p > 0.1$).

Table 3.1 Life stages observed during development until animals fully reached adulthood. Synchronised populations. SMB- ablated strain exhibited signs of a slight delay during day 3 of direct observation.

Strain\Days after hatching	Day 1	Day 2	Day 3	Day 4
WT	l1-l2	l3-l4	young adults/adults	adults
Control ablation	l1-l2	l3-l4	young adults/adults	adults
SAA- (UL4207)	l1-l2	l3-l4	young adults/adults	adults
SMB- (UL4230)	l1-l2	l3-l4	l4/young adults/adults	adults

3.4 Discussion

In this chapter, I sought to shed some light on the role of SAA and SMB neurons during probabilistic (stochastic) and deterministic behaviours (evoked) of the worm. Ablation of SAA and SMB led to worms with very different behavioural phenotypes to controls and wildtype. Similarities in the phenotypes exhibited by SAA and SMB ablation strains suggest they may be part of the same neural circuit. However, there were some clear differences between SAA and SMB ablation phenotypes, hinting at differences in their role/function within the worm's network. Here, I discuss this in more detail.

3.4.1 SAA and SMB neurons are involved in setting the amplitude of head swings

By comparing the curvature of the ablated strains with the controls, by means of the angle curve, I have shown for the first time experimentally that SAA neurons are part of the circuit that sets the amplitude of undulations. This experiment also confirmed what previous laser ablations for SMB had shown; that it has a function in sinusoidal movement regarding the amplitude of undulations (Gray, J.M. *et al.,* 2005). The exaggerated head swings were apparent in all of the contexts the animals were observed under, such as on food, in liquid, off food, prolonged period off food etc. The exaggerated flexing observed after neural ablation suggests an inhibitory activity on the muscles by SMB motor neuron, and an indirect inhibitory effect to the muscles for the SAA interneuron (possibly via dysregulation of SMB motor neuron when SAA is ablated). This hypothesis will be addressed further in Chapter 4 by means of calcium imaging at the body wall muscle.

Being a motor neuron that innervates head and neck muscles, the SMB, was expected to have a role in maintaining some type of body posture as it has a direct effect on the muscles. However, the SAA as an interneuron wasn't necessarily expected to show such a similar phenotype. This result strengthens the hypothesis that SAA controls SMB activity, outlined in the General Introduction. However, the phenotype of SAA ablation is shallower than the SMB one, suggesting that SAA could control another motor neuron and the effect of the ablation that I observed is a combinatorial result. SMD is a good candidate. It is a motor neuron deeply connected to SAA, locally very close and overlapping in gene expression pattern. SMD laser ablation in previous studies has shown a control over the amplitude of omega turns by lowering the steepness of turning dramatically (Gray, J.M. *et al.,* 2005). This result suggests an excitatory activity on the muscles from the SMD neurons, which is the exact opposite effect of the SMB neurons. On that note, and if the SAA controls both, then the result of the ablated worms could be a combination of SMB and SMD dysfunction due to

the SAA ablation. Therefore, one would expect to observe an intermediate phenotype from the SAA- ablated worms.

Two more head neurons have shown an effect in setting the amplitude of the head swings; RME (Gray, J.M. *et al.,* 2005; Shen *et al.,* 2016) and RMD (Pirri, J. K. *et al.,* 2009). However, these motor neurons only innervate the muscles on the tip of the head, and not the neck muscles, and as a result exhibit only a minor foraging/oscillating defect restricted to the end of the head when ablated. Thus far, no other head neural ablation has shown a similar effect.

These results and hypotheses will be further explored in General Discussion, where I will propose a circuit model for the head movement and a network for chemotaxis.

3.4.2 SAA and SMB neurons set the amplitude and inhibit the frequency of omega turns

The coiled turn phenotype observed for the first time in this project by the ablated strains, occurred during both deterministic and probabilistic behaviours. When an SAA- or SMB-ablated worm bent its head to initiate an omega turn, it did so with a deep flex that made the rest of the body coil to the side it was bending. That could occur both at a ventral or a dorsal turn, however, ventral turns were favoured, as previously described in wild types (Gray, J.M. *et al.,* 2005; Broekmans *et al.,* 2016; Croll, 1975). The head once coiled, could not recover and bent to the opposite side, making the omega turn exit very difficult. It seems that without SMB to inhibit the muscles on the side that is initially bending, the turn goes unchecked, and the posture of the head cannot recover. The same happens with the ablation of SAA, but to a lesser extent. The absence of the interneuron seems to render the motor neuron dysfunctional to an extent. Last but not least, in all environments tested, the turn frequency of the ablated strains was significantly increased. This suggests that SAA and SMB, when functioning normally, inhibit the frequency of the turns. As with the previous section, these overlapping results of SAA versus SMB strengthen the hypothesis that one regulates the other.

It was also interesting that the ablated animals did exhibit normal omega turn behaviour as well, but they were deeply flexed and at a very low occurrence. This highlights the fact that SAA and SMB do not work alone on the circuit regulating the amplitude of omega turns. Evidence points to SMD, where in a previous publication investigating the navigational circuit, SMD ablation results in a decrease of omega turns and those turns are shallower (Gray, J.M. *et al.,* 2005). Therefore, whereas SMD promotes the turns, SMB and SAA inhibit them in all tested environments. Once again, SMD seems to have the exact opposite effect on the body posture and muscles to SMB.

These results prompted me to check the activity of the SAA and SMB neurons during this behaviour, which is explored further in the next chapter (Chapter 4).

3.4.3 SAA and SMB neurons promote runs during dispersal behaviour via inhibiting turns

On food, all of the worms exhibited what was previously described as dwelling (Croll, 1975; Gray, J.M. *et al.,* 2005; Fujiwara *et al.,* 2002). A high frequency of pauses, turns and reversals interrupted with the occasional short roam outside of the food boundaries. In contrast, the ablated strains exhibited more turns than the wild-type. This was not explored further in detail due to time constrains, the project's focus on taxis and the fact that the worms' locomotion activities increase once it is removed from food.

Once removed from food, wild-type worms entered a sequence of approximately equal numbers of reversals, and turns. With this behaviour the worm samples its environment while staying relatively close to its starting position. As time went by, the frequency of turns and reversals decreased. In this way, the worm 'runs' more, covers more area and increasingly gets further away from its starting point. These 'runs' are interrupted by short instances of local searches but these diminish in time too. The SAA- and SMB- ablated worms exhibited a significant higher frequency of turns than the control strains, on both local search and dispersal behaviour. It seems with the ablation of either SAA or SMB 'runs' are rarely performed, and when they are, they are not maintained for increasing amounts of time as in wildtype worms. This resulted in the animals getting 'stuck' in the same area, never exploring much further than their starting point. This suggests that the neurons could be controlling the switch between local search and dispersal. During local search mode turns are promoted whereas on the start of the dispersal behaviour turns are inhibited. To sum up, SAA and SMB neurons inhibit 'tumbles' and promote 'runs' while navigating off food. This result is important and will be explored further in Chapter 5, where the two strategies of orientation of the worm will be examined as it hints that SAA and SMB might be suppressing pirouettes during chemotaxis.

On a side note, the time spent in forward, backward movement and pause was no different than the control strains during local search. This indicates that the defect introduced by the ablation of either cells did not affect the switch between backward and forward movement. In fact, other than the increase in short reversals and length of long reversals when SAA is ablated, there was no other significant difference in backward locomotion. This result could be down to the fact that from the two neurons explored here, SAA is the only one with strong

synaptic connections to the backward locomotion circuit, namely RIM and AIB neurons (Piggott *et al.,* 2011).

3.4.4 SAA and SMB neurons might receive and compute proprioceptive information

It has been shown that the worm's forward movement is propagated from head to tail and rhythmically coordinated due to proprioceptive information between adjacent body regions (Leifer *et al.,* 2011; Wen *et al.,* 2012). During swimming the SMB- ablated strain exhibited a stiffness to the lower part of the body, not apparent in the rest of the strains. Under normal conditions, the tail follows the undulation amplitude and general posture of the head (Wen *et al.,* 2012). This suggests that SMB might be expressing stretch receptors that receive and compute proprioceptive information as the body stretches. It is interesting that SMB is pre-synaptically connected to the DVA interneuron, a neuron known for its expression of stretch receptors (*trp-4*), and its regulation on undulatory movement in the body (Li, W. *et al.,* 2006). This connection could provide SMB with feedback proprioceptive information on the extent of muscle activity.

Additional evidence for this comes from the inability of the SMB- ablated strain to recover the position of the head and bend to the opposite side while exiting a coiled omega turn. Moreover, the decreased motility observed in liquid M9 was a result of the difficulty to recover from the exaggerated head swings and exit the coiled omega turns. These observations could be due to a defect in the flow of dorsoventral proprioception information.

Proprioception and the targeted neurons are further explored in Chapter 7, where SAA and SMB are checked for stretch receptor expression.

3.4.5 SAA seems to play a role in 3D head movement

The SAA- ablated animals exhibited a lot of head lifting during local searching, and especially before a turn. This control of head movement could arise from proprioceptive information sensed by stretch receptors and computed in the axons of the SAA neurons extending to the tip of the head.

This evidence of regulation of 3D head movement was very interesting for our group, since my colleague at Computing Robert Holbrook has set up a custom 3D video apparatus. I conducted video-tracking of SAA- ablated worms in the 3D apparatus, but the analysis is not yet concluded at the time this thesis is being written. Not much is known about the circuit in the context of 3D movement and should be explored further in the future.

3.4.6 SAA- and SMB- ablated animals show no significant survival defects

Recently, it has been shown that there is a neuronal regulation of lifespan (Lin *et al.*, 2017). The work by Lin *et al.* (2017) focuses mainly on sensory neurons. However, it seemed interesting to observe if there was a role of SAA or SMB in longevity. There was no evidence of a survival defect of the ablated strains.

3.4.7 The ablation control strain shows no defects

Mock genetic ablation strain, where only one of the two ablation subunits were expressed, didn't show any behavioural defect. In all experiments its behaviour was wild-type like. This confirmed what was observed in Chapter 2; that the ablation occurs only in the presence of both caspase subunits. Moreover, this control showed that no behavioural effects were caused by the genetic manipulations the transgenic strains went through. Therefore, it will not be used in the consequent chapters, and all comparisons are made with the wildtype strain.

Chapter 4
Effect of the SAA and SMB neurons on the body wall muscles and activity of SMB during locomotion

4.1 Introduction

In order to obtain a complete knowledge of neural function a multidisciplinary approach is required. The anatomical and behavioural data must be combined with electrophysiological, molecular and genetic data in order to identify functional pathways between neurons and the electrophysiological properties of these pathways. In this way, we will be able to have a complete picture for such dynamic processes. In recent years, there is been substantial progress in electrophysiological techniques, genetically encoded indicators and optogenetic photo actuators, which are often used in combination in the *C.elegans* field (Leifer *et al.,* 2011; Smedemark-Margulies and Trapani, 2013; Akerboom *et al.,* 2013; Li, Z. *et al.,* 2014). In this chapter, I aimed to observe the effect that the SAA and SMB neurons have on the body wall muscles, and whether this activity causes the postures observed in Chapter 3, by using a genetically encoded calcium indicator (GECI) called Gcamp3 (Tian *et al.,* 2009). In addition, I investigate the activity of the SAA and SMB neurons during spontaneous locomotion, and specifically during omega/delta turns. For this purpose, I generated transgenic strains expressing a GECI in the SAA and SMB neurons, as well as the body wall muscles (BWMs). Due to the lack of a multifaceted video microscopy set up (automatic tracking of freely moving worms for long periods of time combining often calcium imaging with optogenetics) similar to those found in large *C.elegans* labs, or collaboration with any such lab, I instead recorded short consequent videos of freely moving worms under a normal fluorescent stereoscope, but fitted with a dynamic fast capturing camera (see Material and Methods section for more details).

4.1.1 Calcium imaging and GECIs

Calcium imaging is based in the use of calcium indicators that show the calcium ion status of a cell or tissue. Calcium is a messenger molecule that has an essential role in physiology. Calcium ions (Ca^{2+}) are transported into neurons both by action potential firing and synaptic input (Denk *et al.,* 1996; Miyakawa *et al.,* 1992). Neural activity, timing and frequency of action potentials, as well as levels of synaptic input, can all be quantified by measuring changes in intracellular free calcium ions (Pologruto *et al.,* 2004).

In *C.elegans*, calcium imaging is conducted with the use of genetically encoded calcium indicators (GECIs) based on fluorescent proteins that are stably expressed in targeted areas in transgenic strains. These GECIs are actually fluorescent proteins fused with calmodulin which binds to 4 calcium ions and undergoes a conformational change (Miyawaki *et al.,* 1997; Baird *et al.,* 1999; Nagai, Takeharu *et al.,* 2001). After years of research there are a number of available GECIs to work with such as Pericams, GCamps, cameleons etc. Some are FRET-based indicators, like cameleons, where the conformational change caused by the calcium binding to calmodulin brings two fluorescent proteins close and thereby changes the energy transfer between them (Miyawaki *et al.,* 1997; Nagai, T. *et al.,* 2004). Some are non-FRET indicators, like camgaroo and GCamps, where the conformational change alters the environment of only one fluorescent protein (Nakai *et al.,* 2001). Non-Fret indicators have been shown to have a greater dynamic range (Pologruto *et al.,* 2004). The GECI indicators are actually showing the calcium influx into individual neurons which then we translate into action potentials. Since it is very challenging to record these optical signals, a lot of research has gone into the optimization of GECIs. A lot of focus has been put lately on GCamps, which have been largely optimized. The GECI GCamp3, which is used in this chapter, has a higher affinity for calcium than previous GCamps (i.e GCamp and GCamp2), better photo stability and signal-to-noise ratio, and has been widely used since 2009 (Tian *et al.,* 2009).

4.2 Material and methods

4.2.1 Nematode maintenance and strains

Animals were kept at 20°C at all times, fed *E.coli* (OP50 strain) and were maintained as previously described (Brenner, 1974). *C. elegans* variety N2 Bristol wild-type strain was provided by the Caenorhabditis Genetics Centre (CGC), which is funded by the NIH Office of Research Infrastructure Programs (P40 OD010440). The ZW495 strain, which expresses a calcium genetic indicator in the body wall muscle, was also provided by CGC. Ablated strains SAA- (UL4207) and SMB- (UL4230), generated in Chapter 2 for this project, were crossed with the ZW495 and resulted in the strains SAA- x ZW495 (UL4228), SMB- x ZW495 (UL4227) (see Table 4.1). Neural calcium imaging strains, expressing the Gcamp3 calcium imaging indicator in SAA and SMB, were generated in this chapter as explained in the 'Methods and Materials' section 4.2.2; [*lad-2*::GCamp3 (UL4274), *flp-12sp*:: GCamp3 (UL4273), *lad-2*::GCamp3;SMB- (UL4275), *flp-12sp*:: GCamp3;SAA- (UL4276)]. Unfortunately, the strains expressing Gcamp3 in the SAA and SMD neurons (UL4274) (UL4275), as well as the (UL4276) were either not showing a Gcamp3 signal or the transformation marker used in the ablated animals, as well as the GFP expression in nearby

neurons, became an obstacle in tracking and measurement of the targeted cells. More on this discussed in section 4.4.4. Animals were assayed within the first 2 days of adulthood.

Table 4.1 Generated transgenic strains via crossing with the strain ZW495, for the expression of a calcium genetic indicator in the body wall muscle while either SAA or SMB are ablated.

Strains crossed	Screening Markers	Ablated cell	Strain name
SAA- (UL4207) x ZW495	*myo-2p*::mCherry and GCamp3 in the BWM	SAA	UL4228
SMB- (UL4230) x ZW495	*myo-2p*::mCherry and GCamp3 in the BWM	SMB	UL4227

4.2.2 Generation of the neural calcium imaging strains

4.2.2.1 Plasmid used

The *gcy-7p*::GCamp3 plasmid was a kind gift from the Chalasani laboratory (Tian *et al.,* 2009). It was used to drive expression of Gcamp3 calcium indicator in the neurons of interest; SAA and SMB.

4.2.2.2 Molecular biology

Promoter regions *lad-2p* and *flp-12sp*, which were amplified during work conducted in Chapter 2, were cloned into the *gcy-7p*::GCamp3 plasmid at the NaeI(blunt)/BamHI restriction sites once the *gcy-7p* region was excised. Promoter regions were only digested with BamHI before ligation (see appendix Table B.3).

4.2.2.3 Microinjections

The parent wild type strain used for generating the transgenic strains was the *C. elegans* variety N2 Bristol strain (Brenner, 1974), as well as, the main ablated strains generated in Chapter 2 for this project [ablated strains SAA- (UL4207) and SMB- (UL4230)]. Transgenic worms were generated by the means of microinjection (Mello *et al.,* 1991), whereby the constructs mentioned above were microinjected into the distal gonad of a young adult worm alongside with a transformation marker (Hobert, 2002; Evans, 2006). The transformation marker used was the *coel*::GFP that drives GFP expression in the coelomocytes of the worm, and was a gift from Piali Sengupta (Addgene plasmid # 8937) (Miyabayashi *et al.,* 1999). See Table 4.1 below.

Table 4.2 Transgenic strains generated for the expression of a calcium genetic indicator (Gcamp3) in the SAA and SMB neurons. Shown in red are the strains that were not used, as either the Gcamp3 was not expressed (UL4276), or was not visible in the targeted cells due to interference of the transformation marker used in the parent animals and the GFP expression in nearby neurons.

Strain injected	Plasmids injected	Marker	Expected expression of GCamp3	Strain name
N2	*flp-12sp*::GCamp3	*coel*::GFP	SMB	UL4273
N2	*lad-2p*::GCamp3	*coel*::GFP	SAA, SMD, ALN, PLN, SDQ	UL4274
SAA-(UL4207)	*flp-12sp*::GCamp3	*coel*::GFP	SMB	UL4276
SMB-(UL4230)	*lad-2p*::GCamp3	*coel*::GFP	SAA, SMD, ALN, PLN, SDQ	UL4275

4.2.3 Calcium imaging experiments of freely moving worms

4.2.3.1 Body wall muscle calcium imaging

The caps of 0.5ml eppendorf PCR tubes were glued with aquarium sealant onto a clean microscope slide (I dubbed them 'micro-plates') (see Figure 4.1, Image A). Drops of NGM agar were left to solidify in the micro-plates and the micro-plates were immediately sealed with parafilm. Once the worm was transferred, with the use of an eyelash, to the micro-plate, there was a window of approximately 10 minutes of video-tracking before both the plate and the worm dried up. Within the first minute after transfer the worm was left to recover and no video-tracking took place. Since the platform of the fluorescent scope was fixed, the videos were conducted in intervals of 20 seconds, as this was the longest time the worm was in frame at the magnification required to observe muscle activity. When the worm moved out of frame the video tracking was manually terminated. To obtain base line calcium readings in the body wall muscle, animals were anaesthetised by the use of azide (5mM). Images for the body wall muscle were processed with Q-Imaging's Q-capture Pro 7 software, which automatically subtracted the background drawn on the image from the intensity measurements (Figure 4.2). From each worm video captured an independent dorsal and ventral bend was measured unless the quality of the video rendered that impossible. Intensities of the head bends were represented as dorso/ventral or ventral/dorsal ratios. In this way, the comparison between different worms was more accurate, as there is variability in the Gcamp3 expression across individual worms. Moreover, while comparing wild type and the ablated animals' undulation bends, the intensity of calcium in the BWM per se is not as important as the ratio between the

dorsal and ventral part of the head which reflects how contracted and how relaxed each side of muscles are.
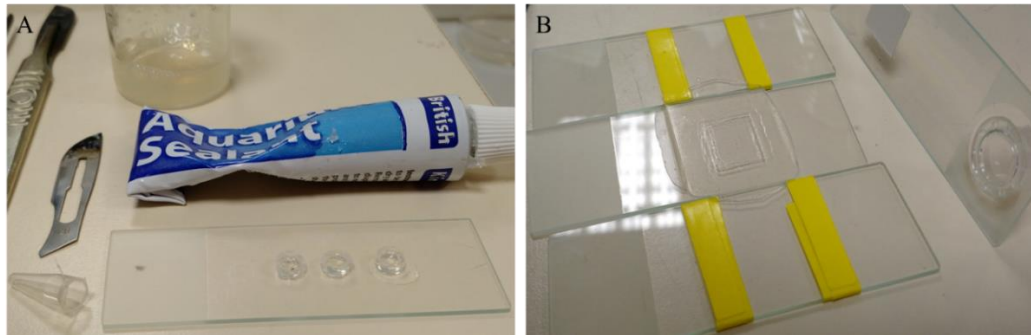
Figure 4.1 Images of NGM agar micro-plates and pads. A) Image showing the construction of NGM agar micro-plates. B) Image showing the construction of NGM agar pads.
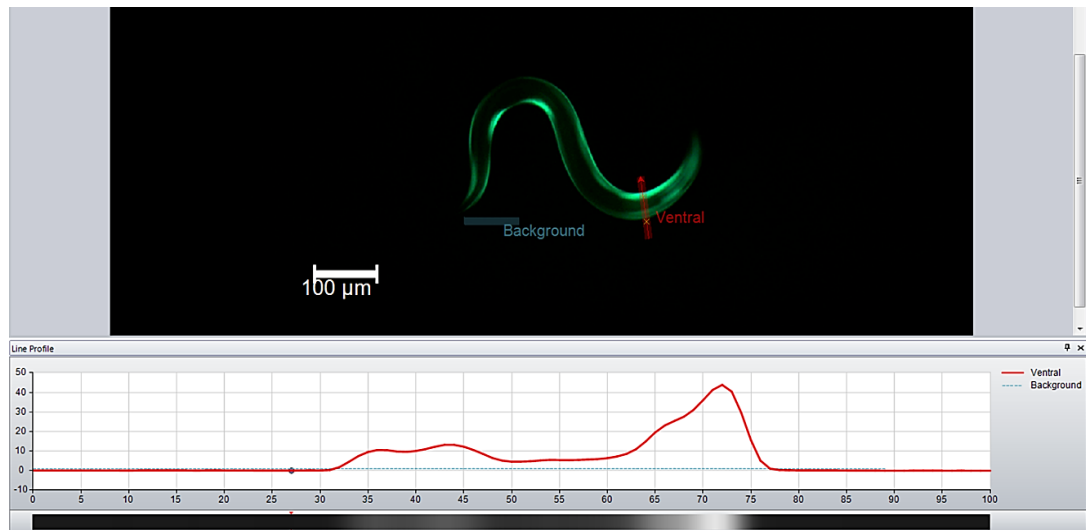
Figure 4.2 Representative snapshot of measurements taken using Q-Imaging's Q-capture Pro 7 software. One line had to be drawn on the area of interest (red: middle area of the head bend), and one had to be drawn on the background (blue: below tail of worm) so corrections could be made for any background fluorescent signal. The line profile below the image shows the intensities measured along the line of interest (left-to-right; dorsal-to-ventral). Red line on the graph reflects the red line drawn on the bend and blue line is the background measurement.

4.2.3.2 Neural calcium imaging

NGM agar pads were made as shown in Image B, Figure 4.1. I followed Monica Driscoll's mounting protocol described in WormBook (Shaham, 2006) with a few changes. I used 1.7% NGM agar for the pads, the worms were alive and freely moving. Once the worm was transferred, with the use of an eyelash, onto the agar pad, a thin cover slip was gently put on

top. The cover slip not only kept the worm and the pad humid enough for long video-tracking, but also slowed down the worm (approximately 3 times lower than its normal velocity; from the ethograms created in Chapter 3 an omega turn takes approximately 4-6 seconds to be performed, here it took approximately 15 seconds). This facilitated the calcium reading of the individual neurons while the worm moved freely. Within the first minute after transfer, the worm was left to recover and no video-tracking took place. Since the platform of the fluorescent scope was fixed, the videos were conducted in intervals of 20 seconds, as this was the longest time the worm was in frame at the magnification required to observe cell activity. When the worm moved out of frame the video tracking was manually terminated. To obtain base line calcium readings of the neurons, animals were anaesthetised by the use of azide (5mM). Images for the individual neural readings were processed, and neurons were tracked, with the use of a custom software scripted by my colleague Christopher Brittin, using a new type of correlation filter for visual tracking; a Minimum Output Sum of Squared Error (MOSSE) filter (Bolme *et al.,* 2010) (Figure 4.3). Background was subtracted from the measurements. Neural calcium intensity was normalised towards the maximum signal and graphed towards time (10^{-1}sec).

Figure 4.3 Representative movie snapshots taken while tracking the SMB neurons with the use of a custom software scripted by my colleague Christopher Brittin, using a new type of correlation filter for visual tracking.

4.2.4 Video Microscopy

A ZEISS stereo Lumar V12 was used to screen for transgenic animals. For the body wall muscle calcium imaging on freely moving worms, a Leica M165 FC fluorescent stereoscope fitted with a Q-imaging Qi-CLICK COOLLED pE-300 camera was used. For the neural calcium imaging on freely moving worms, a Leica M165 FC fluorescent stereoscope fitted with a high dynamic range streak Hamamatsu camera was used. Images were captured with

Q-Imaging's Q-capture Pro 7 software for the body wall muscle readings and Micro-Manager software (version 1.4) for the individual neural readings (Edelstein *et al.,* 2014).

4.2.5 Statistical analysis

Comparisons between tested animals and matched controls were conducted by using one-way analysis of variance (ANOVA) followed by Tukey's multiple comparisons test. Analysis was performed using GraphPad Prism (version 6.01), GraphPad Software, La Jolla California USA, www.graphpad.com.

4.3 Results

4.3.1 BWM calcium activity during head bends in SAA- and SMB- ablated strains compared to controls.

Direct observation of the tested strains revealed a correlation between Gcamp3 expression, and therefore calcium influx in the body wall muscles (BWM), measured as GFP intensity, and body bends. In the part of the bend where the muscle is contracted, calcium influx was high. On the other hand, at the direct opposite part of the bend, where the muscle was relaxed, it was lower. To the naked eye, the dorsoventral (or ventral/dorsal) ratio in GFP intensity seemed to be different between the wild type animals and the ablated strains (Figure 4.4, Images A, B, D, E, G and H; Figure 4.5, Images A-C). Anaesthetised worms, which mostly did not form body bends anymore, but were rather in a straight posture, expressed Gcamp3 at a very low level (Figure 4.4, Images C, F and I). Moreover, specific measurement of a straight anaesthetised animal showed that at this posture muscles have a low and similar calcium influx on both sides of the body (see Appendix section F, Figure F1). Finally, as the worm does not form perfect undulatory postures, calcium influx during body bends decreases posteriorly down the body during forward locomotion (see Appendix section F, Figure F1, Image C and Graph D).
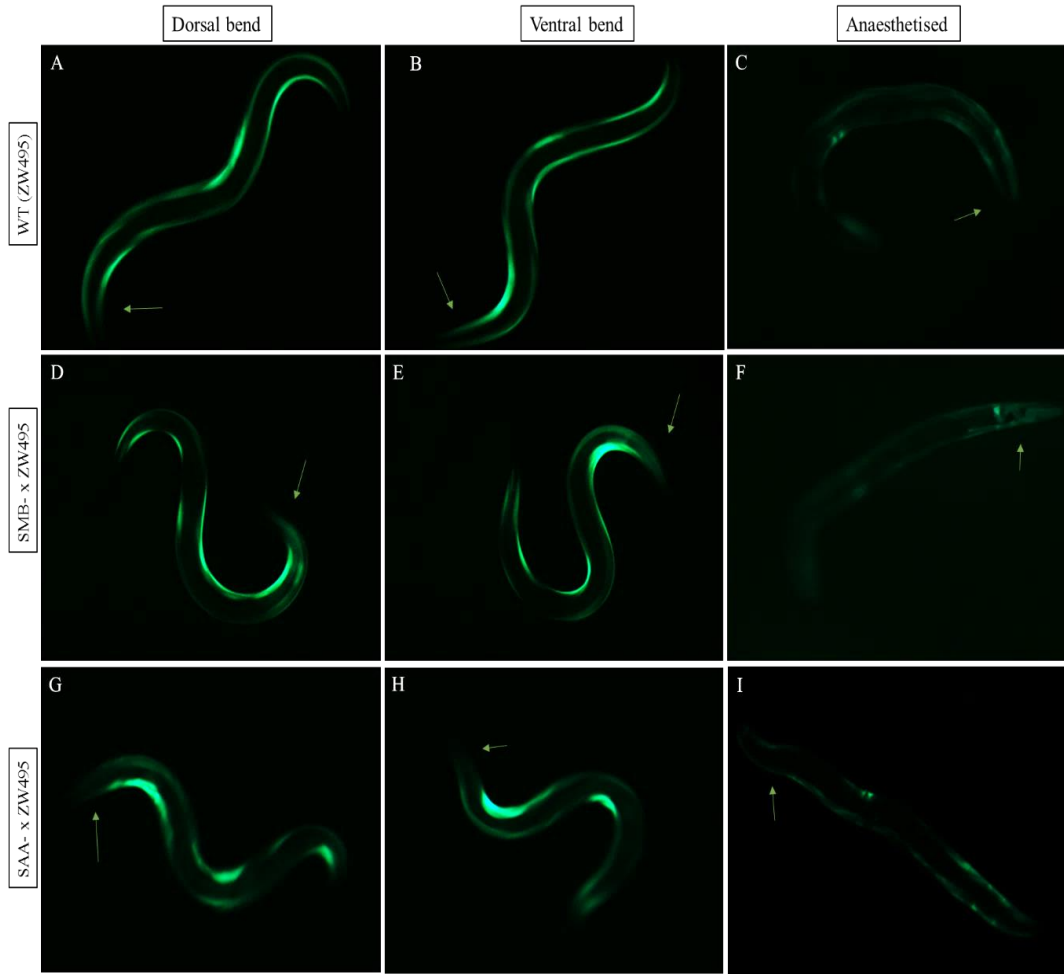
Figure 4.4 Dorsal and ventral head bending images expressing Gcamp3 in the BWM. Wild type (Images A-B), SMB- ablated (Images D-E) and SAA- ablated (Images G-H) animals expressing Gcamp3 in the BWM. Images C, F and I show worms that have just been anaesthetised with azide (control Gccamp3 expression in BWM, for a measurement on this see Appendix section F, Figure F1, Image A and Graph B). Green arrows show the area of the head.
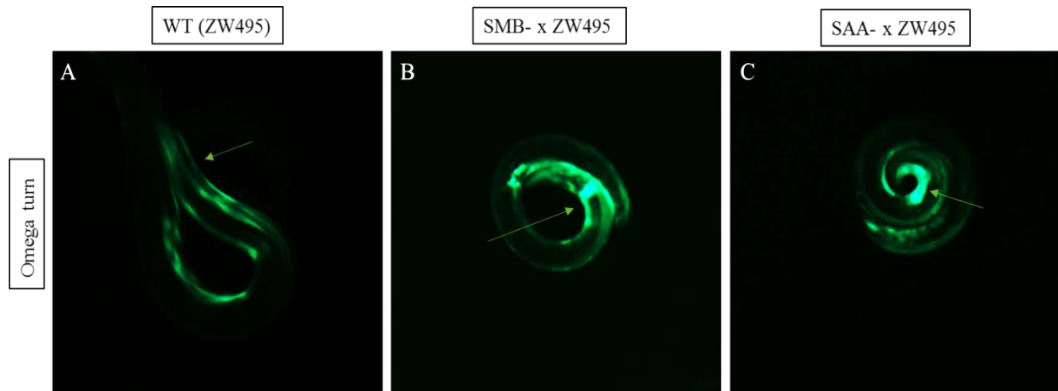
Figure 4.5 Omega turns formed by animals expressing Gcamp3 in the BWMs. Omega turns formed by wild type (A), SMB- ablated (B) and SAA- ablated (C) animals expressing Gcamp3 in the BWM. Green arrows show the area of the head.

Specific measurements of both dorsal and ventral head bends of the assayed animals supported the observations described above, and the results are shown in panel E of Figure 4.6. Both the SAA- and SMB-ablated animals exhibited increased Dorsal/Ventral and Ventral/Dorsal ratios in comparison to wild type animals. The difference was statistically significant. SAA- ablated worms' measured bends were twice as high in intensity as the wild type. SMB- ablated worms' measured bends were three times as high in intensity as the wild type. Interestingly, dorsal head bends of the SMB-ablated animals were different to the ventral ones, with the ventral bends showing a greater ratio. The other two strains (SAA-ablated and wildtype) tested did not exhibit such a difference.
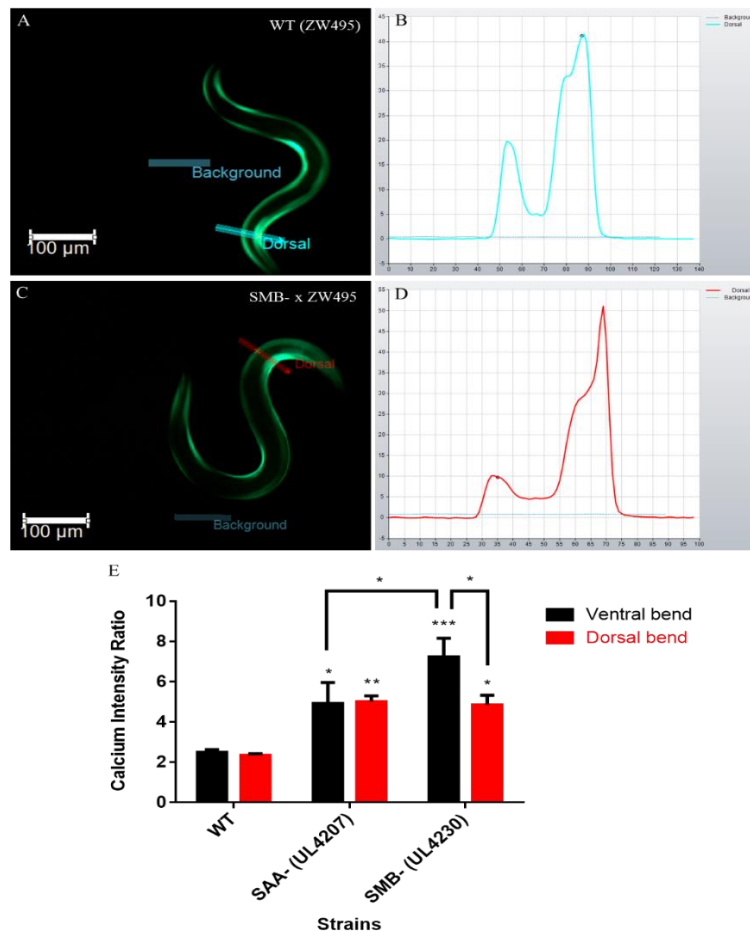
Figure 4.6 Comparison of head bending BWM calcium intensity ratios of wild type, SAA-ablated and SMB-ablated animals. Images A-D show representative head bends (A, C) and their respective graphs (B, D). Graph E shows the Dorsal/Ventral and Ventral/Dorsal ratios of dorsal and ventral bends, respectively, for all tested strains (WT Dorsal bends, n=9 and Ventral bends, n=8; SMB- x ZW495 Dorsal bends, n=9 and Ventral bends, n=11; SAA- x ZW495 Dorsal bends, n=9 and Ventral bends, n=10). Statistical significance and error bars as STDEV, indicated. {A two-way analysis of variance (ANOVA) and Tukey's multiple comparison were used; ***p<0.001; **p<0.01;*p<0.05.

4.3.2 SMB increases its activity at the onset of an omega turn

Continuous measurements of the SMB somas and nerve ring area from six independent worms, showed an increase in intensity in a graded way. An increase was observed on the onset of the omega turn behaviour (Figure 4.7, Images A-D; Figure 4.8, yellow arrow on Graphs A-F), reaching its peak after the onset and right before the exit of the omega turn (Figure 4.7, Image E; Figure 4.8, red star on Graphs A-F). After the peak a decrease in intensity was observed (Figure 4.7, Image F; Figure 4.8, blue arrow on Graphs A-F). The peak of intensity that was recorded after the onset of the omega turn was taking place approximately 2-3 seconds after the onset (Figure 4.8, red star on Graphs A-F). It is at this time when the worms' over flexed head has reached the body and starts to bend on the opposite side (head bend recovery from the deep turn) (Figure 4.7, Image E). The actual measurements from the tracker depict similar results with the observations from the video footage (Figure 4.8, Graphs A-F). Variability between the strains was obvious, however, the pattern in which the calcium slightly increases on the onset and then highly increases within 2 seconds when the head starts to bend on the other side was similar. When the worms were consequently anaesthetised with azide (5mM), calcium intensity was low and constant (grey lines in Graphs A-F, Figure 4.8), even in the worms expressing high levels of Gcamp3 (Figure 4.8, Images C, E and F).
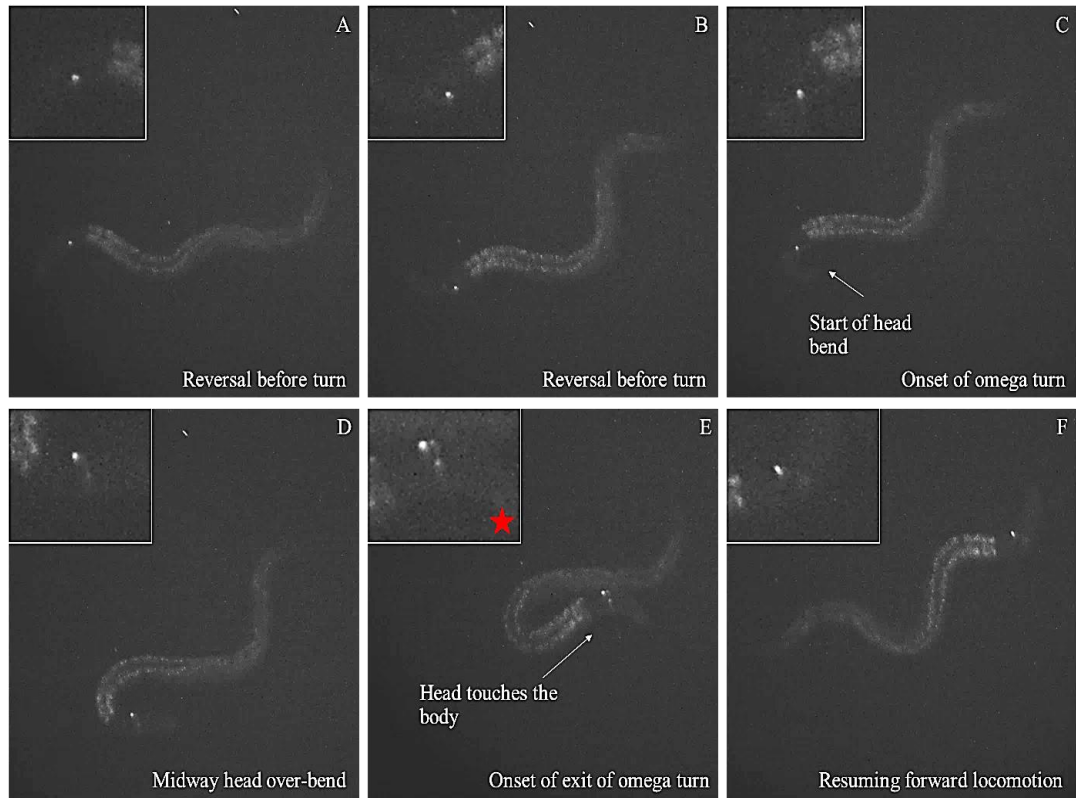
Figure 4.7 Representative video tracking images of an omega turn while measuring activity of SMB via the intensity of calcium influx in the somas of the neurons and the nerve ring (NMJ's localisation). Images A and B depict the reversal before the turn, image C shows the head starting to bend. Image D is a snapshot midway head bending, the first noticeable increase of calcium starts here. Image E shows the snapshot of approximately the highest increase of intensity (red star), where the head has just touched the body and the head bending resets t the opposite side. In image F the worm has finished the turn and resumes its forward crawling.
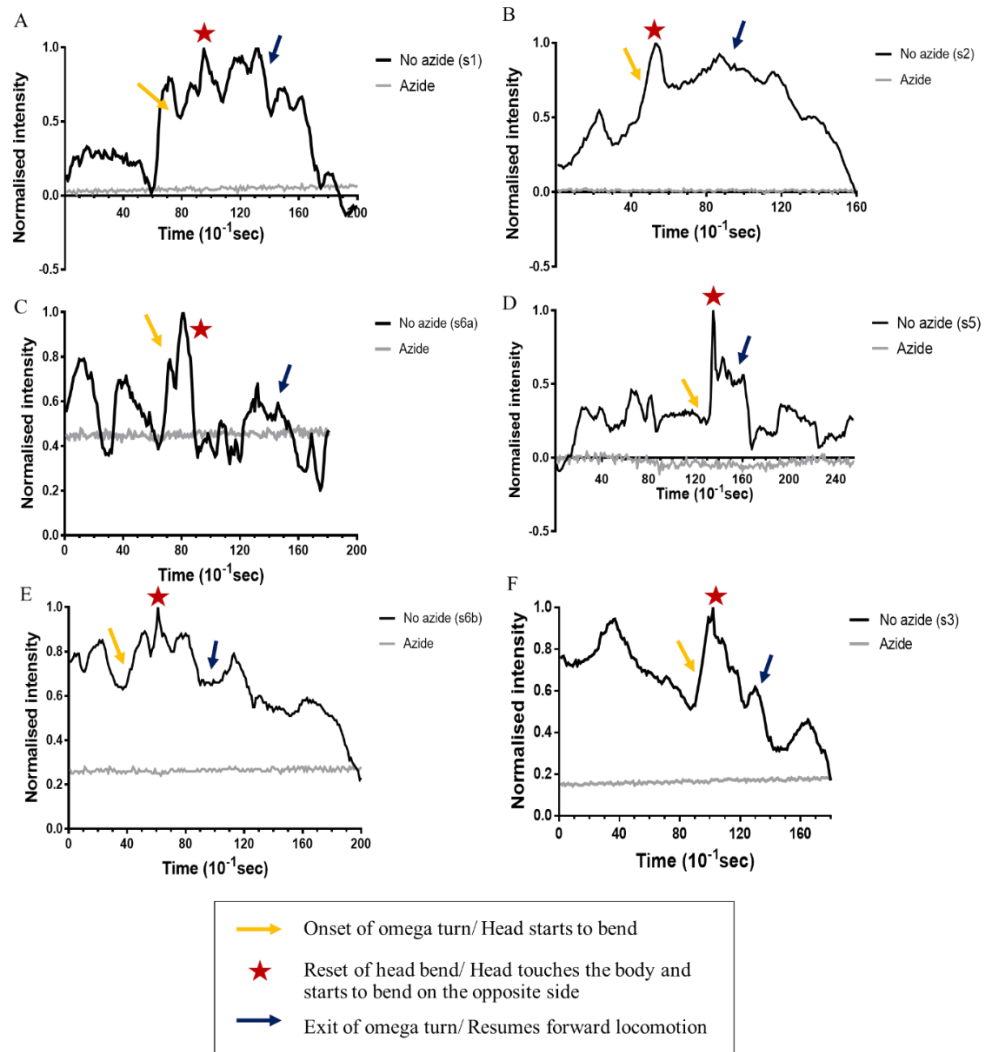
Figure 4.8 Graphs of calcium measurement intensities from freely moving worms while performing an omega turn (black lines) vs graphs of the same worms anaesthetised with azide (5mM)(grey lines). Measurements are shown with the background intensity subtracted and normalised to the maximum signal. Yellow arrow indicates the onset of the omega turn, when the head starts to bend. Red star indicates the approximate time the measured area achieved the highest increase of intensity. Blue arrow indicates the exit of the omega turn, when the worm resumes its forward locomotion.

4.4 Discussion

4.4.1 SMB's activity to the BWMs seems to be either inhibitory or excitatory working in antiphase to the SMD

When SMB is ablated it seems that the calcium influx in the muscles is increased on the one side and decreased on the other. This translates into more contracted muscles on the one side, either dorsal or ventral, and more relaxed on the other, as explained in detail in Chapter 1:

General Introduction. Thus, the body of the worm exhibits more loopy postures, as described in detail during Chapter 3. All of the above, suggest an inhibitory or opposite to the SMD excitatory effect has been lifted from the muscles. This means either SMB is inhibitory to muscles or by ablating SMB- then RME's inhibitory effect to the muscles is been lifted or that SMB is excitatory in antiphase of the excitatory SMD. Previously it has been hypothesised that SMB is excitatory to the muscles by *in silico* models (Izquierdo and Beer, 2013; Karbowski *et al.,* 2008; Sakata and Shingai, 2004), partly due to its neurotransmitter acetylcholine (Ach) which is mainly an excitatory neurotransmitter (Liu *et al.,* 2009). However, Pereira *et al.,* argued recently that acetylcholine (Ach) has also an inhibitory function in *C.elegans* (Pereira *et al.,* 2015). The only head motor neuron with known inhibitory connections to the muscle is RME, which is GABAergic, hence the inhibitory connections (McIntire *et al.,* 1993; Liu *et al.,* 2009). RME- ablation results in a milder loopy phenotype to SMB- and an opposite result to SMD- ablation; i.e. SMD- has is shallower than wildtype (Gray, J.M. *et al.,* 2005; Shen *et al.,* 2016). RME neuron's activity and function in sinusoidal locomotion was shown to act independently to the SMB neuron, but is dependent on the SMD neuron (Shen *et al.,* 2016). This means that the undulatory exaggerated phenotypes I observed because of SMB ablation, is not likely linked to lifting off inhibition of RME through SMB/RME's synaptic connectivity. This leaves us with either SMB being itself inhibitory to muscles or SMB is excitatory in antiphase of the excitatory SMD. However, the nature of connectivity of SMB to the muscles still remains unclear and both possibilities will be taken into consideration in Chapter 8: General Discussion where I propose a testable model circuit for head movement.

The overall indirect effect of the SAA interneuron on the muscle seems to be similar too, but not as much as the SMB motor neuron ablation demonstrates. In line with the hypothesis discussed at the end of Chapter 3, it seems that what one might be observing here is a summative result of SMD dysfunction (loss of excitatory activation to the BWMs) and SMB dysfunction (loss of inhibition or antiphase excitatory to the BWMs) due to the ablation of the SAA that regulates both. Alternatively, it could be that ablation of SAA caused SMD to be less active (SAA is presynaptic to SMD and their connections are dense(White, J.G. *et al.,* 1986)) and thereby RME became less active lifting some of the inhibition it imposes on the BWMs of the head. This would be clarified if activity was measured on the RME's while SAA is being ablated, just as Shen *et al.,* did with RME, SMB and SMD head motor neurons (Shen *et al.,* 2016).

4.4.2 SMB increases its activity after the onset of an omega turn

Continuous measurements of the SMB somas and nerve ring area showed that SMB neurons increase in activity after the onset of an omega turn, when the head over bends from the normal undulation of a head bend. What was descriptively observed in Chapter 3 is now shown in neural activity. It is interesting that calcium influx was not only observed in the somas, but also in the area of the nerve ring, were the SMB neurons are coupled with the muscles via neuromuscular junctions. It is also interesting that the highest activity is recorded after the onset of the omega turn. Given the fact that SMB has just been discussed to be inhibitory to the muscles, it seems possible that the SMB neurons are [predominantly] acting on the side of the body that needs to stay in a relaxed state, so that the other side of the body contracts even more to fulfil the whole posture of the omega turn. However, taking into consideration the coiled omega turn postures observed in Chapter 3 and in this chapter, SMB could also be inhibiting the side of the body that contracts during the omega turn, and thus bring it back to the relaxed state, so that the worm can slide off the body to the opposite side, and resume forward locomotion. Again, I would like to emphasize how SMD seems to work as an antagonistic motor neuron to SMB as ablation of SMD results in shallow omega turns (Gray, J.M. *et al.,* 2005), suggesting that it is excitatory to the muscles and it is the head motor neuron applying the over-bend during the omega turn posture.

4.4.3 Ventral bias observed at the body bends of the ablated SMB strain

Interestingly, a ventral bias was observed while measuring BWM activity on the SMB-ablated worms' body bends. Body bends of the SMB- ablated worms, but not the SAA ablate worms, had higher ventral/dorsal ratios (ventral bends) than dorsal/ventral ratios (dorsal bends). Does the worm have an innate ventral bias in its sinusoidal locomotion that gets accentuated with SMB ablation? We do know that the vulva of the worm is ventrally positioned and that omega turns are ventrally biased (Broekmans *et al.,* 2016), this bias removed by RIV ablation (Gray, J.M. *et al.,* 2005).

It has also been reported that altering the dorsal B-type motor neurons causes a ventral bias in the bending (Goulding, 2012). B-type motor neurons have been suggested to have proprioceptive function (Leifer *et al.,* 2011; Wen *et al.,* 2012). Could it be that by ablating SMB some dorsal proprioceptive information is lost and it results in a ventral over bend? Neurons of interest will be observed for stretch receptor expression in Chapter 7. Skeletonisation of SMB- ablated worms' body postures by an algorithm that can cope with coiled shapes, could also be useful in clarifying this. An experimental algorithm is being

developed by my colleagues in Computing but has not being completed by the time this thesis is being written.

4.4.4 Future direction and troubleshooting for the Gcamp3 strains that did not work

The transformation marker used in the ablated animals (mCherry in the pharynx), as well as the GFP expression in nearby neurons (SMD in the case of Gcamp3 expression driven by *lad-2p*), became an obstacle in tracking and measuring intensities of the targeted cells. Even if the GCapm3 was expressed in the neurons, it was not visible with the equipment at hand. As far as the SAA measurements are concerned, with our set up it was impossible to distinguish between the SAA and the SMD neurons. A collaboration with the Zimmer lab that started the month this thesis is being written will try to bypass these obstacles as their microscopy set up tracks automatically freely moving worms, corrects for worm and neural movement inside the worm and can track at higher magnification. .

If I had to generate these strains again, I would use a transformation marker expressing in the lower part of the body and not the head. Moreover, I would move on to use the better GECIs that have been developed in the meantime, such as GCamp6 and GCamp7, developed from the Nakai laboratory, which produce greater signals than previous versions (Smedemark-Margulies and Trapani, 2013). Finally, I would try to split the Gcamp3 into two subunits and express them, instead of the CED-3 caspase, within the dual-component reconstitute system designed by Chalfie and Chellur (2007) that I used for the ablation of the neurons of interest (Chapter 2). In this way, I could have Gcamp expression targeted to cells that don't have a unique promoter region, such as SAA. This has not been done yet, and if successful, it would not only be novel but also extremely helpful in measuring activity on cells otherwise difficult to measure.

Chapter 5
Role of the SAA and SMB neurons in chemotaxis

5.1 Introduction

Many of the worm's behaviours are achieved through its ability to orient itself towards a targeted destination. When the worm senses an attractive cue it will re-orient itself to follow it, whereas it will try to re-orient itself away from a repellent cue (taxis). Observed behavioural motifs and computational elements have separated two strategies of spatial orientation observed during chemotaxis in the worm; the pirouettes and the weathervane (steering) (Pierce-Shimomura *et al.,* 1999; Iino and Yoshida, 2009; Lockery, Shawn R., 2011; Faumont *et al.,* 2012; Dusenbery, 1980; Ward, S., 1973). In Chapter 1: General introduction, both strategies of orientation and how the worm performs them, were described in detail. Also, the initial hypothesis for SAA and SMB's involvement in steering, via SAA's regulation of SMB motor neuron resulting in the control of head bending, was introduced. This hypothesis was strengthened with the results in Chapter 3. Behavioural analysis showed that both SAA and SMB neurons regulate the amplitude of head swings during undirected locomotion. It has been demonstrated that the worm steers by gradually adjusting the turning angle of its head swings and the body follows it (Iino and Yoshida, 2009; Kim, D. *et al.,* 2011). Regulating how deep or shallow the head swings are, on either the dorsal or the ventral side, is a very important and required element for the worm to be able to steer in a specific direction, as it can lead to gradual turning (Izquierdo and Beer, 2013). The fact that the results in the same chapter also showed that the SAA and SMB inhibit turns to facilitate runs, made me consider that they may play a role in both strategies, as during the pirouette strategy the worm exhibits short runs interrupted by sharp re-orientation turns.

This chapter focuses initially on the role of the SAA and SMB neurons in directed locomotion generally, and consequently on steering specifically. Worms were put into chemotaxis assays where both strategies were observed and their performance noted. Afterwards, I aimed to set up an assay favouring steering over pirouettes, whereby I could observe whether the ablated worms were able to steer, and if so, how efficient they were at that. Efficiency and ability of the worms to orient itself towards the NH_4Cl soluble salt attractant was shown by measuring the chemotaxis index, frequency of pirouettes, weathervane index, time to reach peak of gradient and the visualisation of trajectories. Unfortunately, the coiled phenotypes of the transgenic strains made it impossible to skeletonise their trajectories using either Kerr's multi-worm tracker software (Yemini *et al.,* 2011) or the 'worm' script in Image J (Schindelin *et al.,* 2012), and compare their trajectory angle bearing towards the peak of the gradient as Iino

and Yoshida did in their study (Iino and Yoshida, 2009). An experimental algorithm that can cope with coiled shapes is being developed by my colleagues in Computing, but has not being completed by the time this thesis is being written. High definition visualisation images of the real tracks of the worm I was able to produce though, proved to give a good comparison between the strains.

5.2 Material and methods

5.2.1 Nematode maintenance and strains

Animals were kept at 20°C at all times, fed *E.coli* (OP50 strain) and were maintained as previously described (Brenner, 1974). *C. elegans* variety N2 Bristol wild-type strain was provided by the Caenorhabditis Genetics Centre (CGC), which is funded by the NIH Office of Research Infrastructure Programs (P40 OD010440). The ablated strains SAA-(UL4207) and SMB- (UL4230) used throughout this chapter were generated for this project (see chapter 3). Animals were assayed in the first 2 days of adulthood.

5.2.2 Video-microscopy

For all behavioural experiments in this chapter a custom built multi-worm tracker was used, set up by my postdoc colleague Robert Holbrook, consisting of a Navitar telemetric lens and a XIMEA xiQ super-speed camera mounted on a Fotomate macro slider / Manfrotto 410 geared head, and a Polytech LED red light circular system (Figure 3.2, Image B, Chapter 3).

5.2.3 NH$_4$Cl radial chemotaxis assay

The protocol followed for the NH$_4$Cl radial chemotaxis assay, was adapted from previously published protocols, after preliminary testing of what worked best in the wet lab and for the generated strains (Ward, S., 1973; Pierce-Shimomura *et al.,* 1999; Iino and Yoshida, 2009). Well-fed first day adults of synchronised age were transferred with the use of an eyelash to a 24 well microtiter plate filled with chemotaxis (CTX) buffer (5mM KPi, 1mM CaCl$_2$, 1mM MgSO$_4$ in ddH$_2$O). They were then transferred five times from well to well, with the use of a sterile glass Pasteur pipette, and left in CTX for one hour. The 9cm chemotaxis assay plates (CTX agar) were prepared the day before (5mM KPi, 1mM CaCl$_2$, 1mM MgSO$_4$ and 1.7% agar). The plates were seeded with a 5 μl drop of 500mM NH$_4$Cl in the middle of the plate at two different times, t_1 and t_2, before the experiment ($16 \leq t_1 \leq 17$ hr; $t_2 = 3$ hr), as described

in Pierce-Shimomura *et al.,* (1999) so that the gradient formed was similar to Figure 5.1, Image (A). The washed worms were transferred with a mouth-pipette 2cm away from the centre of the plate and 3 cm from each other. Figure 5.2, Image (A) illustrates the set-up of the plate and Figure 5.3 (top left) a simplified schematic of the radial gradient formed. Video-tracking was initiated immediately and lasted until after the worms reached the peak with a maximum of a 20 minute recording for the wild type and a 60 minute recording for the ablated animals. For the wild type animals 20 minutes was enough for them to reach the peak as previously shown (Ward, S., 1973; Pierce-Shimomura *et al.,* 1999; Iino and Yoshida, 2009), the rare few that did not reach the peak were never aligned to the gradient and went on crawling towards the lid. The ablated worms, however, although most were orienting themselves to the peak their defects in navigation made them take longer to reach it. Therefore, I video tracked them for up to 60 minutes to assess their efficiency. After an hour of recording it was deemed unnecessary to resume as the gradient would have changed largely from the one initially formed (Ward, S., 1973).

Videos were captured at 10fps with the use of StreamPix 7 (version 7.2.1) software built by NorPix. Parafilm was used to seal the plate during the gradient formation, and the petri dish lid was left on throughout the experiment, but unsealed. Eighteen animals were tracked for each strain, 3 animals per plate. Additional animals were tested in control plates were ddH_2O, instead of NH_4Cl, was dropped. Experiments were conducted at 20°C, plates and strains were randomised with the use of a dice. Trajectories were visualised with FIJI software (Schindelin *et al.,* 2012).

5.2.3.1 Chemotaxis index

In order to calculate the chemotaxis index of the tested strains, the assay plates were divided into two regions; A and B. A was the region of the peak of the gradient (5 mm in diameter, which is the approximate surface the 5μl drop of NH_4Cl covers). B was the rest of the plate. The formula used was taken from Bargmann and Horvitz (1993): $CI = (A - B) / (A+B)$, where A is the number of worms reaching and staying in the area of the peak of the gradient and B the others that do not (Bargmann, C. I. and Horvitz, 1991; Bargmann, C. I. *et al.,* 1993). A +1.0 score indicates that 100% of the worms arrived at the peak of the attractant and reflects to high efficiency of navigation. An index of -1.0 is indicates that none of the worms reached the peak and reflects a navigational defect.

5.2.3.2 Pirouette strategy analysis

In order to quantify the extent to which the tested animals performed pirouettes, the frequency and index of that orientation strategy was calculated. The frequency is shown as events of pirouettes per minute. See red tracks representing pirouettes in Figure 5.1, Image (B). Extremely short reversals that didn't change the angle of the trajectory were not counted as

pirouettes (Pierce-Shimomura *et al.,* 1999). When the ablated animals exhibited multiple pirouettes without a run interrupting them, they were counted as individual pirouettes only if the trajectory changed orientation.

5.2.3.3 Weathervane strategy analysis

In order to quantify the weathervane strategy (steering) performed by the different strains, the index of that orientation strategy was calculated. The index is adapted from the original chemotaxis index formula (Bargmann, C. I. *et al.,* 1993) and it represents the time spent on one strategy against the other. When compared to wild type animals it reflects the mutant's inability to steer. The formula is as follows: $WI = (Wt - Pt) / (T)$, where Wt is the time they spent on steering (weathervane), Pt is the time the worms spent performing pirouettes and T the total tracking time until the animal reaches the peak of the gradient (a circular area surrounding the centre of the plate, 5mm in diameter). See Figure 5.1, Image (B).
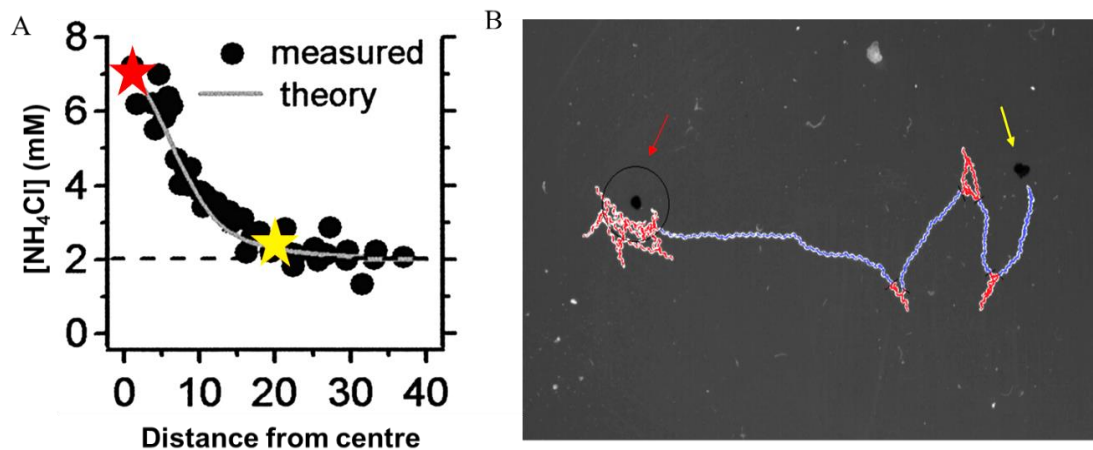
Figure 5.1 The diffusion profile of the radial chemical gradient and an example of a worm navigating it. A) Graph showing concentration of NH_4Cl versus distance from the peak of the gradient, formed by 5μl drops of NH_4Cl at two different time points. The yellow star shows the approximate starting point of the animals in the radial experiments conducted for this project. The red arrow shows the peak of the gradient. Image edited from (Pierce-Shimomura *et al.,* 1999). B) Image showing an actual track of a wild type animal orienting itself up a radial gradient. Tracks while performing the weathervane strategy (runs) are in blue and pirouettes (tumbles) are in red. Yellow arrow indicates the animal's starting point, 2 cm from the NH_4Cl drop. Red arrow and black circle indicates the area the drop occupies, which is considered here as the peak of the gradient.
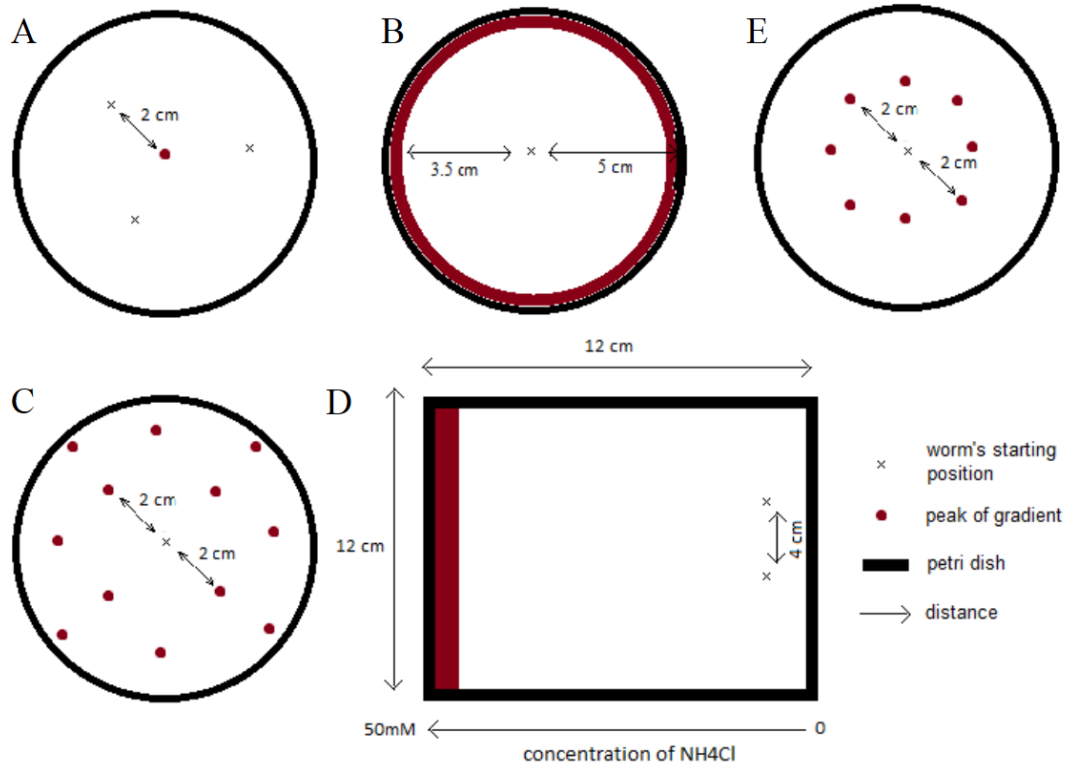
Figure 5.2 Images showing each different experimental set up tested; radial (A), annulus (B), circular grid (C), 12 grid (D) and linear (E) assays. The starting point of animals (X), NH₄Cl drop points (red) and distances are indicated.
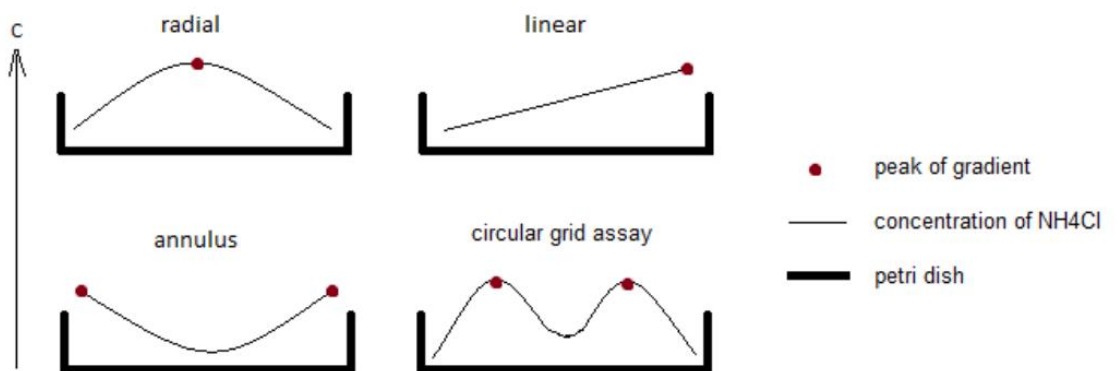
Figure 5.3 Image showing simplified concentration decreases and increases of NH₄Cl in each different experimental set up tested; radial, linear, annulus and circular grid assays.

5.2.4 NH$_4$Cl steering assays

After the orientation performance of the tested strains was observed, I wanted to focus more on steering. I aimed to observe the ability of the ablated strains to perform the weathervane strategy in a more deterministic way by limiting the performance of pirouettes to the minimum. A series of preliminary gradient assays were performed at the multi-worm tracker, in order to pin down the ideal steering assay. The assay that gave the lowest counts of pirouettes but the highest performance possible of steering was favoured. Figures 5.2, Images (B-E) and 5.3 show the simplified experimental set ups and gradients formed in the steering assays, respectively.

I called the assay depicted in Figure 5.3, Image (B) the 'annulus' assay because the peak of the gradient is a uniform area forming an annulus shape at the ends of the 9cm circular petri dish. After the CTX agar (0mM of NH$_4$Cl) was poured (15ml in volume) in the 9cm petri dish assay plate, a sterile petri dish 1.5 cm smaller than the assay plate was used to cut the outer rim out of the plate. The annulus shape formed was filled with CTX agar plus 50mM of NH$_4$Cl, and the plate was left overnight for the NH$_4$Cl to diffuse. The experiments were conducted within 12-34 hours after this pouring took place. The worms were treated as described in methods sub-section 5.3.1, but this time their starting point was at the centre of the plate (see Figure 5.2, Image B).

The 12 grid assays were performed as previously published, by dropping 12 drops of 200mM of the attractant 1 hour before the assay on a 9cm CTX agar petri dish assay plate (see Figure 5.2, Image C) (Iino and Yoshida, 2009).

The linear gradient assay was conducted following a previously published protocol (see Figure 5.2, Image D) (Luo *et al.,* 2014). 12 ml of CTX agar plus 50mM of NH$_4$Cl were poured on a 12.5 cm x 12.5 cm rectangular plate with an inclination. After the agar solidified, the plate was filled with 12 ml of CTX agar (0mM of NH$_4$Cl) while the plate was now sitting level on the bench. The plate was left overnight for the gradient to be formed. Assays were conducted 12 to 24 hours after the pouring of the plate as noted by the published protocol.

5.2.5 Circular NH$_4$Cl assay

I called the assay depicted in Figure 5.3, Image (E) the 'circular' grid assay because the peaks of the gradients are formed by 8 drops of the attractant NH$_4$Cl, placed in the shape of a circle surrounding the centre of the plate. The drops have a distance of 2 cm from the centre. The shape of the set up was drawn on a transparency placed under the petri dish so that the circle formed was always the same size (Figure 5.3, Image E). Again the CTX plate was poured the night before the experiment (15ml in volume), however, the drops this time were placed an

hour before the assay as conducted in the Iino and Yoshida (2009) 12 grid protocol (1μl of 200mM NH$_4$Cl). The worms were treated as described in methods sub-section 5.3.1, but this time their starting point was the centre of the plate.

Video-tracking was initiated immediately and lasted approximately 15 minutes for the wild type (all of them reached a peak before the original 20 minutes tracking time) and 45 minutes for the ablated strains. The radial assay experiments conducted previously on the ablated strains predicted the approximate times needed for recordings (average time required to navigate 2 cm of distance plus the standard deviation). Videos were captured at 5fps with the use of StreamPix 7 (version 7.2.1) software built by NorPix. Parafilm was used to seal the plate during gradient formation, and the petri dish lid was left on throughout the experiment, but unsealed. Twelve animals were tracked for each strain, 1 animal per plate. Additional animals were tested in control plates were ddH$_2$O, instead of NH$_4$Cl, was dropped. Experiments were conducted at 20°C, plates and strains were randomised with the use of a dice. Trajectories were visualised with FIJI software (Schindelin *et al.,* 2012). Chemotaxis index, pirouette frequency and index and weathervane index were calculated as explained in section 5.2.1, above.

5.2.6 Statistical analysis

Comparisons between tested animals and matched controls were conducted by using one-way analysis of variance (ANOVA) followed by Tukey's multiple comparisons test. Analysis was performed using GraphPad Prism (version 6.01), GraphPad Software, La Jolla California USA, www.graphpad.com.

5.3 Results

5.3.1 Navigational tracks of the SAA- and SMB- ablated animals are consistently different to the wild type

Both the SAA- and SMB- ablated animals were able to sense and move up the radial gradient and reach the peak of the radial gradient, albeit in a different manner to wildtype worms. This observation was first and foremost obvious from the trajectories they formed while navigating the gradient (Figure 5.4, Images A-C). The wild type worms' tracks were consistently smooth, curvy and subtly biased when steering towards the direction of the peak. Pirouettes were observed at the very start of the assay, where the worms are at the beginning of the gradient, and they persisted only until the worms adjusted their body up the gradient (Figure 5.1, Graph A, yellow star). While the wild type worms moved up the gradient, from lower to higher concentration, pirouettes were very rare. Some pirouettes were also observed once they reach the area of the peak of the gradient, although these were not counted as part of the experiment. This behaviour ensures that the worms stay in the area of the highest concentration of the attractant. Ablated worms, either SAA or SMB, exhibited inconsistently loopy and thick trajectories from start to end. Pirouettes were observed at a continuously high rate. The ablated worms followed the same pattern in the H_2O control experiments were direction was not deterministic (Figure 5.4, Images D-F). In contrast to wild type and SMB- ablated worms, SAA- ablated worms exhibited often some irregular exaggerated head swings to both the ventral and dorsal sides (compare Images in Figure 5.5, Image A, B, C; red and yellow arrows). The exaggerated head swings were without an obvious period or rhythm.
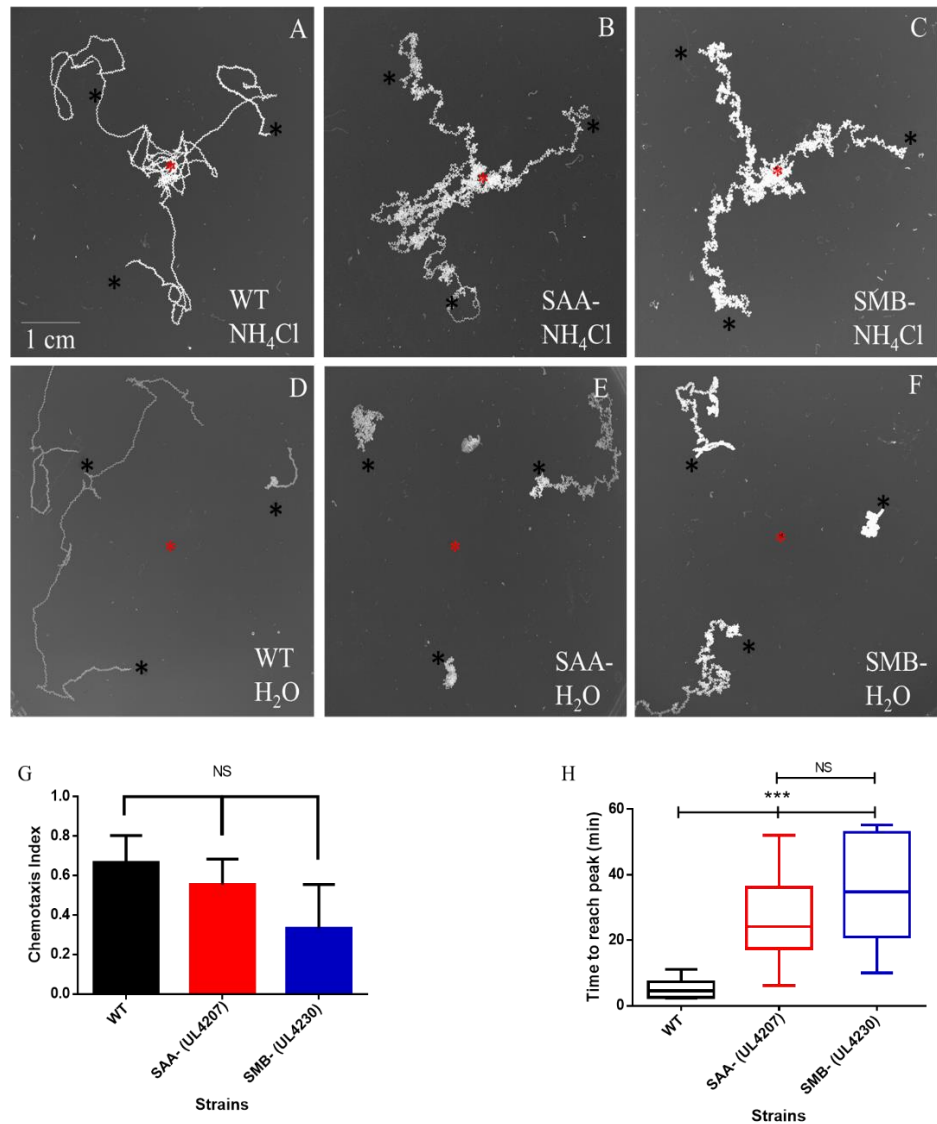
Figure 5.4 Images of the radial gradient experiments and their analysis. Images A, B and C show animals from WT, SAA- (UL4207), SMB- (UL4230) strains. Images D, E and F are the respective controls, where water was used instead of NH_4Cl. None of the animals in the control experiments reached the area of the peak (n=9 for each strain). The black stars indicate the animals' starting points and the red indicates NH_4Cl or H_2O drop points. Graph G shows the chemotaxis index for 18 animals tested from each strain. Graph H shows a box plot of the time required for each tested strain to reach the peak of the gradient. Levels of statistical significance and error bars, as STDEV, are indicated. Index error bars are shown as SEM. (One-way analysis of variance (ANOVA) and Tukey's multiple comparison were used; ***p <0.001; animals that reached the peak: WT n=15 out of 18, SAA- (UL4207) n=14 out of 18, SMB- (UL4230) n=12 out of 18).

5.3.2 SAA- and SMB- ablated animals take longer to reach the peak of the NH$_4$Cl radial gradient

The tested animals were able to sense and reach the gradient in similar numbers. In total, 83.3% (n=18) of the wild type worms, 77.8% (n=18) of the SAA- ablated worms and 66.7% (n=18) of the SMB- ablated worms reached the peak (examples in Figure 5.4, Images A-C). The reproducibility of the experiment was similar to other radial assays with an approximate percentage of 67-83 % (Iino and Yoshida, 2009; Pierce-Shimomura *et al.,* 1999; Ward, S., 1973). As a result, the chemotaxis index for all tested strains was not statistically different (Figure 5.4, Graph G). However, the time it took the worms to reach the area of the peak, was significantly different between the wild type animals and the ablated ones (both SAA and SMB) (Figure 5.4, Graph H). Wild type animals reached the peak within 5 minutes, whereas 27 minutes were required for the SAA- and 34 minutes for the SMB- ablated animals. These mean average times required to navigate a 2cm distance, were considered while conducting subsequent steering assays.

5.3.3 The frequency of pirouettes during chemotaxis increases, while the time spent performing the weathervane strategy is significantly decreased, as a result of the SAA and SMB ablations

The multi-worm setup allowed me to focus on the trajectories at a very high resolution and the ability to replay the movies enabled me to assess the animals' navigational performance (Figure 5.5, Images A-C). The pirouette performance and the weathervane strategy of the worms varied between strains. The frequency of the pirouettes was significantly higher in the ablated animals, more so with the SMB- ablated worms (Figure 5.5, Graph D). Moreover, the ablated worms exhibited pirouettes in the same area, consisting of multiple turns and some reversals in order to readjust the body towards the gradient, whereas for the wild type one reversal and one turn was sufficient (Figure 5.5, Images A-C). The weathervane index of the ablated strains was significantly lower compared to wild type animals (Figure 5.5, Graph E). Long continuous and gradual steering tracks were hardly ever observed in the ablated animals' trajectories, whereas this was commonly seen in wild type worms. SAA- ablated worm's exhibited some tracks of gradual turning (of 10-20 seconds) but were also full of irregularity in their head swings (see red arrows in example in Figure 5.5, Image B).
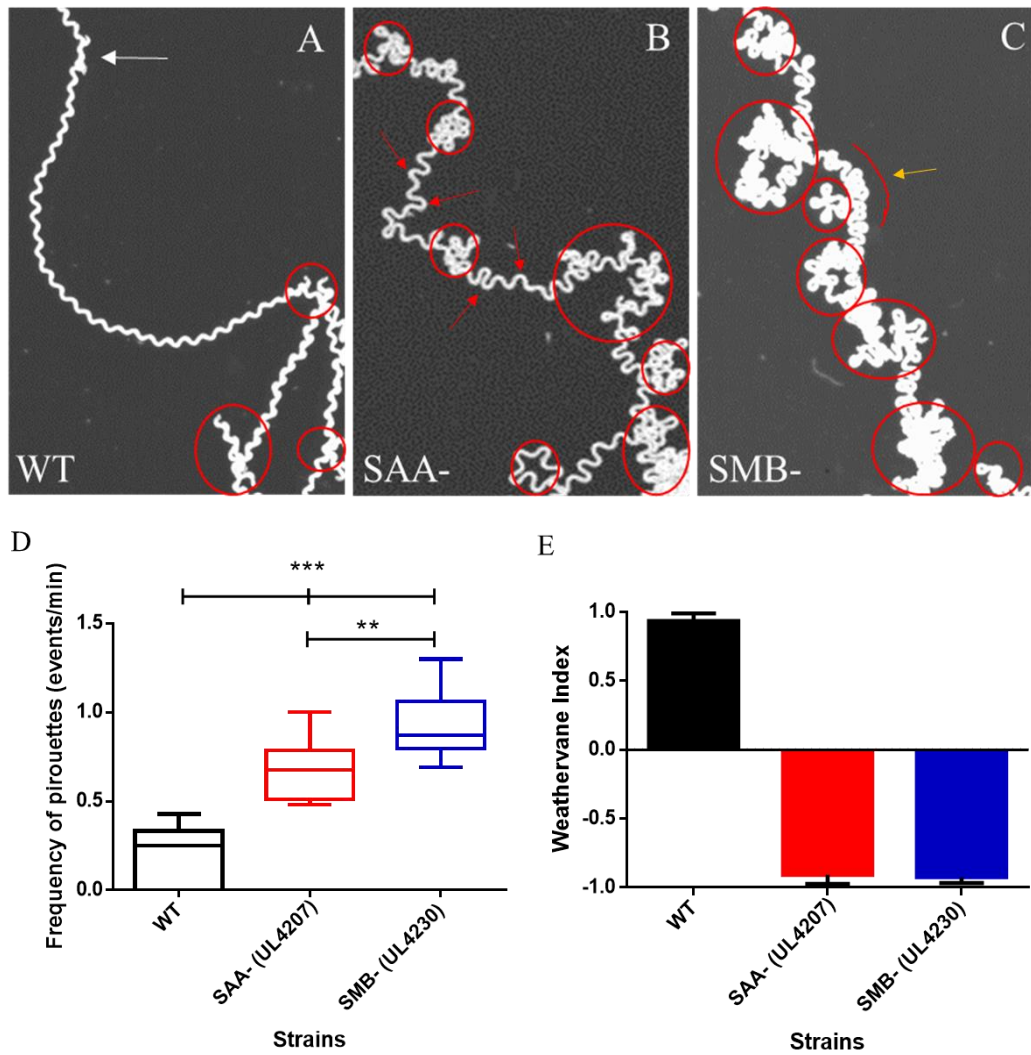
Figure 5.5 Analysis of the NH$_4$Cl radial assays. Images A, B and C show representative tracks of the animals performing the weathervane strategy. Red circles indicate the parts of the tracks were a single pirouette, or a sequence of pirouettes in the case of the ablated strains, was performed. A white arrow points to an example of a short spontaneous reversal that does not change the bearing angle of the trajectory and so was not regarded as a pirouette. The red arrows indicate to examples of the irregularity observed in the SAA- ablated worm tracks. The yellow arrow indicates at an example of the consistency observed in the exaggerated head swings in the SMB- ablated worm tracks. Graph D shows the frequency of pirouettes for each strain as a box plot. Graph E shows the weathervane index. Statistical significance levels and error bars, as STDEV, are indicated. Index error bars are shown as SEM. (One-way analysis of variance (ANOVA) and Tukey's multiple comparison were used; **p<0.01, ***p <0.001; animals that reached the peak: WT n=15 out of 18, SAA- (UL4207) n=14 out of 18, SMB- (UL4230) n=12 out of 18).

5.3.4 The circular grid assay is the ideal steering assay

Different gradient experiments were performed in an endeavour to minimize the frequency of pirouettes while putting the worms in a context where steering would be promoted. In addition, I wanted to conduct an assay where the worm would be already aligned to the gradient of the attractant from the start of the experiment and therefore, the chemotaxis index of the wild type worms would be equal to 1 (all of them given the opportunity would reach the peak). In this case, the defects of the ablated worms would be highlighted. Those preliminary experiments pointed to the ideal assay for assessing the steering ability of the worms (Figure 5.6). Pirouettes were measured until worm's reached the peak of each gradient. Navigating in a linear gradient the worms exhibited a frequency of pirouettes of 0.6 per minute (n=4). The annulus assay gave a frequency of 4 per minute (n=10). The 12 grid assay gave a frequency of 2.6 per minute (n=10), and the circular grid assay a 0.5 pirouettes per minute (n=10). The assay that gave the minimum amount of pirouettes, exhibited the highest performance of the weathervane strategy, and where the worms were reaching the peak most consistently, was the circular gradient assay, which was consequently used to assess the ablated strains (Figure 5.6, Image D).
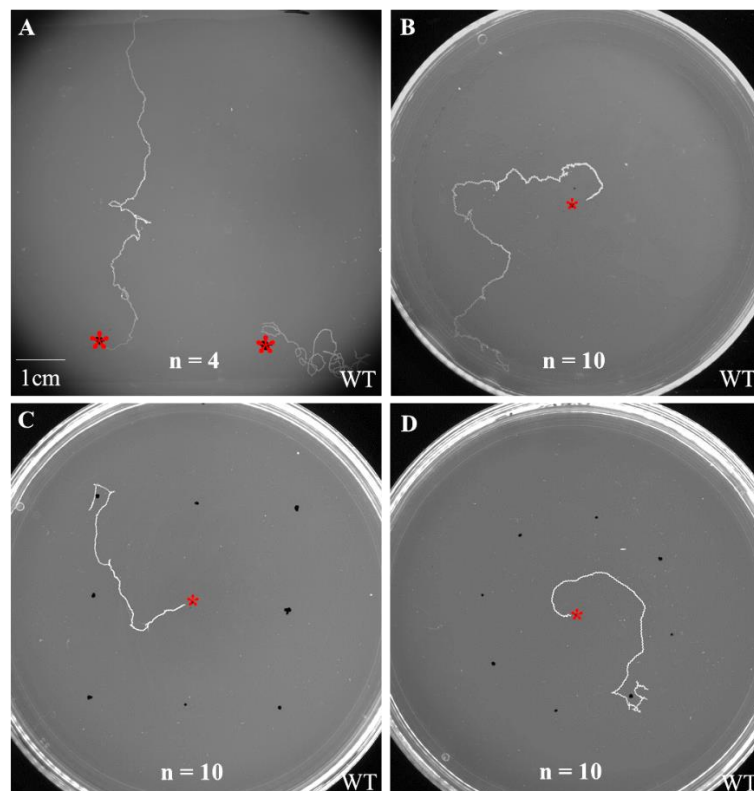
Figure 5.6 Images showing preliminary experiments of all steering assays conducted with the wild type strain; linear (A), annulus (B), 12 grid (C) and circular grid (D). Red star indicates the animals' starting points, black dots indicate NH_4Cl drop points. [linear n=4, annulus n=10, 12 grid n=10, and circular grid n=10].

5.3.5 SAA and SMB ablation promotes pirouettes and introduces defects in the ability of the worm to steer

In the circular grid assay all the wild type animals tested reached a peak of the circular grid within 3 minutes. The ablated strains' overall efficiency to successfully perform chemotaxis was low, with the SAA- ablated worms reaching a peak in 26 minutes on average and the single successful SMB- ablated worm in 39 minutes. Controls with drops of water instead of the attractant did not reach any peak (Figure 5.7).

During the circular grid assays, in wild type worms pirouettes were usually observed when the worm reached the area of the peak. At the starting points in this assay, the worms were already aligned to the gradient and navigated via steering from low to high concentration of the attractant (Figure 5.8, Images A-C). As a result, pirouettes were kept to the minimum and in more than half of the assays (n= 10 out of 18, 55.55%) of the wild type worms they were missing altogether. However, the SAA- and SMB- ablated worms still exhibited a high count of pirouettes. This can be observed both in the trajectories of the worms and in the frequency of pirouettes measured (Figure 5.8, Images D-I), (Figure 5.9, Images A-C and Graph F). The difference in the frequency of pirouettes, between the wild types and the ablated worms, was even higher when the pirouettes were plotted as average number of events per assay and not against time (see Appendix H, Figure H.1 for a comparative graph between the two assays).

Although both the SAA- and SMB- ablated animals were initially aligned with the direction of the gradient, they proved unable to gradually and continuously steer, and follow it up as the wild types did (Figure 5.8, Images A-I). This was most apparent in the SMB- ablated worms, as only one of the 12 managed to reach the peak of the gradient, resulting in its chemotaxis index being negative for this assay (Figure 5.9 Graph D). The SMB- ablated worms exhibited a significantly high count of pirouettes, resulting in them revisiting the same area, and thus never reaching the peak. The SAA- ablated worms' chemotaxis index was significantly lower than the wild type but positive overall. The worms that did reach the peak exhibited some performance of the weathervane strategy, however, with obvious defects and significantly lower in amount than the wild type (Figure 5.9, Images A-C and Graph G).

The defect in steering was also observed in the pattern of the tracks formed while the worms steered (Figure 5.9, Images A-C). As previously described, when a wild type worm steers towards one direction, a dorsoventral asymmetry in the activity of the muscles is introduced and has to be biased towards that direction. That bias is introduced once the worm aligns itself towards the cue sensed and the worm needs to maintain that bias in order for it to slowly turn towards the cue and reach it. Once in a while, a slightly biased head swing course-corrects slightly the trajectory. This can be observed visually in Figure 5.9, Image A (white arrows). The SAA- ablated worms, as with the radial assay, often exhibited some irregular exaggerated

head swings in both ventral and dorsal sides while trying to steer (Figure 5.9, Image B; red arrows). The exaggerated head swings were quite random and seen much more often than the wild type, as the worm was moving towards the peak, where normally not much course correction should have occurred. Overall though, course correction was mostly made by a high frequency of pirouettes (Figure 5.9, Graph F). The SMB- ablated worms exhibited quite similar, but even more obvious, defects. The tracks formed by the very exaggerated head swings are exhibiting hardly any kind of gradual turning, (Figure 5.9, Image C; yellow arrows) but they re-orient via a higher number of pirouettes than any other tested strain (see red circles in Figure 5.9, Image C and Graph F in Figure 5.9). SMB- ablated animals, as with the radial assay, do not exhibited the same irregular exaggerated head swings as the SAA- ablated animals do while steering. Their much exaggerated head swings are sequential and consistent (Figure 5.9, Image C).
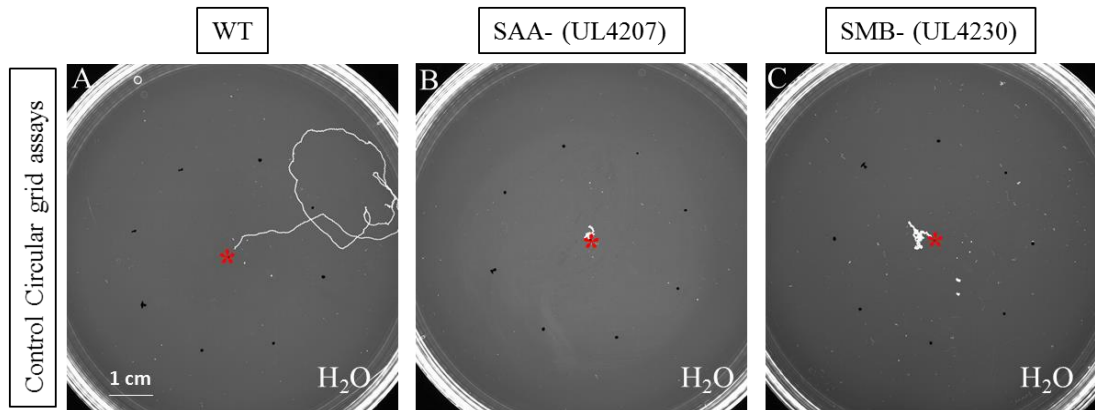
Figure 5.7 Images showing circular grid control assays. The experiments were performed with dH_2O drops instead of NH_4Cl. None of the animals in the control experiments reached and stayed within the area of the peak of the gradient. Red star indicates the animals' starting points, black dots indicate H_2O drop points. [WT n=3, SAA- (UL4207) n=2, SMB- (UL4230) n=2].
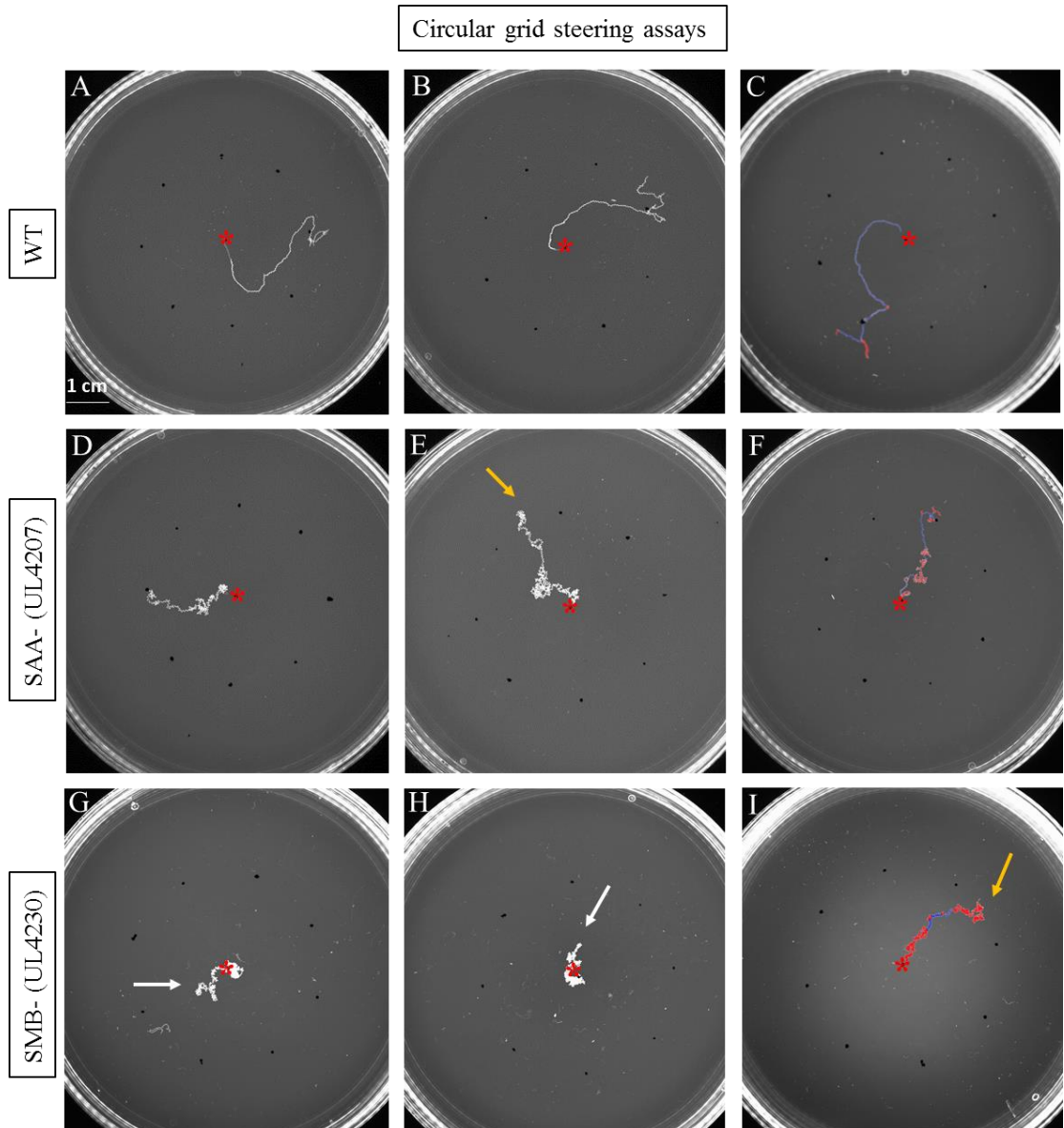
Figure 5.8 Images showing representative circular grid assays. Red star indicates the animals' starting points, black dots indicate NH$_4$Cl drop points. On the third image of each strain trajectories have been coloured as follows: steering (runs) is in blue and pirouettes (tumbles) are in red. White arrows indicate animals that could not steer up the gradient (i.e. didn't reach a black dot). Yellow arrows indicate worms that followed it up but didn't reach a black dot. [Animals tested: WT n=19, SAA- (UL4207) n=14, SMB- (UL4230) n=12].
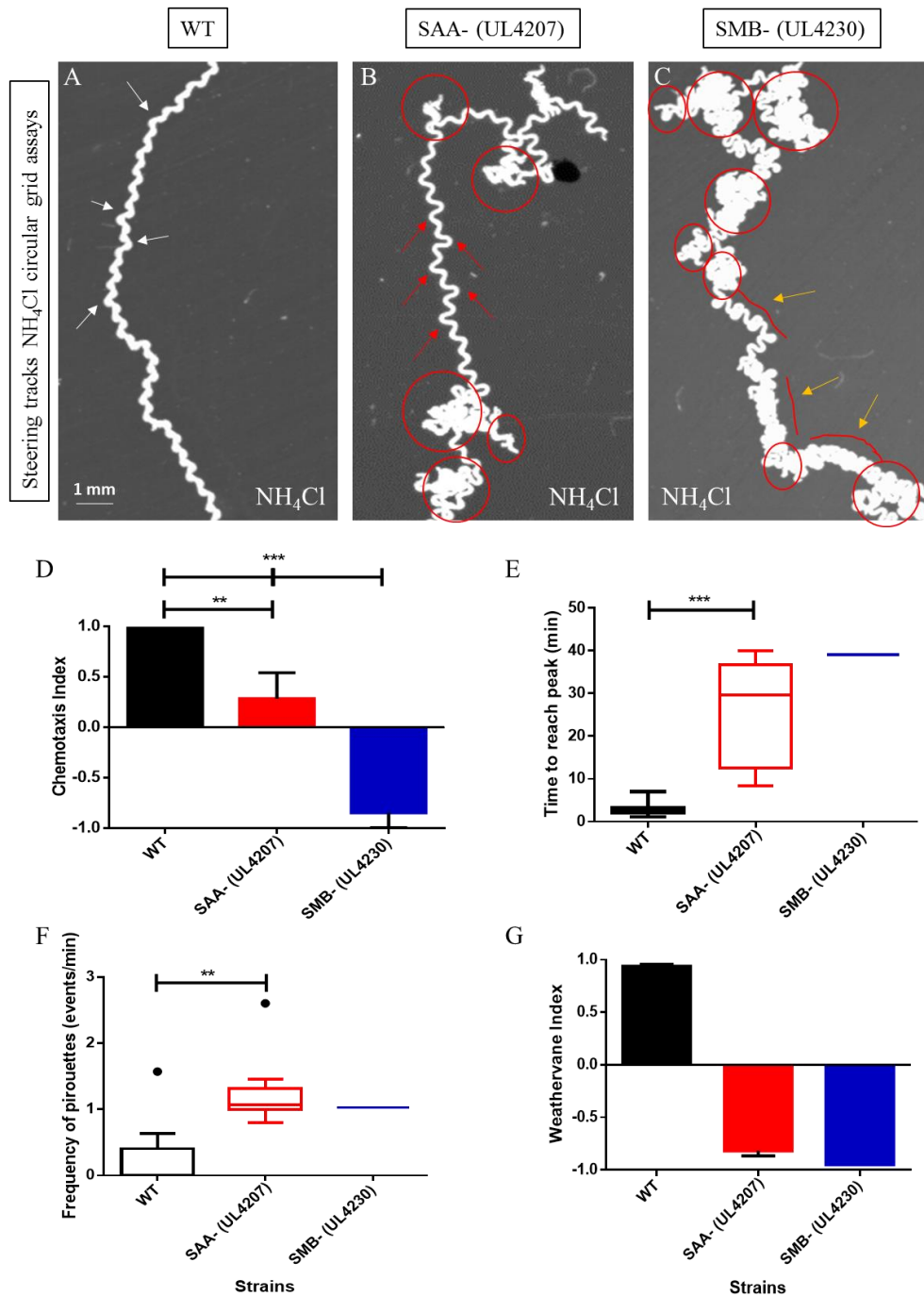
Figure 5.9 Analysis of the NH$_4$Cl circular grid steering assays. Images A, B and C show representative tracks of the animals performing the weathervane strategy. The white arrows show biased head swings that course corrected the trajectory of the wild type worm. The red arrows indicate to examples of the irregularity observed in the SAA-ablated worm tracks while steering. The yellow arrow indicates at an example of the consistency observed in the exaggerated head swings in the SMB- ablated worm tracks. Red circles indicate the parts of the tracks were a single pirouette, or a sequence of pirouettes, was performed. Graph D shows the chemotaxis index for each strain. Graph E shows a box plot of the time required for each tested strain to reach

the peak of the gradient. Graph F shows the frequency of pirouettes for each strain for the worm's that reached the peak as a box plot. Black dots represent two outliers. Graph G shows the weathervane index. Statistical significance levels and error bars, as STDEV, are indicated. Index error bars are shown as SEM. [One-way analysis of variance (ANOVA) and Tukey's multiple comparison were used; **p<0.01, ***p <0.001; Animals reached peak: WT n=19 out of 19, SAA- (UL4207) n=9 out of 14, SMB- (UL4230) n=1 out of 12].

5.4 Discussion

5.4.1 SAA and SMB help set the amplitude of head-swings and suppress turns during chemotaxis

After covering a lot of the worm's probabilistic behaviours in previous chapters, I wanted to address SAA and SMB's role in chemotaxis. Within that directed navigational context the ablated animals, either SAA or SMB, demonstrated an exaggerated amplitude of undulations driven by deep head swings and a high frequency of turns. It seems that the main phenotypic defects observed after ablation in Chapter 3 are not driven by external factors, or in the computation of the input of information, but rather the output of that information; something internally mechanistic has changed due to the ablation of SAA or SMB and their phenotypes are visible in multiple different contexts. This is in accordance to the type of the neural cells ablated, as SAA is a third layer interneuron with direct synaptic connections with numerous head motor neurons, SMB, SMD, RMD, RIV, and SMB is a motor neuron with a direct effect on the head muscles by neuromuscular junctions in the nerve ring. As mentioned numerous times in this project, regulating the amplitude of the head swings is an important element for steering (Izquierdo and Beer, 2013). In addition, regulating the frequency of turns is an important element in chemotaxis (Larsch *et al.,* 2015). First of all, promoting turns is a key element, alongside with reversals, in one of the orientation strategies, the pirouette strategy. Secondly, suppressing turns facilitates long runs and steering during chemotaxis.

Pirouettes most likely occur when an animal is heading down a gradient and less likely when it is following up a gradient. In that sense pirouettes function as the means to stop a run that heads down the gradient and to correct the animal's course during chemotaxis (Pierce-Shimomura *et al.,* 1999). I initially thought that by forming such exaggerated head swings the ablated worms might locally sense that they head down the gradient and initiate readjustment with a pirouette resulting in the high count of pirouettes observed in this chapter. If that was

the case though, then the ablated worms would not exhibit such high frequency of pirouettes without an attractant cue (see controls of this Chapter's assays and roaming experiments in Chapter 3). So part of the sum of the counts of turns observed, are from the intrinsic frequency of pirouettes of the worm, usually regulated by SAA and SMB but following the ablation of these neurons becoming uncontrolled. On the other hand, there was an obvious difference in the level of pirouettes between two assays, the radial and the circular grid, suggesting pirouettes as a means of course correction does indeed take place. It seems likely that the initiation of pirouettes for course correction and the intrinsic frequency of turns in the worms are two independent functions that integrate during navigation, and the neurons of interest are a key element to that, promoting or suppressing them according to context.

On a side note, SMB- ablated worms do exhibit very exaggerated undulations though, and could potentially often sense that they are locally going down the gradient when they are not. That could explain the significant difference in the frequency of pirouettes between SMB- and SAA- ablated worms during the radial gradient and the fact that they exhibit no such difference during the steering circular grid assay. Of course, more SMB- ablated worms should be assayed to make that clear, as only one was able to reach the peak.

5.4.2 The weathervane strategy or both strategies are required for efficient directed navigation

From the radial assays conducted here, it can be observed that wild type animals use both strategies to efficiently navigate towards the peak of the radial gradient. In addition when they were assayed in a gradient favouring steering, some of them could reach the peak without using the pirouette strategy at all and they did so in a remarkably short amount of time. In that sense steering seems to be a more efficient way of course correction, at least in the context of the assays used here. On the other hand, ablated animals could not steer but used mostly pirouettes to navigate in both assays. However, using only the pirouette strategy was sufficient for eventually reaching the peak, albeit not as efficiently as using both demonstrated by the time the worms required to reach the peak.

5.4.3 The Circular grid assay is an ideal steering assay

This assay was conducted in such a way as to favour steering over pirouettes. In the circular grid assay the worm from the very start could only go from low to high concentration of the attractant, its body already aligned to the gradient. In addition, the head of the worm was most of the time moving perpendicular or towards the gradient peak, as this turns out to be the more informative body alignment for the worm generating only small changes in concentration

(Izquierdo *et al.*, 2015). The circular grid gradient demonstrated that wild type animals when required to navigate can use klinotaxis to reach the peak faster than using both strategies together. They will navigate the same distance in significantly less time on average (3.17min) in comparison to the radial assay (5.17min). In this context steering is much more efficient than the pirouette strategy. Ultimately, the assay increased the weathervane index of the wild type worms and lowered the frequency of pirouettes per assay (pirouettes per minute was similar in both assays, as the time to reach peak in the radial assay was higher than the circular). More than half of the wild type animals during the circular grid did not perform any pirouettes at all (n=10 out of 18 worms, 55.55%), whereas during the radial gradient assay one third of the worms did not perform any pirouettes (5 out of 15 worms, 33%). However, the ablated worms needed as long a time to reach the peak as they did in the radial assay, the weathervane index of the SAA was increased (but less so than wild type), whereas the SMB was significantly decreased, and the frequency of pirouettes was even higher than the wild type worms. Indeed, this assay not only highlight the defects of both ablated strains, but also revealed a subtle difference between the effects of the SAA and SMB ablations (compare Figure 5.4, Graph H and Figure 5.5, Graphs D-E with Figure 5.8, Graphs E-G).

5.4.4 SAA and SMB promote steering while inhibiting pirouettes: the integration of two strategies?

It seems the circular grid steering assay put the ablated worms in a context where the inability to steer was highlighted even more. In the case of SMB- ablated worms specifically, the fact that almost all of them didn't reach the peak showed that this motor neuron ablation affected klinotaxis substantially, confirming that SMB is part of the circuit of klinotaxis as previously shown experimentally with optogenetic experiments (Kocabas *et al.*, 2012) and hypothesised in a steering circuit model *in silico* (Izquierdo and Beer, 2013; Izquierdo *et al.*, 2015). As far as SAA is concerned, the SAA- ablated worms fared a bit better than the SMB- ones, with an approximate 60% of the worms tested reaching the peak, however, still at a very slow rate. Overall, the weathervane index was negative (Figure 5.8 G), as it was with the SMB- ablated worms, and significantly lower than the wild type. This is the first time that the SAA neuron has been shown to play a role in klinotaxis. Other neurons that have been shown to play a role in gradual turning are AIZ and AIY, (Kocabas *et al.*, 2012; Iino and Yoshida, 2009), though the latter was lately challenged as AIY was shown to promote negative steering (ipsilateral curving) but not positive steering (contralateral curving), in a more recent publication (Satoh *et al.*, 2014).

In addition to the ablated worms' inability to gradually turn, they both exhibited a high frequency of pirouettes even in the assay favouring steering over the pirouette strategy. This

suggests that SAA and SMB might facilitate steering via suppressing pirouettes. This is the first time SAA and SMB neurons are shown to have a role in the pirouette strategy. Another interneuron shown via ablation to suppress turning rate while facilitating steering is AIY (Larsch *et al.,* 2015; Kocabas *et al.,* 2012; Wakabayashi *et al.,* 2004; Gray, J.M. *et al.,* 2005).

Results from the previous studies mentioned in this section suggest the existence of parallel circuits for steering (via AIZ and/or AIY) and the pirouette strategy (via AIA/AIB/AIY). These circuits have some neurons overlapping (and may have more that are still not known) and those could be the part of the circuit where the two strategies integrate. The combination of the results in this chapter suggests that the SAA, and to a lesser extent the SMB, could be the layer of the neurons within the chemotaxis circuit were the integration of the two strategies takes place. Interestingly, the SAA synaptically is in a direct position to potentially recruit the motor neurons in accordance to sensory context and strategy each time (i.e. SMB, SMD, RIV and RMD). I will elaborate about this hypothesis in detail in Chapter 8: General Discussion, where a potential circuit for chemotaxis will be discussed.

5.4.5 SAA ablation results in undulation irregularity during chemotaxis

Within all chemotaxis assays of this chapter it was observed that SAA- ablated worms exhibited few not continuous exaggerated head swings in a very short but irregular timescale with each other and on both the ventral and dorsal sides (see Figure 5.5, Image A, B, C; and Figure 5.9, Image A, B, C; red arrows). The exaggerated head swings were without an obvious period or rhythm. It could be that this irregularity contributed to the SAA- ablated worms inability to steer efficiently and for long time. They did exhibited some tracks of gradual turning but these were short time-wise (~10-20 seconds). Wild type worms didn't show such an irregularity and were able to steer for the majority of the time required to go up the gradient.. Although, the SMB- ablated worms exhibited even more exaggerated head swings than the SAA- ablated worms, resulting in very thick and dense trajectories, their head swing phenotype was more repetitive and consistent, and had some kind of rhythm, albeit hard to quantify at the moment with such a coiled phenotype.

This observation will be taken into consideration in General Discussion (Chapter 8), while discussing SAA's role within the oscillator and its implication in regulating undulations.

Chapter 6
Ablating the oscillator and breaking dorsoventral symmetry:
Double and Asymmetric genetic ablations

6.1 Introduction

The aim of this chapter was to generate the half ablated strains SAAD, SMBD, SAAV, SMBV and the Double ablation strain (SAA-SMB-). I then tested these strains in NH_4Cl chemotaxis behavioural assays, favouring both or one of the strategies of orientation as in Chapter 5.

The previous chapter highlighted SAA and SMB neuron's individual role in both orientation strategies. It seems both components of the SAA/SMB oscillator are important for steering. But what will happen if the whole hypothesized oscillator is gone? First and foremost, it would be interesting to observe the undulatory phenotype resulted from the double ablation. Is the SAA/SMB oscillator generating the undulations, mediate turns or facilitate steering, or some/all of them? Also, does it act alone or an external input in whatever form, proprioceptive function or an additional oscillator coupled to the SAA-SMB one, might be present? In addition, a double ablation will also be a good way to address any redundancy, as far as the steering circuit is concerned, at the layer of our neurons of interest. The Double ablation strain (SAA-SMB-) was generated by crossing the SAA- ablated and SMB- ablated strains generated in Chapter 2 for this project.

Due to the nature of the mechanism of steering, as described earlier in the General Introduction (Chapter 1), both the muscles and the neurons associated with the steering circuit must be able to introduce and regulate a dorso-ventral (or ventral-dorsal) bias in the worm's undulations. This bias need not be a result of asymmetric connections but of informational flow (Izquierdo *et al.,* 2015). In addition, this bias towards one side has to be maintained and adapted according to continuous sensory feedback for the gradual turning to occur. This requires a dorsoventral regulation that would allow a break in the network symmetry of the head oscillator investigated in this project (see Figure 1.12 for the SAA/SMB head oscillator schematic). Since SMB dorsal cells lack synaptic connectivity to the SMB ventral cells, I have hypothesized early in Chapter 1: General Introduction that SAA could act as an SMB regulator mediating the dorsoventral activity of the SMB neurons. Assaying asymmetrically ablated (i.e. only dorsal or ventral cells are ablated) in chemotaxis behavioural experiments, will give us more insight into SAA and SMB's role in steering, their individual importance in locomotion and steering's requirement of asymmetry. Conversely, it will also highlight how important the network symmetry is during steering. It might also shed some light onto SAA's control of SMB.

Half genetic cell ablation using the two-component system constructed by Chellur and Chalfie, and used throughout this project, is possible by using the promoter of a gene that is expressed only in the dorsal or ventral cells of the neurons (Chelur and Chalfie, 2007). After researching the gene expression patterns of the SAA and SMB cells that was conducted for Chapter 2, I noticed a gene that is expressed only in the dorsal cells of both neurons of interest, SAAD and SMBD (see Table C1 and C2 in the Appendix C). The gene is called *npr-1* and its expression was first described by Coates and de Bono (Coates and de Bono, 2002). By expressing one caspase subunit under the promoter region of *npr-1* and co-expressing it with the other caspase subunit under either *lad-2p* (for SAA dorsal ablation) or *flp-12sp* (for dorsal ablation of SMB), half ablated strains can be created.

Moreover, I found out a way to ablate the ventral cells of SAA and SMB by genetically rescuing the dorsal cells from ablation. It has been observed that the P35 baculovirus protein inhibits CED-3 cell-death protease in *C. elegans* (Xue and Horvitz, 1995). The P35 protein is a substrate for, and therefore a competitive inhibitor of, the *C. elegans* cell-death protease CED-3. Sugimoto *et al*, showed that the P35 protein can be cleaved by CED-3 and found out its cleavage site. In transgenic worms expressing the P35 protein, but wild type in all other ways, they observed extra or 'undead' cells (Sugimoto *et al.,* 1994). They also showed rescued cells by P35 protein in double transgenic animals expressing both the P35 protein and the CED-3 protein.

Driving expression of the P35 protein under the *npr-1* promoter will rescue the dorsal cells of the neurons while the ventral ones will still be killed via the action of CED-3. Table 6.1 in the 'Methods and Materials' section that follows shows the micro-injection experiments that were conducted in order to generate the SAAD-, SMBD-, SAAV- and SMBV- strains. Unfortunately, dorsal cells' genetic rescue did not take place in the ablated strains. Neither cell rescue could be confirmed by imaging nor was an obvious phenotype different to that seen in SAA- or SMB- strains observed.

6.2 Material and methods

6.2.1 Nematode maintenance and strains

Animals were kept at 20°C at all times, fed *E.coli* (OP50 strain) and were maintained as previously described (Brenner, 1974). The *C. elegans* variety N2 Bristol wild-type strain was provided by the Caenorhabditis Genetics Centre (CGC), which is funded by the NIH Office of Research Infrastructure Programs (P40 OD010440). Ablated strains SAA- (UL4207) and SMB- (UL4230) were generated for this project (see Chapter 3). Double ablation strain SAA-

SMB- (UL4278) and successful asymmetrically ablated strains, SAAD- (UL4279) and SMBD- (UL4281), were generated as explained in the 'Methods and Materials' section 6.2.2 of this chapter. Animals were assayed in the first 2 days of adulthood.

6.2.2 Generating the asymmetric ablation strains

6.2.2.1 Plasmids used

CED-3 caspase plasmids carrying the CED-3 large subunit (p17) and the CED-3 small subunit (p15) were a gift from Martin Chalfie (Addgene plasmid # 16081 [TU#807] and Addgene plasmid # 16080 [TU#806], respectively). They originally carried the *mec-18p* promoter region, which had to be excised (see Chapter 2, Figure 2.2).

The pPD95_75 GFP plasmid was a gift from Andrew Fire (Addgene plasmid # 1494). Its backbone was used to carry and express the P-35 protein.

The *npr-1p*::GFP plasmid, a gift from Mario de Bono (Coates and de Bono, 2002), was used as a template to amplify the *npr-1p* promoter region.

Protein P-35's cDNA was a gift from Xue Ding (Xue and Horvitz, 1995) and was carried in a pBluescript II vector.

All plasmids share the pPD95_75 backbone manufactured by Andrew Fire.

6.2.2.2 Molecular biology

The *npr-1p* 2kb promoter region was amplified by PCR from the *npr-1p*::GFP plasmid. Primers are shown in Table A2 in Appendix A. The promoter region was then cloned into the CED-3 p17 subunit plasmid cut with HindIII/BamHI.

Sequence encoding the P35 protein was excised from the pBluescript II vector with the EcoRI enzyme and cloned into the pPD95_75 GFP plasmid without the GFP protein sequence that was also cut using EcoRI. Enzymatic diagnostic digestions were used to make sure the P35 protein sequence was inserted in the correct orientation into the GFP plasmid. Diagnostic enzymatic digestions with BamHI, EcoRI, BstBI or HindIII followed each time to confirm constructs identity.

Table B2 in the Appendix B, shows the cloning steps for the construction of the two additional plasmids required for the asymmetric ablations, *npr-1p*::p17 and *npr-1p*::P35. Table 6.1 in this section, shows the asymmetric ablation strains generated for this chapter via microinjection.

ApE, a plasmid editor v2.0.47 software, was used for the annotation of all genomic regions, predictions of enzymic digestions and ligation results (Paradis *et al.,* 2004). Primer3 v0.4.0

software was used for primer design (Untergasser *et al.,* 2012; Koressaar and Remm, 2007). Oligocalc v3.27 software was used to check self-complementarity of primers and their melting temperature (Tm) (Kibbe, 2007). The restriction enzymes and ligase that were used were purchased from Invitrogen. Primers were purchased from Integrated DNA Technologies (IDT).

6.2.2.3 Microinjections

The parent wild type strain used for generating the transgenic strains was the *C. elegans* variety N2 Bristol strain (Brenner, 1974), the same strain that was used to generate the ablated strains SAA- (UL4207) and SMB- (UL4230) described in Chapter 3. Transgenic worms were generated by the means of microinjection (Mello *et al.,* 1991), whereby the constructs mentioned above were microinjected into the distal gonad of a young adult worm alongside with a transformation marker (Hobert, 2002; Evans, 2006). The *myo-2p*::mCherry plasmid that expresses the red fluorophore mCherry in the pharynx was used as a transformation marker,. pCFJ90 - *myo-2p*::mCherry::unc-54utr was a gift from Erik Jorgensen (Addgene plasmid # 19327) (Frokjaer-Jensen *et al.,* 2008). An additional transformation marker used was the *coel*::GFP and it was a gift from Piali Sengupta (Addgene plasmid # 8937) (Miyabayashi *et al.,* 1999). See Table 6.1. The construct *npr-1p*::P35 injected in the strains that did not result in the expected ventral-ablation phenotypes was sent for sequencing. Sequencing primers are shown in Appendix A section, Table A4. Sequencing BLAST results are shown in Appendix E, Figures 1-3.

Table 6.1 The transgenic asymmetric ablation strains generated for this chapter. In red are the strains where dorsal rescue could not be confirmed and did not result in any obvious phenotype.

Strain injected	Plasmids injected	Marker	Ablated cell	Expected expression/localisation of GFP	Strain name
N2	*flp12sp*::CED-3 (p15) *npr-1p*::CED-3 (p17) *flp12sp*::GFP	*myo-2p*::mCherry	**SMBD**	SMBV Absence of GFP expression in SMBD	UL4281
N2	*lad-2p*::CED-3 (p15) *npr-1p*::CED-3 (p17) *lad-2p*::GFP	*myo-2p*::mCherry	**SAAD**	SAAV, SMD, ALN, PLN, SDQ Absence of GFP expression in SAAD	UL4279
SAA-(UL4207)	*npr-1p*::P35	*coel*::GFP	**SAAV**	SAAD	UL4282
SMB-(UL4230)	*npr-1p*::P35	*coel*::GFP	**SMBV**	SMBD	UL4283
SAA-(UL4207)	*flp-12sp*::CED-3 (p15) *flp-12sp*::CED-3 (p17) *flp-12sp*::GFP	*coel*::GFP	**SMB SAA**	SMD, ALN, PLN, SDQ Absence of GFP expression in SAA and SMB	UL4278

6.2.2.4 Microscopy and imaging

To confirm ablation, transgenic worms were imaged for the expression of GFP, or the lack of it, in the neurons of interest after being anaesthetised by the use of levamisole (2mM). A ZEISS stereo Lumar V12 was used to screen for transgenics. For imaging, a Leica M165 FC fluorescent stereoscope fitted with a Q-imaging Qi-CLICK COOLLED pE-300 camera and a ZEISS Axioplan fluorescent microscope fitted with a Q-imaging RETIGA 2000R camera, were used. Images were captured with Q-Imaging's Q-capture Pro 7 software. Images were processed with the use of FIJI software (Schindelin *et al.,* 2012).

6.2.3 Behavioural assays

For all behavioural experiments in this chapter a custom built multi-worm tracker was used, consisting of a Navitar telemetric lens and a XIMEA xiQ super-speed camera mounted on a Fotomate macro slider / Manfrotto 410 geared head, and a Polytech LED red light circular system (Figure 3.3 B, Chapter 3). Videos were captured at 5fps with the use of StreamPix 7 (version 7.2.1) software built by NorPix. Trajectories were visualised with FIJI software

(Schindelin *et al.,* 2012). Experiments were conducted at 20°C, plates and strains were randomised with the use of a dice.

6.2.3.1 Dispersal (long-range search) behavioural assay

The protocol followed has already been described in Chapter 3 (Methods and Materials section 3.2.3.2). Six animals per strain were video-tracked for one hour, immediately after each worm was transferred at the middle of a 9cm plate. Experiments were conducted at 20°C, plates and strains were randomised with the use of a dice.

6.2.3.2 NH₄Cl radial chemotaxis assay

The protocol followed for the NH_4Cl radial chemotaxis assay, was the same as the one standardised and used in Chapter 5 (Methods and Materials section 5.2.1). As with Chapter 5's chemotaxis experiments, I never exceeded the recordings over 60 minutes for the ablated strains. Video-tracking beyond 60 minutes was avoided, as the gradients would change enough for the assays to not be comparable to the wild type assays where animals reached the gradient peak in a much shorter time. Twelve animals were tracked for the SAAD- (UL4279) strain, 18 for the SMBD- (UL4281) strain and 21 for the double ablation strain (UL4278); 3 animals per plate. Additional animals were tested in control plates were ddH_2O, instead of NH_4Cl, was dropped (n=2 for each strain). Chemotaxis index, pirouette frequency and index, weathervane index were calculated as explained in Chapter 5 (Methods and Materials section 5.2.1).

6.2.3.3 Circular NH₄Cl steering assay

The 'circular' grid assay was conducted as in Chapter 5 (Methods and Materials section 5.2.2.1). As with Chapter 5's circular chemotaxis experiments the suggested approximate times of recordings for the asymmetric ablated strains was 45 minutes. However, for the double ablation animals, so few reached the peak of the radial gradient that I decided to give them the maximum time possible; 60 minutes. Video-tracking beyond 60 minutes was avoided, as the gradients would change enough for the assays to not be comparable to the wild type assays anymore where animals reached the gradient peak in a much shorter time. Ten animals were tracked for each strain, 1 animal per plate. Additional animals were tested in control plates were ddH_2O, instead of NH_4Cl, was dropped. Chemotaxis index, pirouette frequency and index, weathervane index and bearing were calculated as explained in Chapter 5 (Methods and Materials section 5.2.1).

6.2.3.4 Statistical analysis

Comparisons between tested animals and matched controls were conducted by using one-way analysis of variance (ANOVA) followed by Tukey's multiple comparisons test. Analysis was

performed using GraphPad Prism (version 6.01), GraphPad Software, La Jolla California USA, www.graphpad.com.

6.3 Results

6.3.1 Confirmation of half ablation in the new transgenic strains
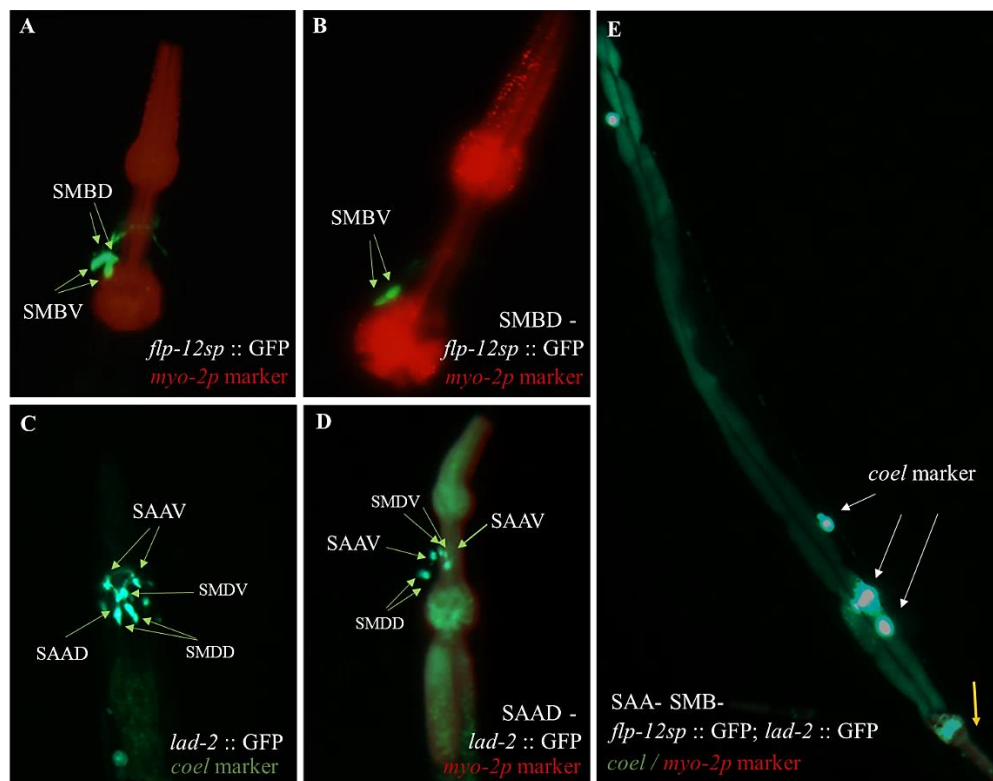
Figure 6.1 Microscopy images of asymmetric ablation, double ablation and wild type strains. Worms expressing the two subunits of the reconstituted CED-3 caspase driven by the *flp-12sp* and *npr-1p* promoter regions (Image B; strain UL4281), and *lad-2p* and *npr-1p* regions (Image D; strain UL4279). GFP expression in the wild type images A and C (strains UL4187, UL4213 respectively), and the lack of it in B and D, confirms the asymmetric genetic ablation. Double ablation strain (Image E) does not express GFP in either SAA or SMB (yellow arrow shows were they should have been). The white arrows show the expression of the GFP marker in the coelomocytes.

SMB dorsal cell ablation occurred in worms expressing the two subunits of the reconstituted CED-3 caspase driven by the *npr-1p* and *flp12-sp* promoter regions (Figure 6.1 Image B; strain UL4281). When the reconstituted CED-3 caspase was driven by the *lad-2p* and *npr-1p* promoter regions, SAA dorsal cell ablation took place (Figure 6.1 Image D; strain UL4279). GFP expression in other cells, and the lack of it in the targeted cells, confirmed the genetic ablation. Wild type animals carrying GFP in the neurons of interest are also included in the

figure for comparison (Figure 6.1 Images A and C; strains UL4187, UL4213 respectively). Both SAA and SMB cells were ablated in the double ablation strain generated (Figure 6.1 Image E; strain UL4278). Therefore, ablation of the dorsal targeted cells with the caspase two-component system occurred successfully as already shown in Chapter 2 and previously described with other neural cells (Chelur and Chalfie, 2007).

Unfortunately, the strains generated for the ablation of the ventral cells of the targeted neurons, strains UL4282 and UL4283, was not successful. The rescue of the dorsal cells by the expression of the protein P35 did not happen in this instance. The rescue could not be confirmed by microscopy, nor was any behavioural phenotype observed that was different to that seen for SAA- and SMB- worms.

A first visual comparison of the undulations formed by the successful half ablated strains and double ablation strains with the wild type and the ablated strains generated in Chapter 2, is shown in Figure 6.2. The double ablation strain gave the strongest phenotype. The curvature of their tracts is so high that the worms seem to move by doing alternate continuous turns, although that is not the case as there was no dorsoventral or ventral-dorsal re-orientation (Figure 6.2, Image D). However, the trajectories of the double ablation worms could follow an approximate straight line (Figure 6.2, Image D). Interestingly, head swings of the double ablation strain seemed to be conducted faster than the other ablated strains. This conclusion comes from direct observations; due to the inability to skeletonize the transgenic strains there are no actual comparisons of velocities). Half dorsal ablation of SAA (Figure 6.2, Image E) and SMB (Figure 6.2, Image F) gave a phenotype that appears more similar to the SAA full ablation strain (Figure 6.2B) than the SBM full ablation strain (Figure 6.2C).
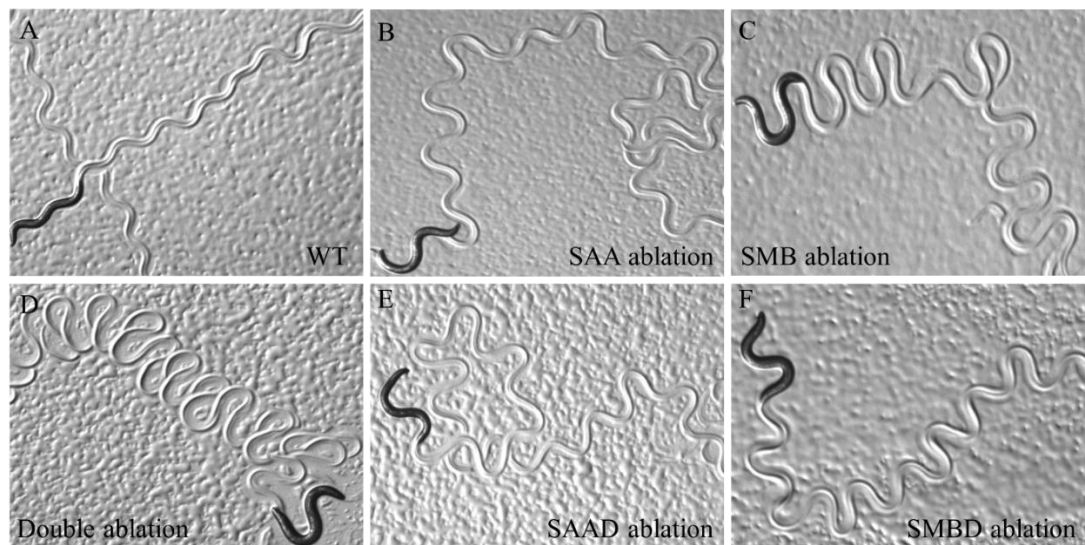
Figure 6.2 Images depict tracks of the ablated and wild type animals on thin bacterial lawns. Images B and C are from the strains generated in Chapter 2. They have been added here for comparison with the double and asymmetrically ablated animals.

6.3.2 Half dorsal and double ablation animals exhibit a decrease in exploratory behaviour

Figure 6.3 below depicts the generated strains' long-range dispersal behaviour. There was a statistically significant decrease in the area explored between the half ablated strains, double ablation strain and the control strains. The SAAD- ablated animals showed a 3-times decrease, similar to the SAA- ablated animals, and the double ablation animals showed a 6-times decrease of the area explored, similar to the SMB ablation strain (Figure 6.3, Graph D). From direct observation of the movies, and as seen in the higher resolution images in Figure 6.4 (Images A, B and C), this was mostly due to the fact that SAA- and SMB- ablated animals performed more turns and less runs during the one hour of video-tracking. On the other hand, the dorsal ablation of SMB didn't result in a significant decrease in dispersal behaviour, as seen for the rest of the tested strains here. In adidition, SMBD- exhibited more contineuous loopy trajectories when revisiting the same areas, rather than abrupt sharp turns as seen for the rest of the ablated strains. This resulted in it covering a bit more area than the rest, but still not as much as the wild type animals.
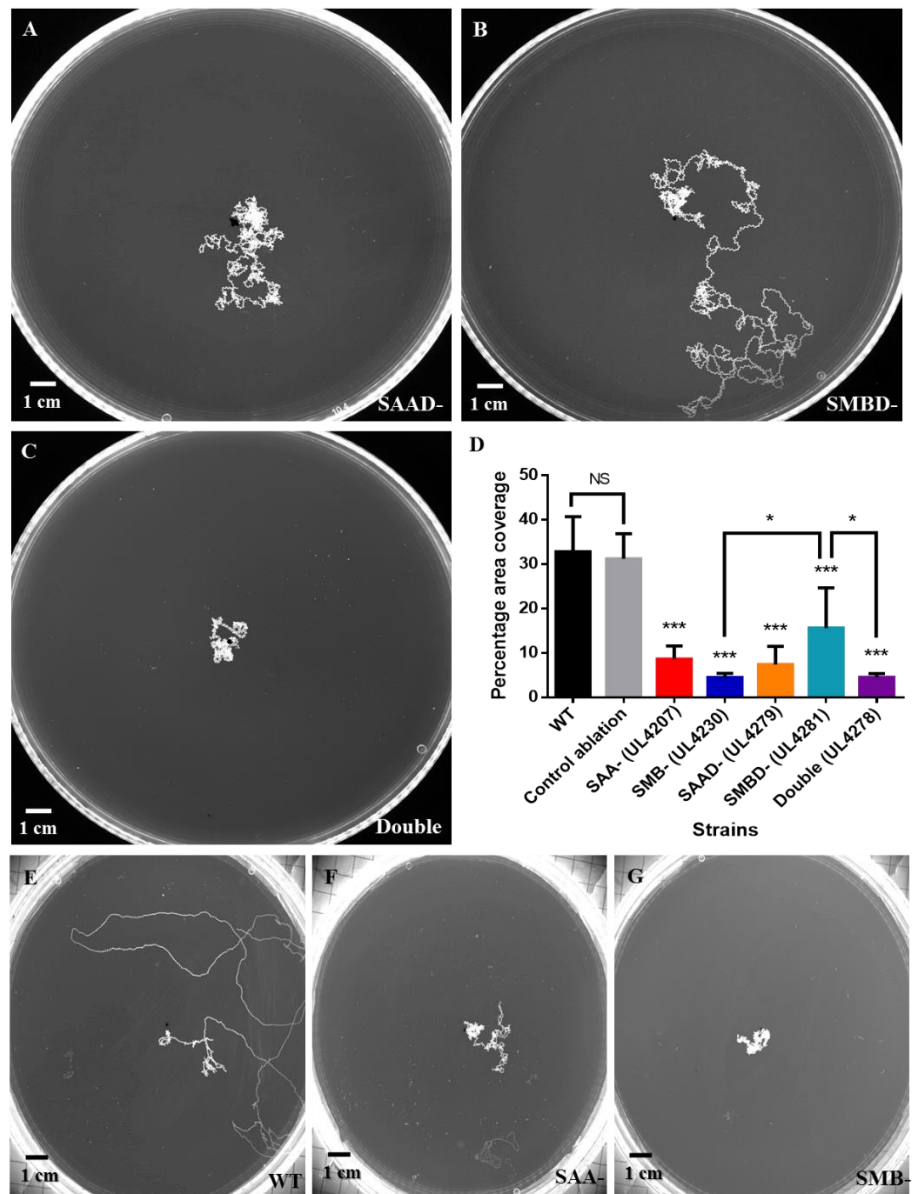
Figure 6.3 Dispersal behaviour of asymmetrically ablated and double ablated strains, including images from wild type, SAA- and SMB- ablated animals from Chapter 5 for comparison. Image A shows the tracks formed by an animal for a whole hour with the dorsal SAA cells ablated (SAAD- UL4279), image B depicts the tracks of a SMBD-ablated animal (SMBD- UL4281) and C the tracks of an animal where both SAA and SMB have been ablated (Double UL4278). Graph D shows the approximate area covered by the animals tracked for 1 hour, including the strains assayed in Chapter 3 [see Images E-C for comparison). Statistical significance and error bars, as STDEV, are indicated. (One-way analysis of variance (ANOVA) and Tukey's multiple comparison were used; ***p <0.001;*p<0.05; n=6 for each strain].
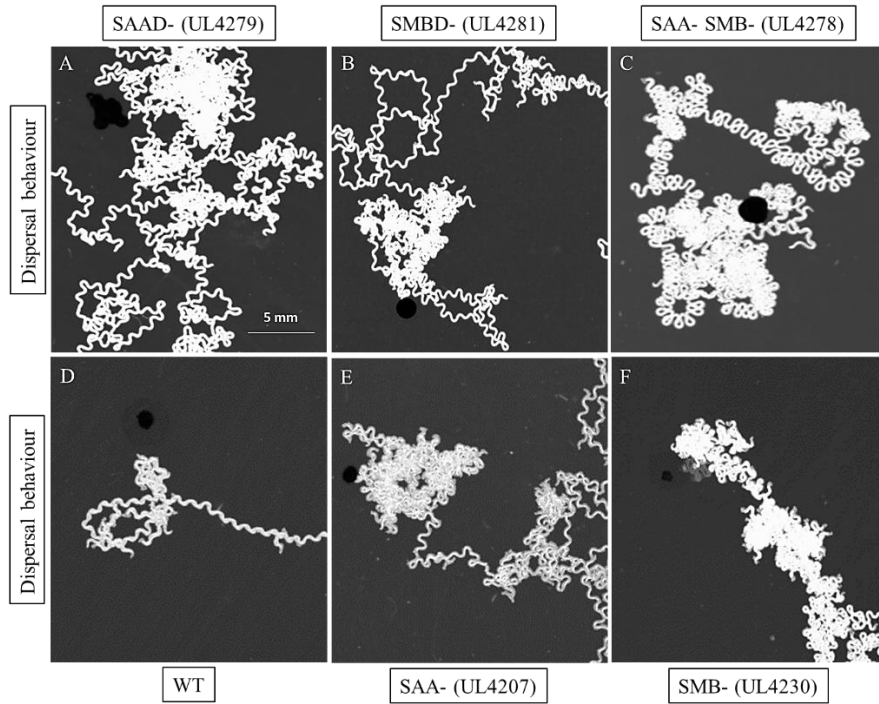
Figure 6.4 Higher resolution images of the dispersal behaviour of the asymmetrically and double ablated strains during local search. Image (A) shows the tracks formed by an SAAD- ablated animal (UL4279), image (B) depicts the tracks of a SMBD- ablated animal (UL4281) and (C) the tracks of an animal where both SAA and SMB have been ablated (UL4278). Images D-F show tracks from wild type, SAA- and SMB- ablated worms for comparison purposes. Black dots indicate the worm's starting point.

6.3.3 The navigational tracks of the asymmetrically ablated and double ablation animals are inconsistent and different to the wild type

Differences in the navigational tracks of half ablated and double ablation animals compared to wildtype were first and foremost obvious from the trajectories they formed while navigating the gradient (Figure 6.5, Images A, C and E). The wild type, SAA- ablated and SMB- ablated worms' navigational tracks in this assay were described in detail in Chapter 5. For comparison see Figure 6.6 that was included from Chapter 5. Half ablated worms, either SAAD- or SMBD-, exhibited quite biased trajectories from start to end where course correction could not happen by steering (modulation of head from being biased from the one side to the other) but with exaggerated irregular undulations and short pirouettes (~75%) (Figure 6.5, Images A and C; close up in Figure 6.7, Images C and D). A minority of half ablation animals (~25%) were not consistent with their undulatory movement during chemotaxis, and they also exhibited tracks were the head swings were very shallow (Figure 6.5, Images A and C; close up in Figure 6.7, Images A and B). Compare panels showing the tract of the half ablated strains in Figures 6.5 and 6.7 with Images A, B and C in Figure 6.8, where the tracks of wild type, SAA and SMB strains from Chapter 5 have been added for comparison purposes. No other strain generated in this study, or in the literature to my knowledge, has exhibited this, only the asymmetric ablation strains here. Pirouettes were observed at a high rate but not as high as the full ablations showed in Chapter 5, judging initially by the thickness of the trajectories left by the worms (compare Figure 6.5 to 6.6). The double ablation strain was generally unable to align itself with the gradient and follow it up. The one worm that reached the peak exhibited thick trajectories directed at the peak, due to the fast exaggerated undulatory movement, but hardly any pirouettes were performed (combination of reversals with very sharp re-orientation turns) (Figures 6.5, Image E and Figure 6.8, Image F). All ablated worms followed the same undulatory pattern in the H_2O control experiments were direction was not deterministic without any bias in direction and without ever reaching the drop of water (Figure 6.5, Images B, D and F).
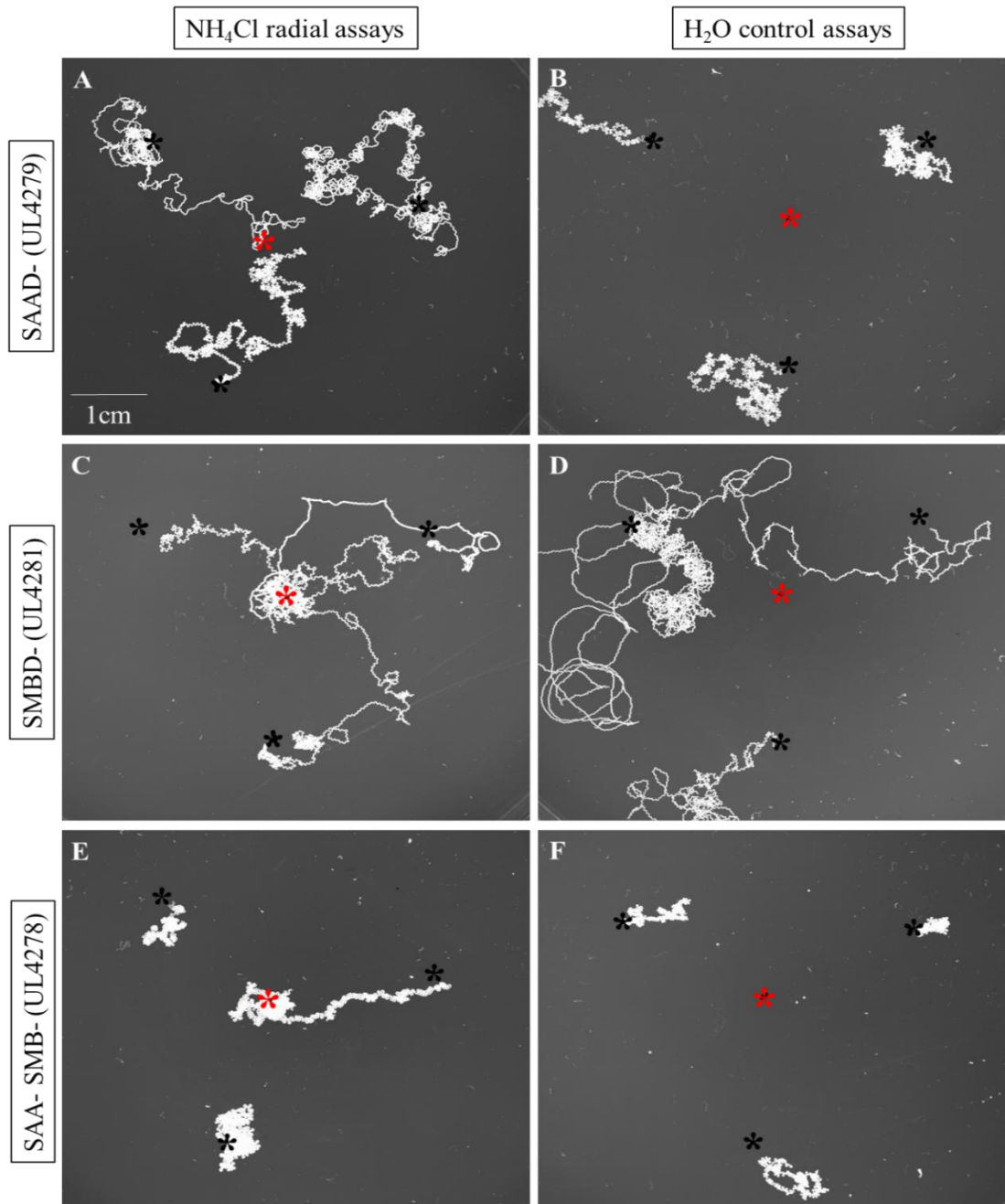
Figure 6.5 Images of the radial gradient experiments when assaying half ablated animals and the double ablation strain. Images A and C show animals where their dorsal neurons have been ablated; SAAD- (UL4279) and SMBD- (UL4281) strains respectively. Image E depicts the trajectories of animals where both SAA and SMB has been ablated; double ablation strain (UL4278). Images B, D and F are the respective controls, where water was used instead of NH_4Cl. None of the animals in the control experiments reached the area of the peak (n=6 for each strain). The black stars indicate the animals' starting points and the red indicates NH_4Cl or H_2O drop points. [Animals tested: SAAD- (UL4279) n=18, SMBD- (UL4281) n=15, Double (UL4278) n=18]. [Animals reached the peak: SAAD- (UL4279) n=11 (61%), SMBD- (UL4281) n=8 (53%), Double (UL4278) n=2 (11%)].
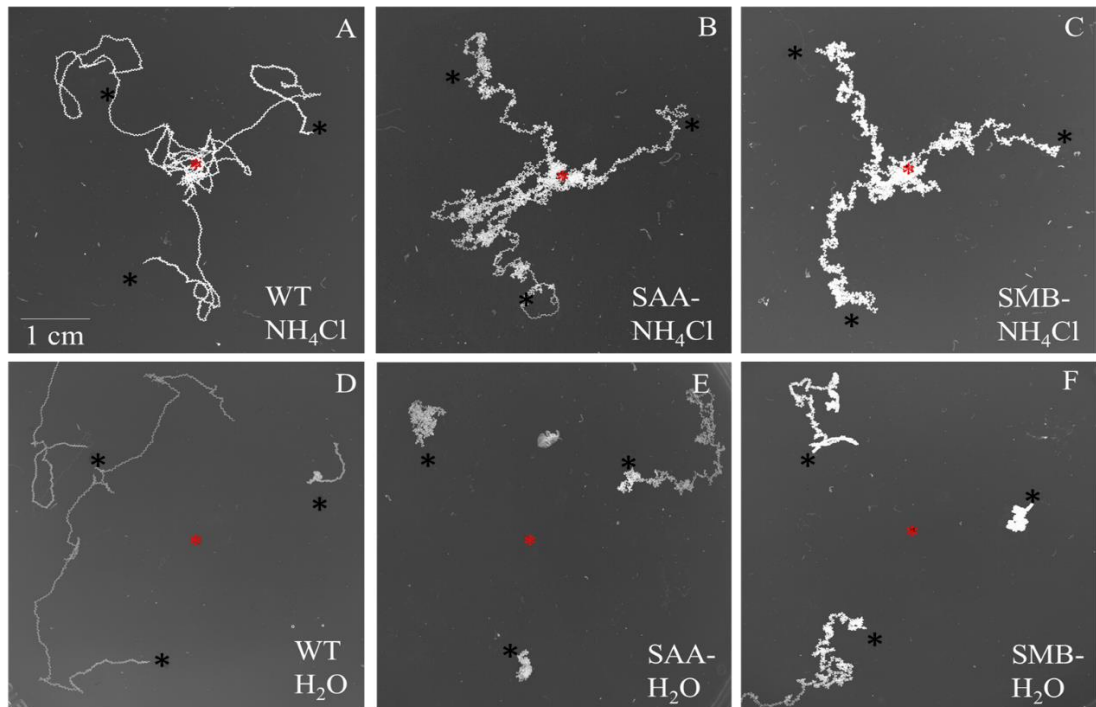
Figure 6.6 Images of the radial gradient experiments inserted here from Chapter 5 for the purpose of comparison with Figure 6.5. Images A, B and C show animals from WT, SAA- (UL4207), SMB- (UL4230) strains. Images D, E and F are the respective controls, where water was used instead of NH_4Cl. The black stars indicate the animals' starting points and the red indicates NH_4Cl or H_2O drop points.
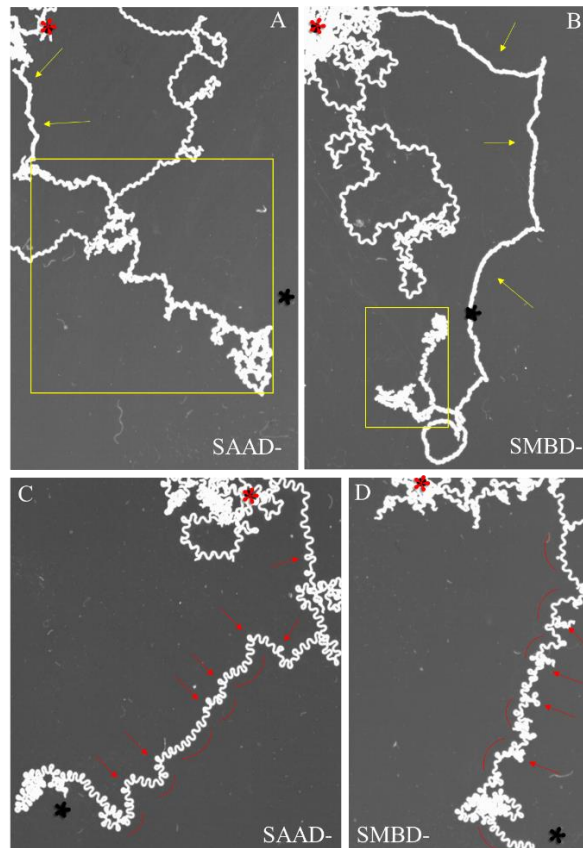
Figure 6.7 Higher resolution images of the two types of trajectories observed by half ablation strains SAAD- (UL4279) and SMBD- (UL4281). Images A (SAAD- ablation) and B (SMBD- ablation), show extreme inconsistent undulatory amplitude from quite normal to very shallow going up a radial chemotaxis gradient (~25%). Yellow square areas include tracks with a deep undulatory movement. Yellow arrows point to tracks with undulation of shallow amplitude. Images C (SAAD- ablation) and D (SMBD- ablation), show a biased trajectory up the gradient in bouts (red lines), where course correction cannot happen by continuous steering but with exaggerated irregular undulations and short pirouettes (~75%) (red arrows). The black stars indicate the animals' starting points and the red indicates NH_4Cl drop points.

6.3.4 Most of the SAAD half ablation and double ablation animals are unable to reach the NH_4Cl radial gradient peak

The ablated animals were often able to sense and begin to follow up the radial gradient but not always reach the peak of the radial gradient (Figure 6.5, Images A-F). In total, 8 out of 18 SAAD- half ablated (61%), 11 out of 15 SMBD- half ablated (53%) and only 2 out of 18 SAA-SMB- double ablation worms reached the peak. As a result, only the chemotaxis index of the SMBD- half ablation animals was similar to wild type (Figure 6.8, Graph G). As a

reminder of the previous chapter's results, wild type animals reached the peak within 5 minutes. In comparison, 27 minutes were required for the SAA- and 34 minutes for the SMB-ablated animals. Interestingly, half ablation animals differed in pattern. The SAAD- strain required on average 33.6 minutes, the SMBD- strain needed 18 minutes and the double ablation strain 20 minutes to reach the peak. The SMBD- and double ablation animals' time to reach the peak was not statistically different to the wild type overall (Figure 6.8, Graph H).
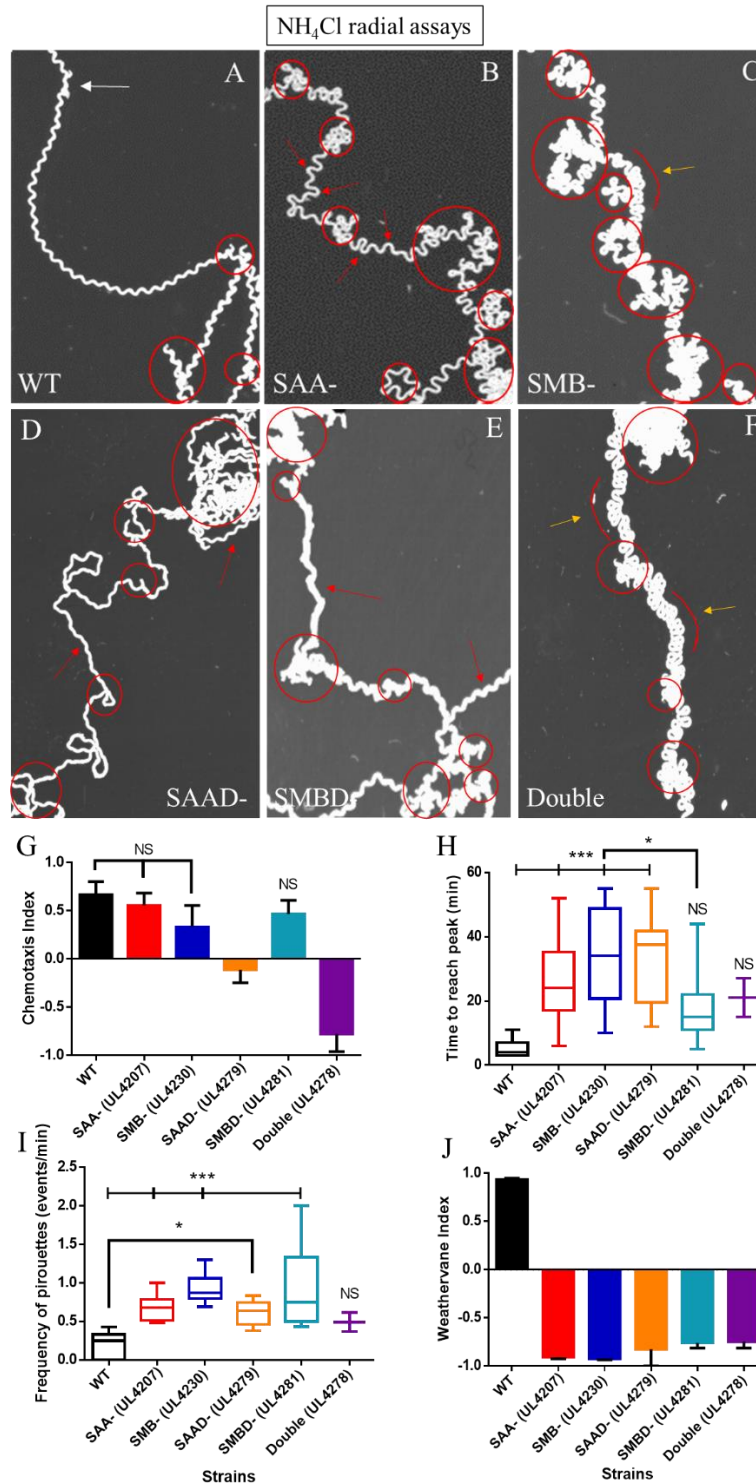
Figure 6.8 Higher resolution images of the radial gradient experiments and their analysis.

Figures and graphs include the strains assayed in Chapter 5 for comparison. Images A to F show representative tracks of the animals performing the weathervane strategy following up the radial gradient. Red circles indicate the parts of the tracks were a single pirouette, or a sequence of pirouettes in the case of the ablated strains, was performed. A white arrow points to an example of a short spontaneous reversal that does not change the bearing angle of the trajectory and so was not regarded as a pirouette. The red arrows indicate at examples of tracks inconsistency (irregularity in the SAA- ablated worm and amplitude inconsistency in the asymmetrically ablated worms). The yellow arrows indicate at an example of the consistency observed in the exaggerated head swings in the SMB- ablated and double ablation worm tracks. Graph G shows the chemotaxis index for the animals tested from each strain. Graph H shows a box plot of the time required for each tested strain to reach the peak of the gradient. Graph I shows the frequency of pirouettes for each strain as a box plot. Graph J shows the weathervane index. Statistical significance and error bars, as STDEV, are indicated. Index error bars are shown as SEM. (One-way analysis of variance (ANOVA) and Tukey's multiple comparison were used; ***p <0.001, *p<0.05; animals that reached the peak: WT n=15 out of 18, SAA- (UL4207) n=14 out of 18, SMB- (UL4230) n=12 out of 18, SAAD- (UL4279) n=8 out of 18, SMBD- (UL4281) n=11 out of 15, Double (UL4278) n=2 out of 18).

6.3.5 The frequency of pirouettes during a radial gradient chemotaxis assay increases while the weathervane strategy is significantly decreased as a result of the asymmetric and double ablations

Examples of the tested animals' navigational performance are shown in Figures 6.5, Images A to F and close up images in Figures 6.7 and 6.8. The performance of pirouettes and the weathervane strategy of the worms varied between strains. The frequency of the pirouettes was significantly higher with the half ablated animals, more so with the SMBD- half ablated worms (Figure 6.8, Graph I). Interestingly the two double ablation worms that managed to reach the peak didn't exhibit a very high frequency of pirouettes (Figure 6.8, Graph I). The ablated worms tested here exhibited a repetition of pirouettes in order to readjust the body towards the gradient, whereas for the wild type a reversal and a turn was sufficient (Figure 6.8, Images A-F). The weathervane index of the ablated strains was significantly lower from the wild type animals (Figure 6.8, Graph J). When the half ablation and double ablation animals were assayed, long continuous steering tracks were few in comparison to the wild type worms, however, slightly higher in number than the full ablation strains (Figure 6.8, Graph J).

6.3.6 Asymmetric and double ablation increases frequency of pirouettes and introduces even more defects in the ability of the worm to steer in a circular gradient chemotaxis assay

Half dorsal ablation and double ablation animals exhibited a high frequency of pirouettes during the circular grid assay as well. This can be observed both in the trajectories of the worms and in the frequency of pirouettes measured (Figure 6.8, Images A-I and Figure 6.10, Images D-F, Graph I). As observed in Chapter 5 during the circular grid steering assays wild type worms kept pirouettes to a minimum, and in most of the assays they were missing altogether. Also, full ablation of SAA and SMB exhibited a high count of pirouettes (see Figure 6.9, Images A-I inserted from Chapter 5 for comparison and Figure 6.10, Images A-C, Graph F).

The ablated animals tested here, although they were able to align themselves with the direction of the gradient initially, were unable to gradually and continuously steer, and efficiently follow the gradient as the wild types could (Figure 6.8, Images A-I; compare with Figure 6.9, Images A-I). Interestingly, this was most apparent at the SAAD- ablated worms, but not the SMBD- ones, as only one of the 12 SAAD- worms tested managed to reach the peak of the gradient, resulting in its chemotaxis index being negative for this assay (Figure 6.10, Graph G). A similar negative chemotaxis result was observed when the double ablation animals were assayed. On the other hand, the SMBD- half ablated worms' chemotaxis index was positive overall, albeit significantly lower than the wild type animals (Figure 6.10, Graph G).

As a reminder of the previous chapter's results, the wild type animals reached the peak in the circular grid assay within 3 minutes. In contrast, 30.4 minutes were required for the SAA- and 39 minutes for the SMB- ablated animals. SAAD- half ablated animals required on average 44 minutes, SMBD- needed 21.4 minutes and the double ablation strain 48.3 minutes to reach the peak. All of the ablation animals' times to reach the peak were statistically different to the wild type overall (Figure 6.10, Graph H).

The SAAD- and double ablated worms that did not reach the peak exhibited a repetition of turns and pirouettes, resulting in them revisiting the same area, and thus never reaching the peak (Figure 6.8, Images B,C and G-I). A high count of pirouettes was observed in the one SAAD- ablated worm that managed to reach the peak (Figure 6.10, Images D and Graph I). The two double ablated worms that reached the peak exhibited a lot of pirouettes in this assay (~33), in contrast to the radial one (~9), but in taking so long to reach the peak the frequency was not that different to the wild type (Figure 6.10, Image F and Graph I). The frequency of

pirouettes of the SMBD- half ablated worms was also higher than wildtype (Figure 6.9, Graph I).

The worms that did reach the peak exhibited some performance of the weathervane strategy, however, with obvious defects and significantly lower in number than the wild type (Figure 6.10, compare Images A-F, and Graph J). To be more specific on the defects, one should observe and compare the high resolution snapshots of tracks formed from the assayed worms while steering up the circular gradient (Figure 6.10, Images A-F). SAAD- half ablated and double ablated worms showed a similar phenotype with each other and with SAA and SMB full ablation. They often exhibited some exaggerated head swings towards both the ventral and the dorsal sides, which made steering towards one direction, as required in this assay, difficult to achieve. The exaggerated head swings were quite random, and seen much more often than the wild type, as the worm was trying to follow up the gradient. Course correction was taking place with extensive use of pirouettes. On the other hand, SMBD- asymmetrically ablated worms exhibited a different pattern of steering defect to SAAD- and the double ablation strains. Most of the tracks formed exhibited some kind of looped and biased gradual turning as the worms seemed to not be able to fine-tune the head movement into steering on the other side (6 out of 11 worms tracked). These circular tracks resulted in the worm visiting the same areas over and over again. Continuous repetition of these biased circle-like trajectories was used for course correction (Figure 6.8, Images D and E; Figure 6.10, Images E). The SMBD- worms were not as able as the rest of the strains to instantly and locally re-align their body towards the gradient with a simple pirouette (wild type animals) or even a barrage of continuous pirouettes (full ablation of SAA and SMB, double ablation and SAAD- half ablation).

None of the animals in the control experiments reached and stayed within the area of the peak of the gradient (Figure 6.11, Images A, B and C).
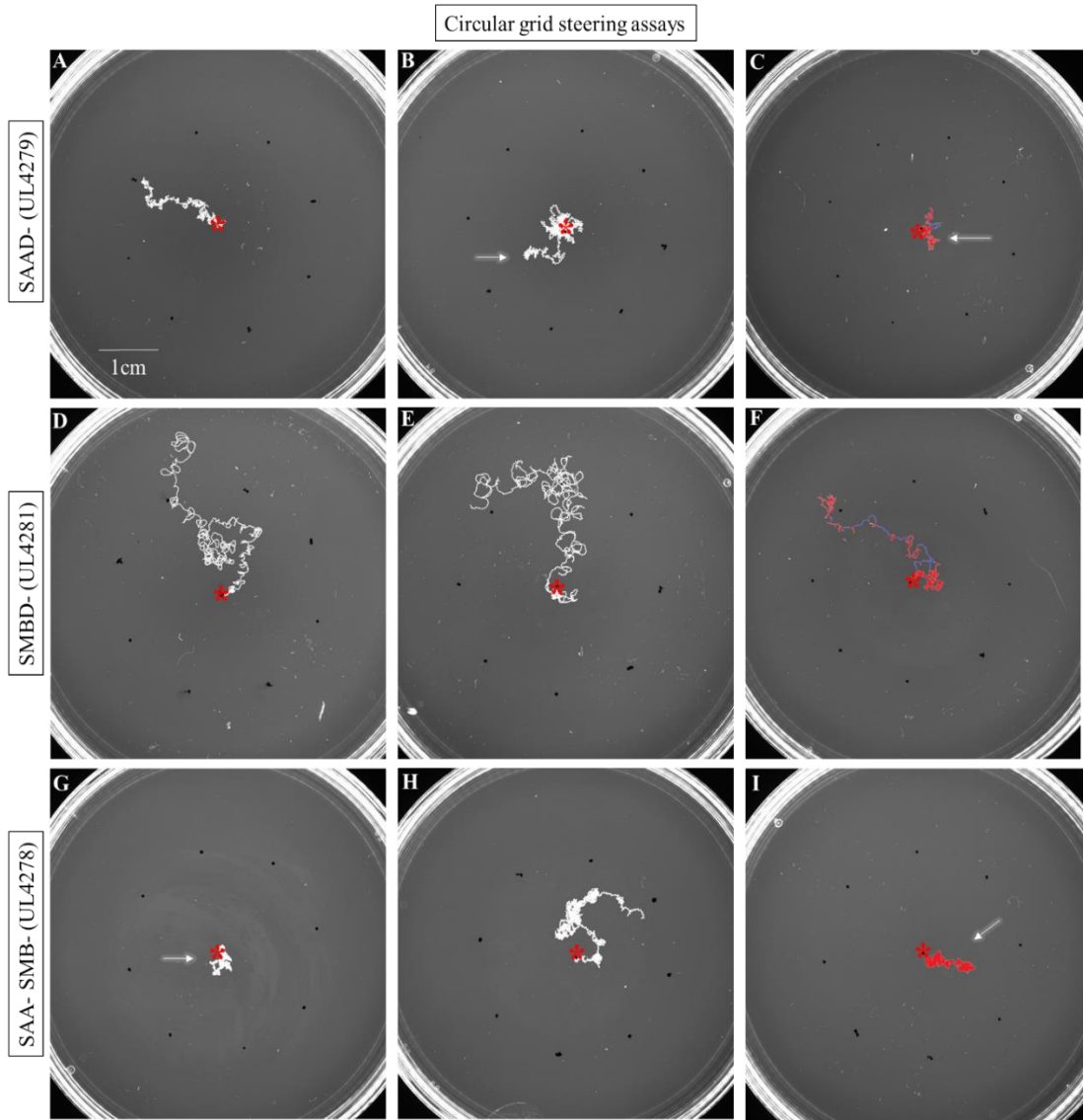
Figure 6.8 Images showing representative circular grid assays from the half ablated and the double ablation strains. Red star indicates the animals' starting points, black dots indicate NH_4Cl drop points. On the third image for each strain, trajectories have been coloured as follows: steering (runs) is in blue and pirouettes (tumbles) are in red. White arrows indicate animals that could not steer up the gradient, or followed it up but didn't reach the peak. [Animals tested: SAAD- (UL4279) n=12, SMBD- (UL4281) n=11, Double (UL4278) n=10].
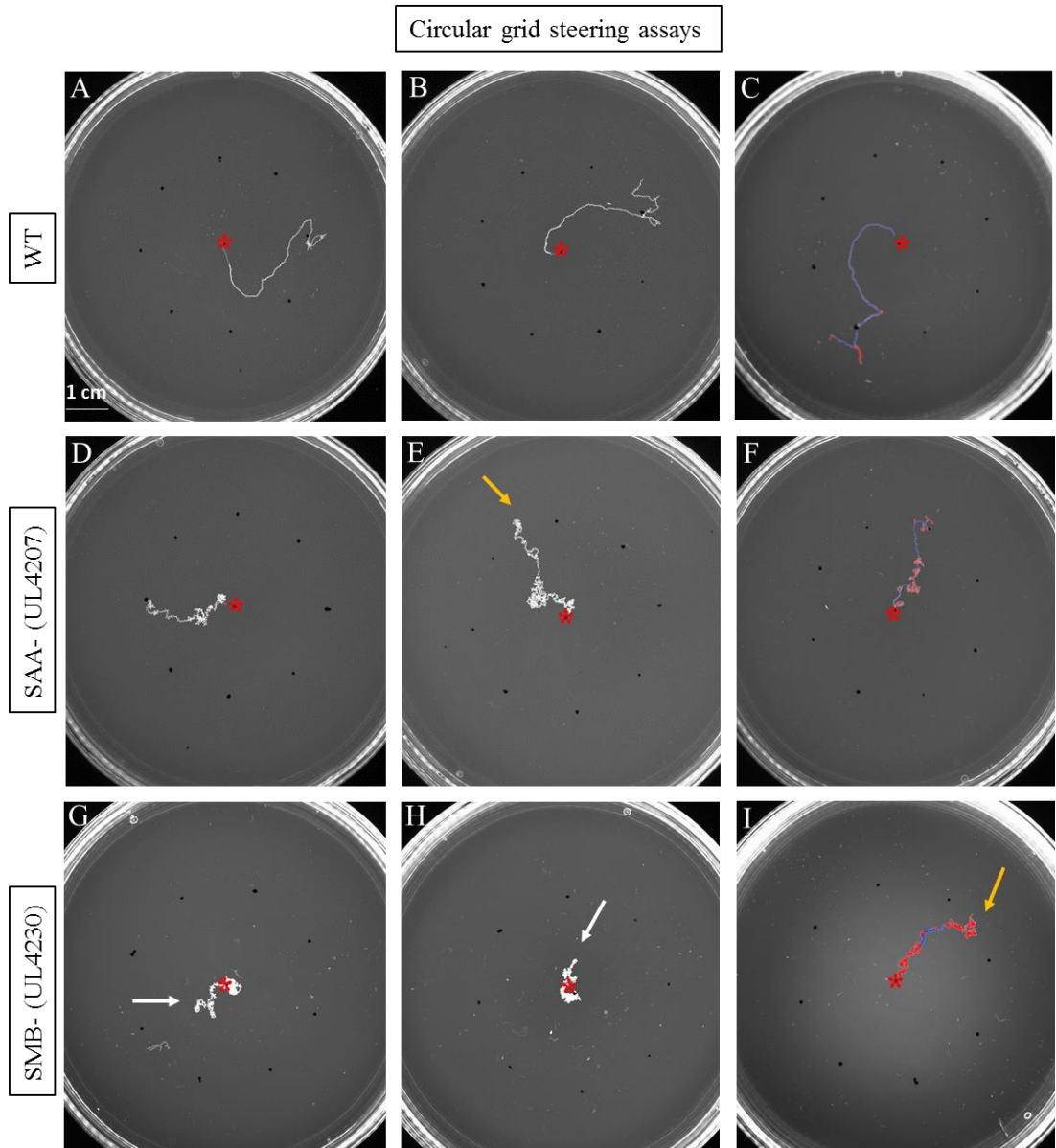
Figure 6.9 Images included from Chapter 5 showing representative circular grid assays for the wild type, SAA- ablated and SMB- ablated animals for comparison purposes. Red star indicates the animals' starting points, black dots indicate NH_4Cl drop points. On the third image of each strain trajectories have been coloured as follows: steering (runs) is in blue and pirouettes (tumbles) are in red. White arrows indicate animals that could not steer up the gradient (i.e. didn't reach a black dot). Yellow arrows indicate worms that followed it up but didn't reach a black dot. [Animals tested: WT n=19, SAA- (UL4207) n=14, SMB- (UL4230) n=12].
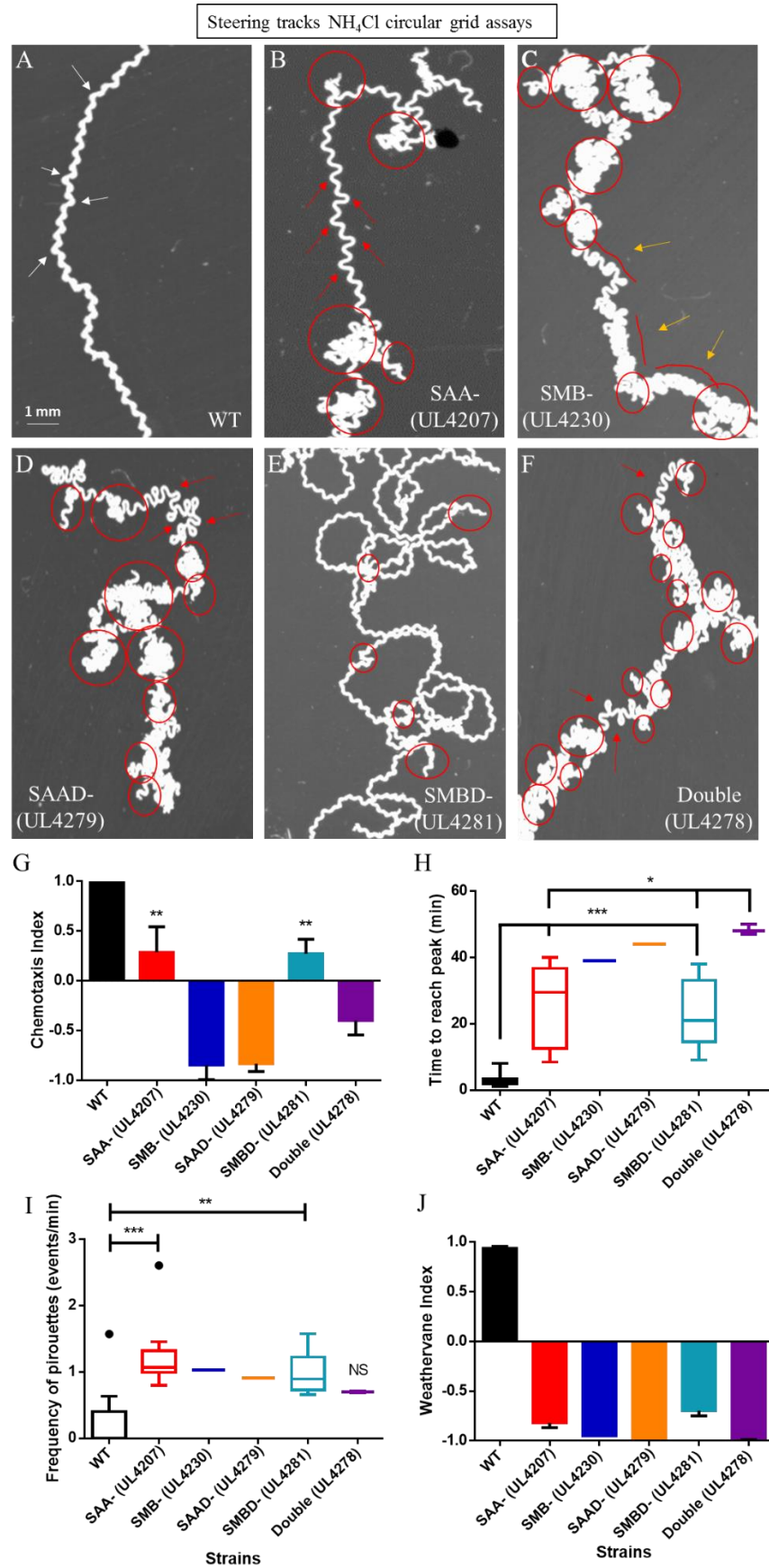
**Figure 6.10** Higher resolution images of the circular grid assays and their analysis. Figures

and graphs include the strains assayed in Chapter 5 for comparison. Images A to F show representative tracks of the different strains performing the weathervane strategy. The white arrows show normal biased head swings that course corrected the trajectory of the wild type worm. The red arrows indicate to examples of the inconsistency in the undulations that the ablated strains demonstrate. The yellow arrow indicates at an example of the consistency observed in the exaggerated head swings in the SMB- ablated worm tracks. Red circles indicate the parts of the tracks were a single pirouette, or a sequence of pirouettes, was performed. Graph G shows the chemotaxis index for each strain. Graph H shows a box plot of the time required for each tested strain to reach the peak of the gradient. Graph I shows the frequency of pirouettes for each strain as a box plot. Black dots represent two outliers. Graph J shows the weathervane index. Statistical significance and error bars, as STDEV, are indicated. Index error bars shown as SEM. (One-way analysis of variance (ANOVA) and Tukey's multiple comparison were used; ***p <0.001; **p<0.01; *p<0.05; animals that reached the peak: WT n=19 out of 19, SAA- (UL4207) n=9 out of 14, SMB- (UL4230) n=1 out of 12, SAAD- (UL4279) n=1 out of 12, SMBD- (UL4281) n=8 out of 11, Double (UL4278) n=2 out of 10).
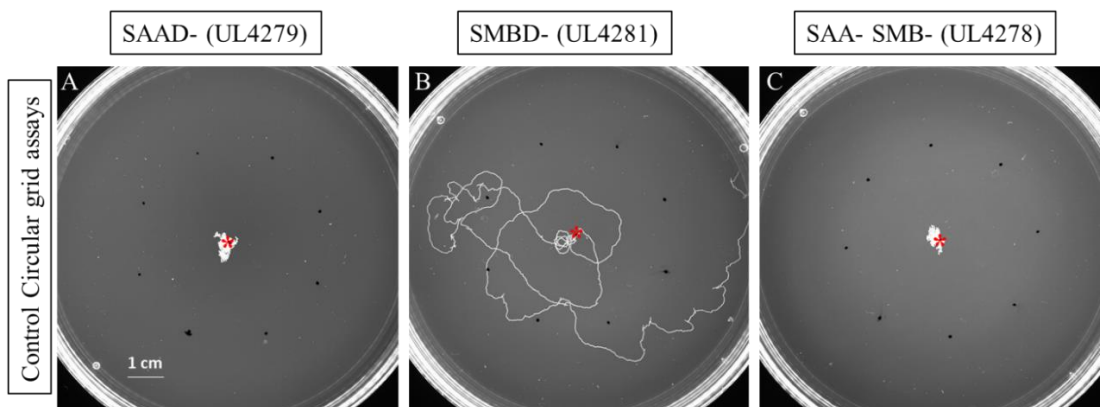
Figure 6.11 Images showing circular grid control assays. The experiments were performed with dH$_2$O drops instead of NH$_4$Cl. None of the animals in the control experiments reached and stayed within the area of the peak of the gradient. Red star indicates the animals' starting point, black dots indicate H$_2$O drop points. (n=2 for each strain).

6.4 Discussion

In this chapter, for the first time to my knowledge genetic ablation was used to kill only half of the cells of one class of neuron. The SAAD- and SMBD- ablation strains generated and explored here have not been generated before. Gray *et al.,* laser ablated the ventral sides of SMB, SMD and RMD (NB. the number of worms they did that on is unknown) and did not observe any effect on turns or undulations other than 'a gentle curvature over the course of several head bends' (Gray, J.M. *et al.,* 2005). This phenotype was not explored further. Asymmetric phenotypes have been explored only via optogenetic activation by shining light only on half of the AIY, AIZ, SMB, and RME neurons to activate them, and noting the turn of the head (Kocabas *et al.,* 2012). That study showed that the worm turns to the same side as the activation for AIY and SMB, whereas it turns to the opposite side of the activation with AIZ and RME.

6.4.1 SAA and SMB are not generating the undulations but regulate the amplitude and frequency of sinusoidal locomotion

Double ablation of the neurons of interest shows that SAA and SMB, together as a potential oscillator, are not the head neurons to generate the undulatory movement of the worm. Double ablation worms still exhibited fast rhythmic undulations, albeit very exaggerated. Double ablation strain's undulations were more exaggerated than in SMB- ablation worms, in turn SMB- ablation exhibited more exaggerated undulations than SAA- ablation (Figure 6.2). This summative defect suggests that SAA regulates the SMB, but also hints again that another neuron, with a function in head movement, is being regulated by SAA. Looking back at the broadened network of the neurons of interest in the head, and taking into consideration connection to SAA and all results so far of this project, SMD still remains a very good candidate, and will be further discussed while forming the proposed network for head movement in the General Discussion: Chapter 8 (see broadened network in Figure 1.5 or in Figure 8.1). Potentially SMD, due to its self-connectivity, forms a self-sustained oscillator that generates the undulatory rhythm in a digital-like rapid fashion (as observed in the double ablation worms). This is supported by the fact that SMD- ablated worms exhibit very shallow undulations (personal communication with Manuel Zimmer). The SMD oscillator could be coupled to a SAA/SMB oscillator, the latter regulating the amplitude and wavelength of the former's generated undulations but also facilitating turning (key part of pirouette strategy and exploratory behaviour) and the break in the undulatory symmetry required to enable the worm to steer (weathervane strategy).

6.4.2 SAA and SMB regulate the symmetry break during steering in a different manner

SAA and SMB's regulation of the amplitude of the generated undulations, which seems so far to translate into modulation of fine-tuned head movement, facilitates both turning (key part of pirouette strategy and exploratory behaviour) and the break in the undulatory symmetry required to enable the worm to steer (weathervane strategy). As mentioned numerous times in this project, indeed regulating the amplitude of the head swings is an important element for steering (Izquierdo and Beer, 2013).

SAA or SMB half ablations, demonstrated a high frequency of pirouettes in both gradient assays (Figures 6.5 and 6.8). Interestingly, whereas SMBD- ablated worms exhibited a milder phenotype than the full ablation of SMB in both chemotaxis assays, SAAD- ablated worms were more defected than SAA- fully ablated and SMBD- half ablated worms. This supports SAA's function as 'the regulator' in the oscillator hypothesis formed in the General Introduction (see Figure 1.8). For the regulator to be able to mediate dorsoventral activity (in general) and introduce bias (during steering and turns), it needs a functional symmetry.

Remarkably, however, half ablated worms were showing an inconsistency of head swing modulation during steering in the chemotaxis assays. Half ablated worms, either SAAD- or SMBD-, exhibited quite biased trajectories from start to end where course correction did not happen by gradual turning (fine-tuned modulation of head from being biased from the one side to the other) but with exaggerated irregular undulations and pirouettes. Few of the half ablation animals were exhibiting some gradual turning but were not consistent with their undulatory movement, switching between deep to very shallow undulations as they were going up the gradient during the radial gradient assay. The two different type of trajectories observed suggests that what I observed here is a result of reaching and aligning to the gradient at different phases of locomotion. As Izquierdo and Beer predicted with their computational model, a change in concentration received at different phases of locomotion produces identical chemosensory signals, however, could result in different turning bias (ventral or dorsal)(Izquierdo *et al.,* 2015). It is possible that some of the dorsally ablated worms (either SAA or SMB) sensed the gradient when in a ventral bend, resulting in ventrally biased loopy trajectories. And some worms sensed the gradient when in a dorsal bend, resulting in the worms demonstrating shallow almost straight line trajectories going up the gradient as the dorsally part of the neuron is ablated and the head cannot either recover at that side or fully undulate at that side. In this case results are also hinting to a defect on possible proprioceptive function within the neurons of interest. In both cases course correction could not happen by fine-tuned modulation of the head and the worm's would keep going at the same direction if not course corrected by exaggerated irregular turns and pirouettes.

Trajectories with loops were more obvious and abundant in SMBD- ablation worms especially during the circular grid assay. On that note, it is extremely interesting that SAAD-ablated worms showed a differential response in these two steering assays compared to the SMBD- ablated strain. Albeit without exhibiting as much steering as the wild types, SMBD-ablated worms chemotaxis index was positive, and time to reach the peak was as low as in the wild type worms. Dorsally ablating the SMB motor neurons seems to result in steering in worms still functioning but not as effectively, modulation of the head is taking place but in a very biased way, unable to recover to the other side, possibly hitning at loss of proprioceptive feedback at the side that SMB was ablated. Dorsally ablating the SAA interneurons, however, resulted in a bigger defect in steering with the worms not able to modulate the gradual head turning at all. SAAD- ablated worms overall performed as badly as SMB- and double ablated (SAA-SMB-) worms did, in both assays. Breaking the symmetry of SMB, which takes place in wild type worms during steering anyway, is not as detrimental to the navigational function of the worm as breaking the symmetry in SAA appears to be. Unexpectedly, SAAD- half ablation resulted in even worse steering defects than the SAA- full ablation. It seems that informational symmetry flow is more important than having the whole regulator present.

Half ablations have 'broken' the SAA/SMB oscillator, and introduced a one side continuous neuronal asymmetry that resulted in a defect in the transition of head swings from normal to a one-side biased undulation during directional movement (SMBD- and SAAD-) or resulted in the absence of functioning steering (SAAD-). SAA seem to be regulating that 'break' in symmetry during steering and SMB seem to translate it, as it is expected from a motor neuron, and modulate it according to feedback it receives (possibly proprioceptive). However, whether these results reflect the breaking of a rhythm oscillator, or a decrease in proprioceptive information from the one side of the worm, or both, is still unclear. For this reason stretch receptor expression will be explored in the next chapter.

6.4.3 SAA more than SMB regulates the frequency of turns thus facilitating runs during local search and dispersal

As mentioned previously, regulating the frequency of turns is an important element in navigation as modulation of it facilitates the switch between local search and dispersal. As with the dispersal assays conducted in Chapter 3, the half ablated, and even more so the double ablated, worms exhibited high frequency of pirouettes and turns without an attractant cue (compare images within Figure 6.3). This was mostly due to the fact that ablated animals performed more turns and less runs during the one hour of video-tracking. Interestingly, the SAAD- ablated animals showed an area coverage similar to the SAA- ablated animals, whereas SMBD- half ablation did not show similar results as the SMB- full ablation. SMBD-

worms exhibited more gradual turns over the course of many undulations, resulting in trajectory loops. This phenotype seems similar to what Gray *et al.,* observed while laser ablations of the ventral somas of the head motor neurons SMB, SMD and RMD (Gray, J.M. *et al.,* 2005). These trajectory loops had the worms revisiting the same areas in a different spatial way than with the abrupt sharp turns as seen with the rest of the ablated strains. This resulted in the SMBD- animals covering a bit more area than the other strains, but still not as much as the wild type animals. This suggests that SAA might have a more integral role in controlling the innate frequency of turns than SMB, highlighting once again that a lot of turns observed in SMB- ablated worms were a result of over bending on either side (see Chapter 3 and Chapter 5 discussion about SMB- ablation and frequency of turns). It also suggests that SAA's symmetrical function might be important to the SAA/SMB oscillator, should the hypothesis of an oscillator prove correct. Indeed, whether the whole regulator (SAA-) or half the regulator (SAAD-) of the oscillator is killed, the defect in the context of explorative behaviour (non-directed locomotion) is the same. In the context of directed locomotion (chemotaxis), as I will discuss below, SAAD- half ablation worms actually exhibit even more defected phenotypes than full SAA- ablation worms, further correlating SAA neuron's function with steering. Finally, on ablating the whole oscillator (double ablation) the worms could no longer perform any runs. All suppression of turns (from both via SAA and SMB) has been lifted and spatial non-directed navigation is almost impossible.

6.4.4 Troubleshooting the ventral half ablations in the future

The plasmids that were injected in the distal gonad of SAA- and SMB- ablated transgenic worms in order to generate a dorsal genetic rescue, were sent for sequencing. Sequencing results showed some unexpected extra nucleotides within the constructed plasmid before the start codon. Protein P35 was provided in a pBluescript II vector and this region was part of the P35 loci not included in the map provided. The reading frame seems not to be shifted with these additional nucleotides. However, expression of P35 could have been defected due to these addition nucleotides. There is also the possibility the promoter regions regulating the ablation of SAA and SMB, were driving expression at an earlier developmental time than the *npr-1* promoter (l3 larval stage). Both *flp-12* and *lad-2* seem to drive expression in the l1 larval stage, earlier than *npr-1*(Wang *et al.,* 2008; Kim, J. *et al.,* 2015b). In this case, it seems likely that ablation of all cells of SAA or SMB took place earlier than the rescue and was irreversible, hence I didn't observe any genetic rescue or change in phenotype.

At the time this thesis is being written there are no obvious means of inducing the expression of the P35 under the *npr-1p* promoter region earlier than the region driving the caspase expression. But perhaps the expression of one of the two caspase subunits could be fused with

an inducible element and delay the ablation. A potential route would be to try and combine the tetracycline inducible element (Das *et al.,* 2016) in one of the two caspase plasmids. Alternatively, the strains could be generated again using a parent strain of heat-shock factor-1 (*hsf-1*) mutants and the caspase plasmids regulated under the expression of the heat shock factor (*hsf-1*). That would allow for spatial and temporal regulation of the caspase plasmid expression as cell-specific expression of *hsf-1* should provide a normal heat-shock response only in targeted cells (Bacaj and Shaham, 2007). It would be interesting to see whether the ventral or the dorsal side has a more important role in turning or steering, and whether there is any innate ventral or dorsal bias in the worm's locomotion in general.

Chapter 7
SAA, SMB and proprioception: The expression patterns of the *trp* mechanosensitive genes

7.1 Introduction

Since White *et al.,*'s 1986 study on the neuroanatomical structure of *C.elegans*, it has been hypothesized that a number of neurons could function as proprioceptors that sense the worm's body postures via stretch receptors. These potential proprioceptive neurons, such as the B-class motor neurons, have processes that can sense body bending, act via stretch receptors and modulate locomotion (White, J.G. *et al.,* 1986). Theoretical studies have showed that the worm's sinusoidal locomotion might not require a central pattern generator but instead is generated by motor neuron sensory feedback via stretch receptors (Boyle *et al.,* 2012; Fang-Yen *et al.,* 2010). As discussed in the General Introduction (Chapter 1), this hypothesis was tested in relation to the B-class of motor neurons, by using microfluidics to bend the worm at specific places along the body and by measuring neuromuscular activity using calcium imaging (Wen *et al.,* 2012). Also, by optogenetic inhibition of the repeated units of VB and DB motor neurons in freely moving worms, Leifer *et al.* were able to suppress undulatory wave propagation along the body (Leifer *et al.,* 2011). In addition, a stretch receptor has been characterised, *trp-4*, a *C.elegans* homologue of the mechanosensitive TRPN channel (Li, W. *et al.,* 2006). That study showed that the DVA neuron functions in proprioception mediated by the expression of the *trp-4* gene. Another study implicated the PVD neuron in proprioceptive function, as ablation of it leads to defective body postures, and this is mediated via the mechanosensory DEG/ENaC channel encoded by the gene *mec-10* (Albeg *et al.,* 2011). Very recent work by Kyuhyung Kim and colleagues (not published yet at the time this thesis is being written) showed that two TRPC channels [encoded by *trp-1*, *trp-2,* (Colbert *et al.,* 1997; Feng *et al.,* 2006)] are co-expressed in SMD and mediate SMD's role in head dorsal movement (and Kyuhyung Kim, personal communication).

As explained in the General Introduction (Chapter 1), proprioceptive function in worms is very important for steering, as it enables the body of the worm to follow the head's direction. In addition, proprioception could aid the maintenance of dorsoventral asymmetry (symmetry breaking) in the head that steering requires.

During Chapter 3 and Chapter 6 my results hinted at SAA and SMB having some proprioceptive function. Observation and description of their anatomy has given the same insight as well (White, J.G. *et al.,* 1986). To investigate whether that function could

potentially be stretch receptor mediated, I wanted to observe the localisation of known stretch receptors of the mechanosensitive TRPN channel. I generated strains expressing reporter constructs for known stretch receptors encoded by the genes *trp-1*, *trp-2* and *trp-4* (Colbert *et al.,* 1997; Feng *et al.,* 2006; Li, W. *et al.,* 2006) (and Kyuhyung Kim, personal communication). The fluorophores I used for the expression of the stretch receptors and the neurons of interest were different, so that I could investigate their co-localisation, if any.

7.2 Material and methods

7.2.1 Nematode maintenance and strains

Animals were kept at 20°C at all times, fed *E.coli* (OP50 strain) and were maintained as previously described (Brenner, 1974). The *C. elegans* variety N2 Bristol wild-type strain was provided by the Caenorhabditis Genetics Centre (CGC), which is funded by NIH Office of Research Infrastructure Programs (P40 OD010440). Stretch receptor expression strains *trp-1*::SAA (UL4229), *trp-2*::SAA (UL4233), *trp-4*::SAA (UL4235), *trp-1*::SMB (UL4232), *trp-2*::SMB (UL4234), and *trp-4*::SMB (UL4236), were generated as explained in the 'Methods and Materials' section 7.2.2 of this chapter.

7.2.2 Generating the stretch receptor expression strains

7.2.2.1 Plasmids used

The *coel*::dsRED plasmid was a gift from Piali Sengupta (Addgene plasmid # 8938) (Miyabayashi *et al.,* 1999). It was used to drive expression of dsRED by the stretch receptors' promoter sequences.

The plasmids to drive GFP expression in the neurons of interest, *lad-2p*::GFP (for the SAA neurons) and *flp12sp*::GFP (for the SMB neurons), were constructed as described in Chapter 2. All plasmids share the pPD95_75 backbone manufactured by Andrew Fire.

7.2.2.2 Molecular biology

Promoter sequences for *trp-1p* (4kb region) and *trp-2p* (3.5kb region) were amplified by PCR from the nematode's genomic fosmid library. The promoter sequence for *trp-4p* (4.5kb region) was amplified by PCR from the worm's genomic DNA. Table A3 in the Appendix A section includes all primers and fosmids used. The promoter regions were then cloned into the *coel*::dsRED plasmid, both digested first with the restriction enzymes SphI/BamHI.

Diagnostic enzymatic digestions with BamHI, EcoRI, EcoRV, KpnI and SphI followed each time to confirm the constructs' identity.

ApE, a plasmid editor v2.0.47 software, was used for the annotation of all genomic regions, predictions of enzymic digestions and ligation results (Paradis *et al.,* 2004). Primer3 v0.4.0 software was used for primer design (Untergasser *et al.,* 2012; Koressaar and Remm, 2007). Oligocalc v3.27 software was used to check self-complementarity in primers and melting temperature (Tm) (Kibbe, 2007). The restriction enzymes and ligase that were used were purchased from Invitrogen. Primers were purchased from Integrated DNA Technologies (IDT).

7.2.2.3 Microinjections

The parent wild type strain used for generating the transgenic strains was the *C. elegans* variety N2 Bristol strain (Brenner, 1974). Transgenic worms were generated by the means of microinjection (Mello *et al.,* 1991), whereby the constructs mentioned above were microinjected into the distal gonad of a young adult worm alongside with a transformation marker (Hobert, 2002; Evans, 2006). The transformation marker used was the *coel*::GFP that drives GFP expression in the coelomocytes of the worm and it was a gift from Piali Sengupta (Addgene plasmid # 8937) (Miyabayashi *et al.,* 1999). Coelomocytes are localised away from either SAA or SMB somas. Therefore, the marker would not obstruct imaging of the nerve ring where the somas of the neurons are situated and it was also a good control against bleed-through from the green channel to the red channel when imaging. See Table 7.1 below.

Table 7.1 Generated transgenic strains for the expression of the stretch receptors in the SAA and SMB neurons.

Strain injected	Plasmids injected	Marker	Expected expression of GFP	Expected expression of dsRED	Strain name
N2	*flp12sp*::GFP *trp-1p*::dsRED	*coel*::GFP	SMB	Cells where *trp-1* is expressed	UL4232
N2	*lad-2p*::GFP *trp-1p*::dsRED	*coel*::GFP	SAA, SMD, ALN, PLN, SDQ	Cells where *trp-1* is expressed	UL4229
N2	*flp12sp*::GFP *trp-2p*::dsRED	*coel*::GFP	SMB	Cells where *trp-2* is expressed	UL4234
N2	*lad-2p*::GFP *trp-2p*::dsRED	*coel*::GFP	SAA, SMD, ALN, PLN, SDQ	Cells where *trp-2* is expressed	UL4233
N2	*flp12sp*::GFP *trp-4p*::dsRED	*coel*::GFP	SMB	Cells where *trp-4* is expressed	UL4236
N2	*lad-2p*::GFP *trp-4p*::dsRED	*coel*::GFP	SAA, SMD, ALN, PLN, SDQ	Cells where *trp-4* is expressed	UL4235

7.2.2.4 Microscopy and imaging

To observe GFP and dsRED expression the worms were put on a slide after being anaesthetised by the use of levamisole (2mM). A ZEISS stereo Lumar V12 was used to screen for transgenic animals. For imaging, a Leica M165 FC fluorescent stereoscope fitted with a Q-imaging Qi-CLICK COOLLED pE-300 camera and a ZEISS Axioplan fluorescent microscope fitted with a Q-imaging RETIGA 2000R camera, were used. Images were captured with Q-Imaging's Q-capture Pro 7 software. Images were processed with the use of FIJI software (Schindelin *et al.,* 2012).

7.3 Results

7.3.1 The gene encoding the *trp-1* stretch receptor is expressed in SAA, SMB & SMD
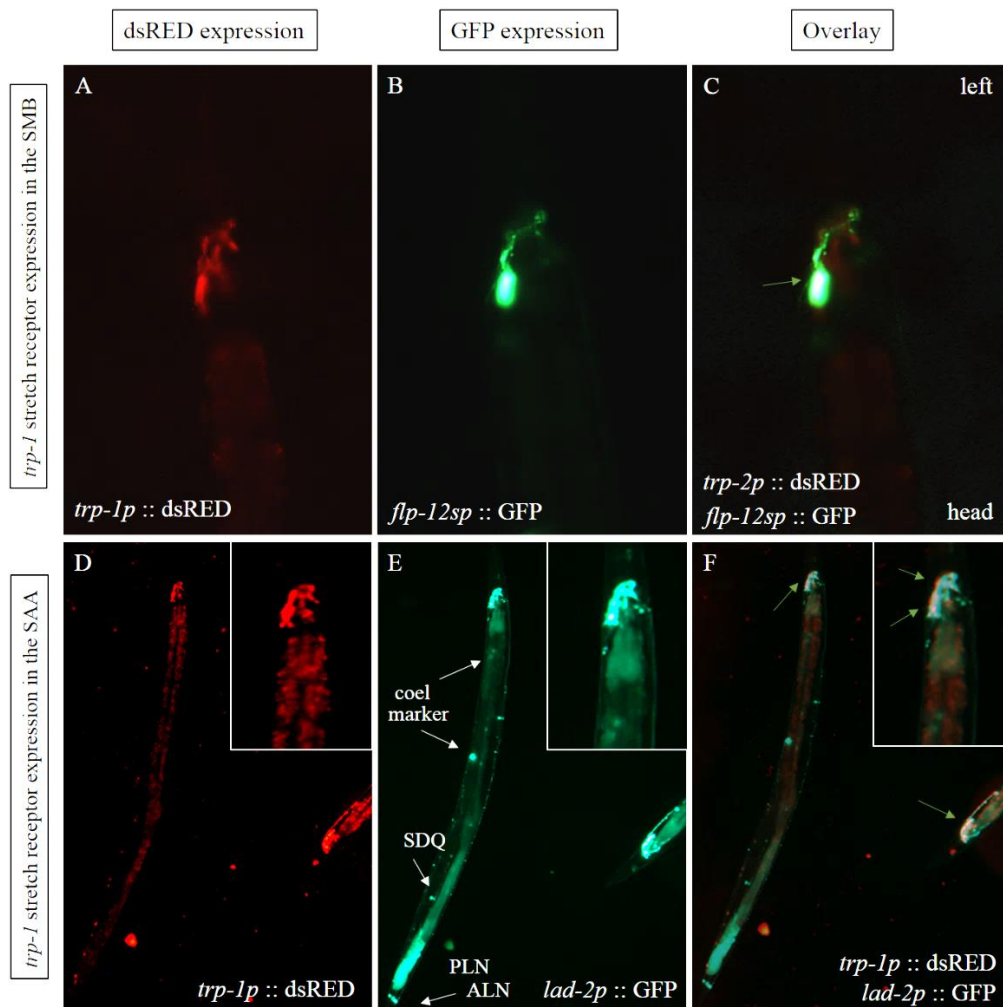
Figure 7.1 Microscopy images of the expression of the *trp-1* stretch receptor in the SMB (images A-C) and SAA (images D-F) neurons. Green arrows in Image F indicate co-localisation of stretch receptor expression with the neurons of interest. Strains imaged here are the *trp-1*::SAA (UL4229) and *trp-1*::SMB (UL4232).

Overlaying images of the GFP and dsRED signal showed expression of *trp-1* in both the SMB (Figure 7.1, Image C) and the SAA (Figure 7.1, Image F) neurons. In addition *trp-1* seems to be expressed in all the nerve ring cells the *lad-2p* promoter region expresses in, not just the SAA, meaning the SMD.

7.3.2 The expression pattern of *trp-2*
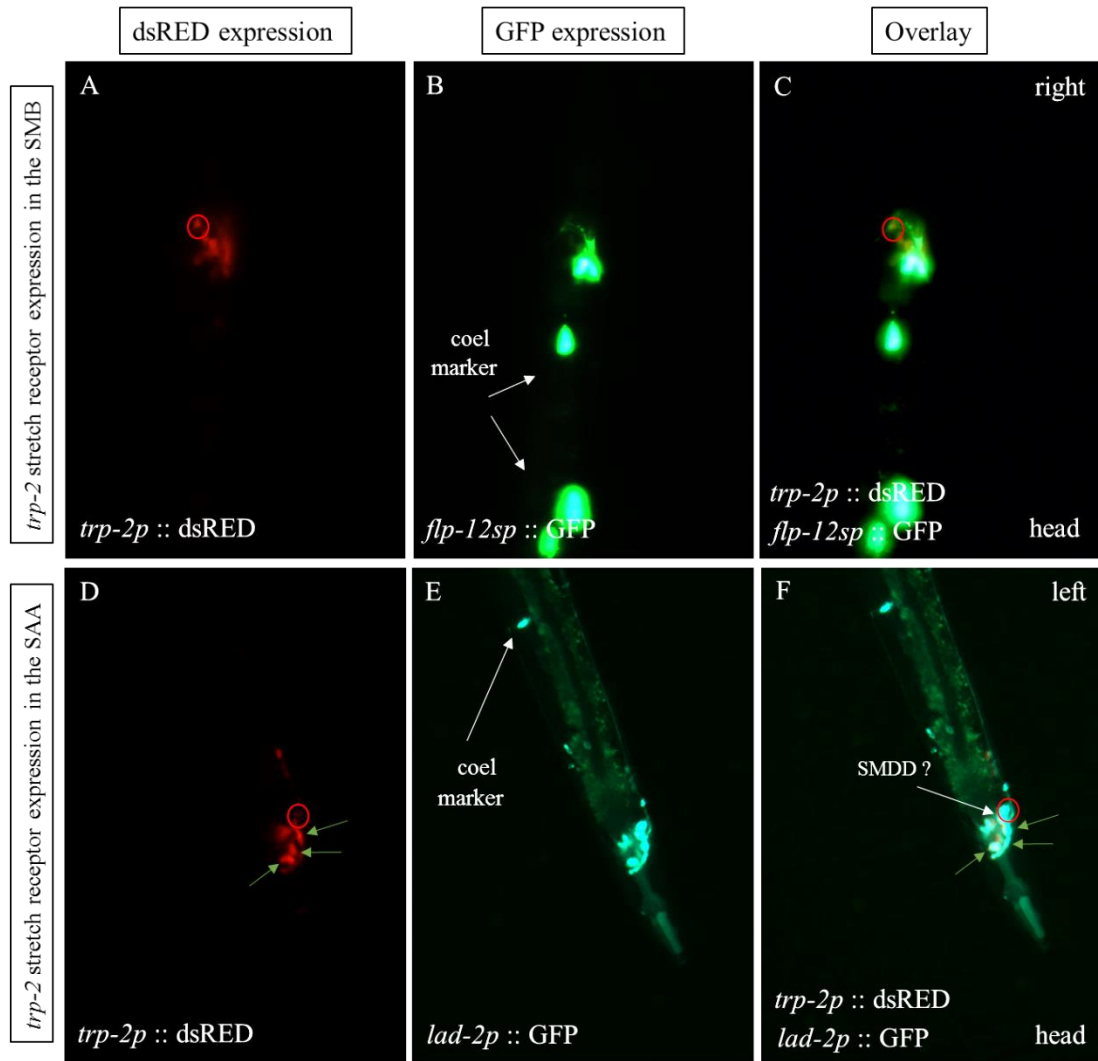
Figure 7.2 Microscopy images of the expression of the *trp-2* stretch receptor in the SMB (images A-C) and SAA (images D-F) neurons. Green arrows in Image F indicate co-localisation of stretch receptor expression and the neurons of interest (including SMD). Green arrows in Image D indicate the cells were co-localisation of stretch receptor expression is seen in Image F. Red circles indicate areas were co-localisation is unclear. Stretch receptor expression strains imaged here are the *trp-2*::SAA (UL4233) and *trp-2*::SMB (UL4234).

Overlaying images of the GFP and dsRED signal showed expression of *trp-2* in the SAA neurons and SMDV (Figure 7.2, Image F). However, the stretch receptor seemed not to be expressed in the somas of the SMB (a potential expression of the stretch receptor in the area

where the axon of SMB circles the nerve ring) and the dorsal cells of SMD (Figure 7.2, Images C and F). Red circles in the two images (Figure 7.2, Image C and F) indicate areas were co-localisation is still unclear.

7.3.3 The expression pattern of *trp-4*
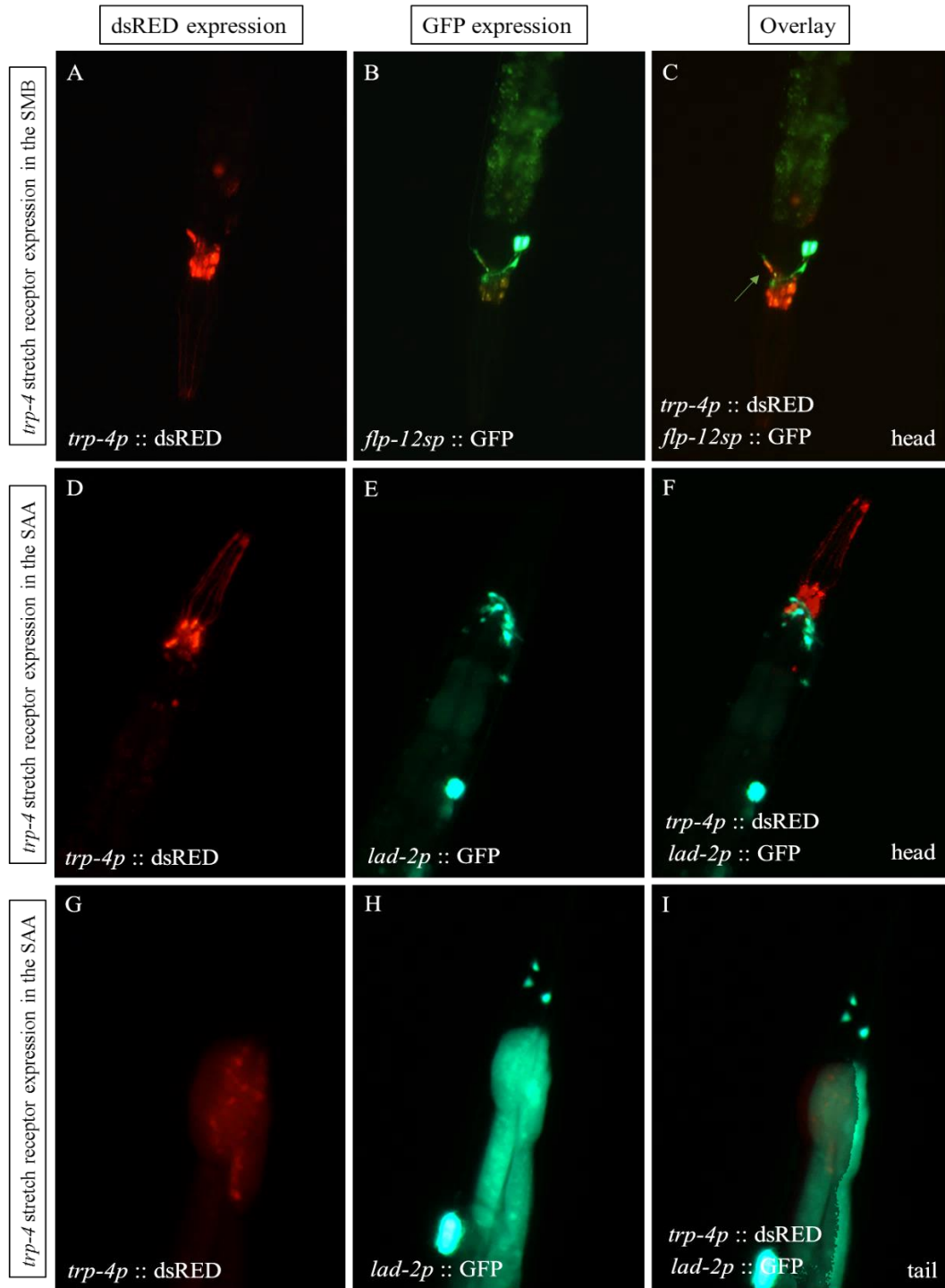
Figure 7.3 Microscopy images of the expression of the *trp-4* stretch receptor in the SMB (images A-C) and SAA (images D-I) neurons. Green arrows indicate co-localisation of stretch receptor expression with the neurons of interest. Stretch receptor expression strains imaged here are the *trp-4*::SAA (UL4235) and *trp-4*::SMB (UL4236).

Overlaying images of the GFP and dsRED signal showed no expression of *trp-4* in the SMB somas (Figure 7.3, Image C) or anywhere in the SAA or SMD neurons (Figure 7.3, Image F, I). There was some minor overlap at the start of SMBD's axon (Figure 7.3, Images A-C; green arrow in C). However, this was not observed elsewhere along the SMB's axons but was a recurring pattern at that specific area across the *trp-4*::SMB (UL4236) strain (approximately 20 worms observed). Finally, there is an orange signal above the nerve ring axon of SMB neurons, however, this is bleed through of the ds-RED signal (flp-12sp is not expressed at that area, see also difference with the axon part that co-localisation of signal is indeed present) (Figure 7.3, Image B). Table 7.2 shows a summary of the results from all the stretch receptor expression strains.

Table 7.2 Summative table of stretch receptor expression in the SAA and SMB neurons.

Neurons	Stretch receptor	Co-localisation of GFP and dsRED	Strain name
SAA/SMD	*trp-1*	YES (SAA, SMD)	UL4281
SMB	*trp-1*	YES (SMB)	UL4279
SAA/SMD	*trp-2*	YES (SAA, SMDV) Unclear (SMDD?)	UL4282
SMB	*trp-2*	Unclear (nerve ring axon?)	UL4283
SAA/SMD	*trp-4*	NO	UL4278
SMB	*trp-4*	Unclear (dorsal axon?)	UL4278

7.4 Discussion

The results reported in this chapter support those in Chapter 3 and Chapter 6 that hinted toward SAA and SMB having some proprioceptive function. The stretch receptors investigated here showed some expression in the neurons of interest. *trp-1* was expressed in both SAA and the SMB. *trp-2* was shown to be expressed in the SAA neurons but results were unclear for the SMB neurons. *trp-4* showed no expression in the somas of either neuron, but was seen in a small part of the axon of SMBD. Due to time constrains, the investigation of the expression of the stretch receptors did not progress further. It would be good to confirm

via means of confocal microscopy whether *trp-2, trp-4* is indeed expressed in SMB's axons and pin down which SAA and SMD cells are indeed expressing the *trp-2* stretch receptor.

If what the results suggest here are true then it is possible that SAA, SMB and SMD together form a proprioceptive mediating oscillator, which is recovering from a ventral bend to a dorsal bend of the head by activation from stretch receptors on the dorsal side of the neural cells (the side that was previously stretched/relaxed). The lack of synaptic connectivity between the dorsal and ventral cells of the SMB could be counterbalanced by a proprioceptive function in those cells, facilitated by the expression of *trp-1* for example. Additional proprioceptive information of the dorsal state and the ventral state of the muscles in the head could also come from the SAA and SMD neurons, and that would bring even more robustness to the undulations. This could be facilitated by both *trp-1* and *trp-2*.

But how is the proprioceptive information of the state of the head passed down along the body and facilitating gradual turning? Where does the integration of this information take place? It is perhaps telling that the DVA neuron - shown previously to be a stretch receptor neuron (Li, W. *et al.,* 2006) - is synaptically connected with SMB and SAA, and that SAA has post-synaptic connections with DB motor neurons that are also known to have a proprioceptive function (Leifer *et al.,* 2011; Wen *et al.,* 2012).

It is also very interesting that alongside the targeted neurons SAA and SMB, *trp-1* and *trp-2* showed expression in the SMD head motor neuron. The stretch receptor expression pattern in SMD looks very similar to that in SAA, supporting the hypothesis discussed in Chapter 3 that SAA could be regulating both SMD and SMB and these motor neurons affect head movement in an opposite manner.

It might be the case that partly (there ought to be other parallel pathways) feedback information on the state of the bending of the head comes from all three neurons (i.e SA, SMB, SMD), thereby forming a proprioceptive-mediated head oscillator. This hypothesis will be further explored in Chapter 8: General discussion.

The next step for this part of the project would be to show whether the locomotory phenotypes observed by SAA and SMB ablation are dependent on the activity of *trp-1* and *trp-2* specifically in those cells. For example, it would be good to test if silencing expression of *trp-1* and *trp-2* in SAA and SMB specifically, results in the observed undulatory phenotypes described in this thesis, and whether rescue of *trp-1* and *trp-2* expression recovers wild type body posture. Finally, relationships between the neurons shown to have proprioceptive function should be investigated. Specifically, interaction of the DVA (*trp-4*), PVD (*mec-10*) stretch interneurons and DB motor neurons with SAA interneuron, SMB and SMD head motor neurons should be observed via a combination of optogenetics and calcium imaging in

freely moving worms, in order to shed more light on the integration of the information of the head bending and its propagation down the body during forward locomotion.

Chapter 8
General Discussion

> 'The movements of animals may be compared with those of automatic puppets, which are set going on the occasion of a tiny movement; the levers are released, and strike the twisted strings against one another…Animals have parts of a similar kind, their organs, the sinewy tendons to wit and the bones; the bones are like the wooden levers in the automaton, and the iron; the tendons are like the strings, for when these are tightened or leased, movement begins.'
>
> Aristotle, 4th century BC
>
> 'On animal movement'

8.1 Discussion

In this project, I used *C.elegans* to investigate the role of two neurons, the SMB motor neuron and the SAA interneuron, in the orientation strategies this animals employs to navigate its environment, and tried to highlight their general function in the worm's locomotion.

I established transgenic ablation strains missing either the SMB or SAA, both of them, or just the dorsal part of them, with the use of a fine-tuned genetic approach. I also expressed calcium indicators and used reporter genes to examine stretch receptor expression to try and answer additional functional questions about the neurons. Finally, I focused on the potential role these neurons have in the orientation strategies observed in the worm, by conducting different types of chemotaxis assays.

Here, I will sum up all of the findings starting with roles in locomotion shared by both neurons of interest. I will go on to discuss the differences observed between them and conclude with focusing just on steering and the pirouette strategies. Some are discussed in the context of the head network involved in undulations and a broadened network regulating the weathervane (steering) and pirouette strategies. For this reason, I include again in Figure 8.1 the broadened network around the neurons of interest first introduced in the General Introduction: Chapter 1, to aid the reader before proposing my own network and model.
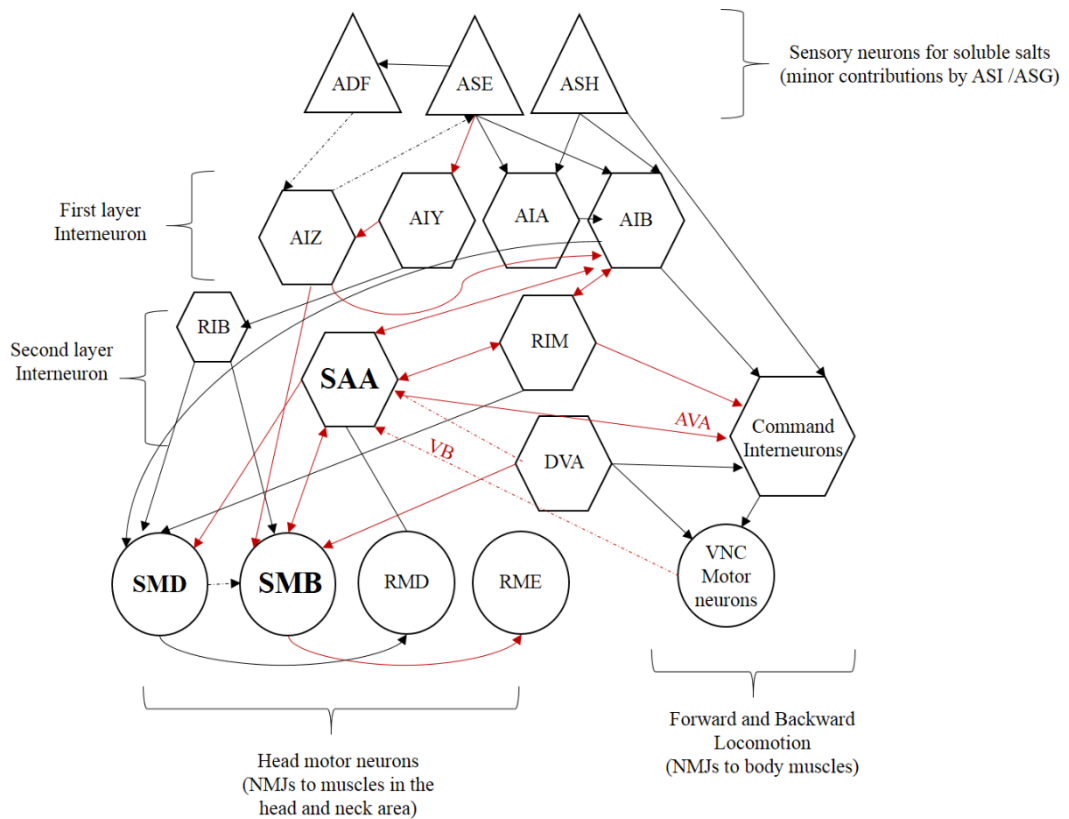
Figure 8.1 A broadened network of postsynaptic and presynaptic partners to the neurons relevant to this project. Starting from the input layer (amphid sensory neurons responding to soluble salts) to the output (muscles). In bold are the neurons of high relevance to the project. Dashed lines are weak connections, solid lines are strong. In red colour are the connections of high relevance to the project.

8.2 The role of the SAA and SMB neurons in locomotion, with a focus on steering

This project provides the first description of the role of the SAA interneuron in locomotion, its regulation of SMB motor neuron and potential regulation of another head motor neuron (probably SMD). The project shows evidence of SAA and SMB's role in head turning, setting the amplitude of head swings, integrating the two orientation strategies (promoting runs while suppressing pirouettes via SAA's connection to the reversal circuits) and showed that they are integral for facilitating steering.

8.2.1 The SAA and SMB neurons are involved in setting the amplitude of sinusoidal locomotion

Consistent with what was previously hypothesized for the SMB neuron due to its anatomy and position (White, J.G. *et al.,* 1986), and later shown by laser ablations (Gray, J.M. *et al.,*

2005; Kim, J. *et al.,* 2015a), my experiments showed that SMB is indeed involved in setting the amplitude of sinusoidal movement. Here, I have provided a more detailed description of the phenotype. The exaggerated head swings were apparent in all contexts the animals were observed under, such as on food, in liquid, off food and during chemotaxis. This function of SMB is not context dependent, but appears more mechanistic, taking place generally during the worm's navigation.

As far as SAA is concerned, I showed for the first time experimentally that SAA neurons are part of the circuit that sets the amplitude of undulations. As for SMB, my results were consistent with what was previously hypothesized for the SMB neurons due to its anatomy and position (White, J.G. *et al.,* 1986); i.e. the exaggerated head swings were apparent in all contexts the animals were observed under, such as on food, in liquid, off food and during chemotaxis. This function of SAA, as with the SMB, seems to be not context dependent, but something more mechanistic, taking place generally during the worm's navigation. However, the SAA ablation phenotype is shallower than the SMB$^-$ one, suggesting that SAA could control another motor neuron, and the effect of the ablation that I observed is a combinatorial result of affecting different motor neurons. SMD is the ideal candidate. It is closely localised to both neurons of interest. In fact, SMD cells wrap round the processes of SAA neurons ventrally and it is densely synaptically connected with SAA (White, J.G. *et al.,* 1986). With SAA- ablated, SMD and SMB are still intact and functioning as opposite motor neurons (as discussed throughout this thesis) but their activity is decreased.

In contrast to what I observed in the sum of my experiments, laser ablation of SAA recently showed no phenotype or change in the wavelength or width of the undulations (Kim, J. *et al.,* 2015a). This is where the advantage of generating genetic ablation strains is highlighted, no matter how much more time and effort it needs than laser ablations do. To this I would like to add that in Kim *et al.,*'s study curvature was not measured by the curving angle but broken into two measurements: the wavelength and width. By doing so perhaps subtle differences were not observed. However, the SAA curvature phenotype can be observed by direct observation in snapshots, as provided in Chapter 3 here.

In addition, it is important to mention that SAA- ablated worms exhibited irregular exaggerated head swings in a very short timescale with each other and to both ventral and dorsal sides. The exaggerated head swings were without an obvious period or rhythm. Wild type and SMB- ablated worms didn't show such an irregularity. This hints at an additional role for SAA in setting the rhythm of undulation and supports its role as the 'regulator' in the SAA/SMB head oscillator hypothesis mentioned in the Introduction and discussed below in Section 8.4.

That SAA might have a function in head swings has been hypothesised by two *in silico* computational models investigating head movement and its integration with body movement (Sakata and Shingai, 2004; Karbowski *et al.,* 2008). The Sakata and Shingai model though did not include some of SAA's connections to the SMD head motor neurons and the reciprocal inhibition of the SAA by the SMB neuron. It also included neurons that have since been shown to be part of initiating reversals and not head movement. The Karbowski model placed SMD and SMB as one component, where both were excitatory and completely ignored their connections with SAA.

8.2.2 The SAA and SMB neurons are involved in setting the amplitude of omega/delta turns

For the first time I have shown that SAA and SMB control the amplitude of the omega/delta turns, their individual ablation resulting in similar coiled phenotypes.

Specifically for SMB, calcium imaging of the neuron on freely moving worms showed its activity peaking after the onset of the turn in what seems to be a graded response. Ablation of SMB resulted in a coiled turn phenotype. This phenotype was not observed or explored by Gray *et al.,*'s study as they didn't differentiate between undulatory exaggerated movement of SMB ablation and an omega turn. I counted as omega/delta turns only the turns where the head touched the body, which accounts for most of the re-orientation turns anyway (Gray, J.M. *et al.,* 2005; Broekmans *et al.,* 2016).

SMD has been shown to regulate the amplitude of the omega/delta turns but in an opposite fashion. Its ablation resulted in shallow turns (Gray, J.M. *et al.,* 2005), again highlighting the antithetical role SMD has to SMB. No other head neuron has been shown to have any effect on the amplitude of the turns. These past data will be taken into consideration when forming the proposed network model for the two orientation strategies and the head movement oscillator model.

8.2.3 The SAA and SMB neurons are involved in regulating the innate frequency of turns

For the first time I have shown that in all environments tested the turn frequency of the SAA- and SMB - ablated worms was significantly increased. This suggests that SAA and SMB, when functioning normally, inhibit the frequency of the turns. In addition, the level of the increase in turn frequency was different between the strains, with SMB showing a greater increase. Interestingly, SMB also showed an increase in the amplitude of head swings

compared to SAA. This might suggest that increase in turns is the result of overbending due to the head swings often passing a threshold that results to the performance of a turn. It's also worth pointing out the ventral bias observed while measuring calcium influx ratios in the BWMs of only SMB- ablated worms, which may also account for the greater increase in turns since omega turns are ventrally biased.

8.2.4 The SAA and SMB neurons facilitate the local search/dispersal switch

By inhibiting the innate frequency of spontaneous turns SAA and SMB facilitate in this way long runs that in turn facilitate exploratory behaviour during dispersal. For the first time I have shown that SAA and SMB is involved in the switch of local search to dispersal (long-range exploratory behaviour) by supressing the frequency of turns enabling in this way long runs. The level of involvement is differential here, with SAA being more important than SMB, as the half ablation strains demonstrated. SAAD- ablated worms exploratory decrease was much greater than SMBD- (and similar to SAA- ablated worms) in contrast to the SMBD-ablated worms that were milder in defect.

8.2.5 The SAA and SMB neurons have a proprioceptive function

The results of behavioural assays in Chapter 3 and Chapter 6 hinted toward SAA and SMB having some proprioceptive function. Ablation of SMB resulted in stiffness in the lower part of the body while swimming, and ablation of SAA could not recover body bend to the other side while swimming resulting in a decrease in motility. Both instances hinted at a loss of proprioceptive function. In addition, few half ablated worms, from both the SAAD- and SMBD- ablated strains, exhibited a change from deep to shallow undulations during chemotaxis, and that change could not recover to the normal undulatory phenotype for that strain for long periods of time.

I validated this idea in Chapter 7, where expression of known stretch receptor genes was observed. For the first time since it was hypothesised (White, J.G. *et al.,* 1986), stretch receptor expression was shown in the SAA and SMB neurons. Both *trp-1* and *trp-2* showed expression in SAA. Both *trp-1* and likely *trp-4* showed expression in SMB. The SMD neuron was also recently shown to express *trp-1* and *trp-2* (personal communication Kuyung Kim) and was confirmed by my experiments as well. SAA and SMB's synaptic connection to the DVA stretch receptor neuron and this neurons' expression of the TRP-4 stretch receptor (Li, W. *et al.,* 2006) might be partly responsible for the propagation of the wave of undulatory movement from head along the body.

8.2.6 The SAA interneuron regulates the SMB motor neuron

All results so far have strengthened the hypothesis that SAA is regulating the activity of the SMB head motor neurons. Similar phenotypes, albeit sometimes of differing strength, has causally linked them as a pairing working in unison in most of the behaviours investigated.

8.2.7 The SAA neuron has a subtle function in backward movement which may be linked to its function of suppressing pirouettes

SAA- ablated worms, but not the SMB- ablated worms, showed an increase in short reversals and length of long reversal. This result is reflecting the fact that from the two neurons explored here, SAA is the only one with strong postsynaptic and presynaptic connections to the backward locomotion circuit, namely the RIM and AIB neurons (Piggott *et al.,* 2011). SAA is also connected to the AVA command interneurons regulating backward movement (Chalfie *et al.,* 1985). SAA's strong role in suppressing pirouettes (i.e. even when half of its cells were ablated when SMBD- did not exhibit this), may be linked to its subtle function with backward movement and connections to the backward circuits.

Similar results for the frequency of pirouettes were shown for the AIZ interneuron in a large study of neural ablations and chemotaxis assays (Iino and Yoshida, 2009). AIZ's function in pirouettes was shown to probably be facilitated by the command interneurons AVA and AVE. A more recent study via chemotaxis assays using isoamyl alcohol confirmed previous findings and added AVD command interneuron and AIB first layer interneuron to their neural circuit model (Yoshida *et al.,* 2012).

8.2.8 The activity of the SMB neuron on the head and neck muscles is antithetical to SMD

The exaggerated head swings, the increased ratio of calcium influx on the body wall muscle and the omega turn phenotype observed following neural ablation together suggest an inhibitory effect has been lifted from the muscles. This is opposite to the excitatory effect reported for SMD (Shen *et al.,* 2016). The only head motor neuron with known inhibitory connections to the muscle is RME, which is GABAergic, hence the inhibitory connections (McIntire *et al.,* 1993; Liu *et al.,* 2009). This means either SMB is inhibitory to muscles, or by ablating SMB- then RME's inhibitory effect to the muscles has been lifted, or that SMB is excitatory in antiphase to the excitatory action of SMD. Previously it has been hypothesised that SMB is excitatory to the muscles by *in silico* models (Izquierdo and Beer, 2013; Karbowski *et al.,* 2008; Sakata and Shingai, 2004), partly due to its neurotransmitter acetylcholine (Ach) which is mainly an excitatory neurotransmitter (Liu *et al.,* 2009). However, Pereira *et al.,* argued recently that acetylcholine (Ach) has also an inhibitory

function in *C.elegans* (Pereira *et al.,* 2015). RME- ablation results in a milder loopy phenotype to SMB- and an opposite result to SMD- ablation; i.e. SMD- has shallower undulations than wildtype (Gray, J.M. *et al.,* 2005; Shen *et al.,* 2016). The RME neuron's activity and function in sinusoidal locomotion was shown to act independently to the presence or absence of the SMB neuron, but is dependent on the SMD neuron (Shen *et al.,* 2016). This means that the undulatory exaggerated phenotypes I observed because of SMB ablation, is not likely linked to the lifting of inhibition by RME through their SMB/RME synaptic connectivity. This leaves us with either SMB being itself inhibitory to muscles or SMB is excitatory in antiphase to the excitatory SMD.

The nature of connectivity of SMB to the muscles still remains unclear and both possibilities will be taken into consideration in the head oscillator function below, including SMD and RME both linked to head movement (Kocabas *et al.,* 2012)(personal communication with Manuel Zimmer).

8.2.9 The SAA and SMB neurons are integral for steering and pirouettes with a difference in their contribution to both orientation strategies

8.2.9.1 Steering, the regulator (SAA) and the translator (SMB)

Double ablation of both SAA- and SMB- exhibited a total inability to steer in both types of assays. Indeed, with their much exaggerated head swings, fine modulation of the head swings was impossible. As mentioned numerous times in this project, regulating the amplitude of the head swings is an important element for steering (Izquierdo and Beer, 2013). The phenotype of the double ablation strain alone highlights the importance of SAA and SMB in steering but also renders them as key players in that strategy. All parts of SAA and SMB's function in locomotion discussed so far, each and every one of them, are important for facilitating efficient steering. However, the neurons exhibited a differential level of importance in steering suggested by the half ablation strains in Chapter 6. Asymmetric ablation, being a not as invasive ablation as the full ablation of the neurons performed in Chapter 5, highlighted the subtle differences between the neurons and showcased their level of importance during steering.

In the SAAD- line, the worm's ability to fine tune its gradual turning was lost, even if the major steering motor neuron (SMB) was still intact. What is interesting is that the half ablation defect was even stronger than the full ablation of SAA- steering defect, in both assays conducted. In the radial assays for example, few SAAD- half ablated worms reached the peak in comparison to the SAA- full ablation strain that exhibited no difference to the wild type ones. In the circular steering assay the difference was even greater, with only one of the half

ablated worms reaching a peak. The SAAD- worms in this case performed as badly as the SMB- ablated and the double ablated worms did (SAA-SMB-). On the other hand, SMBD-ablated worms, while not steering as efficiently as the wild type ones, were performing better than the SAAD-, SMB- and double ablated (SAA-SMB-) worms overall; in terms of worms reaching the peak, average time it took to reach the peak, frequency of pirouettes and overall time of steering. Their trajectories were biased or loopy, therefore they did exhibit a higher amount of pirouettes than the wild types for course correction, and their undulatory movement was inconsistent in comparison to the wild type worms, but their overall performance was significantly better than the SAAD- ablated worms. Steering was still present and performed, albeit not 'translated' well enough. Taking out a small part of the SMB motor neuron is not as detrimental as taking a small part out of the 'regulator' (SAA). The worm either by the activity of other head motor neurons (redundancy) or proprioception can still cope, whereas, when SAA is half ablated it introduces a dysfunction/irregularity to more neurons than just the SMB (probably SMD), and an informational asymmetry that breaks the whole system down. SAA has a 'dominant negative' like effect in the steering circuit at the output layer.

8.2.9.2 Pirouettes, the regulator (SAA) and the translator (SMB)

Regulating the frequency of turns is an important element in chemotaxis (Larsch *et al.,* 2015). Suppressing turns facilitates steering during chemotaxis. Turns mechanistically are an integral part of a pirouette, as a pirouette is really a course-correction turn. SAA- and SMB- ablated worms exhibited a high frequency of pirouettes even in the assay favouring steering over the pirouette strategy, where many wild types did not perform a single pirouette for course correction. This increase could not be accounted for by only the pirouettes being performed for course correction, as ablated strains in plates without a stimuli performed a lot of turns as well. This suggests that both neurons of interest facilitate steering also via suppressing the frequency of pirouettes. This is the first time SMB neurons have been shown to have a role in the pirouette strategy. Its connection to SAA that in turn has connections to the backward movement circuits suggests that this function of SMB comes via SAA. However, the neurons exhibited a differential level of importance in pirouettes again suggested by the half ablation strains in Chapter 6.

SAAD- ablated worms exhibited a high frequency of pirouettes during both chemotaxis assays just as SMBD- ablated worms did as means of course correction to their biased and loopy trajectories. However, dispersal behaviour assays told a different story highlighting SAA's regulation of innate frequency of turns even more. When the SAAD- ablated worms were transferred on a plate without any stimuli they still covered as little area as the SAA-ablated worms did, due to a lot of turning and a decreased performance of runs. The SMBD-ablated worms explored more area than any of the other ablated strains including SMB-

ablation strain. The SMBD- ablated worms performed quite a lot of runs, albeit with bouts of loops. This highlights SAA's being more important than SMB in regulating turning rates and consequently in the pirouettes strategy. SAA's post- and presynaptic connections to the backward movement circuits supports this idea. It makes sense for the 'regulator' (SAA) of the motor neuron enabling the 'translating' of steering (SMB) to have connections to backward locomotion circuits in order to suppress or promote turning rates depending on context; in this instance I am referring to SAA's connectivity with AIB, RIM interneurons (dense post- and presynaptic connections) and AVA command neuron (presynaptic connections) (Piggott *et al.,* 2011; Gray, J.M. *et al.,* 2005).

8.2.10 Additional neurons that past studies have shown to contribute to either orientation strategies

Other neurons that have been shown to play a role in gradual turning are AIZ and AIY, (Kocabas *et al.,* 2012; Iino and Yoshida, 2009), though the latter was lately challenged as AIY was shown to promote negative steering (ipsilateral curving) rather than positive steering (contralateral curving), in a more recent publication (Satoh *et al.,* 2014). In addition, double ablation of AIA and AIB neurons causes a significant decrease in curving bias on both sides (Satoh *et al.,* 2014) rendering them redundant interneurons for chemotaxis.

As far as the pirouette strategy is concerned, it has been previously observed that AIB interneurons promotes turning rates (Larsch *et al.,* 2015; Gray, J.M. *et al.,* 2005; Wakabayashi *et al.,* 2004) and sets reversal rates during the pirouette strategy (Luo *et al.,* 2014; Iino and Yoshida, 2009). On the other hand, AIY has been shown to suppress turning rate while facilitating steering (Larsch *et al.,* 2015; Kocabas *et al.,* 2012; Wakabayashi *et al.,* 2004; Gray, J.M. *et al.,* 2005). Similar results for the frequency of pirouettes were shown with AIZ interneuron in a large study of neural ablations and chemotaxis assays (Iino and Yoshida, 2009). AIZ's function in pirouettes was shown to probably be facilitated via the command interneurons AVA and AVE. A more recent study via chemotaxis assays using isoamyl alcohol confirmed previous findings and added the AVD command interneuron and the AIB first layer interneuron to their neural circuit model (Yoshida *et al.,* 2012). These past data will be taken into consideration when forming the proposed network model for the two orientation strategies.

8.3 Integration of two parallel strategies for chemotaxis: a proposed network involving the SAA and SMB neurons

Taken together, all previous studies mentioned in this discussion chapter, and the sum of my results on salt soluble attractants, suggest the existence of a neural circuit regulating the pirouette strategy (via AIY/AIZ/ AIA /AIB /RIM / command interneurons/ SAA/ SMB/ SMD) with neural overlaps to the weathervane (steering) neural circuit (AIY/ AIZ/ SAA/ SMB). I am in agreement with Iino and Yoshida (2009) that the two strategies are employed by the worm in parallel. My results are also in agreement with all networks hypothesising SMB's role in steering (Sakata and Shingai, 2004; Karbowski *et al.,* 2008; Iino and Yoshida, 2009; Izquierdo and Beer, 2013). However, not all of them proposed a role to SMB for sharp turns, more likely because of a perceived distinction between steering (shallow gradual turning) and sharp turning (part of pirouettes). This is a distinction that is becoming more blurry than originally thought as more studies are conducted on chemotaxis.

Previous work on AIY showing that it regulates turning to facilitate steering (Larsch *et al.,* 2015; Kocabas *et al.,* 2012; Wakabayashi *et al.,* 2004; Gray, J.M. *et al.,* 2005), work on AIZ showing it to be a 'direction switch' (Li, Z. *et al.,* 2014) and my experiments on SAA and SMB, together suggest that they are part of the broadened network mediating the integration of the pirouette and weathervane strategies. Specifically, the SAA, AIZ and AIY interneurons, and to a lesser extent the SMB motor neuron, could be the part of the neurons within the chemotaxis circuit were the integration of the two strategies takes place. Interestingly, the SAA is synaptically in a direct position to potentially recruit the motor neurons in accordance to sensory context and strategy each time [(i.e SMB, SMD (and RIV, RMD not included in the schematic)] and suppress/promote backward movement at the same time due to its dense synaptic connections to RIM and AIB (reversals are part of the pirouette response). SAA could therefore be a second layer interneuron 'puppet master'.

I have added on this network the sensory layer for soluble attractants; ASEL and ADF sensing up-steps in concentration and ASER and ASH sensing down-steps in concentration (Suzuki *et al.,* 2008; Thiele *et al.,* 2009; Iino and Yoshida, 2009). In addition, I have included ASI as a sensory neuron shown to have a minor role in both strategies (Iino and Yoshida, 2009). The RIB interneuron was also added as it has been shown to regulate speed (Li, Z. *et al.,* 2014) and the worm modulates its speed during chemotaxis (Iino and Yoshida, 2009; Pierce-Shimomura *et al.,* 1999). Finally, the DVA stretch neuron was added as it has been shown to have a negative and positive effect on body bending via the expression of the *trp-4* stretch receptor (Li, W. *et al.,* 2006). Not only was *trp-4* shown to be expressed in the axon in the SMB in my experiments, but DVA and *trp-4* mutants result in exaggerated body bends as

shown by Li et al's study. My proposed network for the two strategies can be seen in Figure 8.2.
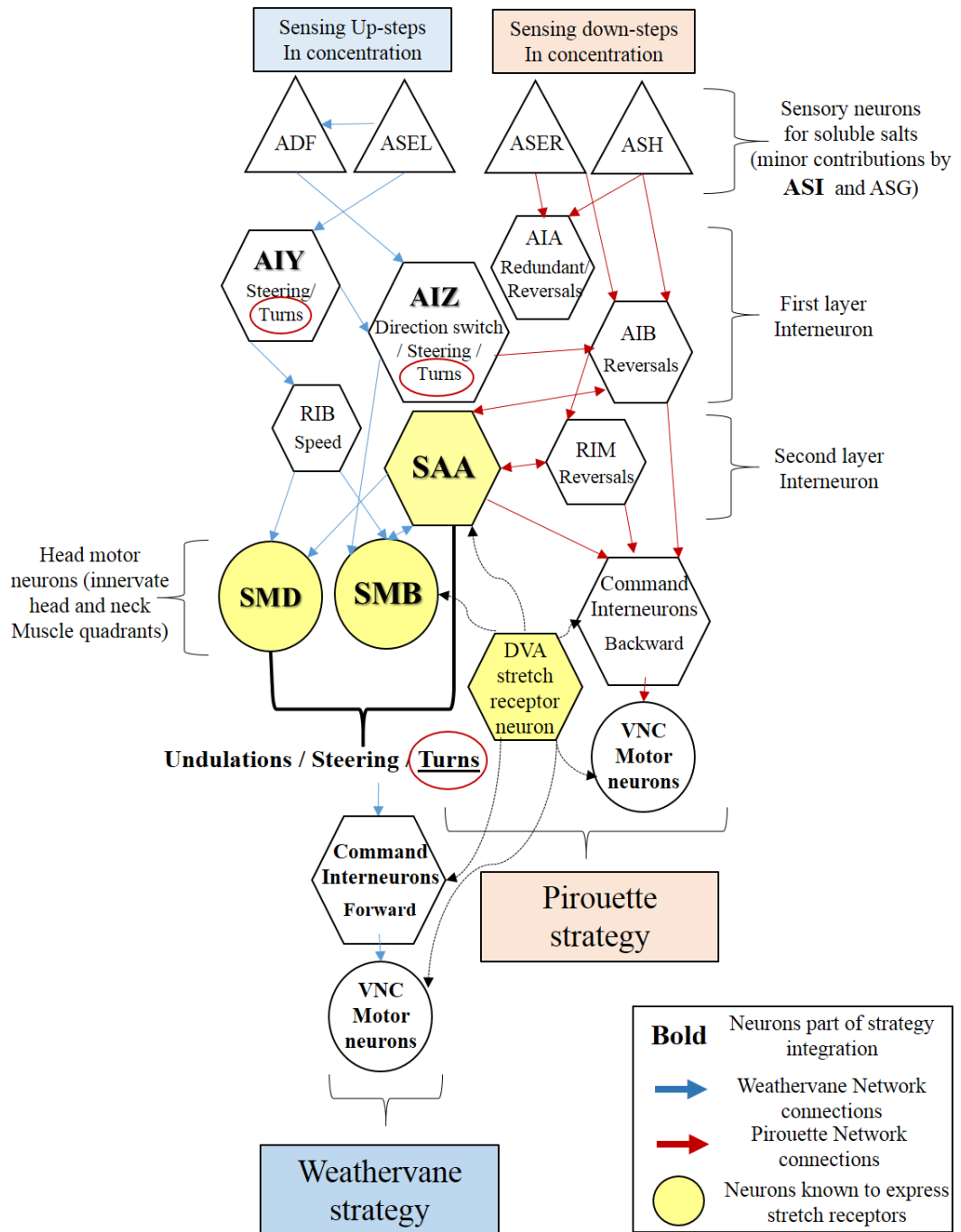
Figure 8.2 A network integrating the two orientation strategies of the worm formed from experimental data of past studies and this project. Nothing is assumed. Starting from the input layer (amphid sensory neurons responding to soluble salts) to the output (muscles). In bold font are the neurons that regulate both strategies. Blue arrows indicate weathervane strategy network connections. Red arrows indicate pirouette strategy network connections. In yellow colour are the neurons with stretch receptor expression.

8.4 A revised model for the head oscillator and its involvement in undulations/head movement: SAA the puppet master interneuron

8.4.1 Double ablation : killing the oscillator and the importance of SMD in the head oscillator

The double ablation of the SAA and SMB neurons showed that, together as an oscillator, they are not the head neurons generating the undulatory movement of the worm. Double ablation worms still exhibited fast rhythmic undulations, albeit very exaggerated. Throughout this thesis it has been hinted that SAA is regulating another head motor neuron other than the SMB. This probed me to add another player in my head oscillator model. Looking back at the broadened network of the neurons of interest in the head, and taking into consideration connection to SAA and all results so far of this project, SMD still remains a very good candidate. It is closely localised to both neurons of interest. In fact, SMD cells wrap round the processes of SAA neurons ventrally and it is densely synaptically connected with SAA (White, J.G. *et al.,* 1986). The totality of the experimental results of SMD ablation so far from other studies, mentioned in other parts of this thesis, shows that SMD is an antithetical motor neuron to the SMB neuron (Shen *et al.,* 2016; Gray, J.M. *et al.,* 2005) (and personal communication with Manuel Zimmer's lab). See Figure 8.3, Image A for a schematic reminder of ablation results postures).
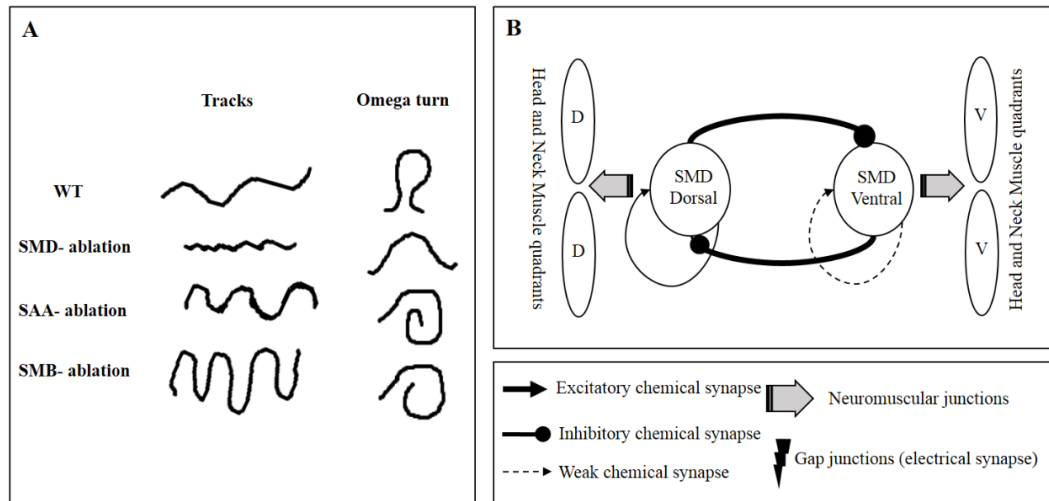
Figure 8.3 A schematic representation of neural ablation results and the self-synaptic connectivity in SMD. A) A schematic representation of neural ablation results. Tracks and omega turn postures are shown for SAA-, SMB- and SMD- ablations. B) Schematic showing the self-synaptic connectivity in SMD. Connection information in Left and Right neurons was merged and the schematic has a dorso-ventral perspective, reflecting the worm's movement on the agar plates. The nature of the connection are assumed, and have not yet been confirmed.

Potentially SMD, due to its self-connectivity, forms a self-sustained oscillator that generates the undulatory rhythm in a digital-like fast fashion (remember the double ablation worms' fast exaggerated undulatory phenotype with SAA- and SMB- ablated in Chapter 6) (see Figure 8.3, Image B for the schematic of the SMD self-oscillator). The fact that SMD- ablated worms exhibit very shallow undulations (Shen *et al.*, 2016)(personal communication with Manuel Zimmer) supports this idea. The SMD self-oscillator could be coupled then to the SAA/SMB oscillator hypothesised in Chapter 1: General Introduction, the latter being slower (due to dampening having to generate the rhythm through two neurons) and both oscillators potentially working in antiphase (Figure 8.4). This would explain SMB neurons and SMD neuron's opposite phenotypes (whatever the SMB connection to the muscles may be, either excitatory or inhibitory; this will be further explored in Figures 8.5 and 8.6). The slow oscillator regulates the amplitude and wavelength of the fast oscillator's generated undulations in a dynamic range, thus facilitating turning (key part of pirouette strategy and exploratory behaviour) and the break in the undulatory symmetry required to enable the worm to steer (weathervane strategy). Interplay between a fast and a slow oscillator would not only provide robustness to the system, but it would also account for the versatile movement of the worm's head (accounting head swings and foraging head movements) and explain the worms ability to navigate and adapt in both slow and fast fashion.
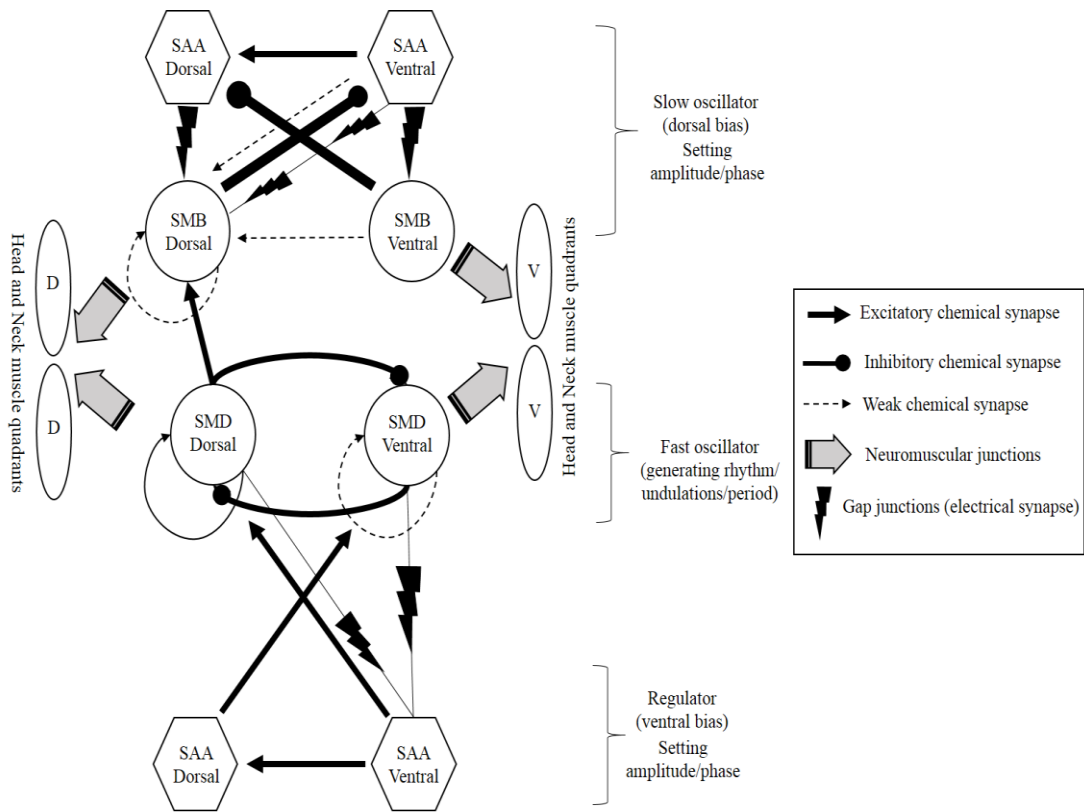
Figure 8.4 A schematic of synaptic connectivity between potential slow (SAA, SMB) and fast (SMD) oscillators. Connection information in Left and Right neurons was merged and the schematic has a dorso-ventral perspective. The nature of the connection are assumed, and have not yet been confirmed. The SAA neuron is shown twice to highlight connections to both head motor neurons.

8.4.2 A model of head movement with two oscillators

Based on the revised head oscillator model in Figure 8.4, I have drawn a head movement circuit model (Figure 8.5 and Figure 8.6, in the former SMB is assumed inhibitory and in the latter SMB is excitatory), taking into consideration known synaptic connections (White, J.G. *et al.,* 1986), the results of this thesis on SAA and SMB function, previous work done on RME highlighting as important for head movement (Shen *et al.,* 2016; Kocabas *et al.,* 2012), the laser ablation work on head motor neurons (Gray, J.M. *et al.,* 2005) and the neurotransmitters of each cell (Pereira *et al.,* 2015; McIntire *et al.,* 1993). In Figure 8.5 a dorsal and ventral bend is shown, while highlighting each neurons' activity. Note that the RME does not innervate neck muscle quadrants, only the head ones, and SMB is assumed to be inhibitory to the muscle in this instance. SMD works as an on/off component on its own resulting in a digital-like response, contracting the muscles of the side of the bend (ventral

muscles for a ventral bend and vice versa). SMB works as an antithetical motor neuron to SMD, inhibiting the opposite neuron (as RME does (Shen *et al.,* 2016)) to keep it relaxed as the other side is contracting. An additional role of SMB is to inhibit parts of the neck and head muscle quadrants of the contracted muscles in a graded response during steering, to prevent SMD from over bending the head, and fine tune head turning according to the worm's direction. SAA is controlling regularity and activity of SMB and SMD and keeps their antiphase rhythm in check. Dense gap junctions of SAA with SMB renders the slow oscillator moving as a unit activity-wise, and reciprocal inhibition makes their activity on/off as well, but with a delay.

The RME inhibitory neuron has been included in the proposed circuit model, as it has some role in regulating the foraging head movement (movement restricted to the end of the head, not the 'neck') during undulations (Gray, J.M. *et al.,* 2005; Shen *et al.,* 2016), it innervates head muscles (White, J.G. *et al.,* 1986), it was shown to be regulated by extrasynaptic connectivity from SMD and finally, RME limits the head over bending that the excitatory SMD is causing (Kocabas *et al.,* 2012). On that note, after exploring the SMD neuron in relation to SAA and SMB (see future prospect section below), RME is definitely the next neural target to aim for while dissecting head movement.

For example, in Figure 8.5 where SMB is assumed inhibitory, when the dorsal side of the slow oscillator is active, via SAAD it is activating the ventral side of SMD that contracts the muscle. The ventral side of SAA, after being inhibited by the dorsal side of SMB (due to their reciprocal inhibition) goes through a post-inhibitory rebound and turns on, thereby turning on the dorsal side of SMD.
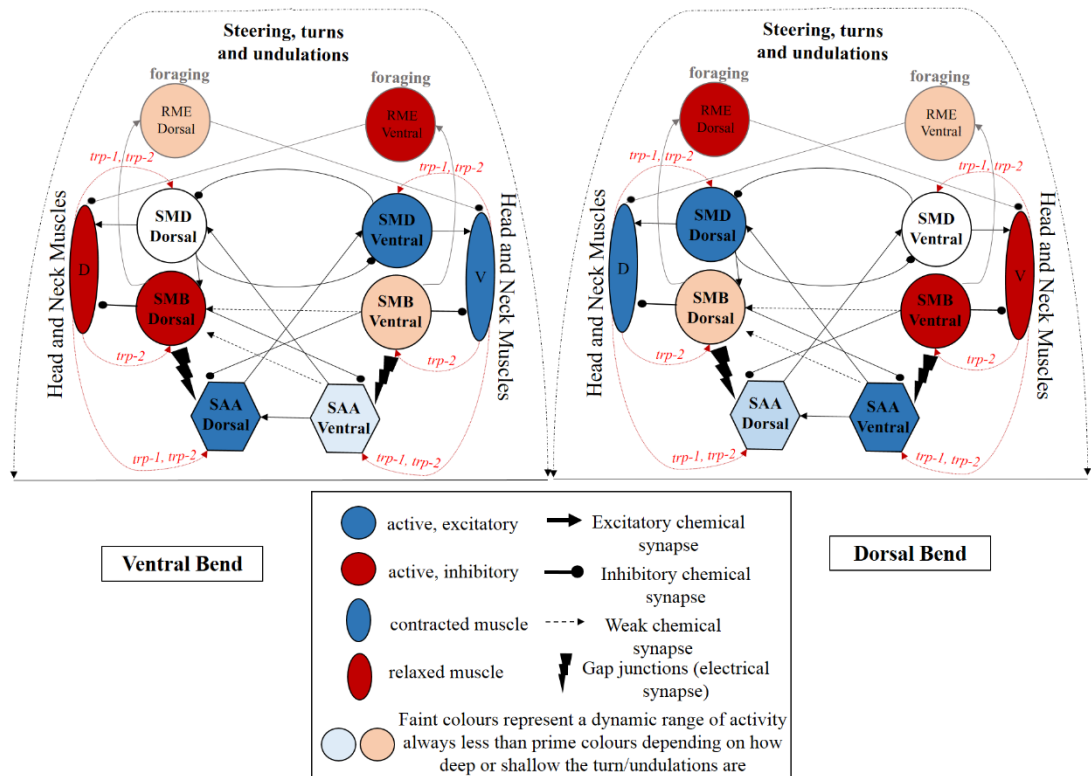
Figure 8.5 Head movement model with SMB being inhibitory. The model is based on synaptic connectivity, experimental data and the slow - fast oscillator hypothesis shown in Figure 8.4. Connection information in Left and Right neurons was merged and the schematic has a dorso-ventral perspective. Activity of the neurons is shown in a very simplistic way. RME head motor neuron and its known inhibitory connections are included. Note that the RME does not innervate neck muscle quadrants, only the head ones. The rest of inhibitory connections are based on assumptions. Red connections show stretch receptor expression.

Figure 8.6 shows the same head circuit model, however, exploring the possibility that SMB motor neurons are excitatory to the head and neck muscle but still antithetical to the SMD neurons. Regulation of the SMB's strong or weak excitation via the SAA neurons, to the expanded side of the head during bends, would work against the excitation of SMD on the contracting side. In this way modulation of gradual head turning could be achieved. Note that strengths of neural activity in this possibility would vary. SAA's and RME's would work the same way as before. Until this is modelled computationally, and more experimental data becomes available, both possibilities remain equally possible.
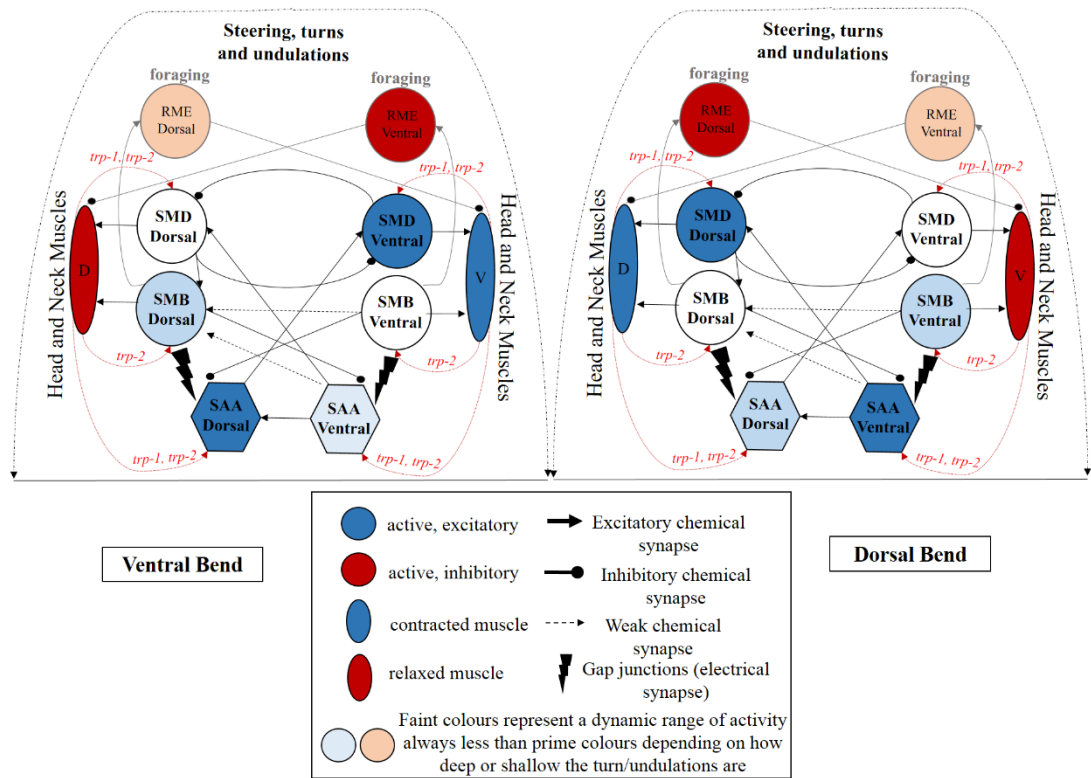
Figure 8.6 Head movement model with SMB being excitatory. Connection information in Left and Right neurons was merged and the schematic has a dorso-ventral perspective. Activity of the neurons is shown in a very simplistic way. RME head motor neuron and its known inhibitory connections are included. Note that the RME does not innervate neck muscle quadrants, only the head ones. The rest of the inhibitory connections are based on assumptions. Red connections show stretch receptor expression.

Looking at this model (with SMB being either inhibitory or excitatory), if the SMB neurons are gone a lot of force opposing the action of the SMD is gone, so one would expect exaggerated head swings. My results were consistent with that. Given the subtle dorsal bias in the connectivity one would expect a mild ventral bias as a result of SMB ablation too. My calcium imaging results on the muscles showing a ventral bias in the body bends, were consistent with that. If the SAA neurons are gone both SMB and SMD receive less activity, with SMB being more dysregulated than the SMD neurons. One would expect a milder phenotype than losing just the SMB neurons, as SMBs and SMDs are antithetical in their effect on the undulatory movement. My results were consistent with that. If both SAA and SMB are gone the excitation to the muscle (via SMD) is overpowering so that one would expect fast exaggerated undulations. My results are consistent with that, SAA had indeed an in-between phenotype (Figure 8.3). If the dorsal SAA is gone regulation of SMB dorsal is defective leading to a slight bias on one side and SMD activity would be irregular leading to

irregularities in the rhythm of undulations. SAAD- ablated results, especially during the chemotaxis assays, are consistent with that. If SMBD- ablated cells are gone, all it does is creating a ventral bias to the system but the head should still be able to cope and respond to undulations and steering with mild defects. One would expect loops in the trajectories of the worms. SMBD- ablation results during the chemotaxis assays were consistent with that. The dorsal ablations also showed a defect in recovery to the other side during steering. This could be explained by the worm entering the gradient in the phase where the dorsal side was aligned to the gradient at that time and continued steering in that defected state, not being able to recover the bias to the other side.

Stretch receptors in the system might stimulate neurons on the relaxed side to activate the neurons on the other side, thereby enforcing the undulatory movement and regulation of it. Having a feedforward rhythm and feedback from stretch receptors would make this double oscillator able to respond to weak signals with normal undulations and to strong signals with turns (gradual or sharp). Why would the worm need to have such a complexity? As Kuo 2002 showed in his study, a combination of feedforward rhythm and feedback control can improve performance, as it can filter sensory noise and disturbances from the environment (D Kuo, 2002). *C.elegans* in nature is found in the soil and rotten fruit, therefore such a complexity would enable it to cope with its turbulent and uneven niche.

Finally, since SAA is regulating SMB and SMD, it is essentially regulating differential types of response, both digital-like (SMD but also turn and pirouette frequency) and one with a dynamic range (SMB/steering). How could one interneuron with one type of neurotransmitter be able to facilitate both types of response? Li *et al.,* demonstrated in their recent study that this can be achieved by differential biophysical properties of the postsynaptic receptors on the postsynaptic neurons. They showed that AIY can achieve the regulation of two behaviours that differ in their mechanistic quality (speed via RIB and forward/backward movement switch via AIZ) using one neurotransmitter (Ach), and graded transmission (Li, Z. *et al.,* 2014). It would be extremely interesting to look into how and if SAA achieves regulation of SMB and SMD in a similar manner.

In my opinion, there is enough data and insight here for an updated head movement computational model including SAA and SMB, since Sakata's and Karbowski's was proposed more than 10 years ago (Sakata and Shingai, 2004; Karbowski *et al.,* 2008).

8.5 Future prospects

There are a number of directions for future work. First and foremost, a close investigation of the SMD motor neuron should be conducted, including detailed observation of SMD's genetic ablation phenotype and chemotaxis assays to assess its role in the weathervane or pirouette strategy. Finally, it should be ablated alongside the SAA and SMB neurons and observe whether undulations are still generated.

The combination of calcium imaging and optogenetics on freely moving worms measuring activity in SAA, SMB and/or SMD during certain behaviours, such as omega turns or reversals, and during chemotaxis, would also be highly informative. Measurements should be taken on one of the three neurons of interest, while the others are either activated by channel-rhodopsin or de-activated by halo-rhodopsin. These experiments will show us the activity of the neurons during locomotion and how that changes during chemotaxis, but will also assess the overall nature of their connections to each other.

To pin down the proprioceptive function of SAA, SMB and SMD, one should observe whether the neurons of interest are activated by head bending via a combination of calcium imaging in the neurons and optogenetic activation of the muscles. The next step on that would be to observe if that response is dependent on the activity of *trp-1* and *trp-2* specifically to those cells. Also, whether expression of *trp-1* and *trp-2* in SAA, SMB or SMD specifically rescues any observed locomotion phenotype could be tested, and it should be confirmed that *trp-4* is indeed expressed in SMB's axons. Finally, interaction between DVA (*trp-4*), PVD (*mec-10*) and DB motor neurons, SAA, SMB and SMD should be observed via a combination of optogenetics and calcium imaging in freely moving worms, in order to shed more light on the integration of the information of the head bending and its propagation down the body during forward locomotion.

Unfortunately it proved impossible to conduct ventral genetic ablations of SAA and SMB. Generating successful strains with their ventral neural cells ablated and assaying them in comparison to the dorsal genetic ablation strains assayed and generated here, could highlight any subtle asymmetry present in the worm's undulatory movement during exploratory locomotion or chemotaxis (for proposed genetic manipulations that could result in successful ventral genetic ablations see Discussion section of Chapter 6). It is telling that SAA and SMD stretch receptor expression is localised in the ventral somas of the neurons and that omega turns are ventrally biased for example.

Additional taxis assays could be conducted with stimuli sensed in sensory neurons other than the chemotaxis ones, such as odor attractants, temperature, light etc. These experiments could support the mechanistic function SAA, SMB and SMD have in the worm's navigation. Within

this context it would be of a potential interest to investigate RIA interneuron as it has been shown to be involved in thermotaxis and aid in undulatory movement via SMD (Hendricks *et al.,* 2012).

In addition, there is growing evidence of extrasynaptic modulation of the behaviour of the worm as discussed in Chapter 1: General Introduction (i.e monoamines, neuropeptides) (Alkema *et al.,* 2005; Donnelly *et al.,* 2013). Investigation of any extrasynaptic modulation of the observed behaviours, while linking them to the neurons of interest, would be extremely interesting and would connect the neurons of interest with neural partners that are anatomically not as close.

Finally, the neuronal model integrating steering and pirouettes proposed here should be integrated with an updated model of forward and backward movement with a better understanding on the circuitry of command and ventral cord neurons and the switch between forward and backward movement. The head movement slow/fast oscillator hypothesis proposed here should also be considered in this context.

8.6 The contributions of this work to the field

This is the first study to investigate the role of the SAA neuron in worm locomotion. This project provided evidence on SAA's role in the frequency and performance of head turning, setting the amplitude of head swings, integrating the two orientation strategies and showed that it has an integral role in steering via regulating SMB motor neurons. Finally, it suggested some proprioceptive function for the SAA.

For the first time this study has shown that SMB controls the amplitude of the omega/delta turns, the activity of SMB peaks after the onset of the turn and the response is graded. In addition, this work has shown that SMB has an integral role in steering, has potential proprioceptive function and its function is antagonistic to the known SMD neuron's functions from the literature. Finally, it provided supporting evidence for the SMB motor neuron's previously proposed function in setting the amplitude of head swings and head turning.

There was also some behavioural evidence supporting that both orientation strategies are required for efficient navigation, with weathervane being more efficient than the pirouette strategy (in the context of the worm reaching the stimuli faster). That informational symmetry is important in steering was also shown.

By investigating both neurons individually, but also as a pair, in a lot of different contexts, this project has identified a potential integrated neural circuit regulating undulations, turns and steering. It provided additional neural targets of interest and proposed a neural network

of chemotaxis integrating the two orientation strategies. Finally, it proposed a testable model for head movement. The network integrating the two strategies of orientation and the head oscillator hypothesis are combined in Figure 8.7 below.
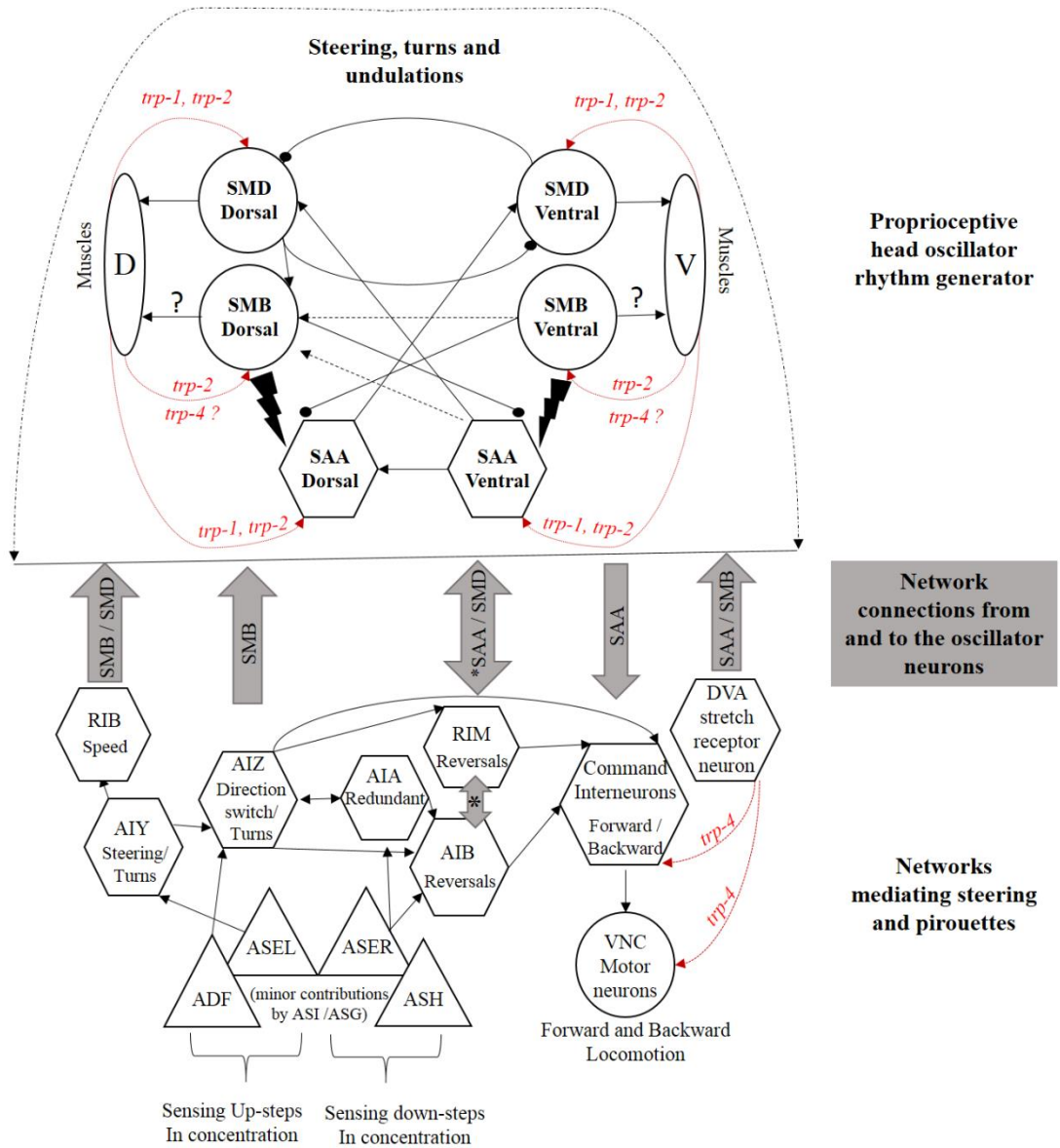
Figure 8.7 Head oscillator (top) combined with the network regulating the two orientation strategies (bottom). Connection information in Left and Right neurons was merged and the schematic has a dorso-ventral perspective for the head oscillator (Top). Nature of connections is assumed. Connections in the network circuit at the bottom are showing direction of informational flow. Red connections reflect proprioceptive function.

8.7 Musings on an interneuron / motor neuron pairing

During my PhD, it has never ceased to amaze me how predictions about the function of SAA and SMB, made by White and colleagues over 30 years ago, only by observing anatomical structures, were on the right track (White, J.G. *et al.,* 1986). It has always been the case that 'biology' is there, in front of us and it is our job to interpret how it works. Via a lot of effort, painstakingly manual annotations and observations, time-consuming genetic and electrophysiological techniques, connectomics etc. we are beginning to identify the pieces of the 'puzzle' that together explain the worm's neural control of behaviour. Once all the pieces are identified, computational modelling can help us make more sense of them.

It is my hope that my work here adds to our understanding of neural function. I hope both experimental data and consequent hypothesis rising from it, will be modelled or used to guide *in silico* models of klinotaxis, chemotaxis, head movement or models integrating any or all of them. Only by adding experimental data to the field will the modelling more accurately reflect biological reality, and give us a better understanding of how the worm works at a systems levels.

List of Abbreviations

WT = wild type

GFP = green fluorescent protein

RFP = red fluorescent protein

BWM = body wall muscle

NMJ = neuromuscular junction

NGM = nematode growth medium

P = promoter region

DNA = deoxyribonucleic acid

VNC = ventral nerve cord

V = ventral

D = dorsal

L = left

R = right

Ach = acetylcholine

GABA = gamma-aminobutyric acid

Appendix A
Tables of primers used for cloning

Table A.1 Primers used for the amplification of the selected promoter regions targeting full ablation of the SAA and SMB neurons.

SAA	Primer sequence	Restriction site	Fosmid	Length
lad-2p	Forward: aaaCTCGAGccagggtgttgagaaattag	XhoI	WRM0641dD06	4 kb
	Reverse: ggccGGATCCtgttggaaaaatccaaaaaa	BamHI		
unc-42p	Forward: cagaAAGCTTgtaggagcaagaggaag	HindIII	WRM0624cE10	2.8 kb
	Reverse: aaaaGAGCTCtgtgtgagtgaaagcggaga	SacI/Ecl136II		
SMB	**Primer sequence**	**Restriction site**	**Fosmid**	**Length**
flp-12sp*	Forward: caaaAAGCTTccgggattcctctatcctt	HindIII	WRM063Be06	350 bp
	Reverse: ccaaGGATCCtgtttactgaaagttcagc	BamHI		
flp-12lp*	Forward: aaaaCTCGAGgccataacgagtcggaacta	XhoI	WRM063Be06	2.6 kb
	Reverse: ccaaGGATCCtgtttactgaaagttcagc	BamHI		
odr-2p	Forward: caaaCTCGAGcgacatgaaaacaactttg	XhoI	WRM0636aF03	2.4 kb
	Reverse: cccGGATCCtttctgtctgaaatataaatg	BamHI		

* sp = small promoter region, lp = large promoter region

Table A.2 Primers used for the amplification of the selected promoter region *npr-1p* targeting half ablation of the SAA and SMB neurons.

Region	Primer sequence	Restriction site	Plasmid	Length
npr-1p	Forward: ccccAAGCTTcagtatctaataaatttgat	HindIII	*npr-1p*::GFP	2 kb
	Reverse: ttttGGATCCttggcctatgtctgaaattt	BamHI		

Table A.3 Primers used for the amplification of the stretch receptors promoter regions *trp-1, trp-2* and *trp-4.*

Stretch receptor	Primer sequence	Restriction site	Fosmid	Length
trp-1p	Forward: tatGCATGCtctgatttgaacgcttaagtag	SphI	WRM0611bF07	4 kb
	Reverse: aaaGGATCCtcaaattgctcaggcagtaga	BamHI		
trp-2p	Forward: aaaaGCATGCtttcgcatcttgccatatac	SphI	WRM0621aD02	3.5 kb
	Reverse: aaaGGATCCtggctggaaaatggaagggtt	BamHI		
trp-4p	Forward: aaaaGCATGCtttggggcaattgatatggt	SphI	Genomic DNA	4.5 kb
	Reverse: aaaaGGATCCaaccgggggtaatgtataatg	BamHI		

Table A.4 Sequencing primers used for confirmation of *npr-1p*::P35::GFP backbone construct.

Target Region	Primer sequence	Sequencing direction	Identity
npr-1p to P35	ttctataagccataagccatgc	Forward	96%
P35 to PD95.75 backbone	gtggacagtgtgcagtttgatg	Forward	100%
PD95.75 backbone to *npr-1p*	cccaggctttacactttatgcttc	Forward	100%

Appendix B
Tables of cloning steps

Table B.1 Plasmid construction of projects' ablations, reporter GFP and reconstitute GFP plasmids

Targeted neuron	Promoter region digest	Plasmid digest	Result of ligation
SAA	*lad-2p* cut XhoI/BamHI	CED-3 (p15) plasmid cut XhoI/BamHI	SAA ablation plasmid
SAA	*unc-42p* cut Ecl/HindIII	CED-3 (p17) plasmid cut BamHI blunt by Klenow/HindIII	SAA ablation plasmid
SAA	*lad-2p* cut XhoI/BamHI	rec-GFP (707) plasmid cut SalI/BamHI	SAA rec-GFP reporter plasmid
SAA	*lad-2p* cut XhoI/BamHI	rec-GFP (708) plasmid cut SalI/BamHI	SAA rec-GFP reporter plasmid
SAA	*unc-42p* cut Ecl/HindIII	rec-GFP (707) plasmid cut BamHI blunt by Klenow/HindIII	SAA rec-GFP reporter plasmid
SAA	*unc-42p* cut Ecl/HindIII	rec-GFP (708) plasmid cut BamHI blunt by Klenow/HindIII	SAA rec-GFP reporter plasmid
SAA	*lad-2p* cut XhoI/BamHI	GFP plasmid cut SalI /BamHI	SAA GFP reporter plasmid
SAA	*unc-42p* cut Ecl/HindIII	GFP plasmid cut HindIII/SmaI	SAA GFP reporter plasmid
SMB	*flp-12sp* cut HindIII/BamHI	CED-3 (p15) plasmid cut HindIII/BamHI	SMB ablation plasmid
SMB	*flp-12sp* cut HindIII/BamHI	CED-3 (p17) plasmid cut HindIII/BamHI	SMB ablation plasmid
SMB	*flp-12sp* cut HindIII/BamHI	rec-GFP (707) plasmid cut HindIII/BamHI	SMB rec-GFP reporter plasmid
SMB	*flp-12sp* cut HindIII/BamHI	rec-GFP (708) plasmid cut HindIII/BamHI	SMB rec-GFP reporter plasmid
SMB	*flp-12sp* cut HindIII/BamHI	GFP plasmid cut HindIII/BamHI	SMB GFP reporter plasmid
SMB	*flp-12lp* cut XhoI/BamHI	rec-GFP (707) plasmid cut SalI/BamHI	SMB rec-GFP reporter plasmid
SMB	*flp-12lp* cut XhoI/BamHI	rec-GFP (708) plasmid cut SalI/BamHI	SMB rec-GFP reporter plasmid
SMB	*flp-12lp* cut XhoI/BamHI	GFP plasmid cut SalI/BamHI	SMB GFP reporter plasmid
SMB	*flp-12lp* cut BamHI	CED-3 (p15) plasmid cut HindIII blunt by Klenow/BamHI	SMB ablation plasmid
SMB	*flp-12lp* cut BamHI	CED-3 (p17) plasmid cut HindIII blunt by Klenow/BamHI	SMB ablation plasmid
SMB	*odr-2p* cut XhoI/BamHI	GFP plasmid cut SalI/BamHI	SMB GFP reporter plasmid
SMB	*odr-2p* cut XhoI/BamHI	rec-GFP (707) plasmid cut SalI/BamHI	SMB rec-GFP reporter plasmid
SMB	*odr-2p* cut XhoI/BamHI	rec-GFP (708) plasmid cut SalI/BamHI	SMB rec-GFP reporter plasmid
SMB	*odr-2p* cut BamHI	CED-3 (p15) plasmid cut HindIII blunt by Klenow/BamHI	SMB ablation plasmid
SMB	*odr-2p* cut BamHI	CED-3 (p17) plasmid cut HindIII blunt by Klenow/BamHI	SMB ablation plasmid

Table B.2 Plasmid construction of the project's half ablation plasmids

Targeted neuron	Promoter region digest	Plasmid digest	Result of ligation
SAAD and/ or SMBD ablation	*npr-1p* cut HindIII/BamHI	CED-3 p17 cut HindIII/BamHI	*npr-1p*::p17 plasmid
SAAD and/ or SMBD genetic rescue	*npr-1p* cut HindIII/BamHI	pPD95_75 cut AgeI/EcoRI to excise GFP, then blunted and religated, then cut HindIII/BamHI to insert *npr-1* promoter region, finally cut EcoRI to insert P35 protein.	*npr-1p*::p35 plasmid

Table B.3 Plasmid construction of the project's GCamp3 plasmids

Targeted neuron	Promoter region digest	Plasmid digest	Result of ligation
SAA/SMD	*lad-2p* cut BamHI	*gcy-7p*::GCamp3 cut NaeI(blunt)/BamHI	*lad-2p*::GCamp3 plasmid
SMB	*flp-12sp* cut BamHI	*gcy-7p*::GCamp3 cut NaeI(blunt)/BamHI	*flp-12sp*::GCamp3 plasmid

Appendix C
Tables of neuronal gene expression patterns

Table C.1 SAA neuronal gene expression pattern. Underlined are the pair of genes used to target the SAA neurons in this project. In bold font is the neuron of interest.

Gene	Neurons expressed	Reference
flp-12	AVH/AVJ, BAG, PDA, PVR, **SAA**, SDQ, SMB, BDU (?)	(Kim, K. and Li, 2004)
flp-7	ALA, AVG, PHB, PDA, PVW, RIC, **SAA**, RMDV, SMDV(?), PHA(?)	(Kim, K. and Li, 2004)
glr-4	AVA(?), RMD, SMD, **SAA**, SIB, RIB, RIM, AVH, FLP, RMG, DVA, AUA, PVD, URY, URA, SAB, RIF, DB(?), PVU(?)	(Brockie *et al.*, 2001)
<u>*lad-2*</u>	SMD, **SAA**, SDQ, ALN, PLN	(Aurelio *et al.*, 2002)
lim-4	AWB, RMEV, RMD, RID, RIV, **SAA**, SIA	(Sagasti *et al.*, 1999)
<u>*npr-1*</u>	AQR, ASE, ASG, ASH, URX, IL2, QLQ, AUA, **SAAD**, RMG, SMBD, M3, VD, DD, PQR, PHA, PHB, RIV, RIG, SDQ	(Coates and de Bono, 2002)
rig-6a	AVA, AVB, AVE, PVC, AIB, AUA, AVG, RIB, RIC, **SAA**, SIA, SIB, RIF, RIM, RMD, RME, SMD, DA, DB, VA, VB, M5, NSM, MC, I3	(Schwarz *et al.*, 2009)
syg-1	**SAA(?)**, ADF, ADL, AVH (?), AIN, RIG, RIS, SIA, SIB, RIF OR SAB, RIM, DA, DB, DD, VA, VB, M3(?), M4	(Schwarz *et al.*, 2009)
unc-17	IL2, URA, URB, **SAA**, SAB, SIA, SIB, SMB, SMD, RMD, AIY, M1-2-5, I1F, I6F, VA, VB, VC, DA, DB, AS, SDQ, HSNF, ALN, PLN	Shawn Lockery (unpublished)
<u>*unc-42*</u>	AVA, AVD, AVE, ASH, RMD, SMB, AIN, AVH, AVJ, AVK, RIV, **SAA**, SIB, DD, PVT	(Brockie *et al.*, 2001)
pdf-1	**SAA**, SIAV, AVB, AIM, RMG, ASK/AFD (?)	(Barrios *et al.*, 2012)
unc-7	numerous neurons, not a good candidate	(Starich *et al.*, 2009)
(?)	uncertain of neural identity or faint expression	

Table C.2 SMB neuronal gene expression pattern. Underlined are the pair of genes used to target the SMB neuron in this project. In bold font is the neuron of interest.

Gene	Neurons expressed	Reference
flp-12	AVH, AVJ, BAG, PDA, PVR, SAA, SDQ, **SMB**, BDU (?)	(Kim, K. and Li, 2004)
npr-1	AQR, ASE, ASG, ASH, URX, IL2, QLQ, AUA, SAAD, RMG, **SMBD**, M3, VD, DD, PQR, PHA, PHB, RIV, RIG, SDQ	(Coates and de Bono, 2002)
unc-17	IL2, URA, URB, SAA, SAB, SIA, SIB, **SMB**, SMD, RMD, AIY, M1-2-5, I1F, I6F, VA, VB, VC, DA, DB, AS, SDQ, HSNF, ALN, PLN	Shawn Lockery (unpublished)
unc-42	AVA, AVD, AVE, ASH, RMD, **SMB**, AIN, AVH, AVJ, AVK, RIV, SAA, SIB, DD, PVT	(Brockie _et al.,_ 2001)
odr-2	**SMB**, RME, ALN, PLN, RIG	(Chou _et al.,_ 2001)
unc-7	numerous neurons, not a good candidate	(Starich _et al.,_ 2009)
vab-8	numerous neurons expressed in the larval and embryonic stage	(Wolf _et al.,_ 1998)
(?)	uncertain of neural identity or faint expression	

Appendix D
Examples of Ethograms

A

strain/subject	WT s4											
	1min	2min	3min	4min	5min	6min	7min	8min	9min	10min	11min	TOTAL
FW locomotion (sec)	45	46	40	57	50	58	51	49	45	56	54	551
STOPS (sec)	1	2			1	2		2	2			10
BW locomtion (sec)	14	12	20	3	9		9	9	13	4	6	99
LONG REVERSAL (counts)	2	1	4	1	1		1	1	1	1	1	14
SHORT REVERSAL (counts)	4	2	1		2		2	2	2			15
Ω TURN (counts)	3	2	4	1	3		1	1	1	3	1	20
	60	60	60	60	60	60	60	60	60	60	60	

B

strain/subject	UL4230 SMB s7											
	1min	2min	3min	4min	5min	6min	7min	8min	9min	10min	11min	TOTAL
FW locomotion (sec)	50	40	43	58	40	41	56	55	23	57	53	516
STOPS (sec)	1	6	3			1			2	1	2	16
BW locomtion (sec)	9	14	14	2	20	18	4	4	35	2	5	127
L REVERSAL (counts)		3	2		2	1		1	3	1		13
S REVERSAL (counts)	2		1	1	1	4	1		1		2	13
Ω TURN (counts)	3	4	4	10	3	6	7	9	5	4	6	61
	60	60	60	60	60	60	60	60	60	60	60	

C

strain/subject	UL4207 SAA s3											
	1min	2min	3min	4min	5min	6min	7min	8min	9min	10min	11min	TOTAL
FW locomotion (sec)	54	48	37	39	27	56	30	53	40	48	51	483
STOPS (sec)	3	4	4	1	1	1	1	4	2	3	6	30
BW locomtion (sec)	3	8	19	20	32	3	29	3	18	9	3	144
L REVERSAL (counts)			1	1	1		3		1			7
S REVERSAL (counts)	2	6	1	1		1		2	1		2	16
Ω TURN (counts)	1	1	1	3	2	1	3	6	4	3	5	30
	60	60	60	60	60	60	60	60	60	60	60	

Figure D.1 Representative ethograms of the main strains tested in Chapter 2. Images show 11 minutes of continuous locomotion of: A) a wild type animal (N2), B) a SAA- ablated animal (UL4207), and C) a SMB- ablated animal (UL4230).

Appendix E
Sequencing BLAST Result Figures

Figure E.1 Sequencing BLAST results of PD95.75 backbone to *npr-1p* region. Highlighted in blue the exact region where the ligation of PD95.75 backbone and *npr-1p* took place. Constructed plasmid sent for sequencing and expected sequence identity is highlighted with a red circle (100% identity).

Download ∨ Graphics

Sequence ID: Query_226185 Length: 1320 Number of Matches: 1

Range 1: 1 to 528 Graphics   ▼ Next Match ▲ Previous Match

Score	Expect	Identities	Gaps	Strand
839 bits(454)	0.0	507/528(96%)	21/528(3%)	Plus/Plus

```
Query  1    ATAGGATTTTATTTTTTATCTATTAATCTATTTGGTTAACACCCTCTTTCATCTTTGTTT  60
            ||||||||||||||||||||||||||||||||||||||||||||||||||||||||||||
Sbjct  1    ATAGGATTTTATTTTTTATCTATTAATCTATTTGGTTAACACCCTCTTTCATCTTTGTTT  60

Query  61   CCTCAATTTTTCTTTCCTCCATTAGACTaaaaaaaaTTTCAGACATAGGCCAAGGATCCCC  120
            |||||||||||||||||||||||||||||        |||||||||||||||||||||||
Sbjct  61   CCTCAATTTTTCTTTCCTCCATTAGACTAAAAAAAATTTCAGACATAGGCCAAGGATCCCC  120

Query  121  GGGATTGGCCAAAGGACCCAAAGGTATGTTTCGAATGATACTAACATAACATAGAACATT  180
            ||||||||||||||||||||||||||||||||||||||||||||||||||||||||||||
Sbjct  121  GGGATTGGCCAAAGGACCCAAAGGTATGTTTCGAATGATACTAACATAACATAGAACATT  180

Query  181  TTCAGGAGGACCCTTGGAGGGTA---G-A----A----T----T--C---ATGTGTGTAA  219
            |||||||||||||||||||||||   | |    |    |    | |   |||||||||
Sbjct  181  TTCAGGAGGACCCTTGGAGGGTACCGGAATTCGATCTTTACCATAGCAAAATGTGTGTAA  240

Query  220  TTTTTCCGGTAGAAATCGACGTGTCCCAGACGATTATTCGAGATTGTCAGGTGGACAAAC  279
            ||||||||||||||||||||||||||||||||||||||||||||||||||||||||||||
Sbjct  241  TTTTTCCGGTAGAAATCGACGTGTCCCAGACGATTATTCGAGATTGTCAGGTGGACAAAC  300

Query  280  AAACCAGAGAGTTGGTGTACATTAACAAGATTATGAACACGCAATTGACAAAACCCGTTC  339
            ||||||||||||||||||||||||||||||||||||||||||||||||||||||||||||
Sbjct  301  AAACCAGAGAGTTGGTGTACATTAACAAGATTATGAACACGCAATTGACAAAACCCGTTC  360

Query  340  TCATGATGTTTAACATTTCGGGTCCTATACGAAGCGTTACGCGCAAGAACAACAATTTGC  399
            ||||||||||||||||||||||||||||||||||||||||||||||||||||||||||||
Sbjct  361  TCATGATGTTTAACATTTCGGGTCCTATACGAAGCGTTACGCGCAAGAACAACAATTTGC  420

Query  400  GCGACAGAATAAAATCAAAAGTCGATGAACAATTTGATCAACTAGAACGCGATTACAGCG  459
            ||||||||||||||||||||||||||||||||||||||||||||||||||||||||||||
Sbjct  421  GCGACAGAATAAAATCAAAAGTCGATGAACAATTTGATCAACTAGAACGCGATTACAGCG  480

Query  460  ATCAAATGGATGGATTCCACGATAGCATCAAGTATTTTAAAGATGAAC     507
            |||||||||||||||||||||||||||||||||||||||||||||||
Sbjct  481  ATCAAATGGATGGATTCCACGATAGCATCAAGTATTTTAAAGATGAAC     528
```

Figure E.2 Sequencing BLAST results of *npr-1p* to P35 protein region. Highlighted in blue the exact region where the ligation of *npr-1p* to P35 took place. The yellow box highlights the area where additional unmatched nucleotides were found in the constructed plasmid. Protein P35 was provided in a pBluescript II vector and this region was part of the P35 loci not included in the map provided. However, the reading frame is not rearranged with these additional nucleotides. Constructed plasmid sent for sequencing and expected sequence identity is highlighted with a red circle (96% identity).

Figure E.3 Sequencing BLAST results of P35 protein to PD95.75 backbone region. Highlighted in blue is the end of P35 protein. In a red square the stop codon can be observed. Green box encircles the exact region where the ligation of *npr-1p* to PD95.75 backbone took place. Constructed plasmid sent for sequencing and expected sequence identity is highlighted with a red circle (100% identity).

Appendix F
Additional BWM calcium imaging Figures
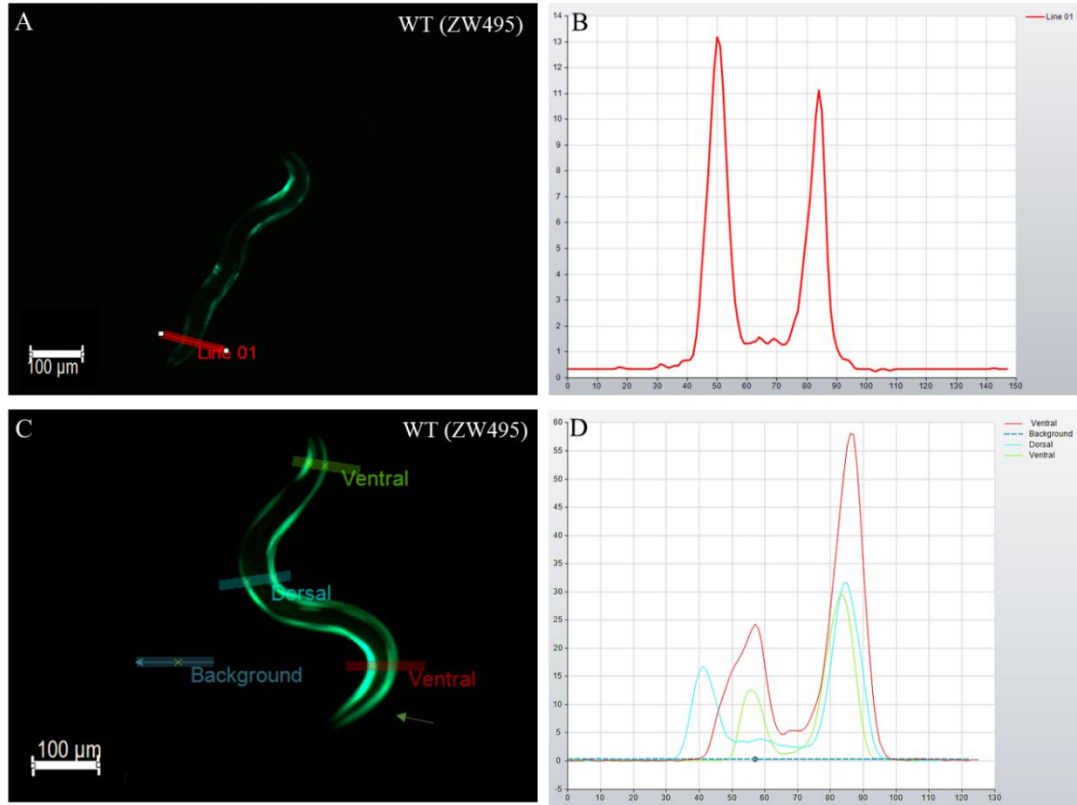
Figure F.1 Various measurements on wild type (ZW495) animals expressing Gcamp3 in the BWM. Image A and Graph B show measurement of the area of the head when an animal is anaesthetised. Image C and Graph D show measurements of all the animal's body bends. Green arrows show the area of the head.

Appendix G
Sensory neurons table

Table G.1 Amphid sensory neurons referred to or relevant (underlined bold font) to this
project.

Neuron name	Function: what is it sensing?	References
ASE	water-soluble chemicals (Na , Cl, Cu, biotin, lysine)	(Bargmann, C. I. and Horvitz, 1991; Suzuki *et al.,* 2008)
AWC	odor attractants (benzaldehyde,butanone,isoamyl alcohol etc)	(Bargmann, C. I. *et al.,* 1993; Kocabas *et al.,* 2012)
AWA	odor attractants (diacetyl, pyrazine, and 2,4,5-trimethylthiazole)	(Bargmann, C. I. *et al.,* 1993)
ASK	avoidance, minor chemotaxis, pheromone sensing, promotes local search	(Gray, J.M. *et al.,* 2005)
AFD	temperature	(Mori and Ohshima, 1995; Beverly *et al.,* 2011)
ASI	minor chemotaxis(sodium & Cl), dauer formation	(Bargmann, C. I. and Horvitz, 1991)
AWB	odor repellant (volatile avoidance)	(Troemel *et al.,* 1999)
ASH	nociception: Harsh nose touch avoidance, Osmotic avoidance, Chemical avoidance(Cu, bitter), Social feeding	(Bargmann, C. I. and Horvitz, 1991)
ADF	minor chemotaxis(sodium & Cl), dauer formation	(Bargmann, C. I. and Horvitz, 1991)
ASJ, ASG	dauer formation, minor chemotaxis(sodium & Cl)	(Bargmann, C. I. and Horvitz, 1991)
ADL	social feeding, avoidance	(de Bono *et al.,* 2002)

Appendix H
Frequency of pirouettes as events per assay between radial and circular
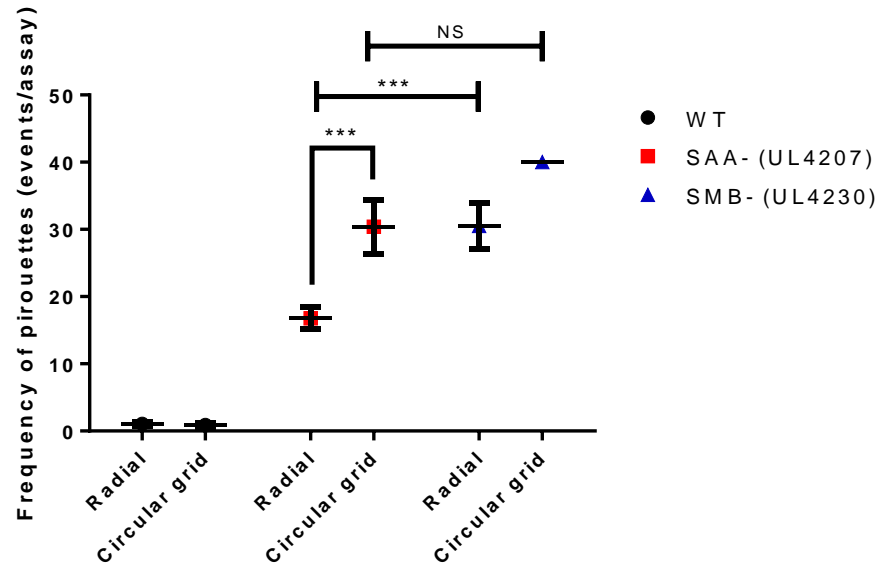
Figure H.1 Graph showing a summative comparison of frequency of pirouettes amongst strains and assays. Statistical significance levels and error bars, as STDEV, are indicated. Index error bars are shown as SEM. [Two-way analysis of variance (ANOVA) and Sidak's multiple comparison were used; ***p <0.001;].

Appendix I
Examples of annotated DNA maps of plasmids generated for this project
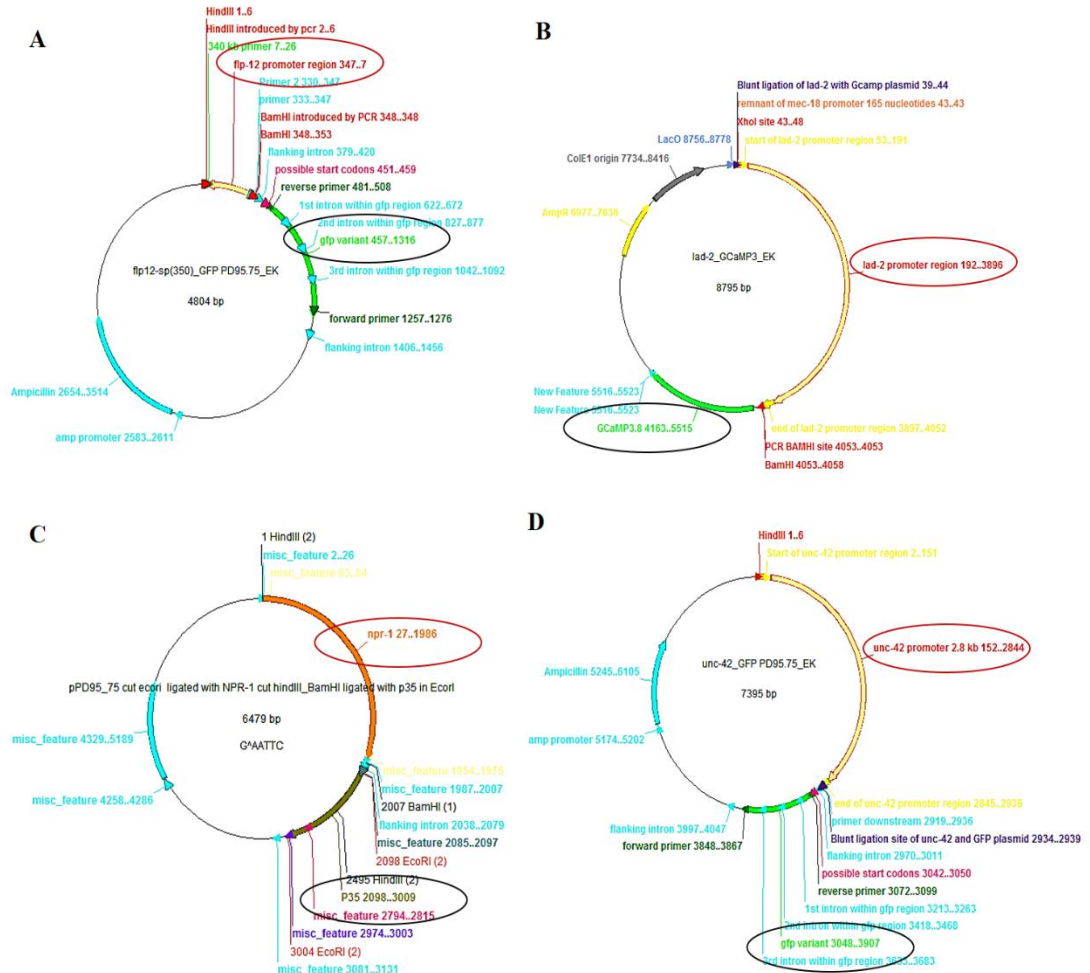
Figure I.1 Examples of various DNA maps of plasmids constructed for this project. Image (A) shows the *flp-12sp*::GFP plasmid, Image (B) shows the *lad-2p*::GCamp3 plasmid, Image (C) shows the *npr-1*::P35 plasmid and Image (D) shows the *unc-42p*::GFP plasmid.

References

Akerboom, J., Carreras Calderon, N., Tian, L., Wabnig, S., Prigge, M., Tolo, J., Gordus, A., Orger, M.B., Severi, K.E., Macklin, J.J., Patel, R., Pulver, S.R., Wardill, T.J., Fischer, E., Schuler, C., Chen, T.W., Sarkisyan, K.S., Marvin, J.S., Bargmann, C.I., Kim, D.S., Kugler, S., Lagnado, L., Hegemann, P., Gottschalk, A., Schreiter, E.R. and Looger, L.L. 2013. Genetically encoded calcium indicators for multi-color neural activity imaging and combination with optogenetics. *Front Mol Neurosci.* **6**, p2.

Albeg, A., Smith, C.J., Chatzigeorgiou, M., Feitelson, D.G., Hall, D.H., Schafer, W.R., Miller, D.M., 3rd and Treinin, M. 2011. *C. elegans* multi-dendritic sensory neurons: morphology and function. *Mol Cell Neurosci.* **46**(1), pp.308-317.

Alkema, M.J., Hunter-Ensor, M., Ringstad, N. and Horvitz, H.R. 2005. Tyramine Functions independently of octopamine in the *Caenorhabditis elegans* nervous system. *Neuron.* **46**(2), pp.247-260.

Aurelio, O., Hall, D.H. and Hobert, O. 2002. Immunoglobulin-domain proteins required for maintenance of ventral nerve cord organization. *Science.* **295**(5555), pp.686-690.

Avery, L. and Horvitz, H.R. 1987. A cell that dies during wild-type *C. elegans* development can function as a neuron in a ced-3 mutant. *Cell.* **51**(6), pp.1071-1078.

Bacaj, T. and Shaham, S. 2007. Temporal Control of Cell-Specific Transgene Expression in *Caenorhabditis elegans*. *Genetics.* **176**(4), pp.2651-2655.

Baird, G.S., Zacharias, D.A. and Tsien, R.Y. 1999. Circular permutation and receptor insertion within green fluorescent proteins. *Proc Natl Acad Sci U S A.* **96**(20), pp.11241-11246.

Bargmann, C.I. 1993. Genetic and cellular analysis of behavior in *C. elegans*. *Annu Rev Neurosci.* **16**, pp.47-71.

Bargmann, C.I. 1998. Neurobiology of the *Caenorhabditis elegans* genome. *Science.* **282**(5396), pp.2028-2033.

Bargmann, C.I. 2012. Beyond the connectome: How neuromodulators shape neural circuits. *BioEssays.* **34**(6), pp.458-465.

Bargmann, C.I., Hartwieg, E. and Horvitz, H.R. 1993. Odorant-selective genes and neurons mediate olfaction in *C. elegans*. *Cell.* **74**(3), pp.515-527.

Bargmann, C.I. and Horvitz, H.R. 1991. Chemosensory neurons with overlapping functions direct chemotaxis to multiple chemicals in *C. elegans*. *Neuron.* **7**(5), pp.729-742.

Barrios, A., Ghosh, R., Fang, C., Emmons, S.W. and Barr, M.M. 2012. PDF-1 neuropeptide signaling modulates a neural circuit for mate-searching behavior in *C. elegans*. *Nat Neurosci.* **15**(12), pp.1675-1682.

Bendesky, A., Tsunozaki, M., Rockman, M.V., Kruglyak, L. and Bargmann, C.I. 2011. Catecholamine receptor polymorphisms affect decision-making in *C. elegans*. *Nature.* **472**(7343), pp.313-318.

Bernhardt, R.R., Nguyen, N. and Kuwada, J.Y. 1992. Growth cone guidance by floor plate cells in the spinal cord of zebrafish embryos. *Neuron.* **8**(5), pp.869-882.

Beverly, M., Anbil, S. and Sengupta, P. 2011. Degeneracy and neuromodulation among thermosensory neurons contribute to robust thermosensory behaviors in *C. elegans*. *The Journal of neuroscience : the official journal of the Society for Neuroscience.* **31**(32), pp.11718-11727.

Bolme *et al*. 2010. Visual object tracking using adaptive correlation filters. In: *2010 IEEE Computer Society Conference on Computer Vision and Pattern Recognition*, *05 August 2010, San Francisco, CA, 2010*. IEEE, pp.2544-2550.

Boyle, J.H., Berri, S. and Cohen, N. 2012. Gait Modulation in *C. elegans*: An Integrated Neuromechanical Model. *Front Comput Neurosci.* **6**, p10.

Breitman, M.L., Clapoff, S., Rossant, J., Tsui, L.C., Glode, L.M., Maxwell, I.H. and Bernstein, A. 1987. Genetic ablation: targeted expression of a toxin gene causes microphthalmia in transgenic mice. *Science.* **238**(4833), pp.1563-1565.

Brenner, S. 1974. The genetics of *Caenorhabditis elegans*. *Genetics.* **77**(1), pp.71-94.

Brockie, P.J., Mellem, J.E., Hills, T., Madsen, D.M. and Maricq, A.V. 2001. The *C. elegans* glutamate receptor subunit NMR-1 is required for slow NMDA-activated currents that regulate reversal frequency during locomotion. *Neuron.* **31**(4), pp.617-630.

Broekmans, O.D., Rodgers, J.B., Ryu, W.S. and Stephens, G.J. 2016. Resolving coiled shapes reveals new reorientation behaviors in *C. elegans*. *Elife.* **5**.

Chalfie, M., Sulston, J.E., White, J.G., Southgate, E., Thomson, J.N. and Brenner, S. 1985. The neural circuit for touch sensitivity in *Caenorhabditis elegans*. *J Neurosci.* **5**(4), pp.956-964.

Chalfie, M., Tu, Y., Euskirchen, G., Ward, W.W. and Prasher, D.C. 1994. Green fluorescent protein as a marker for gene expression. *Science.* **263**(5148), pp.802-805.

Chalfie, M. and White, J. 1988. The nervous system. In the nematode *Caenorhabditis elegans*. In: Wood, W.B. ed.   NY: Cold Spring Harbor, p.667.

Chelur, D.S. and Chalfie, M. 2007. Targeted cell killing by reconstituted caspases. *Proc Natl Acad Sci U S A.* **104**(7), pp.2283-2288.

Chen, B.L., Hall, D.H. and Chklovskii, D.B. 2006. Wiring optimization can relate neuronal structure and function. *Proc Natl Acad Sci U S A.* **103**(12), pp.4723-4728.

Chou, J.H., Bargmann, C.I. and Sengupta, P. 2001. The *Caenorhabditis elegans* odr-2 gene encodes a novel Ly-6-related protein required for olfaction. *Genetics.* **157**(1), pp.211-224.

Coates, J.C. and de Bono, M. 2002. Antagonistic pathways in neurons exposed to body fluid regulate social feeding in *Caenorhabditis elegans*. *Nature.* **419**(6910), pp.925-929.

Cohen, N. and Sanders, T. 2014. Nematode locomotion: dissecting the neuronal-environmental loop. *Curr Opin Neurobiol.* **25**, pp.99-106.

Colbert, H.A., Smith, T.L. and Bargmann, C.I. 1997. OSM-9, a novel protein with structural similarity to channels, is required for olfaction, mechanosensation, and olfactory adaptation in *Caenorhabditis elegans*. *J Neurosci.* **17**(21), pp.8259-8269.

Croll, N.A. 1975. Behavioural analysis of nematode movement. *Adv Parasitol.* **13**, pp.71-122.

D Kuo, A. 2002. *The Relative Roles of Feedforward and Feedback in the Control of Rhythmic Movements.*

Darwin, C. 1859. *On the Origin of Species by Means of Natural Selection, Or, The Preservation of Favoured Races in the Struggle for Life.* J. Murray.

Das, A.T., Tenenbaum, L. and Berkhout, B. 2016. Tet-On Systems For Doxycycline-inducible Gene Expression. *Current Gene Therapy.* **16**(3), pp.156-167.

de Bono, M. and Maricq, A.V. 2005. Neuronal substrates of complex behaviors in *C. elegans*. *Annu Rev Neurosci.* **28**, pp.451-501.

de Bono, M., Tobin, D.M., Davis, M.W., Avery, L. and Bargmann, C.I. 2002. Social feeding in *Caenorhabditis elegans* is induced by neurons that detect aversive stimuli. *Nature.* **419**(6910), pp.899-903.

Denk, W., Yuste, R., Svoboda, K. and Tank, D.W. 1996. Imaging calcium dynamics in dendritic spines. *Curr Opin Neurobiol.* **6**(3), pp.372-378.

Donnelly, J.L., Clark, C.M., Leifer, A.M., Pirri, J.K., Haburcak, M., Francis, M.M., Samuel, A.D. and Alkema, M.J. 2013. Monoaminergic orchestration of motor programs in a complex *C. elegans* behavior. *PLoS Biol.* **11**(4), pe1001529.

Dusenbery, D.B. 1980. Chemotactic behavior of mutants of the nematode*Caenorhabditis elegans* that are defective in osmotic avoidance. *Journal of comparative physiology.* **137**(1), pp.93-96.

Edelstein, A.D., Tsuchida, M.A., Amodaj, N., Pinkard, H., Vale, R.D. and Stuurman, N. 2014. Advanced methods of microscope control using μManager software. *2014.*

Ellis, H.M. and Horvitz, H.R. 1986. Genetic control of programmed cell death in the nematode *C. elegans*. *Cell.* **44**(6), pp.817-829.

Evans, T.C. 2006. *Transformation and microinjection.* [Online]. The *C.elegans* Research community. Available from: http://www.wormbook.org

Fang-Yen, C., Wyart, M., Xie, J., Kawai, R., Kodger, T., Chen, S., Wen, Q. and Samuel, A.D. 2010. Biomechanical analysis of gait adaptation in the nematode *Caenorhabditis elegans*. *Proc Natl Acad Sci U S A.* **107**(47), pp.20323-20328.

Faumont, S., Lindsay, T.H. and Lockery, S.R. 2012. Neuronal microcircuits for decision making in *C. elegans*. *Current opinion in neurobiology.* **22**(4), pp.580-591.

Feng, Z., Li, W., Ward, A., Piggott, B.J., Larkspur, E.R., Sternberg, P.W. and Xu, X.Z. 2006. A *C. elegans* model of nicotine-dependent behavior: regulation by TRP-family channels. *Cell.* **127**(3), pp.621-633.

Flavell, S.W., Pokala, N., Macosko, E.Z., Albrecht, D.R., Larsch, J. and Bargmann, C.I. 2013. Serotonin and the neuropeptide PDF initiate and extend opposing behavioral states in *C. elegans*. *Cell.* **154**(5), pp.1023-1035.

Fraenkel, G. and Gunn, D. 1940. The Orientation of Animals: Kineses. *Taxes and Compass Reactions Clarendon Press: Oxford, UK.*

Fraenkel, G.S. and Gunn, D.L. 1961. *The orientation of animals.* Dover Publications, Inc; New York.

Frisch, K.v. 1954. *The Dancing Bees.* 1 ed. Springer-Verlag Wien.

Frokjaer-Jensen, C., Davis, M.W., Hopkins, C.E., Newman, B.J., Thummel, J.M., Olesen, S.P., Grunnet, M. and Jorgensen, E.M. 2008. Single-copy insertion of transgenes in *Caenorhabditis elegans*. *Nat Genet.* **40**(11), pp.1375-1383.

Fujiwara, M., Sengupta, P. and McIntire, S.L. 2002. Regulation of body size and behavioral state of *C. elegans* by sensory perception and the EGL-4 cGMP-dependent protein kinase. *Neuron.* **36**(6), pp.1091-1102.

Gallagher, T., Kim, J., Oldenbroek, M., Kerr, R. and You, Y.-J. 2013. ASI regulates satiety quiescence in *C. elegans. The Journal of neuroscience : the official journal of the Society for Neuroscience.* **33**(23), pp.9716-9724.

Gao, S., Guan, S.A., Fouad, A.D., Meng, J., Kawano, T., Huang, Y.-C., Li, Y., Alcaire, S., Hung, W., Lu, Y., Qi, Y.B., Jin, Y., Alkema, M., Fang-Yen, C. and Zhen, M. 2018. Excitatory motor neurons are local oscillators for backward locomotion. *Elife.* **7**, pe29915.

Ghosh, I., Hamilton, A.D. and Regan, L. 2000. Antiparallel leucine zipper-directed protein reassembly: application to the green fluorescent protein. *J. Am. Chem. Soc.* **122**(23), pp.5658-5659.

Glauser, D.A., Chen, W.C., Agin, R., MacInnis, B.L., Hellman, A.B., Garrity, P.A., Tan, M.-W. and Goodman, M.B. 2011. Heat Avoidance Is Regulated by Transient Receptor Potential (TRP) Channels and a Neuropeptide Signaling Pathway in *Caenorhabditis elegans. Genetics.* **188**(1), pp.91-103.

Goodman, M.B., Hall, D.H., Avery, L. and Lockery, S.R. 1998. Active currents regulate sensitivity and dynamic range in *C. elegans* neurons. *Neuron.* **20**(4), pp.763-772.

Goulding, M. 2012. Motor Neurons that Multitask. *Neuron.* **76**(4), pp.669-670.

Gray, J. and Lissmann, H.W. 1964. The Locomotion of Nematodes. *Journal of Experimental Biology.* **41**(1), pp.135-154.

Gray, J.M., Hill, J.J. and Bargmann, C.I. 2005. A circuit for navigation in *Caenorhabditis elegans. Proc Natl Acad Sci U S A.* **102**(9), pp.3184-3191.

Gray, J.M., Karow, D.S., Lu, H., Chang, A.J., Chang, J.S., Ellis, R.E., Marletta, M.A. and Bargmann, C.I. 2004. Oxygen sensation and social feeding mediated by a *C. elegans* guanylate cyclase homologue. *Nature.* **430**(6997), pp.317-322.

Ha, H.-i., Hendricks, M., Shen, Y., Gabel, C.V., Fang-Yen, C., Qin, Y., Colón-Ramos, D., Shen, K., Samuel, A.D.T. and Zhang, Y. 2010. Functional organization of a neural network for aversive olfactory learning in *Caenorhabditis elegans. Neuron.* **68**(6), pp.1173-1186.

Hall, D.H. and Russell, R.L. 1991. The posterior nervous system of the nematode *Caenorhabditis elegans*: serial reconstruction of identified neurons and complete pattern of synaptic interactions. *J Neurosci.* **11**(1), pp.1-22.

Harris, G., Korchnak, A., Summers, P., Hapiak, V., Law, W.J., Stein, A.M., Komuniecki, P. and Komuniecki, R. 2011. Dissecting the serotonergic food signal stimulating sensory-mediated aversive behavior in *C. elegans*. *PLoS One.* **6**(7), pe21897.

Hedgecock, E.M., Culotti, J.G., Hall, D.H. and Stern, B.D. 1987. Genetics of cell and axon migrations in *Caenorhabditis elegans*. *Development.* **100**(3), pp.365-382.

Hedgecock, E.M. and Russell, R.L. 1975. Normal and mutant thermotaxis in the nematode *Caenorhabditis elegans*. *Proc Natl Acad Sci U S A.* **72**(10), pp.4061-4065.

Hendricks, M., Ha, H., Maffey, N. and Zhang, Y. 2012. Compartmentalized calcium dynamics in a *C. elegans* interneuron encode head movement. *Nature.* **487**(7405), pp.99-103.

Hobert, O. 2002. PCR fusion-based approach to create reporter gene constructs for expression analysis in transgenic *C. elegans*. *Biotechniques.* **32**(4), pp.728-730.

Hodgkin, J., Horvitz, H.R., Jasny, B.R. and Kimble, J. 1998. C. elegans: Sequence to Biology. *Science.* **282**(5396), pp.2011-2011.

Hohenwarter, M. 2002. *{G}eo{G}ebra: Ein {S}oftwaresystem fur dynamische {G}eometrie und {A}lgebra der {E}bene*. MSc thesis, Paris Lodron University, Salzburg, Austria.

Hong, K. and Driscoll, M. 1994. A transmembrane domain of the putative channel subunit MEC-4 influences mechanotransduction and neurodegeneration in *C. elegans*. *Nature.* **367**(6462), pp.470-473.

Horvitz, H.R., Chalfie, M., Trent, C., Sulston, J.E. and Evans, P.D. 1982. Serotonin and octopamine in the nematode *Caenorhabditis elegans*. *Science.* **216**(4549), pp.1012-1014.

Iino, Y. and Yoshida, K. 2009. Parallel use of two behavioral mechanisms for chemotaxis in *Caenorhabditis elegans*. *J Neurosci.* **29**(17), pp.5370-5380.

Integrated Publishing, I. 2013. *Elements of a horizontal curve.* [Online]. [Accessed 03 January 2018]. Available from: http://www.tpub.com/inteng/11a.htm

Izquierdo, E.J. and Beer, R.D. 2013. Connecting a connectome to behavior: an ensemble of neuroanatomical models of *C. elegans* klinotaxis. *PLoS Comput Biol.* **9**(2), pe1002890.

Izquierdo, E.J. and Beer, R.D. 2016. The whole worm: brain-body-environment models of *C. elegans*. *Curr Opin Neurobiol.* **40**, pp.23-30.

Izquierdo, E.J. and Lockery, S.R. 2010. Evolution and analysis of minimal neural circuits for klinotaxis in *Caenorhabditis elegans*. *J Neurosci.* **30**(39), pp.12908-12917.

Izquierdo, E.J., Williams, P.L. and Beer, R.D. 2015. Information Flow through a Model of the *C. elegans* Klinotaxis Circuit. *PLoS One.* **10**(10), pe0140397.

Jarrell, T.A., Wang, Y., Bloniarz, A.E., Brittin, C.A., Xu, M., Thomson, J.N., Albertson, D.G., Hall, D.H. and Emmons, S.W. 2012. The Connectome of a Decision-Making Neural Network. *Science.* **337**(6093), pp.437-444.

Karbowski, J., Schindelman, G., Cronin, C.J., Seah, A. and Sternberg, P.W. 2008. Systems level circuit model of *C. elegans* undulatory locomotion: mathematical modeling and molecular genetics. *Journal of Computational Neuroscience.* **24**(3), pp.253-276.

Kibbe, W.A. 2007. OligoCalc: an online oligonucleotide properties calculator. *Nucleic Acids Res.* **35**(Web Server issue), pp.W43-46.

Kim, D., Park, S., Mahadevan, L. and Shin, J.H. 2011. The shallow turn of a worm. *J Exp Biol.* **214**(Pt 9), pp.1554-1559.

Kim, J., Yeon, J., Choi, S.-K., Huh, Y.H., Fang, Z., Park, S.J., Kim, M.O., Ryoo, Z.Y., Kang, K. and Kweon, H.-S. 2015a. The evolutionarily conserved LIM homeodomain protein LIM-4/LHX6 specifies the terminal identity of a cholinergic and peptidergic *C. elegans* Sensory/Inter/Motor neuron-type. *PLOS Genetics.* **11**(8), pe1005480.

Kim, J., Yeon, J., Choi, S.-K., Huh, Y.H., Fang, Z., Park, S.J., Kim, M.O., Ryoo, Z.Y., Kang, K., Kweon, H.-S., Jeon, W.B., Li, C. and Kim, K. 2015b. The Evolutionarily Conserved LIM Homeodomain Protein LIM-4/LHX6 Specifies the Terminal Identity of a Cholinergic and Peptidergic *C. elegans* Sensory/Inter/Motor Neuron-Type. *PLOS Genetics.* **11**(8), pe1005480.

Kim, K. and Li, C. 2004. Expression and regulation of an FMRFamide-related neuropeptide gene family in *Caenorhabditis elegans*. *J Comp Neurol.* **475**(4), pp.540-550.

Kocabas, A., Shen, C.H., Guo, Z.V. and Ramanathan, S. 2012. Controlling interneuron activity in *Caenorhabditis elegans* to evoke chemotactic behaviour. *Nature.* **490**(7419), pp.273-277.

Koelle, M.R. and Horvitz, H.R. 1996. EGL-10 regulates G protein signaling in the *C. elegans* nervous system and shares a conserved domain with many mammalian proteins. *Cell.* **84**(1), pp.115-125.

Koressaar, T. and Remm, M. 2007. Enhancements and modifications of primer design program Primer3. *Bioinformatics.* **23**(10), pp.1289-1291.

Kramer, J.M., French, R.P., Park, E.C. and Johnson, J.J. 1990. The *Caenorhabditis elegans* rol-6 gene, which interacts with the sqt-1 collagen gene to determine organismal morphology, encodes a collagen. *Mol Cell Biol.* **10**(5), pp.2081-2089.

L. Gunn, D. 1975. *The meaning of the term 'klinokinesis'.*

Larsch, J., Flavell, S.W., Liu, Q., Gordus, A., Albrecht, D.R. and Bargmann, C.I. 2015. A Circuit for Gradient Climbing in *C. elegans* Chemotaxis. *Cell Rep.* **12**(11), pp.1748-1760.

Lebois, F., Sauvage, P., Py, C., Cardoso, O., Ladoux, B., Hersen, P. and Di Meglio, J.M. 2012. Locomotion control of *Caenorhabditis elegans* through confinement. *Biophys J.* **102**(12), pp.2791-2798.

Leifer, A.M., Fang-Yen, C., Gershow, M., Alkema, M.J. and Samuel, A.D. 2011. Optogenetic manipulation of neural activity in freely moving *Caenorhabditis elegans*. *Nat Methods.* **8**(2), pp.147-152.

Li, W., Feng, Z., Sternberg, P.W. and Xu, X.Z. 2006. A *C. elegans* stretch receptor neuron revealed by a mechanosensitive TRP channel homologue. *Nature.* **440**(7084), pp.684-687.

Li, Z., Liu, J., Zheng, M. and Xu, X.Z.S. 2014. Encoding of Both Analog- and Digital-like Behavioral Outputs by One C. elegans Interneuron. *Cell.* **159**(4), pp.751-765.

Lin, C.-T., He, C.-W., Huang, T.-T. and Pan, C.-L. 2017. Longevity control by the nervous system: Sensory perception, stress response and beyond. *Translational Medicine of Aging.* **1**, pp.41-51.

Lindsay, T.H., Thiele, T.R. and Lockery, S.R. 2011. Optogenetic analysis of synaptic transmission in the central nervous system of the nematode *C. elegans*. *Nature Communications.* **2**, pp.306-306.

Liu, Q., Hollopeter, G. and Jorgensen, E.M. 2009. Graded synaptic transmission at the *Caenorhabditis elegans* neuromuscular junction. *Proceedings of the National Academy of Sciences.* **106**(26), pp.10823-10828.

Lockery, S.R. 2011. The computational worm: spatial orientation and its neuronal basis in *C. elegans*. *Current opinion in neurobiology.* **21**(5), pp.782-790.

Lockery, S.R. and Goodman, M.B. 2009. The quest for action potentials in *C. elegans* neurons hits a plateau. *Nat Neurosci.* **12**(4), pp.377-378.

Lockery, S.R., Lawton, K.J., Doll, J.C., Faumont, S., Coulthard, S.M., Thiele, T.R., Chronis, N., McCormick, K.E., Goodman, M.B. and Pruitt, B.L. 2008. Artificial dirt: microfluidic substrates for nematode neurobiology and behavior. *J Neurophysiol.* **99**(6), pp.3136-3143.

Lorenz, K. 1970. *Studies in animal and human behaviour.* Harvard University Press.

Luo, L., Clark, D.A., Biron, D., Mahadevan, L. and Samuel, A.D. 2006. Sensorimotor control during isothermal tracking in *Caenorhabditis elegans*. *J Exp Biol.* **209**(Pt 23), pp.4652-4662.

Luo, L., Wen, Q., Ren, J., Hendricks, M., Gershow, M., Qin, Y., Greenwood, J., Soucy, E.R., Klein, M., Smith-Parker, H.K., Calvo, A.C., Colon-Ramos, D.A., Samuel, A.D. and Zhang, Y. 2014. Dynamic encoding of perception, memory, and movement in a *C. elegans* chemotaxis circuit. *Neuron.* **82**(5), pp.1115-1128.

Marder, E. and Bucher, D. 2001. Central pattern generators and the control of rhythmic movements. *Current Biology.* **11**(23), pp.R986-R996.

Mariol, M.C., Walter, L., Bellemin, S. and Gieseler, K. 2013. A rapid protocol for integrating extrachromosomal arrays with high transmission rate into the *C. elegans* genome. *J Vis Exp.* (82), pe50773.

McIntire, S.L., Jorgensen, E., Kaplan, J. and Horvitz, H.R. 1993. The GABAergic nervous system of *Caenorhabditis elegans*. *Nature.* **364**(6435), pp.337-341.

Mello, C.C., Kramer, J.M., Stinchcomb, D. and Ambros, V. 1991. Efficient gene transfer in *C.elegans*: extrachromosomal maintenance and integration of transforming sequences. *EMBO J.* **10**(12), pp.3959-3970.

Miyabayashi, T., Palfreyman, M.T., Sluder, A.E., Slack, F. and Sengupta, P. 1999. Expression and function of members of a divergent nuclear receptor family in *Caenorhabditis elegans*. *Dev Biol.* **215**(2), pp.314-331.

Miyakawa, H., Ross, W.N., Jaffe, D., Callaway, J.C., Lasser-Ross, N., Lisman, J.E. and Johnston, D. 1992. Synaptically activated increases in Ca2+ concentration in hippocampal CA1 pyramidal cells are primarily due to voltage-gated Ca2+ channels. *Neuron.* **9**(6), pp.1163-1173.

Miyawaki, A., Llopis, J., Heim, R., McCaffery, J.M., Adams, J.A., Ikura, M. and Tsien, R.Y. 1997. Fluorescent indicators for Ca2+ based on green fluorescent proteins and calmodulin. *Nature.* **388**(6645), pp.882-887.

Mori, I. and Ohshima, Y. 1995. Neural regulation of thermotaxis in *Caenorhabditis elegans*. *Nature.* **376**, p344.

Nagai, T., Sawano, A., Park, E.S. and Miyawaki, A. 2001. Circularly permuted green fluorescent proteins engineered to sense Ca2+. *Proceedings of the National Academy of Sciences.* **98**(6), pp.3197-3202.

Nagai, T., Yamada, S., Tominaga, T., Ichikawa, M. and Miyawaki, A. 2004. Expanded dynamic range of fluorescent indicators for Ca(2+) by circularly permuted yellow fluorescent proteins. *Proc Natl Acad Sci U S A.* **101**(29), pp.10554-10559.

Nagel, G., Brauner, M., Liewald, J.F., Adeishvili, N., Bamberg, E. and Gottschalk, A. 2005. Light activation of channelrhodopsin-2 in excitable cells of *Caenorhabditis elegans* triggers rapid behavioral responses. *Curr Biol.* **15**(24), pp.2279-2284.

Nakai, J., Ohkura, M. and Imoto, K. 2001. A high signal-to-noise Ca(2+) probe composed of a single green fluorescent protein. *Nat Biotechnol.* **19**(2), pp.137-141.

O'Hagan, R. and Chalfie, M. 2005. Mechanosensation in *Caenorhabditis elegans*. *International Review of Neurobiology.* Academic Press, pp.169-203.

Paradis, E., Claude, J. and Strimmer, K. 2004. APE: Analyses of Phylogenetics and Evolution in R language. *Bioinformatics.* **20**(2), pp.289-290.

Pereira, L., Kratsios, P., Serrano-Saiz, E., Sheftel, H., Mayo, A.E., Hall, D.H., White, J.G., LeBoeuf, B., Garcia, L.R., Alon, U. and Hobert, O. 2015. A cellular and regulatory map of the cholinergic nervous system of *C. elegans*. *Elife.* **4**, pe12432.

Pfeffer. 1888. Uber chemotaktische Bewegungen von Bakterien, Flagellaten und Volvocineen. . *Untersuchungen Bot. Inst. Tübingen.* **2**, pp.582–661.

Pierce-Shimomura, J.T., Dores, M. and Lockery, S.R. 2005. Analysis of the effects of turning bias on chemotaxis in *C. elegans*. *J Exp Biol.* **208**(Pt 24), pp.4727-4733.

Pierce-Shimomura, J.T., Morse, T.M. and Lockery, S.R. 1999. The fundamental role of pirouettes in *Caenorhabditis elegans* chemotaxis. *J Neurosci.* **19**(21), pp.9557-9569.

Piggott, B.J., Liu, J., Feng, Z., Wescott, S.A. and Xu, X.Z. 2011. The neural circuits and synaptic mechanisms underlying motor initiation in *C. elegans*. *Cell.* **147**(4), pp.922-933.

Pirri, J.K. and Alkema, M.J. 2012. The neuroethology of *C. elegans* escape. *Current opinion in neurobiology.* **22**(2), pp.187-193.

Pirri, J.K., McPherson, A.D., Donnelly, J.L., Francis, M.M. and Alkema, M.J. 2009. A tyramine-gated chloride channel coordinates distinct motor programs of a *Caenorhabditis elegans* escape response. *Neuron.* **62**(4), pp.526-538.

Pologruto, T.A., Yasuda, R. and Svoboda, K. 2004. Monitoring neural activity and [Ca2+] with genetically encoded Ca2+ indicators. *J Neurosci.* **24**(43), pp.9572-9579.

Qi, Y.B., Garren, E.J., Shu, X., Tsien, R.Y. and Jin, Y. 2012. Photo-inducible cell ablation in *Caenorhabditis elegans* using the genetically encoded singlet oxygen generating protein miniSOG. *Proc Natl Acad Sci U S A.* **109**(19), pp.7499-7504.

Rankin, C.H., Beck, C.D. and Chiba, C.M. 1990. *Caenorhabditis elegans*: a new model system for the study of learning and memory. *Behavioural brain research.* **37**(1), pp.89-92.

Rich, J.T., Neely, J.G., Paniello, R.C., Voelker, C.C.J., Nussenbaum, B. and Wang, E.W. 2010. A PRACTICAL GUIDE TO UNDERSTANDING KAPLAN-MEIER CURVES. *Otolaryngology--head and neck surgery : official journal of American Academy of Otolaryngology-Head and Neck Surgery.* **143**(3), pp.331-336.

Richmond, J.E. and Jorgensen, E.M. 1999. One GABA and two acetylcholine receptors function at the *C. elegans* neuromuscular junction. *Nature Neuroscience.* **2**, p791.

Ryu, W.S. and Samuel, A.D. 2002. Thermotaxis in *Caenorhabditis elegans* analyzed by measuring responses to defined thermal stimuli. *Journal of Neuroscience.* **22**(13), pp.5727-5733.

Sachs. 1887. *Vorlesungen iiber Pflanzenphysiologie.* 2nd Ed. ed. Leipzig.

Sagasti, A., Hobert, O., Troemel, E.R., Ruvkun, G. and Bargmann, C.I. 1999. Alternative olfactory neuron fates are specified by the LIM homeobox gene lim-4. *Genes Dev.* **13**(14), pp.1794-1806.

Sakata, K. and Shingai, R. 2004. Neural network model to generate head swing in locomotion of *Caenorhabditis elegans*. *Network.* **15**(3), pp.199-216.

Sanders, T. 2016. *Sensory computation and decision making in C. elegans: a computational approach*. PhD thesis thesis, University of Leeds.

Satoh, Y., Sato, H., Kunitomo, H., Fei, X., Hashimoto, K. and Iino, Y. 2014. Regulation of experience-dependent bidirectional chemotaxis by a neural circuit switch in *Caenorhabditis elegans*. *J Neurosci.* **34**(47), pp.15631-15637.

Schindelin, J., Arganda-Carreras, I., Frise, E., Kaynig, V., Longair, M., Pietzsch, T., Preibisch, S., Rueden, C., Saalfeld, S., Schmid, B., Tinevez, J.Y., White, D.J., Hartenstein, V., Eliceiri, K., Tomancak, P. and Cardona, A. 2012. Fiji: an open-source platform for biological-image analysis. *Nat Methods.* **9**(7), pp.676-682.

Schofield, W. 2001. *Engineering surveying: theory and examination problems for students.* Elsevier.

Schwarz, V., Pan, J., Voltmer-Irsch, S. and Hutter, H. 2009. IgCAMs redundantly control axon navigation in *Caenorhabditis elegans*. *Neural Dev.* **4**, p13.

Shah, E.M. and Jay, D.G. 1993. Methods for ablating neurons. *Curr Opin Neurobiol.* **3**(5), pp.738-742.

Shaham, S. 2006. *WormBook: Methods in Cell Biology.* [Online]. [Accessed (last viewed 25/03/2018)]. Available from: http://www.wormbook.org.

Shen, Y., Wen, Q., Liu, H., Zhong, C., Qin, Y., Harris, G., Kawano, T., Wu, M., Xu, T., Samuel, A.D. and Zhang, Y. 2016. An extrasynaptic GABAergic signal modulates a pattern of forward movement in *Caenorhabditis elegans*. *Elife.* **5**.

Smedemark-Margulies, N. and Trapani, J.G. 2013. Tools, methods, and applications for optophysiology in neuroscience. *Front Mol Neurosci.* **6**, p18.

Starich, T.A., Xu, J., Skerrett, I.M., Nicholson, B.J. and Shaw, J.E. 2009. Interactions between innexins UNC-7 and UNC-9 mediate electrical synapse specificity in the *Caenorhabditis elegans* locomotory nervous system. *Neural Dev.* **4**, p16.

Strasburger. 1878. Wirkung des Lichtes und der Warme auf Schwarm- sporen. *Jena. Zeit., N.F., Bd.* **XII**, pp.551-625.

Sugimoto, A., Friesen, P.D. and Rothman, J.H. 1994. Baculovirus p35 prevents developmentally programmed cell death and rescues a ced-9 mutant in the nematode *Caenorhabditis elegans*. *EMBO J.* **13**(9), pp.2023-2028.

Sulston, J.E. and Horvitz, H.R. 1977. Post-embryonic cell lineages of the nematode, *Caenorhabditis elegans*. *Dev Biol.* **56**(1), pp.110-156.

Sulston, J.E., Schierenberg, E., White, J.G. and Thomson, J.N. 1983. The embryonic cell lineage of the nematode *Caenorhabditis elegans*. *Dev Biol.* **100**(1), pp.64-119.

Sulston, J.E. and White, J.G. 1980. Regulation and cell autonomy during postembryonic development of *Caenorhabditis elegans*. *Dev Biol.* **78**(2), pp.577-597.

Suzuki, H., Thiele, T.R., Faumont, S., Ezcurra, M., Lockery, S.R. and Schafer, W.R. 2008. Functional asymmetry in *Caenorhabditis elegans* taste neurons and its computational role in chemotaxis. *Nature.* **454**, p114.

Thiele, T.R., Faumont, S. and Lockery, S.R. 2009. The Neural Network for Chemotaxis to Tastants in *Caenorhabditis elegans* Is Specialized for Temporal Differentiation. *The Journal of Neuroscience.* **29**(38), pp.11904-11911.

Tian, L., Hires, S.A., Mao, T., Huber, D., Chiappe, M.E., Chalasani, S.H., Petreanu, L., Akerboom, J., McKinney, S.A., Schreiter, E.R., Bargmann, C.I., Jayaraman, V., Svoboda, K. and Looger, L.L. 2009. Imaging neural activity in worms, flies and mice with improved GCaMP calcium indicators. *Nat Methods.* **6**(12), pp.875-881.

Tinbergen, N. 1951. *The study of instinct.* Clarendon Press.

Tolstenkov, O., Van der Auwera, P., Liewald, J.F., Steuer Costa, W., Bazhanova, O., Gemeinhardt, T.M., Bergs, A.C.F. and Gottschalk, A. 2018. Functionally asymmetric motor neurons coordinate locomotion of *Caenorhabditis elegans*. *bioRxiv.*

Troemel, E.R., Sagasti, A. and Bargmann, C.I. 1999. Lateral signaling mediated by axon contact and calcium entry regulates asymmetric odorant receptor expression in *C. elegans.* *Cell.* **99**(4), pp.387-398.

Untergasser, A., Cutcutache, I., Koressaar, T., Ye, J., Faircloth, B.C., Remm, M. and Rozen, S.G. 2012. Primer3--new capabilities and interfaces. *Nucleic Acids Res.* **40**(15), pe115.

Vidal-Gadea, A., Topper, S., Young, L., Crisp, A., Kressin, L., Elbel, E., Maples, T., Brauner, M., Erbguth, K., Axelrod, A., Gottschalk, A., Siegel, D. and Pierce-Shimomura, J.T. 2011. *Caenorhabditis elegans* selects distinct crawling and swimming gaits via dopamine and serotonin. *Proc Natl Acad Sci U S A.* **108**(42), pp.17504-17509.

Von Stetina, S.E., Treinin, M. and Miller, D.M. 2005. The Motor Circuit. *International Review of Neurobiology.* Academic Press, pp.125-167.

Wakabayashi, T., Kitagawa, I. and Shingai, R. 2004. Neurons regulating the duration of forward locomotion in *Caenorhabditis elegans.* *Neurosci Res.* **50**(1), pp.103-111.

Wang, X., Zhang, W., Cheever, T., Schwarz, V., Opperman, K., Hutter, H., Koepp, D. and Chen, L. 2008. The *C. elegans* L1CAM homologue LAD-2 functions as a coreceptor in MAB-20/Sema2 mediated axon guidance. *J Cell Biol.* **180**(1), pp.233-246.

Ward, A., Liu, J., Feng, Z. and Xu, X.Z. 2008. Light-sensitive neurons and channels mediate phototaxis in *C. elegans*. *Nat Neurosci.* **11**(8), pp.916-922.

Ward, S. 1973. Chemotaxis by the nematode *Caenorhabditis elegans*: identification of attractants and analysis of the response by use of mutants. *Proc Natl Acad Sci U S A.* **70**(3), pp.817-821.

Ward, S. and Carrel, J.S. 1979. Fertilization and sperm competition in the nematode *Caenorhabditis elegans*. *Dev Biol.* **73**(2), pp.304-321.

Ward, S., Thomson, N., White, J.G. and Brenner, S. 1975. Electron microscopical reconstruction of the anterior sensory anatomy of the nematode *Caenorhabditis elegans*.?2UU. *J Comp Neurol.* **160**(3), pp.313-337.

Ware, R.W., Clark, D., Crossland, K. and Russell, R.L. 1975. The nerve ring of the nematode *Caenorhabditis elegans*: Sensory input and motor output. *The Journal of Comparative Neurology.* **162**(1), pp.71-110.

Wen, Q., Po, M.D., Hulme, E., Chen, S., Liu, X., Kwok, S.W., Gershow, M., Leifer, A.M., Butler, V., Fang-Yen, C., Kawano, T., Schafer, W.R., Whitesides, G., Wyart, M., Chklovskii, D.B., Zhen, M. and Samuel, A.D. 2012. Proprioceptive coupling within motor neurons drives *C. elegans* forward locomotion. *Neuron.* **76**(4), pp.750-761.

White, J.G., Southgate, E., Thomson, J.N. and Brenner, S. 1976. The structure of the ventral nerve cord of *Caenorhabditis elegans*. *Philos Trans R Soc Lond B Biol Sci.* **275**(938), pp.327-348.

White, J.G., Southgate, E., Thomson, J.N. and Brenner, S. 1986. The structure of the nervous system of the nematode *Caenorhabditis elegans*. *Philos Trans R Soc Lond B Biol Sci.* **314**(1165), pp.1-340.

White, J.Q., Nicholas, T.J., Gritton, J., Truong, L., Davidson, E.R. and Jorgensen, E.M. 2007. The sensory circuitry for sexual attraction in *C. elegans* males. *Curr Biol.* **17**(21), pp.1847-1857.

Wolf, F.W., Hung, M.S., Wightman, B., Way, J. and Garriga, G. 1998. vab-8 is a key regulator of posteriorly directed migrations in *C. elegans* and encodes a novel protein with kinesin motor similarity. *Neuron.* **20**(4), pp.655-666.

Xu, M., Jarrell, T.A., Wang, Y., Cook, S.J., Hall, D.H. and Emmons, S.W. 2013. Computer Assisted Assembly of Connectomes from Electron Micrographs: Application to *Caenorhabditis elegans*. *PLoS One.* **8**(1), pe54050.

Xue, D. and Horvitz, H.R. 1995. Inhibition of the *Caenorhabditis elegans* cell-death protease CED-3 by a CED-3 cleavage site in baculovirus p35 protein. *Nature.* **377**(6546), pp.248-251.

Yemini, E., Kerr, R.A. and Schafer, W.R. 2011. Tracking Movement Behavior of Multiple Worms on Food. *Cold Spring Harbor protocols.* **2011**(12), pp.1483-1487.

Yoshida, K., Hirotsu, T., Tagawa, T., Oda, S., Wakabayashi, T., Iino, Y. and Ishihara, T. 2012. Odour concentration-dependent olfactory preference change in *C. elegans*. *Nature Communications.* **3**, p739.

Zhang, S., Ma, C. and Chalfie, M. 2004. Combinatorial marking of cells and organelles with reconstituted fluorescent proteins. *Cell.* **119**(1), pp.137-144.

Zhao, B., Khare, P., Feldman, L. and Dent, J.A. 2003. Reversal frequency in *Caenorhabditis elegans* represents an integrated response to the state of the animal and its environment. *Journal of Neuroscience.* **23**(12), pp.5319-5328.

Zheng, Y., Brockie, P.J., Mellem, J.E., Madsen, D.M. and Maricq, A.V. 1999. Neuronal Control of Locomotion in C. elegans Is Modified by a Dominant Mutation in the GLR-1 Ionotropic Glutamate Receptor. *Neuron.* **24**(2), pp.347-361.